Cytohesins are cytoplasmic ErbB receptor activators

Dissertation

zur Erlangung des Doktorgrades (Dr. rer. nat.) der Mathematisch-Naturwissenschaftlichen Fakultät der Rheinischen Friedrich-Wilhelms-Universität Bonn

vorgelegt von

Anke Bill

Bonn, März 2011

1. Gutachter: Prof. Dr. Michael Famulok

2. Gutachter: Prof. Dr. Thorsten Lang

Tag der mündlichen Prüfung: 30.06.2011

Erscheinungsjahr 2011

Eidesstattliche Erklärung

Hiermit erkläre ich, dass ich die vorliegende Arbeit selbst verfasst habe und keine anderen als die angegebenen Quellen und Hilfsmittel benutzt habe.

Bonn, März 2011

_____

Anke Bill

Parts of this thesis are published in:

- **Bill, A**., A. Schmitz, B. Albertoni, J. N. Song, L. C. Heukamp, D. Walrafen, F. Thorwirth, P. J. Verveer, S. Zimmer, L. Meffert, A. Schreiber, S. Chatterjee, R. K. Thomas, R. T. Ullrich, T. Lang and M. Famulok (2010). "Cytohesins are cytoplasmic ErbB receptor activators." Cell 143(2): 201-211.
- Stumpfe, D., **A. Bill**, N. Novak, G. Loch, H. Blockus, H. Geppert, T. Becker, A. Schmitz, M. Hoch, W. Kolanus, M. Famulok and J. Bajorath (2010). "Targeting multifunctional proteins by virtual screening: structurally diverse cytohesin inhibitors with differentiated biological functions." ACS Chem Biol 5(9): 839-849.

To my parents

Acknowledgments

It is a pleasure to thank those you made this thesis possible.

I would like to express my sincere gratitude to Professor Dr. Michael Famulok. His understanding, encouraging and personal guidance has provided the basis for my career in life science from the very beginning.

I am heartily thankful to my colleague and supervisor, PD Dr. Anton Schmitz, whose expertise, understanding, encouragement and patience enabled me to achieve this work.

I am indebted to my many cooperation partners for their patience in teaching me new techniques and their willingness and dedication to support my work.

I want to thank my lab colleagues for providing a perfect working atmosphere, for additional help and interesting discussions.

Many friends have helped me to weather all these exciting years. Their support and care helped me overcome setbacks and stay focused on my study. I greatly value their friendship and I deeply appreciate their belief in me.

My special thanks goes to Barbara Albertoni for helping me get through the difficult times, for all her camaraderie and the many long evenings we spent together in the lab.

Finally, I owe my deepest gratitude to my parents for the love and support they have provided through my entire life.

Table of contents

TABLE OF CONTENTS **7**

I SUMMARY **11**

II INTRODUCTION **12**

II.1 THE ERBB RECEPTOR FAMILY OF RECEPTOR TYROSINE KINASES 12

II.1.1 Receptor tyrosine kinases (RTKs) *12*

II.1.2 The ErbB family of RTKs *13*

II.1.3 Signaling of ErbB receptors – An Overview *14*

II.1.4 Activation of ErbB receptors *15*

II.1.4.1 Ligand-induced dimerization of the extracellular domain 15

II.1.4.2 Activation of the kinase domain 16

II.1.4.3 MIG6 – a negative regulator of ErbB receptor activation 17

II.1.5 Downstream signaling of ErbB receptors *18*

II.2 ERBB RECEPTORS AND CANCER 20

II.2.1 Lung cancer *20*

II.2.2 Breast cancer *23*

II.2.3 Glioblastoma *24*

II.3 CYTOHESINS AND ARF-GTPASES 26

II.3.1 Adenosine diphosphate ribosylation factors (ARFs) *26*

II.3.2 The cytohesin family of ARF-GEFs *28*

II.3.3 The small molecule SecinH3 ..... *29*

III OBJECTIVES **31**

IV RESULTS **32**

IV.1 CYTOHESINS ARE CYTOPLASMIC ERBB RECEPTOR ACTIVATORS 32

IV.1.1 Inhibition of cytohesins decreases ErbB receptor signaling *32*

IV.1.1.1 Chemical inhibition of cytohesins reduces EGFR phosphorylation and signaling 32

IV.1.1.2 Chemical inhibition of cytohesins reduces HER3 phosphorylation and signaling 33

IV.1.2 Cytohesins enhance ErbB receptor activation *34*

IV.1.2.1 Overexpression of the cytohesin ARNO enhances both EGFR and HER3 phosphorylation 34

IV.1.2.2 The Sec7 domain of ARNO is sufficient for EGFR activation 35

IV.1.2.3 Activation of ErbB receptors by ARNO is independent of its GEF activity 36

IV.1.3 Cytohesins facilitate a conformational rearrangement of the intracellular domains of ErbB receptor dimers *38*

IV.1.3.1 SecinH3 does not alter EGF-triggered internalization or cluster size of EGFR 38

IV.1.3.2 Cytohesins enhance the phosphorylation but not the dimerization of ErbB receptors 40

IV.1.3.1 SecinH3 does not alter HER2/HER3 heterodimerization 43

IV.1.3.2 Cytohesins facilitate the phosphorylation of constitutively dimerized EGFR 44

IV.1.3.3 ARNO facilitates a conformational rearrangement of the intracellular domains in EGFR dimers 47

IV.1.3.3.1 Principles of steady-state fluorescence anisotropy 47

IV.1.3.3.2 Evaluation of the system 50

IV.1.3.3.3 ARNO induces a change in steady-state fluorescence anisotropy of lz-EGFR-mCitrine 51

IV.1.3.3.4 Control measurements 53
IV.1.4 Cytohesins interact with the EGFR *53*
IV.1.4.1 ARNO forms a complex with EGFR in cells 53
IV.1.4.2 Cytohesins directly bind to the intracellular domain of the EGFR 54
IV.1.5 ARNO stimulates autophosphorylation of EGFR by direct interaction *58*
IV.1.6 Chemical inhibition of cytohesins diminishes proliferation of human lung cancer cell lines in vitro and in vivo *59*
IV.1.6.1 SecinH3 decreases proliferation of human lung cancer cell lines expressing wild-type EGFR 60
IV.1.6.1.1 SecinH3 inhibits proliferation of H460 and A549 cells 60
IV.1.6.1.2 SecinH3 reduces growth of H460 cell tumor xenografts in nude mice 61
IV.1.6.2 SecinH3 also reduces growth of lung cancer cell lines with EGFR mutations 63
IV.1.6.3 SecinH3 induces cell-cycle arrest in PC9 cells 63
IV.1.6.4 SecinH3 induces apoptosis in PC9 cells 65
IV.1.6.5 SecinH3 reduces growth of PC9 tumor xenografts in nude mice 67
IV.1.6.6 Chemical inhibition of cytohesins decreases proliferation in various EGFR-dependent cell lines independent of the EGFR mutation status 69
IV.1.7 Overexpression of cytohesins in human lung adenocarcinoma correlates with enhanced EGFR signaling *71*
IV.1.7.1 Cytohesins are overexpressed in human lung adenocarcinoma 71
IV.1.7.2 Cytohesin overexpression correlates with enhanced EGFR signaling in human lung adenocarcinomas 72
IV.2 IDENTIFICATION OF IMPROVED CYTOHESIN ANTAGONISTS IN VITRO 74
IV.2.1 Virtual screening *74*
IV.2.2 Establishment of a GDP/GTP-exchange assay for ARF1 ..... *74*
IV.2.3 Screening of second generation SecinH3 chemotypes *76*
IV.2.4 Structure-activity-relationship studies for Secin16 ..... *77*
IV.2.5 Screening of third generation SecinH3 chemotypes *80*
IV.3 EVALUATIONS OF 3RD GENERATION SECINH3 CHEMOTYPES IN HUMAN GLIOBLASTOMA CELL LINES . 82
IV.3.1 Third generation Secins are potent inhibitors of glioblastoma cell proliferation *82*
IV.3.2 GDP/GTP- exchange assay versus glioma cell proliferation *86*
IV.3.3 Third generation SecinH3 chemotypes induce distinct phenotypes in glioblastoma cells *88*
IV.3.4 Compounds A11, C1 and C10 induce apoptosis selectively in EGFRvIII expressing glioblastoma cells *90*
IV.3.5 Effect of compounds A11, C1 and C10 on EGFR phosphorylation *91*
IV.3.6 Compounds A11, C1 and C10 influence repair of DNA double strand breaks in glioblastoma cells *91*
IV.3.7 EGFRvIII expressing glioblastoma cell lines show an increase in ARF6 expression *94*
IV.4 A NEW REAL-TIME FRET-BASED ASSAY TO MONITOR GDP/GTP EXCHANGE ON NΔ17ARF1 96
IV.4.1 Recent approaches *96*
IV.4.2 A new FRET-based assay for the cytohesin catalyzed GDP/GTP exchange on NΔ17ARF1 ..... *98*
IV.4.2.1 Proof of principle I: The FRET signal depends on the concentration of YPET-GGA3 98
IV.4.2.2 Proof of principle II: The FRET signal depends on the amount of Δ17ARF-CyPET-GTP 100
IV.4.2.3 Proof of principle III: The FRET-based assay is suitable for screening 101
V DISCUSSION 102
V.1 CYTOHESINS ARE CYTOPLASMIC ERBB RECEPTOR ACTIVATORS 102
V.1.1 Inhibition of cytohesins reduces ErbB receptor signaling *102*
V.1.2 Cytohesins enhance ErbB receptor activation independently of their GEF activity *103*
V.1.3 Cytohesins facilitate a conformational rearrangement in the intracellular domains of EGFR dimers *104*

V.2 PATHOPHYSIOLOGICAL RELEVANCE OF CYTOHESINS IN LUNG CANCER 109
V.2.1 Cytohesins are overexpressed in human lung adenocarcinomas 109
V.2.2 Chemical inhibition of cytohesins diminishes proliferation of EGFR dependent lung cancer cell lines 110
V.3 IDENTIFICATION OF IMPROVED CYTOHESIN ANTAGONISTS IN VITRO 112
V.3.1 2nd generation Secin chemotypes 113
V.3.2 Secin16 114
V.3.3 3rd generation Secin chemotypes 115
V.3.4 Further directions 116
V.4 THIRD GENERATION SECINS ARE POTENT INHIBITORS OF GLIOBLASTOMA CELL PROLIFERATION 117
V.4.1 Inhibition of glioblastoma cell proliferation 117
V.4.2 Inhibition of proliferation versus inhibition of GDP/GTP-exchange 118
V.4.3 EGFRvIII selective compounds 120
V.5 CYTOHESINS AS NEW TARGETS IN CANCER THERAPY 123

VI METHODS 126

VI.1 CELL CULTURE 126
VI.1.1 Cell lines 126
VI.1.2 Plasmids 126
VI.1.3 Transfection 128
VI.2 CELLULAR ASSAYS 128
VI.2.1 Protein biochemistry 128
VI.2.1.1 Preperation of cell lysates 128
VI.2.1.2 Immunoprecipitation 129
VI.2.1.3 SDS-PAGE 129
VI.2.1.4 Blotting 131
VI.2.1.5 Immunodetection 132
VI.2.1.6 Crosslinking 133
VI.2.2 Analysis of expression levels 133
VI.2.2.1 RNA purification 133
VI.2.2.2 Reverse Transcription (RT) 134
VI.2.2.3 Quantitative real time PCR 134
VI.2.3 Microscopy 135
VI.2.3.1 Immunofluorescence 135
VI.2.3.2 STED 136
VI.2.3.3 Anisotropy Microscopy 136
VI.2.3.4 FLIM measurements 137
VI.2.4 Proliferation assays 137
VI.2.5 Apoptosis assays 138
VI.2.6 Cell-cycle analysis 139
VI.3 MOUSE EXPERIMENTS 139
VI.3.1 Xenograft models 139
VI.3.1.1 H460 cells 139
VI.3.1.2 PC9 cells 139
VI.3.2 [18F]FLT PET imaging 140

VI.4 ANALYSIS OF HUMAN TUMOR SAMPLES 140
VI.5 CELL-FREE ASSAYS 141
VI.5.1 Proteins *141*
VI.5.2 Fluorescence anisotropy *141*
VI.5.2.1 Labeling of proteins 141
VI.5.2.2 Anisotropy measurements 142
VI.5.2.3 Aggregation of EGFR-ICD 142
VI.5.3 EGFR-ICD autophosphorylation assays *143*
VI.5.4 GDP/GTP-exchange assays *143*
VI.5.4.1 Tryptophan fluorescence 143
VI.5.4.2 FRET 143
VI.6 STATISTICS 146
VI.7 MATERIALS 146
VI.7.1 Instruments *146*
VI.7.2 Materials *147*
VI.7.3 Cell culture reagents *147*
VI.7.4 Standards for DNA- and protein-gels *148*
VI.7.5 Kits *148*
VII LITERATURE 149

I Summary

Signaling by ErbB receptors requires the activation of their cytoplasmic tyrosine kinase domains which is initiated by ligand binding to the receptor ectodomains. Up to now, cytoplasmic factors contributing to the activation of ErbB receptors have been unknown. This thesis introduces members of the cytohesin family of guanine nucleotide exchange factors as the first cytoplasmic ErbB receptor activators.

Chemical inhibition or knock-down of cytohesins decreased ErbB receptor autophosphorylation and signaling whereas cytohesin overexpression stimulated receptor activation. Crosslinking experiments and studies with a constitutively dimerized EGFR construct showed that cytohesins act on already dimerized receptors. Cell-free reconstitution of cytohesin-dependent receptor autophosphorylation as well as monitoring EGFR conformation by fluorescence anisotropy microscopy indicate that cytohesins facilitate conformational rearrangements in the intracellular domains of dimerized receptors. Thus cytohesins may represent an additional layer of regulation of ErbB receptor activation which would allow the cell to modulate the number of activated ligand-bound receptors according to cellular needs.

Consistent with cytohesins playing a prominent role in ErbB receptor signaling, cytohesins were found to be overexpressed in human lung adenocarcinomas. Furthermore, the overexpression correlated with increased activation of the EGF signaling pathway. Inhibition of cytohesins by the cytohesin-specific small-molecule inhibitor SecinH3 resulted in reduced proliferation and induction of apoptosis in EGFR-dependent lung cancer cells in vitro, as well as in tumor xenografts in mice. These findings underline the functional importance of cytohesin-dependent EGFR activation for tumor growth. Furthermore, chemical inhibition of cytohesins led to a strong reduction of glioblastoma cell proliferation.

In order to optimize the inhibitory potential of SecinH3 , new Secin chemotypes were analyzed. In addition, a new assay for the screening of small molecules that interfere with cytohesin-catalyzed guanine nucleotide exchange on ARFs was established.

The work in hand establishes cytohesins as an unprecedented, pathophysiologically relevant class of cytoplasmic conformational ErbB receptor activators and opens up new, entirely unexplored avenues for fighting ErbB receptor-dependent cancers by targeting not the receptors themselves but their activators.

II Introduction

II.1 The ErbB receptor family of receptor tyrosine kinases

II.1.1 Receptor tyrosine kinases (RTKs)

Cells are continuously exposed to diverse extracellular stimuli. The correct interpretation of these signals is of great importance for the cell and the whole organism, in order to achieve the appropriate response. A large group of genes in all eukaryotes encodes for proteins that function as membrane spanning cell surface receptors. By binding of specific ligands they are able to perceive extracellular stimuli and to relay these signals to internal signal transduction pathways, enabling the cell to respond correctly to its environment. One large sub-class of cell surface receptors is characterized by their intrinsic tyrosine kinase activity. These receptor tyrosine kinases (RTKs) catalyze the transfer of the γ phosphate of ATP to hydroxyl groups of tyrosine residues on target proteins.

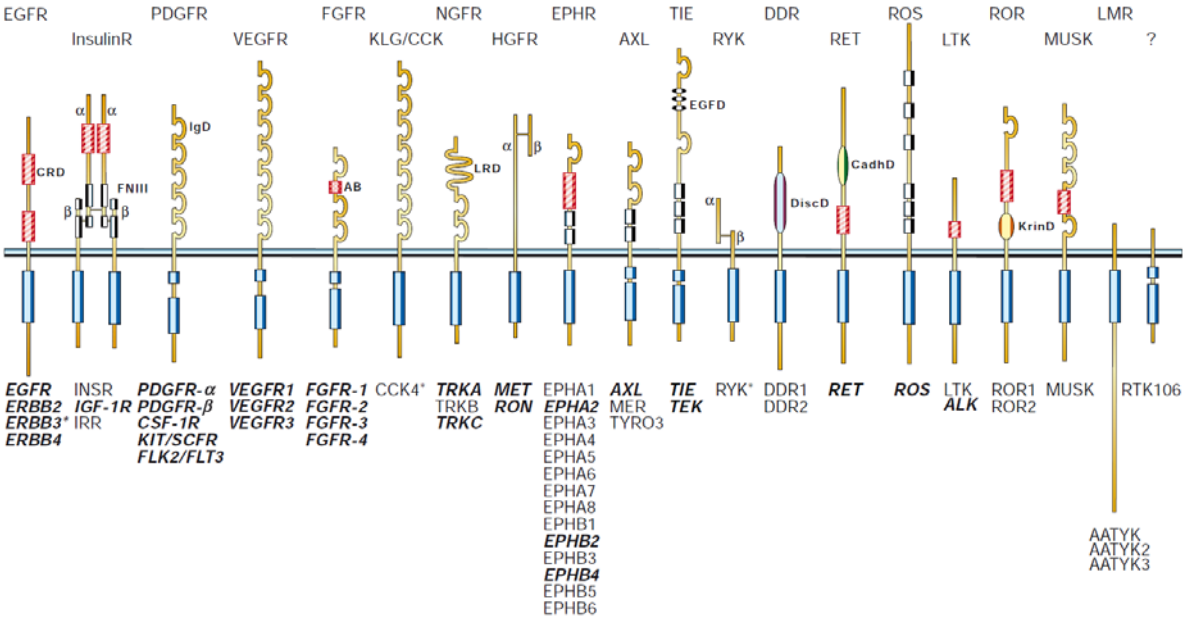

Figure 1 Human receptor tyrosine kinases

The prototypic receptor for each family is indicated above and the known members are listed below. EGFR, epidermal growth factor receptor; InsR, insulin receptor; PDGFR, platelet-derived growth factor receptor; VEGFR; vascular endothelial growth factor receptor; FGFR, fibroblast growth factor receptor; KLG/CCK, colon carcinoma kinase; NGFR, nerve growth factor receptor; HGFR, hepatocyte growth factor receptor, EphR, ephrin receptor; Axl, a Tyro3 PTK; TIE, tyrosine kinase receptor in endothelial cells; RYK, receptor related to tyrosine kinases; DDR, discoidin domain receptor; Ret, rearranged during transfection; ROS, RPTK expressed in some epithelial cell types; LTK, leukocyte tyrosine kinase; ROR, receptor orphan; MuSK, muscle-specific kinase; LMR, Lemur. AB, acidic box; CadhD, cadherin-like domain; CRD, cysteine-rich domain; DiscD, discoidin-like domain; EGFD, epidermal growth factor-like domain; FNIII, fibronectin type III-like domain; IgD, immunoglobulin-like domain; KrinD, kringle-like domain; LRD, leucine-rich domain. The symbols α and β denote distinct RTK subunits. RTK members in bold and italic type are implicated in human malignancies. An asterisk indicates that the member is devoid of intrinsic kinase activity. [1]

Binding of ligands to the extracellular domain of these receptors leads to the activation of the intracellular kinase domain and subsequently to the phosphorylation of various target proteins [2]. Although all human RTKs display the common structure of an usually glycosylated extracellular ligand-binding domain, a single transmembrane-helix and a cytoplasmic domain harboring the tyrosine kinase unit, they can be further grouped into families, based on their primary structures. Figure 1 summarizes the families of human receptor tyrosine kinases.
RTKs are important regulators of fundamental cellular processes like metabolism, proliferation and differentiation. Aberrant signaling of the normally tightly controlled RTKs results in deregulated activity of downstream kinases and is a common feature of malignant transformation [1].

II.1.2 The ErbB family of RTKs

ErbB proteins (named after v-erb-B, a transforming protein of avian erythroblastosis virus [3]) are typical receptor tyrosine kinases that constitute subclass I (EGFR family) of RTKs. They are key regulators of cell differentiation, survival, proliferation and migration. Aberrant ErbB receptor function is a hallmark of many human cancers [4]. The ErbB receptor family is comprised of four known members (Figure 2): epidermal growth factor receptor 1 (EGFR, also referred to as ErbB1), human epidermal growth factor 2 (p185, neu, HER2, ErbB2), HER3 (ErbB3) and HER4 (ErbB4) [5]. They all show the typical structure of RTKs: a glycosylated extracellular ligand binding domain which is connected to an intracellular domain by a single transmembrane helix. The cytoplasmic domain harbors the protein tyrosine kinase core and additional regulatory sequences.

Figure 2 Receptors of the ErbB family of receptor tyrosine kinases and their ligands
All four receptors share high homology in the extracellular domain and the kinase domain. However, HER3 lacks kinase activity. Although there is no known ligand for HER2 (p185), HER2 has been found to be the preferred dimerization partner for the other ErbB family members. Only few examples of possible receptor dimers are shown [6].

Numerous ligands for the ErbB receptor family have been described. With respect to their binding affinities they can be divided into three groups: the first group, consisting of epidermal growth factor (EGF), transforming growth factor α (TGFα) and amphiregulin, shows high specificity for the EGFR; betacellulin, epiregulin and heparin-binding EGF, the second group, bind both EGFR and HER4. The third group, consisting of the neuregulins (NRGs), can be divided into the HER3 and HER4 binding NRG1 and NRG2 on one hand, and the HER4 specific NRG3 and NRG4 on the other hand [7]. With the exception of EGF, ErbB ligands exclusively act over short distances as autocrine or paracrine growth factors. No direct ligand for HER2 has yet been described.

II.1.3 Signaling of ErbB receptors – An Overview

Binding of the ligand to the extracellular domain of ErbB receptors favors receptor dimerization. The ligand-induced conformational change in the receptor ectodomains results in the association of the cytoplasmic tyrosine kinase domains of two receptor molecules, which has been considered to be sufficient for kinase activation. The activated kinase catalyzes the intermolecular autophosphorylation of tyrosine residues in the intracellular domain of an adjacent ErbB receptor molecule which in turn keeps the kinase active. Phosphorylated tyrosine residues in the cytoplasmic domain serve as docking sites for signaling proteins containing SH2 and PTB domains. These signaling proteins get activated by recruitment to the receptor and /or phosphorylation and are responsible for onward transmission of the signal [8]. The downstream signal transduction pathways are determined by the specific set of recruited signaling proteins which reflects the identity of the ligand and the receptor oligomer composition. Although there is no known ligand for HER2, this ErbB receptor can act as a co-receptor and is the preferred heterodimerization partner for all other ErbB family members [9]. HER3 is a distinct member of the EGFR family because its kinase domain lacks certain residues that are known to be essential for catalytic activity in other kinases. That is why HER3 shows only impaired kinase activity [10-11]. Nevertheless, HER3 functions as a signaling entity based on its ability to bind specific ligands and its tyrosine residues that can be transphosphorylated in a heterodimeric complex with another ErbB receptor. In this way HER3 is capable of providing specific docking sites for downstream signaling proteins, despite its impaired kinase activity. This feature makes HER3 an important player in the ErbB signaling. That is why the horizontal network of interactions is crucial for ErbB signaling [12].

II.1.4 Activation of ErbB receptors

Crystallographic data obtained in the past few years have shed new light on the structural basis of receptor activation and have introduced a detailed two-step model of ErbB receptor activation, embodied by receptor dimerization and kinase activation.

II.1.4.1 Ligand-induced dimerization of the extracellular domain

Two models for the induction of receptor dimerization by ligand binding have been proposed. Gullick et al. postulated a ligand-mediated mechanism, in which the bivalency of the ligand mediates receptor dimerization, resulting in an 1:2 ligand:receptor complex [13]. On the other hand, the receptor-mediated mechanism for dimerization, hypothesized by Lemmon et al. [14], requires the binding of two molecules of monomeric ligands to two receptor molecules, resulting in a 2:2 ligand:receptor complex formed by stable intermediates of 1:1 ligand:receptor complexes. Further studies confirmed the receptor-mediated mechanism for ErbB receptor dimerization [15-18]. Burgess et al. showed that binding of EGF to the monomeric EGFR leads to a dramatic conformational change and the exposition of a dimerization arm [19]. The extracellular part of the EGFR consists of four domains (I to IV) and exists in two distinct conformations (Figure 3). In the inactive conformation, the interaction of domains II and IV results in a tethered form of the receptor preventing domains I and III from forming the ligand binding site. This conformation is in equilibrium with a ligand stabilized, open active state of the receptor, in which domains I and III interact to form the ligand-binding pocket. Since domain II is no longer bound to domain IV it can form a dimerization loop for the interaction with the domain II of another EGFR molecule to form a receptor dimer.

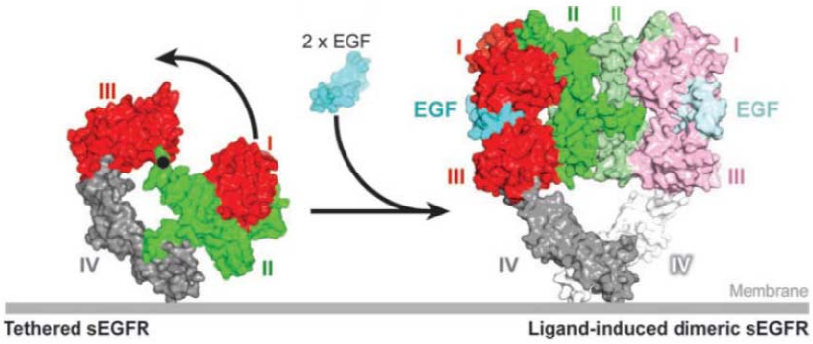

Figure 3 Model of ligand induced dimerization of the extracellular domain of EGFR

A molecular surface model of the extracellular domain of monomeric EGFR in the tethered, inactive form (left part) and EGF stabilized, dimeric, active conformation (right part). Domains I and III are shown in red/pink, domain II in green and domain IV in grey/white [17].

Studies of the structure of HER2 revealed a constitutively exposed dimerization arm, explaining its ability to dimerize with other members of the ErbB family despite the lack of ligand-binding activity [20-21].

II.1.4.2 Activation of the kinase domain

Dimerization of the extracellular domain of EGFRs also leads to the dimerization of the intracellular domains, which was thought to be sufficient for kinase activation [8, 22]. However, recent findings suggest an additional step of receptor activation: the formation of an asymmetric dimer between the intracellular kinase domains, in which one kinase domain (the activator) acts as an allosteric activator of the other (the receiver) kinase [23], similar to the activation mechanism of cyclin-dependent kinases [24]. The asymmetric dimer conformation enables the interaction of the carboxy-terminal lobe of one kinase domain with the amino-terminal lobe of the other, required for the activation of the kinase [23].

In this model, (ligand-independent) dimerization of the intracellular domain leads to the formation of an inactive symmetric kinase dimer, which shows an autoinhibited conformation of the kinase domains. In this conformation a catalytically critical helix of the N-terminal part of the kinase (helix αC) is rotated outward with respect to its conformation in the active state, enabling the centrally located activation loop to be tightly packed inside the active site in a way that blocks substrate binding [23]. Furthermore, parts of the juxtamembrane domain interact with the kinase domain, holding it in the inactive orientation. However, the precise orientation of the kinase domains in these (ligand-independent) preformed dimers is unknown (Figure 4) [25-26].

Upon ligand-binding, the extracellular domains of EGFRs dimerize. The involved conformational changes in the extracellular domain lead to the approaching of the membrane-near segments of the receptors at the junction with the transmembrane segments [19]. Ligand binding relieves the inhibitory association between the juxtamembrane region and the kinase domain, facilitating dimerization between the two juxtamembrane domains that stabilizes the kinase domain dimer (juxtamembrane latch). Furthermore, ligand binding results in the re-orientation of the kinase domains relative to each other, with the carboxy-terminal lobe of one kinase domain facing the amino-terminal lobe of the other, the so called asymmetric dimer (Figure 4). At the same time, helix αC rotates toward the active site, resulting in an open conformation of the activation loop that is compatible with substrate binding [23].

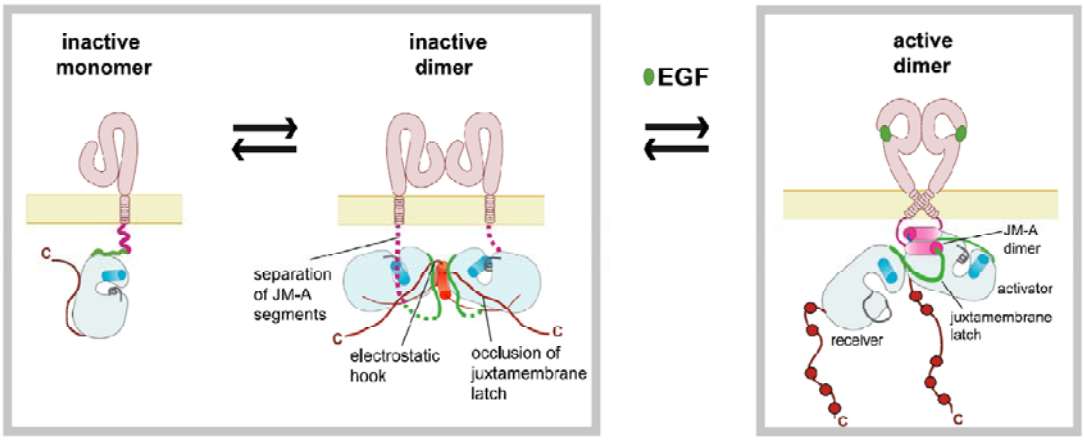

Figure 4 A schematic representation of the activation mechanism of EGFR [25]

Recently, the described model for EGFR activation was extended to HER3 [11, 27], explaining its important role in ErbB receptor heterodimers despite its impaired kinase activity: Sequence comparisons between HER3 and EGFR suggested that although the kinase domain of HER3 cannot be activated it can serve as the activator in asymmetric dimers. The sequences of HER3 in the region spanning the helix αC (favors outward rotation) or the juxtamembrane segment (prevents juxtamembrane latch) are divergent from that of other EGFR family members. In addition residues that are important for docking the activator kinase are missing in HER3. In summary, the (C-lobe) kinase domain of HER3 acts as a constitutively active activator for other members of the ErbB family, although it shows no or only low kinase activity [27].

II.1.4.3 MIG6 – a negative regulator of ErbB receptor activation

The cytoplasmic protein MIG6 (mitogen-induced gene 6, also known as ERRFI1 or RALT) interacts with and is a feedback inhibitor of both EGFR and HER2 [28-29]. Deletion of the MIG6 gene leads to hyper-activation of EGFR and may indicate its role as a tumor-suppressor gene [30-32]. Crystal structures of complexes between EGFR and MIG6 show that a region spanning residues 323-372 of MIG6 is critical for EGFR binding (MIG6-EBR, EGFR binding region). However, only residues 337-361 (denoted as segment1) bind to the distal surface of the C-lobe of the kinase domain and stabilize the inactive, symmetric conformation of the receptor [33-35]. Furthermore, a second segment of MIG6 (residues 362-412, denoted as segment 2) binds to the activation loop of the activated kinase domain. Therefore, MIG6 uses a double-headed mechanism for inhibiting EGFR: first by the blockage of the asymmetric dimer interface and second by directly interacting with the active site of the kinase (Figure 5).

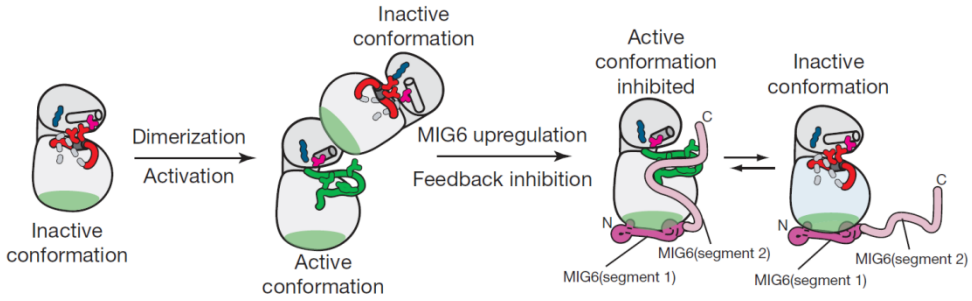

Figure 5 Schematic for EGFR inhibition by MIG6 involving both segment 1 and segment 2 [34]

Recently obtained structural data have revealed an additional mechanism for MIG6 induced EGFR inhibition. A six residue motif in the juxtamembrane latch of EGFR is almost identical in sequence with six residues in MIG6, indicating that part of the function of MIG6 is to prevent formation of the juxtamembrane latch [25].

II.1.5 Downstream signaling of ErbB receptors

Activated ErbB receptors stimulate many intracellular signaling pathways and different ErbB receptors preferentially activate certain signaling pathways, owing to the ability of individual ErbB receptors to bind specific effector proteins (Figure 6).

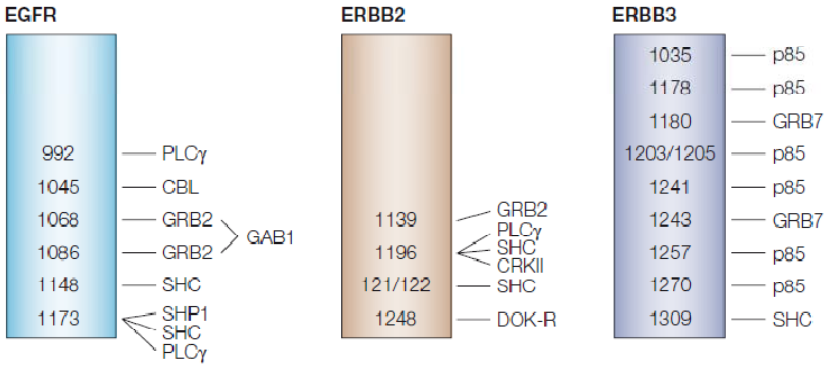

Figure 6 Schematic for the main phosphorylation sites of ErbB receptors and the corresponding adaptor proteins [7]

Two of the main pathways activated by the receptors are the mitogen-activated protein kinase (MAPK) and the phosphatidylinositol 3-kinase (PI3K)–AKT pathway (Figure 7).

The MAPK-pathway is initiated by binding of the adaptor protein Grb2 via its SH2-domain to phosphorylated tyrosine residues in the intracellular domain of the receptor or to the adaptor protein Shc. Grb2 itself recruits the guanine-nucleotide exchange factor Sos via its SH3-domain (binds to prolin-rich sequences): Sos catalyzes the GDP/GTP exchange on the small GTPase Ras, which subsequently binds the serin-threonine-kinase Raf. The following activation cascade involves the mitogen activated protein kinase kinase (MEK) and leads to

the phosphorylation of the extracellular-signal-regulated kinases ERK1 and ERK2 (p44/42), important regulators of cell proliferation, differentiation and apoptosis [36].

PI3-kinases (phosphatidylinositol-3-kinase) are heterodimeric molecules composed of a regulatory (p85) and a catalytic subunit (p110). The regulatory subunit (p85) interacts with phosphorylated tyrosine residues in the intracellular part of ErbB or on the adaptor proteins IRS (insulin receptor substrate 1) or Gab1, thereby recruiting the catalytic subunit (p110) to the membrane. Once both subunits are combined, the PI3-kinase catalyzes the phosphorylation of the inositol ring of the phospholipid phosphatidylinositol (4,5) bisphosphate (PIP2) at position 3 to phosphatidylinositol (3,4,5)-trisphosphate (PIP3). The pleckstrin homology domain of Akt binds directly to PIP3 resulting in the translocation of Akt to the plasma membrane. Likewise, the phosphoinositide-dependent protein kinase 1 (PDK1) is recruited to the plasma membrane upon activation of PI3-kinase. The colocalization of activated PDK1 and Akt allows Akt to become phosphorylated by PDK1 on threonine 308, leading to partial activation of Akt. Full activation of Akt occurs upon phosphorylation of serine 473 by the TORC2 complex of the mTOR protein kinase. The PI3K-Akt signal has been shown to regulate various cellular functions, but is mainly involved in cell proliferation and survival [37].

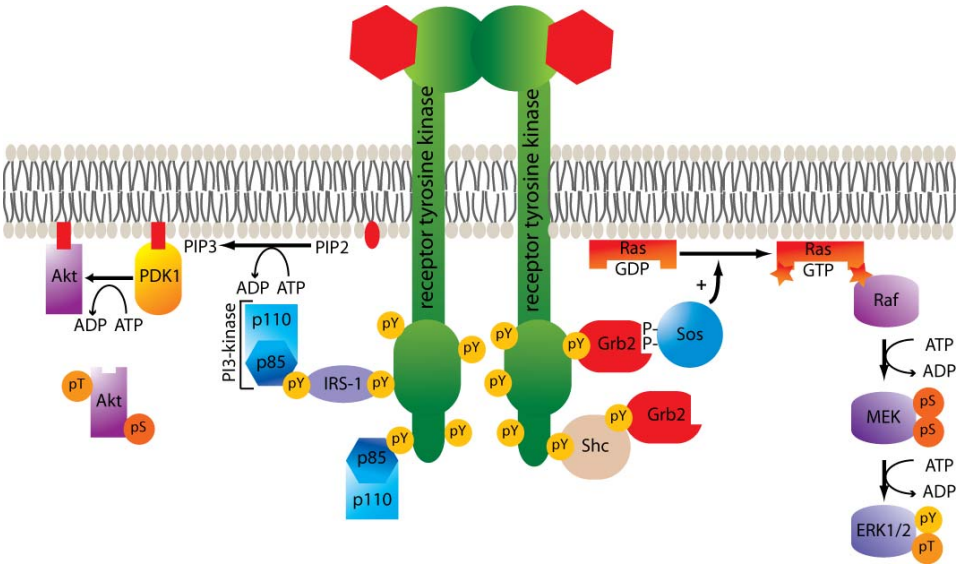

Figure 7 Downstream signaling of ErbB receptors

Other important ErbB receptor signaling effectors are the signal transducer and activator of transcription proteins (STATs) [38], SRC tyrosine kinase [39], and mammalian target of rapamycin (mTOR), a serine/threonine kinase [40].

II.2 ErbB receptors and cancer

Deregulated or autonomous cell growth is the defining feature of all neoplasms. In contrast to benign neoplasms, malignant neoplasms have the capacity to invade normal tissues and metastasize to and grow at distant body sites, the other main defining criterion of cancer. Deregulated cell growth occurs as a result of perturbed signal transduction disturbing the critical balance between the rate of cell-proliferation/growth on one hand and programmed cell death on the other [41]. Receptor tyrosine kinases are important regulators of intracellular signal-transduction pathways, and hence often mutated in cancers. More than half of the known RTKs have been found to be associated with human malignancies [1].

One example is provided by the family of ErbB receptors. In many different cancer cell types, the ErbB receptor pathway becomes hyperactivated by a range of mechanisms, including overproduction of ligands, overexpression of receptors, or constitutive activation of receptors [8]. The ErbB receptors were first implicated in cancer in the early 1980s, when the avian erythroblastosis tumor virus was found to encode an aberrant form of the human EGFR [42-43]. Activated EGFR provides signals that drive dysregulated proliferation, invasion, metastasis, angiogenesis as well as cell survival. Over the past several decades, the role of ErbB receptors in malignant processes has been the content of intensive studies. Today deregulated signaling of ErbB receptors is known to be involved in the initiation and progression of various human cancer types. Thus, the ErbB receptors are attractive candidates for targeted therapy, and, to date, several anti-ErbB monoclonal antibodies and small-molecule tyrosine kinase inhibitors (TKIs) have been developed.

II.2.1 Lung cancer

Lung cancer is one of the leading causes for death, accounting for one third of all cancer-related deaths [44]. Lung cancer can be broadly divided into Small Cell Lung Cancer (SCLC; representing (10–15% of lung cancers, commonly associated with smoking), Non-Small Cell Lung Cancer (NSCLC; representing 85–90% of lung cancers) and carcinoid tumors of the lung (less than 5% of lung cancers). While carcinoid tumors of the lung and SCLC generally respond well to surgery, chemotherapy and/or radiation therapy, NSCLC is largely refractory to these treatments, explaining the short overall survival time of patients with this disease. NSCLC can be further sub-classified into Squamous Cell Carcinoma (30% of NSCLC, often linked to a history of smoking), Adenocarcinoma (50% of NSCLC) and Large Cell Carcinoma (20% of NSCLC) [44].

Among the potential therapeutic targets that could be exploited in the management of lung cancer, the ErbB proteins have emerged as key players. The EGFR was first found to be overexpressed in NSCLC nearly 25 years ago [45], identifying it as a new target for NSCLC therapy. However, more recent studies have shown that EGFR overexpression is found in 60% of NSCLC, but only counts as a weak prognostic marker in NSCLC. On the other hand, overexpression of ErbB2 which is found in 40% of NSCLC correlates with poor overall survival. In addition to the overexpression of ErbB receptor family members, NSCLC often show autocrine expression of three EGFR ligands, namely TGFα, EGF and amphiregulin, leading to sustained activation of the downstream signaling of these receptors [45-46].

Mutations in the intracellular domain of EGFR have been identified as the most common cause of aberrant EGFR activation. Whereas mutations in the extracellular part of the receptor (for example EGFRvIII, see glioblastoma chapter for more details) are rare, 25-40% of NSCLC show mutations in the tyrosine kinase domain of EGFR (Figure 8). These mutations involve exons 18-21 of EGFR and cluster around the ATP binding site of the kinase. Mutations in exon18 (commonly at position G719) count for 5% off all mutations and target the nucleotide binding loop of the receptor. 50% of all mutations are found within exon 19, mostly in frame deletions at position 747-750. Together with mutations in exon 21, these modifications cluster around the helix αC, thereby destabilizing the inactive conformation of the EGFR kinase [23, 47]. Exon 20 harbors 5% off all mutations (for example T790M), which render NSCLC tumors insensitive to EGFR kinase inhibitors. The remaining 40% of all mutations are found in the activation loop of the receptor (exon21, for example L858R, destabilizing the inactive conformation of the EGFR kinase [23]) [48].

Interestingly, with exception of mutations in exon 20, kinase-mutated EGFR proteins expressed in NSCLC are generally more sensitive to tyrosine kinase inhibitors (TKIs) as the wild-type expressing tumors. This phenomenon may be explained by the weakened affinity for ATP of these receptors, as reported by some groups. On the other hand, it appears that tumor cells harboring oncogenic EGFR alleles acquire dependency on the survival signals transduced by the hyperactivated EGFR, such that inhibition of these signals leads to rapid cell death of the tumor cells. However, the precise mechanism underlying increased TKI sensitivity of these tumors has yet to be established [49].

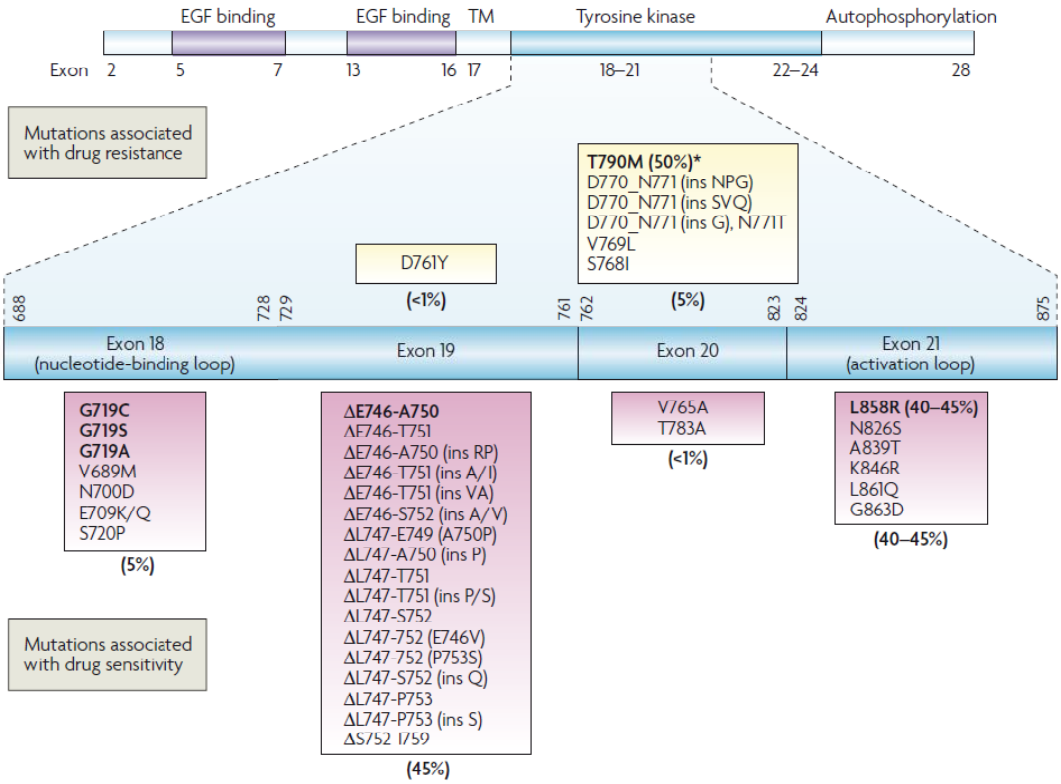

Figure 8 EGFR mutations in lung cancer
Schematic illustrating the EGFR and the relevant mutations located in the in Exons 18-21 (regions expanded). A detailed list of EGFR mutations located in these exons that are associated with sensitivity (magenta boxes) or resistance (yellow boxes) to gefitinib or erlotinib is shown. The main mutations in each class are shown in bold type. TM: transmembrane domain.[46]

Based on the structure and function of EGFR, two therapeutic strategies have been developed (Figure 9) [50]. The first uses humanized monoclonal antibodies (mAbs) generated against the receptor's ligand-binding extracellular domain. These mAbs block binding of receptor-activating ligands, and, in some cases, can induce receptor endocytosis and downregulation. The second approach uses small molecules (TKI, tyrosine kinase inhibitors) that compete with adenosine triphosphate for binding to the receptor's kinase pocket, thereby blocking receptor activation and the transduction of downstream signals.

However, the acquisition of resistance to EGFR TKIs in NSCLC therapy remains an important limitation to the utility of such treatments [51]. Two molecular mechanisms for TKI resistance have been postulated. The first mechanism involves the acquisition of secondary mutations within the EGFR catalytic domain. One mutation T790M, also referred to as gate-keeper mutation, restores the ATP affinity of the catalytic domain which accounts for the reduced susceptibility to TKIs, is found in 50% in all cases of acquired resistance. The second mechanism of acquired EGFR TKI resistance in NSCLC is based on the amplification of the gene encoding for the MET receptor kinase. MET transduces signals to similar set of

effectors as EGFR and it appears that it restores EGFR signaling by providing redundant survival signals [49, 52].

Drug name	Class of action	Target	Stage of development (completed)
Cetuximab	Chimeric MAB	EGFR	Phase III
Panitumumab	Humanized MAB	EGFR	Phase I/II
Matuzumab	Humanized MAB	EGFR	Phase I
Nimotuzumab	Humanized MAB	EGFR	Phase I
Trastuzumab	Humanized MAB	HER2	Phase II
Pertuzumab	Humanized MAB	HER2	Phase II
Erlotinib	Reversible TKI	EGFR	In clinical use
Gefitinib	Reversible TKI	EGFR	In clinical use
EKB-569	Irreversible TKI	EGFR	Phase I
CL-3877785	Irreversible TKI	EGFR	Preclinical
HKI-272	Irreversible TKI	EGFR, HER2	Phase I
BIBW-2992	Irreversible TKI	EGFR, HER2	Phase I
PKI-166	TKI	EGFR, HER2	Phase I
Lapatinib	Reversible TKI	EGFR, HER2	Phase II
CI-1033	Irreversible TKI	EGFR, HER2, HER4	Phase II
PF-00299804	Irreversible TKI	EGFR, HER2, HER4	Phase I
Vandetanib	TKI	EGFR, VEGF, RET	Phase II
XL647	Reversible TKI	EGFR, HER2, EphB4, VEGF	Phase II
AEE788	TKI	EGFR, HER2, VEGF	Phase I
EGF Cancer Vaccine	Vaccine	EGFR	Phase I/II

EGF, epidermal growth factor; EGFR, epidermal growth factor receptor; MAB, monoclonal antibody; TKI, tyrosine kinase inhibitor.

Figure 9 EGFR inhibitors in development and in practice [50]

Taken together, ErbB receptor signaling plays a major role in NSCLC, but, although it represents a promising target for cancer therapy, new approaches are needed to circumvent acquired TKI resistance.

II.2.2 Breast cancer

Breast cancer is the most common malignancy in women, accounting for 32% of all female cancers and is responsible for 15% of cancer deaths in women, making it the number-two cause of cancer death. Breast cancer can be classified based on its origin in the ducts or lobules. Approximately 80% of all breast cancers are described as infiltrating ductal carcinoma (IDC), 15% as medullary carcinoma (MC), 5% as infiltrating lobular carcinoma (ILC). In addition, breast cancer is categorized by the expression level of the surface receptors for estrogen and progesterone and the human epidermal growth factor receptor 2 (HER2) [53]. The first frontier in the treatment of breast cancer is surgery, followed by radiation therapy. Patients with estrogen receptor positive tumors will typically also receive hormone therapy. Typical hormonal treatments include Tamoxifen (antagonist of the estrogen receptor), aromatase inhibitors or GnRH (Gonadotropin-releasing hormone)-analogues [53].

The HER2 gene is amplified and overexpressed in about 25% of breast cancers, conferring a more aggressive biology [54] and it makes a compelling case that HER2 plays a dominant role in causing and maintaining the transformed phenotype. The association between HER2 overexpression and a poor prognosis is supported by the significantly shorter overall survival

rate and time to relapse in patients with HER2-overexpressing breast cancer relative to patients with tumors without HER2 overexpression [54-55].

The apparent dependency of HER2-overexpressing tumors on constitutive HER2 function has made HER2 an attractive target for anti-cancer drug development (Figure 9). Two drugs are currently FDA-approved for treatment of HER2-positive cancers. Trastuzumab (Herceptin) is a humanized monoclonal antibody that recognizes the external domain of HER2 [56]. Its mechanism of action is still not totally clear, but it seems to have its greatest effects in tumors with increased HER2 homodimers. Although it does not block autophosphorylation of HER2, it does inhibit HER2 downstream signaling [57]. Lapatinib (GW572016, Tykerb) is a dual tyrosine kinase inhibitor targeting EGFR and HER2, binding to the ATP-binding pocket with the consequence of blocking the downstream signaling pathways from these receptors [58-59]. In addition, Pertuzumab (2C4, Omnitarg) [60], a monoclonal antibody directed against extracellular domain II of HER2, sterically blocking dimerization of HER2 with EGFR and HER3, has entered clinical testing for the treatment of breast cancer. However first clinical trials have shown only limited activity [61].

Despite these new therapeutic possibilities the problem of acquired resistance has still to be conquered. Mutations in the PTEN gene are found in 50% of patients with breast cancer and have been shown to be associated with resistance and poorer prognosis. In addition, mutations in the extracellular domain of HER2 prevent trastuzumab from binding to the domain, resulting in trastuzumab resistance. Also, increased signaling form other receptors activating the MAPK- or PI3K-pathway are known to render cells resistant to HER2 targeted therapy. Although the discovery of trastuzumab and lapatinib represents a real breakthrough in treating HER2 positive breast cancer, each has only a response rate around 30% as single agent in first-line treatment of HER2 positive breast cancer, meaning that around 70% of patients will not derive any benefit from treatment with either agent [62-63].

II.2.3 Glioblastoma

Gliomas (glia cells = supporting cells of the nervous system including oligodendrocytes, astrocytes and Schwann cells) are the most common subtype of primary (a subtype which arises *de novo*) brain tumors and are responsible for about 2% off all deaths from cancer. Gliomas are classified according to their line of differentiation and are afterward graded according to their malignancy. Glioblastomas are the most frequent form of gliomas and represent grade IV astrocytomas. As all grade IV tumors glioblastomas are highly malignant, usually resistant to chemotherapy and infiltrate throughout the brain. This invasive nature

results in the inability of surgery and the very short median survival of 9-12 month of glioblastoma patients [64]. The epidermal growth factor receptor (EGFR) is a primary contributor to glioblastoma initiation and progression. EGFR amplification and overexpression is the most common genetic alteration in primary glioblastoma with a frequency of 40-70%, but is not observed in lower grade astrocytomas. Of the glioblastoma that overexpress EGFR ~75% are also found to have mutations in the EGFR gene, ranging from point mutations or deletions in the extracellular domain to deletions in the cytoplasmic part of the receptor [65-66]. A number of mutations in the extracellular domain of the EGFR are exclusively found in glioblastoma. They reside primarily at the interfaces of extracellular domain I/II or II/IV and are thought to prevent tethering of domain II and IV and therefore keep the receptor in an active conformation. The most abundant mutation, which is found in approximately 50-60% of glioblastoma that overexpress the EGFR but not in normal tissue, is the EGFR variant III (EGFRvIII). This mutant lacks domains I and II of the extracellular part of the EGFR as a result of the deletion of exons 2 to 7 of the EGFR gene. Although EGFRvIII is incapable of ligand binding it is constitutively tyrosine phosphorylated, even though to a lesser extent than the ligand-stimulated EGFR [67]. Loss of the domain II is thought to prevent the formation of the closed inactive conformation, favoring a shift in the equilibrium to the open active conformation of the receptor. Additionally the signaling potency of EGFRvIII is increased by its constitutive localization at the plasma membrane due to impaired endocytosis and degradation of the receptor [68]. EGFRvIII also influences signaling of the wild type receptor, as it can signal through EGFRvIII homodimers or through heterodimers with either EGFR or ErbB2. The glioblastoma cell line U87 stably transfected with EGFRvIII (U87 EGFRvIII) shows a significant growth advantage compared to the parental cell line (which expresses only wt EGFR) when grown as tumour xenografts and in vitro under serum starvation conditions [66]. The growth advantage is thought to result from an elevated proliferation rate coupled with a reduction in apoptosis. Although EGFRvIII is phosphorylated on the same tyrosine residues as the wild-type receptor, signaling in response to EGFRvIII is distinct from that in response to activation of the wild-type receptor. PI3K signaling is the dominant signaling pathway activated as a result of EGFRvIII expression. Upregulation of PI3K activity activates Akt-mTOR signaling which decreases the abundance of the cyclin-dependent kinase inhibitor p27 and consequently inhibits G1 arrest under conditions of serum starvation. Amplification of EGFRvIII also leads to activation of the Ras-Raf-MEK pathway but does not result in high phosphorylation of extracellular signal regulated kinase 1 and 2 (Erk1/2). Similarly, unlike wild-type EGFR, EGFRvIII does not appear to activate the STAT3 pathway. The reduced apoptotic rate of EGFRvIII expressing

cells is due to an increase in apoptosis inhibitor Bcl-X_L expression [65-66]. Nevertheless, forced expression of EGFRvIII alone was insufficient to form high-grade tumors in mouse models, which implies that although EGFRvIII is an important driver of transformation in primary glioblastoma, its transformation activity requires additional genetic aberrations [69].
The invasive nature and high malignancy of glioblastomas together with the resistance to classical chemo- and radiotherapy contribute to the very poor prognosis of glioblastoma patients. The high prevalence of EGFRvIII in glioblastomas and the lack of expression in normal tissue make it a very attractive therapeutic target. The absence of domains I and II give rise to a tumor specific epitope in EGFRvIII, against which monoclonal antibodies have been generated. The EGFRvIII-specific monoclonal antibody Y10 showed a high potency to inhibit the growth of subcutaneous glioblastoma xenografts but not of orthotopic tumors, due to its inability to cross the blood-brain barrier [70]. MAb806, another EGFRvIII-targeting monoclonal antibody, which was able to cross the blood brain barrier, led to tumor shrinkage in both, subcutaneous and orthotopic tumor models and is currently under investigation for clinical use [71]. Several EGFR specific tyrosine kinase inhibitors (TKI) have also been evaluated for their efficacy against gliomas but they appear relatively ineffective for tumors expressing EGFRvIII, although the EGFR specific TKI AG1478 showed an additive effect on tumor size shrinkage if combined with classical chemotherapeutics like temozolomide or cisplatin [72]. More recently, another novel small molecule inhibitor was reported to show a slightly selective inhibitory effect on the growth of several glioma cells expressing EGFRvIII compared to matched glioma cells negative for EGFRvIII [73]. However the target or mechanism of action for this small molecule is still unknown.

II.3 Cytohesins and ARF-GTPases

II.3.1 Adenosine diphosphate ribosylation factors (ARFs)

Adenosine diphosphate ribosylation factors (ARFs) are small guanine nucleotide-binding proteins and belong to the Ras superfamily. Like all small GTPases, these proteins act as molecular switches that cycle between two conformations: the active guanosine triphosphate (GTP)-bound conformation and the inactive guanosine diphosphate (GDP)-bound state. They are controlled, on one hand, by factors that lead to the dissociation of GDP and the binding of GTP, the GEFs (guanine nucleotide exchange factors), and on the other hand by proteins that stimulate the intrinsic GTP hydrolase activity (GAPs, GTPase-activating proteins).

Guanine nucleotide exchange factors (GEFs) catalyze the dissociation of the nucleotide from the G protein by modifying the nucleotide-binding site in such a way, that the nucleotide affinity is decreased, which results in the release of the nucleotide. Since G proteins show a nanomolar to picomolar affinity for GDP and GTP, the GEF is subsequently replaced by a new nucleotide. Cytohesins, a class of ARF GEFs (see next chapter), bind to the binary complex between ARF and GDP, in which the GDP is sandwiched between two loops called switch 1 and switch 2 (residues 38–52 and 69–84 in ARF1), which are connected by an interswitch region comprising two ß-strands. Switch regions 1 and 2 interact with the phosphates of GDP and a coordinating magnesium ion, thereby stabilizing the GDP bound conformation of ARF. In the cytosolic full-length form of ARF-GDP the myristoylated amphipathic amino-terminal helix locks the interswitch in a retracted conformation that blocks nucleotide exchange. Its reversible binding to membrane releases the hasp and opens up the locked conformation of the interswitch to enable nucleotide exchange [74-76]. Binding of cytohesin displaces switch 1 to open up the nucleotide binding site and GDP is subsequently kicked out of the transiently formed ternary complex between cytohesin, ARF and GDP [77-78]. The detailed function of cytohesins in these mechanisms was described by Beraud-Dufour et al. [79]: A glutamic acid finger of the cytohesin Sec7 domain approaches the negatively charged phosphate of GDP and displaces the coordinated magnesium ion thereby perturbing the interaction surface in the phosphate-binding region, which leads to nucleotide release. In the course of the exchange reaction a new nucleotide displaces the GEF, since the nucleotide weakens the affinity of the G protein for the GEF. The affinity of G proteins for GDP or GTP is similar, that is why the ratio of concentration between GDP and GTP determines the exchange. Thus the resulting increase in GTP-bound over GDP-bound ARF in cells is due to the approximately ten times higher cellular concentration of GTP compared to GDP [77].

ARF proteins control essential cellular functions including cytoskeletal dynamics, cell migration or vesicular trafficking [80]. There are six mammalian ARF proteins which can be categorized into three classes, based on amino-acid sequence identity. Class I ARF proteins (ARF1, ARF2 and ARF3) are involved in coat complex formation along the secretory pathway in ER and Golgi. The functions of the class II ARF proteins (ARF4 and ARF5) are still unclear, however, some studies have indicated that ARF5 might have a role in early Golgi transport. ARF6, which is the sole member of class III, is thought to regulate endosomal membrane traffic and structural organization at the cell surface [81-82].

II.3.2 The cytohesin family of ARF-GEFs

Cytohesins are guanine nucleotide exchange factors (GEFs) for ARFs. There are four known human cytohesins: cytohesin-1 [83], cytohesin-2 (ARNO) [84], cytohesin-3 (Grp1) [85] and cytohesin-4 [86]. They are proteins of approximately 47 kDa which share a conserved domain structure: the amino-terminal coiled-coil domain, which is used for interaction with cellular-binding partners, the central Sec7 domain, which contains the GEF function, and the carboxy-terminal pleckstrin homology (PH) domain, which can bind to inositol phospholipids and therefore regulate the protein's membrane association.

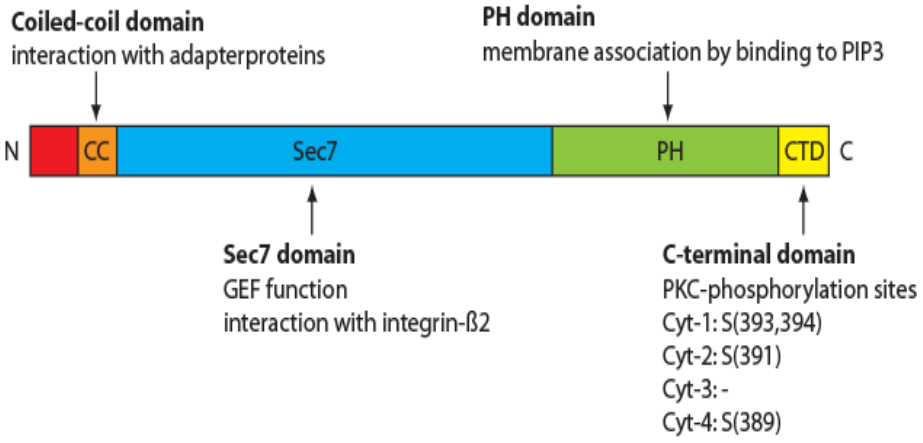

Figure 10 Domain structure of cytohesins

Cytohesins have been shown to be involved in signal transduction in vertebrates and invertebrates. Kolanus et al. identified cytohesin-1 as a regulator of integrin β binding to ICAM-1 in immune cells. Interestingly, this effect is independent of the GEF activity of cytohesin-1 [87]. Kliche et al. have shown, that cytohesin-1 binds to the transmembrane protein kaposin A, which is known for its transforming potential in tumor cells by selective activation of the mitogen-associated protein (MAP)-signaling pathway [88]. Our group developed an aptamer that specifically binds to cytohesin-2, without disturbing the GEF activity toward ARF1. Transfected into HeLa cells this aptamer abrogated MAP-signaling and reporter gene transcription directed by serum response elements [89]. However, our discovery of the small molecule inhibitor of cytohesins (SecinH3) has opened up new possibilities to directly target cytohesins and to shed new light into their function [90].

II.3.3 The small molecule SecinH3

Until very recently, only one small molecule inhibitor of GDP/GTP exchange on ARF was available, the fungal macrolide Brefeldin A, which binds to Sec7 domains of large GEFs, but shows no inhibitory effect on small GEFs like the cytohesins [91]. By a similar mechanism, the small molecule LM11 targets the complexes of ARF1-GDP with the large GEF BIG1 as well as with BFA-insensitive ARNO (cytohesin-2). Both molecules have been shown to inhibit ARF-regulated traffic at the Golgi apparatus in cells [92].

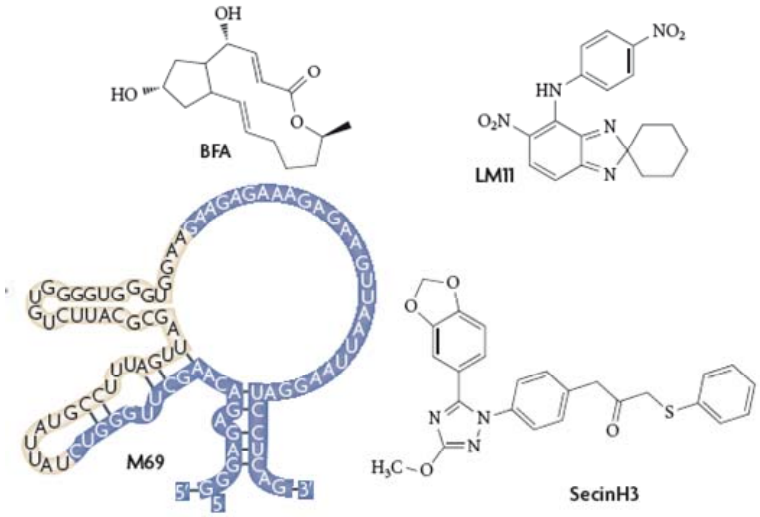

Figure 11 Known GEF inhibitors

Brefeldin A (BFA) binds to the complex between large GEFs an ARF, whereas LM11 targets the complex between ARF1 and BIG1 or ARNO. The RNA aptamer M69 binds selectively to the cytohesin family of small GEFs and inhibits its GEF activity. SecinH3 is the first known small molecule inhibitor that specifically targets small GEFs. Modified from [93].

A novel Sec7 inhibitor for cytohesins has been recently identified by our group in an aptamer displacement screen using the cytohesin specific aptamer M69 [90, 94-95]. The small organic compound SecinH3 specifically inhibits GDP/GTP exchange catalyzed by the human cytohesins 1-3 and by the Drosophila melanogaster cytohesin homolog Steppke [90], while showing only weak affinity to large GEFs. Various studies have proven the potential of SecinH3 (**Sec**7-**in**hibitor H3) as an indirect inhibitor of ARF1 and ARF6 [90, 96-101].

With the help of this new tool the involvement of cytohesins in insulin signaling was demonstrated. SecinH3 blocks the transcription of insulin-dependent genes in human HepG2 cells and in murine liver cells in vivo most likely by inhibiting the binding of adapter molecules like IRS-1 (insulin receptor substrate 1) to the activated insulin receptor (Figure 12) [90].

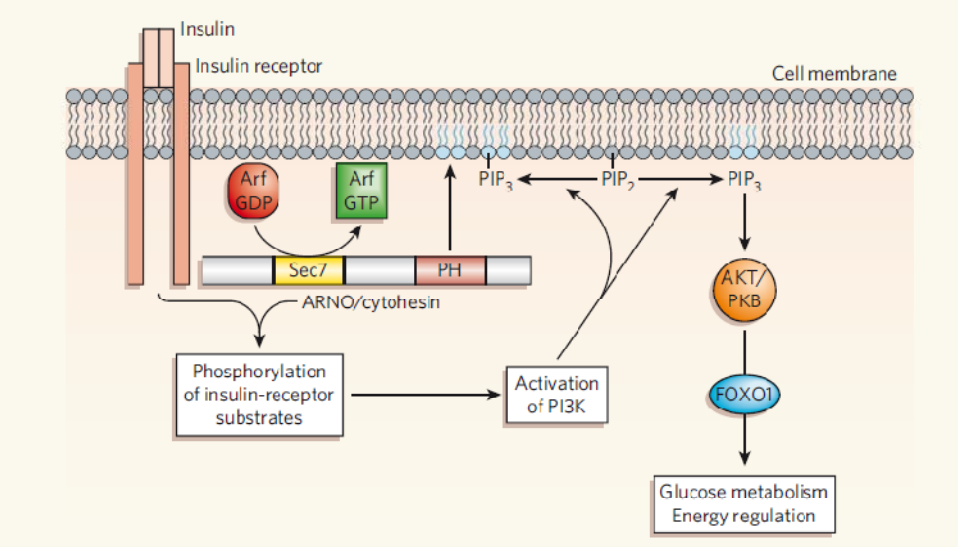

Figure 12 Function of cytohesin in insulin signaling

Cytohesins bind to the insulin-receptor and facilitate the binding and phosphorylation of further substrates of the receptor in an ARF-dependent mechanism.

In parallel Fuss et al. described a Drosophila mutant in which expression of the only cytohesin homolog Steppke is strongly reduced [102]. These flies show a significantly smaller size and a drastic weight reduction of the larvae as compared with wild-type larvae. Biochemical studies revealed that PI3K signaling induced by the insulin receptor was strongly reduced in the Steppke mutants. Feeding wildtype larvae with SecinH3 led to the same phenotype as seen for the Steppke mutants, indicating that a cytohesin ARF-GEF is essential in an important and conserved signaling pathway as the insulin pathway. The modulation of insulin signaling describes a new ARF-dependent function of cytohesins. Recently these findings where substantiated by an additional study of Lim et al. showing that cytohesins interact with the Connector Enhancer of KSR1 (CNK1), thereby promoting insulin receptor signaling [96].

III Objectives

Cytohesins have been shown to be involved in insulin receptor signaling [90]. Preliminary data, obtained in my diploma thesis, suggests a further involvement of cytohesins in ErbB receptor signaling.

From this background, the aim of this thesis was to dissect the mechanism of cytohesin mediated ErbB receptor activation.

As a first step towards this goal, the involvement of cyohesin in ErbB receptor signaling had to be confirmed. After establishing an appropiate cell culture system, the effect of cytohesin inhibition or overexpression had to be evaluated.

In a second step, the underlying mechanism of cytohesin mediated ErbB receptor activation had to be dissected with respect to the direct impact of cytohesins on receptor trafficking, dimerization or on the conformation of the receptor. For this purpose, appropriate test systems to analyze the indicated steps of ErbB receptor activation had to be established.

Furthermore, additional questions about the mechanism of cytohesin mediated ErbB receptor activation had to be answered: Do cytohesins directly bind to and activate the EGFR? Which domain of cytohesins is responsible for this effect? Is the GEF-activity of cytohesins required?

As a further objective, a potential pathophysiological relevance of cytohesins in EGFR-dependent human cancers were to be elucidated, and the impact of cytohesin inhibition on these cancers were to be evaluated.

Another part of this thesis was focused on the optimization of the small molecule inhibitor specific for cytohesins, SecinH3 [90]. New Secin chemotypes obtained in structure activity relationship studies and virtual screening approaches had to be characterized in vitro and in cell culture for their potential to interfere with cytohesin mediated functions.

IV Results

IV.1 Cytohesins are cytoplasmic ErbB receptor activators

IV.1.1 Inhibition of cytohesins decreases ErbB receptor signaling

IV.1.1.1 Chemical inhibition of cytohesins reduces EGFR phosphorylation and signaling

It has recently been shown that cytohesins are important regulators of insulin signaling [90]. To investigate whether cytohesins are also involved in EGFR signaling, I tested the effect of the cytohesin antagonist SecinH3 on the activation of the EGFR.

I used a human lung adenocarcinoma-derived cell line, named H460, which expresses normal levels of wild-type EGFR [103]. Before stimulation with 50ng/ml EGF for 5min, the cells were starved overnight (basal medium without fetal bovine serum) in the presence of 15µM SecinH3 or solvent (0.4% DMSO). Cell lysates were analyzed by SDS-PAGE and western blotting. Phosphorylation of the indicated proteins was determined by immunodetection using the indicated (phosphospecific) antibodies. Heat shock cognate protein 70 (Hsc70) served as loading control.

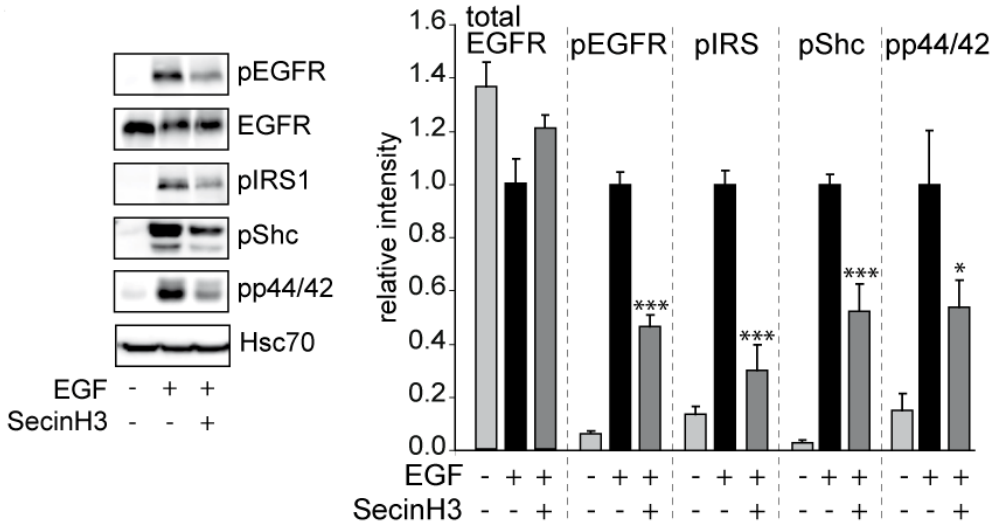

Figure 13 Chemical inhibition of cytohesins inhibits EGFR signaling

Western blot analysis of H460 cells treated with SecinH3 or solvent and stimulated with EGF. Phosphorylation of the indicated proteins was determined by immunodetection using phosphospecific antibodies (pEGFR_Y1086, pIRS_Y612, pAkt_T308, pShc_Y239/240, pp44/42_T202/Y204). Heat shock cognate protein 70 (Hsc70) served as loading control. The diagrams show relative phosphorylation levels after normalization for Hsc70 with the untreated ligand-stimulated cells set as 1 (n=6). Data represented as mean ± SEM, *: $p<0.05$ ***: $p<0.001$.

SecinH3 treated cells showed an about 50% inhibition of EGFR activation, using autophosphorylation as readout (Figure 13). The inhibitory effect was also found on the levels

of the adaptor proteins IRS1 and Shc and of the downstream kinases p44/p42 (Erk1/Erk2). XH1009, a control compound which is structurally related to SecinH3 but does neither bind nor inhibit cytohesins, had no effect on EGFR activation and signaling (Figure 14).

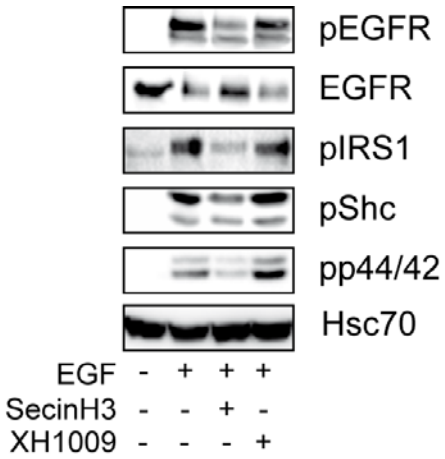

Figure 14 Secinh3 but not XH1009 inhibits EGFR signaling

Representative western blot analysis of H460 cells treated with the control compound XH1009, SecinH3 or solvent and stimulated with EGF. Phosphorylation of the indicated proteins was determined by immunodetection using phosphospecific antibodies (pEGFR_Y1086, pIRS_Y612, pAkt_T308, pShc_Y239/240, pp44/42_T202/Y204). Heat shock cognate protein 70 (Hsc70) served as loading control.

To obtain SecinH3-independent evidence, the cytohesin-specific aptamer M69 or cytohesin-specific siRNAs were used. Inhibition of EGFR activation was observed in both experiments (data not shown, experiments done by Jin-Na Song [104]).

These results show an involvement of cytohesins in EGFR signaling.

IV.1.1.2 Chemical inhibition of cytohesins reduces HER3 phosphorylation and signaling

In order to examine whether cytohesins also affect the signaling of other ErbB receptors, a HER2/HER3 expressing human breast adenocarcinoma derived cell line (SkBr3 cells) was used [105]. SkBr3 cells were starved overnight (basal medium without fetal bovine serum) in the presence of 15μM SecinH3 or solvent (0.4% DMSO) and stimulated with the HER3-ligand heregulin (HRG, 5min, 25ng/ml) in order to induce formation of HER2/HER3 heterodimers. Cell lysates were analyzed by SDS-PAGE and western blotting. Phosphorylation levels were analyzed as described.

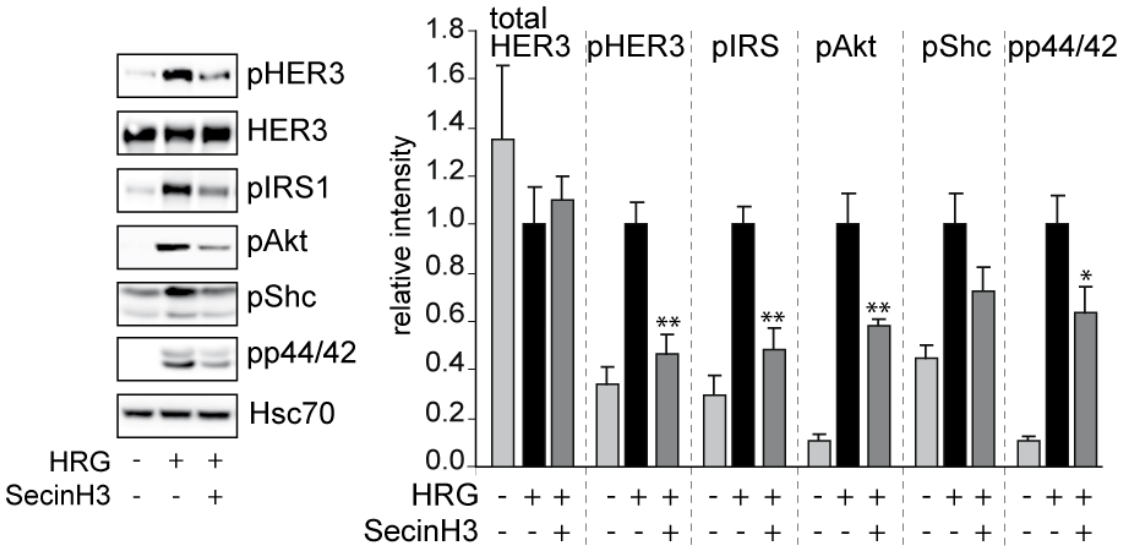

Figure 15 Chemical inhibition of cytohesins inhibits HER3 signaling

Western blot analysis of SkBr3 cells treated with SecinH3 or solvent and stimulated with heregulin (HRG). Phosphorylation of the indicated proteins was determined by immunodetection using phosphospecific antibodies (pHER3_Y1289, pIRS_Y612, pAkt_T308, pShc_Y239/240, pp44/42_T202/Y204). Heat shock cognate protein 70 (Hsc70) served as loading control. The diagrams show relative phosphorylation levels after normalization for Hsc70 with the untreated ligand-stimulated cells set as 1 (n=6). Data represented as mean ±SEM, *: $p<0.05$ ***: $p<0.001$.

Again, SecinH3 reduced the phosphorylation of HER3 by about 50%, which was also reflected in reduced activation of the adaptor protein IRS1 and the downstream kinases Akt and p44/p42 (Figure 15). The control compound XH1009 had no inhibitory effect (data not shown [104]). Once more the involvement of cytohesins in the activation of HER3 was confirmed by the aptamer M69 and by cytohesin specific siRNAs (data not shown, experiments done by Jin-Na Song [104]).

Taken together, these results imply that cytohesins are involved in the regulation of ErbB receptor signaling.

IV.1.2 Cytohesins enhance ErbB receptor activation

IV.1.2.1 Overexpression of the cytohesin ARNO enhances both EGFR and HER3 phosphorylation

Having shown that cytohesin inhibition reduces ErbB signaling one might ask whether overexpression of cytohesins leads to an enhancement of ErbB receptor activation. To examine this question, I transfected H460 and SkBr3 cells with increasing amounts of FLAG-tagged wild-type ARNO or empty vector for 48h. All cells were transfected with equal total amounts of plasmid, i.e. empty vector was added to fill in. Before harvesting, cells were starved overnight in the absence of FBS and were stimulated with EGF or HRG, respectively.

Receptor activation was analyzed as previously described. I selected ARNO for this analysis since it showed the highest expression in both cell types (determined by quantitative PCR, data not shown).

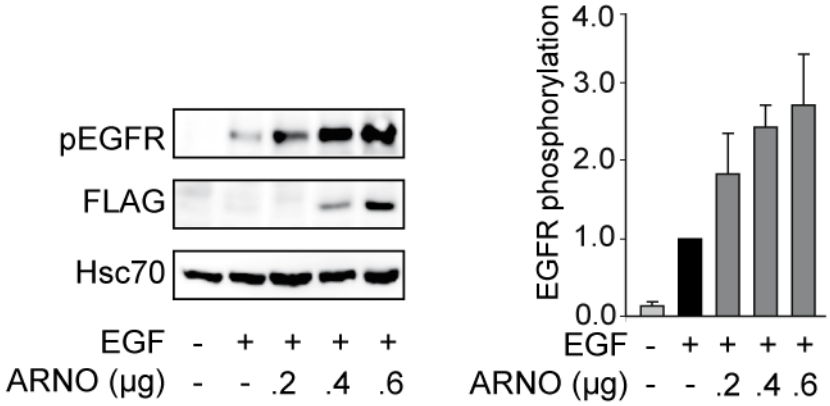

Figure 16 Overexpression of the cytohesin ARNO enhances EGFR autophosphorylation

H460 cells were transfected with the indicated amounts of FLAG-tagged ARNO and were stimulated with EGF. Receptor autophosphorylation was analyzed as above and transfected ARNO was detected with an anti-FLAG antibody (n=3). The diagram shows relative phosphorylation levels (pEGFR_Y1086) after normalization for Hsc70. The phosphorylation level of empty-vector transfected, ligand-stimulated cells was set as 1. Data represented as mean ±SEM.

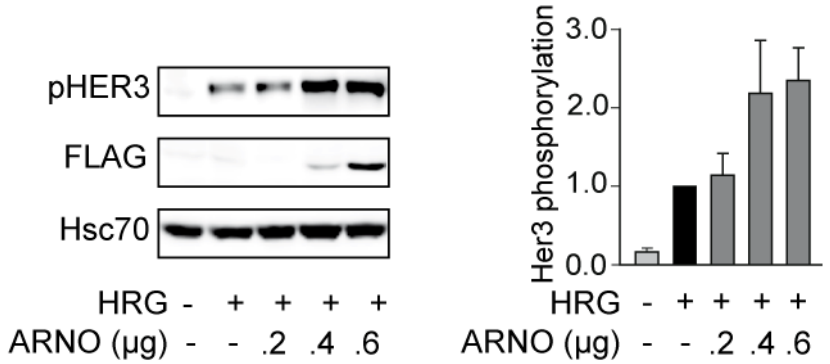

Figure 17 Overexpression of the cytohesin ARNO enhances HER3 phosphorylation

SkBr3 cells were transfected with the indicated increasing amounts of FLAG-tagged ARNO and were stimulated with HRG. HER3 phosphorylation was analyzed as above and transfected ARNO was detected with an anti-FLAG antibody (n=3). The diagram shows relative phosphorylation levels (pHER3_Y1289) after normalization for Hsc70. The phosphorylation level of empty-vector transfected, ligand-stimulated cells was set as 1. Data represented as mean ±SEM.

Overexpression of ARNO increased the phosphorylation of both EGFR (H460 cells, Figure 16) and HER3 (SkBr3 cells, Figure 17) in an expression level dependent manner.

These results show that overexpression of ARNO enhances the ligand-dependent activation of ErbB receptor family members.

IV.1.2.2 The Sec7 domain of ARNO is sufficient for EGFR activation

Cytohesins are multidomain proteins. They share a conserved domain structure consisting of the amino-terminal coiled-coil domain, which is used for interaction with cellular-binding

partners, the central Sec7 domain, which contains the GEF function and the carboxy-terminal pleckstrin homology (PH) domain, which can bind to inositol phospholipids and therefore regulate the protein's membrane association [80].

To determine which domain of ARNO is responsible for the enhancement of EGFR activation, I transfected H460 cells with either empty vector (mock) or the following FLAG-tagged ARNO constructs: full length protein (FL), ARNO lacking the coiled-coil (Δcc) or the pleckstrin homology (ΔPH) domain or the isolated Sec7 domain (Sec7). After stimulation with EGF the phosphorylation of the EGFR was analyzed as above.

All ARNO constructs were expressed equally in the cells and stimulated EGFR autophosphorylation as efficient as the full-length protein (Figure 18). As the lowest common denominator, all tested constructs contained the Sec7 domain of ARNO, attributing the EGFR-activating capability of the cytohesins to this domain.

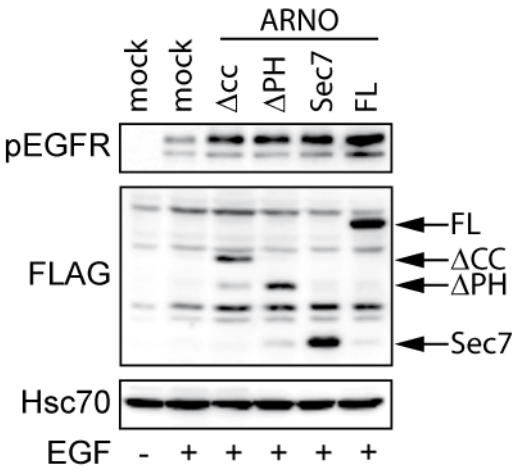

Figure 18 The Sec7 domain of ARNO is sufficient to enhance EGFR activation

Representative western blot of H460 cells transfected with full-length ARNO (FL), with ARNO lacking the coiled-coil (Δcc) or the pleckstrin homology (ΔPH) domain or the isolated Sec7 domain (Sec7). Autophosphorylation of EGFR (pEGFR_Y1086) was determined as above. mock: empty vector

IV.1.2.3 Activation of ErbB receptors by ARNO is independent of its GEF activity

The known function of ARNO is to act as a GEF on ARF proteins. This activity resides in the Sec7 domain of cytohesins, which is in turn also sufficient to activate ErbB receptors. Hence, it is important to analyze whether the GEF activity of ARNO is also required for the activation of the EGFR.

Therefore, I transfected H460 cells and SkBr3 cells with either empty vector, ARNO wild-type or the GEF-inactive ARNO mutant ARNO-E156K and analyzed EGFR autophosphorylation as described above.

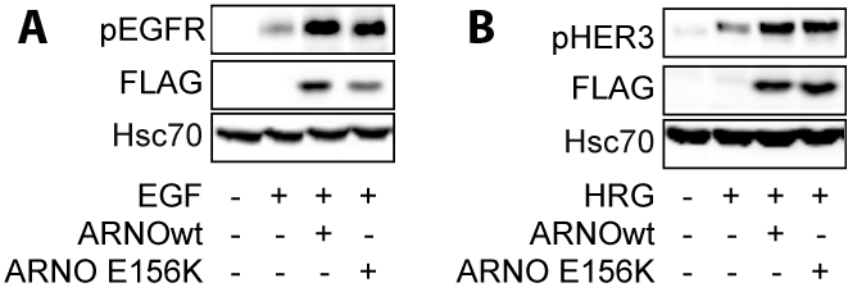

Figure 19 ARNO enhances ErbB receptor autophosphorylation independently of its GEF activity

Representative western blot analysis of H460 (A) or SkBr3 (B) cells transfected with FLAG-tagged wild-type ARNO or GEF-inactive ARNO-E156K. Cells were stimulated with EGF or heregulin (HRG), respectively. Receptor autophosphorylation (pEGFR_Y1086, pHER3_Y1289) and ARNO expression was analyzed as described.

Unexpectedly, overexpressed wild-type ARNO and ARNO-E156K were equally potent in enhancing EGFR autophosphorylation in H460 cells (Figure 19A). ARNO-E156K also stimulated HER2/HER3 autophosphorylation in SkBr3 cells (Figure 19B), suggesting that the GEF activity is not required for the ARNO-mediated activation of ErbB receptors.

One explanation for this observation could be that the effect of the E156K-mutation might be overcome due to high expression levels.

To rule out this possibility, I transfected H460 cells with ARNO-specific siRNA (to knock down endogenous ARNO expression) and increasing amounts of plasmid encoding ARNO or ARNO-E156K. To exclude interference between ARNO knockdown and overexpression, a siRNA which bound to the untranslated region of endogenous ARNO mRNA (not included in the plasmid coding for ARNO or ARNOE156K) was used. EGF-induced EGFR autophosphorylation was analyzed as above. Knock-down of endogenous ARNO was controlled using an ARNO specific antibody (the lower band in the ARNO blot represents a non-specific cross-reactivity of the antibody, ARNO is the upper band).

As Figure 20 shows, ARNO-E156K expressed at endogenous protein level rescued the inhibition of EGFR autophosphorylation induced by knockdown of endogenous ARNO, showing that the ability of ARNO-E156K to enhance EGFR activation was not due to its overexpression.

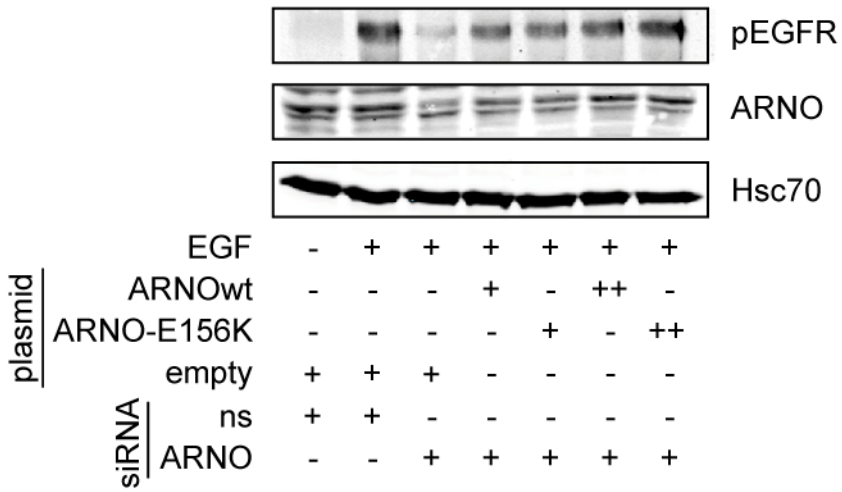

Figure 20 Re-expression of ARNO or the GEF-inactive ARNO-E156K rescues the effect of ARNO knockdown on EGFR autophosphorylation

Representative western blot of H460 cells transfected with ARNO-specific siRNA and increasing amounts (+ or ++) of plasmid encoding ARNO or ARNO-E156K. EGFR autophosphorylation was detected using a phosphospecific antibody (pEGFR_Y1086). Hsc70 served as loading control. Empty: empty vector, ns: non-silencing siRNA.

Furthermore, knockdown of ARF1 or ARF6 had no influence on the activation of the EGFR or HER2/Her3 (data not shown, experiments done by Jin-Na Song [104]).

These results indicate that the cytohesin-mediated activation of ErbB receptors does not involve ARF1 or ARF6, nor does it require the GEF function of the Sec7 domain, and thus implicate a hitherto unknown GEF-independent function of cytohesins.

IV.1.3 Cytohesins facilitate a conformational rearrangement of the intracellular domains of ErbB receptor dimers

The enhancement of EGFR activation by cytohesins could be due to different effects: First, cytohesins are known to be involved in endocytosis and may augment EGFR activation indirectly by modulating the endocytosis or degradation of the EGFR. Second, the increase of EGFR activation by cytohesins could be caused by alterations in the clustering of EGFR. Third, cytohesins may promote EGFR dimerization or, fourth, may induce a conformational change in the cytoplasmic domains of EGFR which facilitates EGFR autophosphorylation. To distinguish between these possibilities I conducted the following experiments.

IV.1.3.1 SecinH3 does not alter EGF-triggered internalization or cluster size of EGFR

As the enhancement of EGFR activation by cytohesins could be indirectly caused by modulations in EGFR endocytosis or degradation, the effect of SecinH3 on the amount of

EGFR on the plasma membrane of H460 cells was analyzed. SecinH3-treated or untreated H460 cells were stimulated with EGF and the EGFR remaining at the plasma membrane was quantified on plasma membrane sheets by immunofluorescence microscopy (experiments were done together with David Walrafen, AG Lang, University of Bonn).

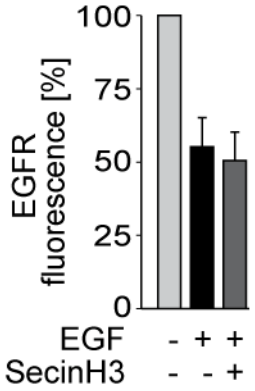

Figure 21 SecinH3 does not affect EGF-triggered internalization of EGFR

SecinH3 treated or untreated H460 cells were stimulated with EGF and the EGFR remaining at the plasma membrane was quantified on plasma membrane sheets by immunofluorescence microscopy. The diagram shows the mean of three independent experiments, comprising 22-26 membrane sheets each. Experiments were done in cooperation with T. Lang, University of Bonn).

As expected, EGF stimulation enhanced EGFR internalization and led to a decrease in the amount of EGFR at the plasma membrane (Figure 21). However, quantification of the EGFR at the plasma membrane after EGF stimulation revealed no difference between untreated and SecinH3-treated cells, arguing against the assumption that cytohesins enhance EGFR activation by modulating endocytosis.

One might expect that reduced EGFR activation after cytohesin inhibition would slow down EGFR endocytosis. But, recently it had been shown that receptor dimerization rather than receptor phosphorylation triggers EGFR endocytosis [106]. Thus, these results furthermore indicate that cytohesins do not affect EGFR dimerization.

Depending on determinants that are as yet incompletely understood, ErbB receptor activation by growth factors may be accompanied by receptor clustering. To further rule out an effect of cytohesins on EGFR clustering, EGF-dependent EGFR clustering was examined by superresolution light microscopy using stimulated emission depletion (STED) on plasma membrane sheets. SecinH3-treated or untreated H460 cells were stimulated with EGF and EGFR cluster sizes were determined by STED microscopy on plasma membrane sheets (experiments were done by David Walrafen and Arne Schreiber, AG Lang, University of Bonn). EGF led to a slight increase in the measured EGFR cluster size at the plasma membrane of H460 cells, which was not affected by SecinH3, indicating that the reduction of

EGFR signaling observed after cytohesin inhibition is not a result of alterations in cluster size at the observed ~100nm scale (data not shown [104]).

Taken together, these results indicate, that the cytohesins-dependent enhancement in EGFR autophosphorylation is not due to altered endocytosis or increased clustering of the receptor.

IV.1.3.2 Cytohesins enhance the phosphorylation but not the dimerization of ErbB receptors

One possible scenario for the positive effect of cytohesins on EGFR autophosphorylation could be that cytohesins induce receptor dimerization.

To analyze the effect of cytohesins on EGFR homodimerization, H460 cells were preincubated with SecinH3 or transfected with ARNO, stimulated with EGF and dimeric receptors on the cell membrane were "trapped" by crosslinking with BS3.

Bis(sulfosuccinimidyl)suberate (BS3) is a commonly used, water-soluble and membrane impermeable crosslinker [107]. It contains an amine-reactive N-hydroxysulfosuccinimide (NHS) ester at each end of an 8-carbon spacer arm (11.4 angstrom). NHS esters react with primary amines (found in the side chain of lysine residues and at the N-terminus of proteins) to form stable amide bonds, along with release of the N-hydroxysulfosuccinimide leaving group. BS3 can be used to crosslink adjacent proteins on the cell membrane and it has been often used to crosslink ErbB receptors. Due to its stability under reducing conditions crosslinked EGFR dimers can be analyzed by SDS-PAGE using low-percentage polyacrylamide gradient gels. Because of the high molecular weight of crosslinked EGFR dimers (>300kDa) western blotting has to be done using the wet blot system (tank-system). Transferred proteins were detected with the indicated antibodies.

Figure 22 (upper blot) shows the amount of monomeric (indicated by an asterisk) and dimeric (indicated by an arrow) EGFR before/after stimulation with EGF and incubation with SecinH3. Stimulation with EGF led to a strong induction of EGFR dimer, which was not altered by SecinH3 treatment. The lower blot displays the phosphorylation levels of monomeric and dimeric receptors. As expected, EGF stimulated the phosphorylation of EGFR dimers which was clearly diminished by SecinH3. The diagram shows the phosphorylation of the crosslinked, i.e. dimeric receptors after normalization for total dimeric receptor.

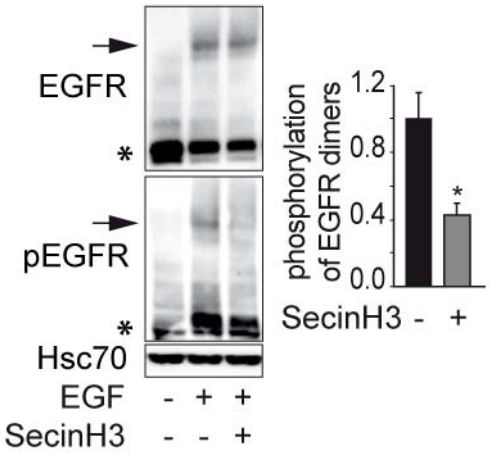

Figure 22 SecinH3 inhibits the phosphorylation but not the dimerization of EGFR

H460 cells were treated with SecinH3, stimulated with EGF for 5min and treated with crosslinker. Receptor phosphorylation was analyzed by a phosphospecific antibody (pEGFR_Y1086). Arrows indicate receptor dimers, asterisks indicate receptor monomers. The diagram summarizes the relative phosphorylation of the crosslinked, i.e. dimeric receptors only, after normalization for total dimeric receptor (n=9). Data are shown as mean ±SEM, *: $p<0.05$.

These results show that cytohesin inhibition does not affect receptor dimerization but clearly reduces the phosphorylation of the dimerized receptors.

I repeated the same experiment for H460 cells overexpressing ARNO instead of SecinH3 treatment. Consistently, ARNO overexpression in H460 cells led to a more than 2fold increase in phosphorylation of EGFR dimers, whereas it had no effect on EGFR dimerization (Figure 23).

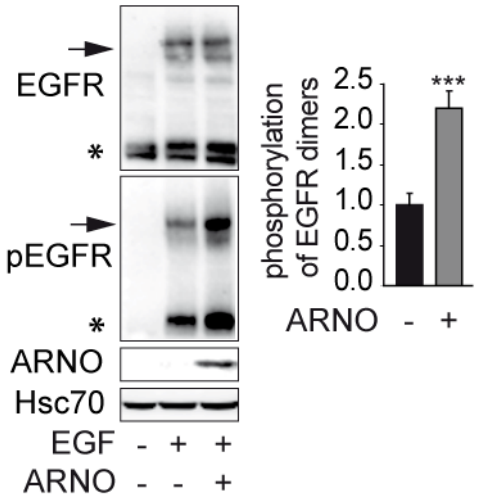

Figure 23 ARNO enhances the phosphorylation but not the dimerization of EGFR

H460 cells were transfected with ARNO or empty vector for 48h, stimulated with EGF for 5min and treated with crosslinker. Receptor phosphorylation was analyzed by a phosphospecific antibody (pEGFR_Y1086). Arrows indicate receptor dimers, asterisks indicate receptor monomers. The diagram summarizes the relative phosphorylation of the crosslinked, i.e. dimeric receptors only, after normalization for total dimeric receptor (n=5). Data are shown as mean ±SEM, ***: $p<0.001$.

Having shown that cytohesins facilitate EGFR autophosphorylation without altering the dimerization of the receptor, I analyzed whether the same was true for HER3. Therefore, I treated SkBr3 cells with SecinH3, stimulated with HRG and chemically crosslinked the receptor. Analysis of crosslinked receptors were performed as described for the H460 cells.

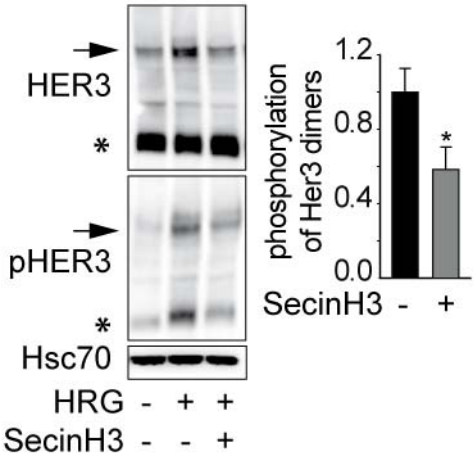

Figure 24 SecinH3 inhibits the phosphorylation but not the dimerization of HER3

SkBr3 cells were treated with SecinH3, stimulated with HRG for 5min and treated with crosslinker. Receptor phosphorylation was analyzed by a phosphospecific antibody (pHER3_Y1289). Arrows indicate receptor dimers, asterisks indicate receptor monomers. The diagram summarizes the relative phosphorylation of the crosslinked, i.e. dimeric receptors only, after normalization for total dimeric receptor (n=9). Data are shown as mean ±SEM, *: $p<0.05$.

In agreement with the results obtained for the EGFR, chemical inhibition of cytohesins with SecinH3 led to strong reduction in the phosphorylation if dimeric HER3, but did not alter the amount of dimeric HER3 (Figure 24).

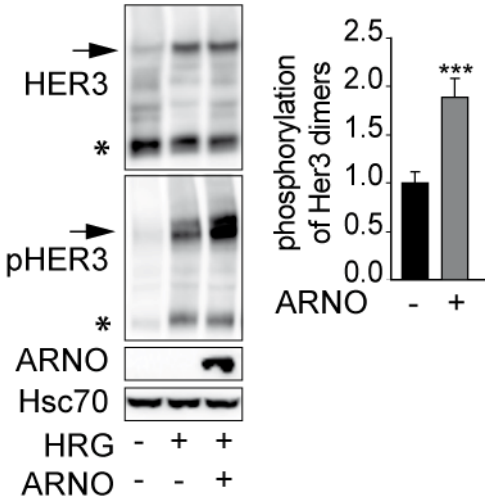

Figure 25 ARNO enhances the phosphorylation but not the dimerization of HER3

SkBr3 cells were transfected with ARNO or empty vector for 48h, stimulated with HRG for 5min and treated with crosslinker. Receptor phosphorylation was analyzed by a phosphospecific antibody (pHER3_Y1289). Arrows indicate receptor dimers, asterisks indicate receptor monomers. The diagram summarizes the relative phosphorylation of the crosslinked, i.e. dimeric receptors only, after normalization for total dimeric receptor (n=5). Data are shown as mean ±SEM, ***: $p<0.001$.

Furthermore, overexpression of ARNO in SkBr3 cells increased HER3 phosphorylation without altering HER3 dimerization. (Figure 25)

Taken together, these data suggest that ARNO facilitates the activation of already dimerized ErbB receptors.

IV.1.3.1 SecinH3 does not alter HER2/HER3 heterodimerization

In order to gain more insight into the effect of cytohesins on HER3 activation, I analyzed the amount of HER2/HER3 heterodimers in SkBr3 cells after treatment with SecinH3.
I performed coimmunoprecipitation studies for the HER2/HER3 heterodimer. SkBr3 cells, which express both HER2 and HER3, were treated with SecinH3 or solvent, starved overnight and stimulated with heregulin to induce HER2/HER3 heterodimer formation. The cell lysate was subjected to immunoprecipitation using a HER3 specific antibody coupled on agarose beads. After washing, I eluted precipitated HER3 and analyzed the eluate by SDS-PAGE, western blotting and immunodetection with a HER2 specific antibody.

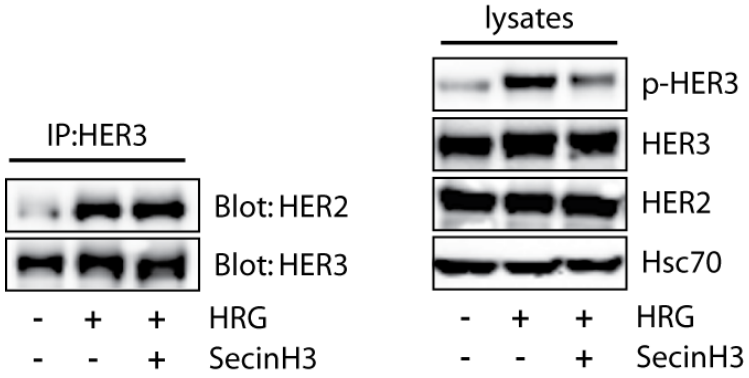

Figure 26 SecinH3 does not alter the amount of HER3/HER2 dimers in SkBr3 cells
SkBr3 cells were treated with SecinH3 and the lysates were subjected to immunoprecipitation using an HER3 specific antibody. Precipitated HER3 and coprecipitated HER2 were analyzed by immunoblotting of the eluate.
Left: representative western blot of precipitate.
Right: Control of receptor levels in the lysates used for immunoprecipitation. Proteins were detected as described above.

As expected, stimulation with heregulin induced the formation of HER2/HER3 heterodimers which was manifested in a distinct coimmunoprecipitation of HER2 and phosphorylation of HER3 (Figure 26). Treatment with SecinH3 did not alter the amount of coprecipitated HER2 nor did it change total receptor expression levels, even so it clearly decreased HER3 phosphorylation. Taken together these results implement that cytohesins do not affect HER2/HER3 heterodimer formation.

IV.1.3.2 Cytohesins facilitate the phosphorylation of constitutively dimerized EGFR

To substantiate the assumption that cytohesins facilitate the activation of already dimerized ErbB receptors, a constitutively dimerized EGFR (lz-EGFR) was constructed by replacing the extracellular domain of the receptor with a dimerization module consisting of a leucine zipper and a single cysteine residue that forms a disulfide bridge upon dimerization (Figure 27, cloning done by Anton Schmitz). If the mode of action for cytohesins is to facilitate the activation of already dimerized receptors they should also be able to increase the activity of the constitutively dimerized lz-EGFR.

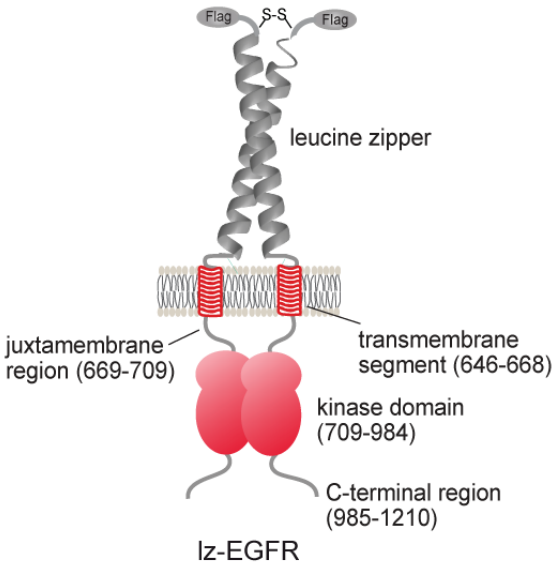

Figure 27 Schematic of the constitutively dimerized lz-EGFR
The extracellular domain of EGFR was replaced by a FLAG-tagged disulfide-bridged leucine zipper module.

I used HEK293 cells for transfection of lz-EGFR to avoid interference with endogenous wild-type EGFR. HEK293 have only a very low endogenous level of EGFR and can be easily transfected using Metafectene (Biontex) and are therefore perfectly suited for these kinds of experiments.

First, I had to test the integrity of the lz-EGFR. HEK293 cells were transfected with increasing amounts of lz-EGFR (+ and ++) or empty vector (-). After 48h, cells were harvested and proteins were separated by reducing or non-reducing SDS-PAGE and lz-EGFR was detected by anti-FLAG antibody.

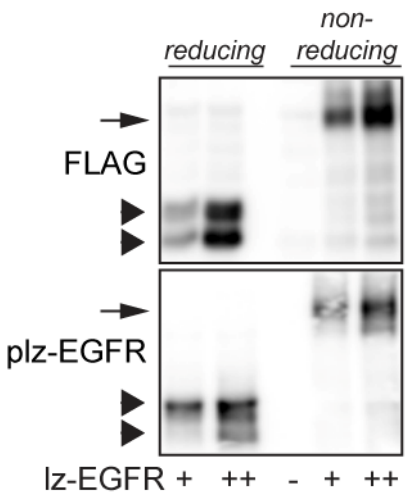

Figure 28 lz-EGFR is expressed as a constitutive dimer

Western blot of HEK293 cells transfected with increasing amounts of lz-EGFR (+ and ++) or empty vector (-). Proteins were separated by reducing or non-reducing SDS-PAGE and lz-EGFR was detected by anti-FLAG antibody, phosphorylated lz-EGFR (plz-EGFR) by anti pEGFR_Y1086) antibody. The arrow indicates receptor dimers, the arrowheads monomers. The double bands under non-reducing conditions correspond to unphosphorylated (lower) and phosphorylated (upper) lz-EGFR.

Under non-reducing conditions, I found the lz-EGFR exclusively expressed as dimer (Figure 28, arrow, upper panel, right half). Consistent with its constitutive dimerization lz-EGFR was phosphorylated (lower panel). The double bands (arrow heads) under reducing conditions correspond to unphosphorylated (lower) and phosphorylated (upper) forms of monomeric lz-EGFR (plz-EGFR). Under non-reducing conditions the two forms were not separated.

Secondly, I had to test whether the activation of the lz-EGFR kinase domain was still dependent on the formation of the asymmetric dimer. Therefore I analyzed the effect of MIG6 on the autophosphorylation of the lz-EGFR. MIG6 is known to inhibit receptor autophosphorylation by preventing the formation of the active asymmetric EGFR dimer [34]. I transfected HEK293 cells with either lz-EGFR alone or in combination with a myc-tagged form of the EGFR-binding domain of MIG6 (MIG6-EBR), which was shown to be sufficient for inhibiting EGFR signaling [34]. Cell lysates were analyzed as above under reducing conditions. Hsc70 served as a loading control.

As Figure 29 shows, coexpression of MIG6-EBR reduced lz-EGFR autophosphorylation (please also note the shifting of the upper band of lz-EGFR), suggesting that the activation of the lz-EGFR still depends on the formation of the asymmetric dimer. Thus, regarding the allosteric activation of the kinase domains, the lz-EGFR appears to behave like an authentic EGFR. Therefore, the lz-EGFR is a suitable model to ask whether cytohesins enhance the activation of the EGFR kinase after its dimerization.

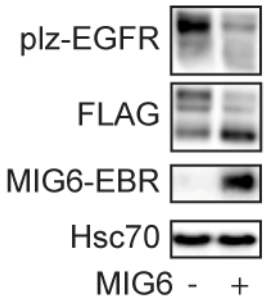

Figure 29 MIG6 inhibits the autophosphorylation of lz-EGFR

Representative western blot of HEK-293 cells transfected with lz-EGFR alone or in combination with a myc-tagged form of MIG6-EBR. Proteins were separated by reducing SDS-PAGE and lz-EGFR was detected by an anti-FLAG antibody, MIG6-EBR by an anti-myc antibody and the phosphorylation of lz-EGFR by a phosphospecific antibody (pEGFR_Y1086). Hsc70 served as loading control.

To address this question I transfected HEK293 cells with lz-EGFR and incubated the cells with SecinH3. Cell lysates were analyzed as described. In the presence of SecinH3 the autophosphorylation of lz-EGFR was reduced, whereas there was no change in total lz-EGFR expression (Figure 30). The control compound XH1009 had no effect (data not shown [104]). The diagram shows lz-EGFR phosphorylation after normalization for total receptor, with solvent-treated cells set as 1.

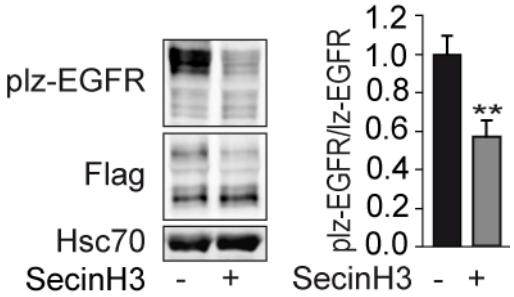

Figure 30 SecinH3 decreases the autophosphorylation of constitutively dimerized EGFR

HEK293 cells were transfected with lz-EGFR and treated with SecinH3. The phosphorylation of lz-EGFR (plz-EGFR) was analyzed by a phosphospecific antibody (pEGFR_Y1086) and total expression level of lz-EGFR by an anti-FLAG antibody (Flag). The diagram shows receptor phosphorylation after normalization for total receptor. Data are represented as mean ± SEM, n=5.

These results show that SecinH3 is capable to inhibit autophosphorylation of already dimerized receptors.

To test whether ARNO is capable of activating already dimerized EGFR, I co-transfected HEK293 cells with both lz-EGFR and ARNO and analyzed lz-EGFR phosphorylation 48h after transfection as described.

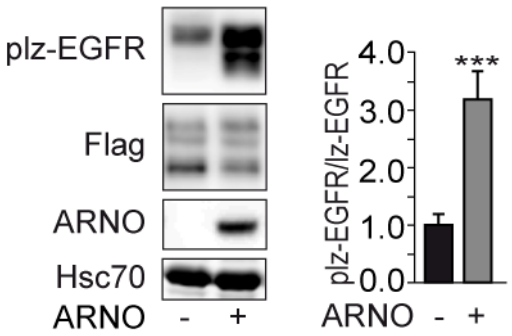

Figure 31 ARNO enhances autophosphorylation of lz-EGFR

HEK293 cells were co-transfected with lz-EGFR and ARNO. The phosphorylation of lz-EGFR (plz-EGFR) was analyzed 48h after transfection by immunoblotting using a phosphospecific antibody (pEGFR_Y1086) and total expression level of lz-EGFR by an anti-FLAG antibody (Flag). The diagram shows receptor phosphorylation after normalization for total receptor. Data are represented as mean ± SEM, n=5.

Consistently, coexpression of ARNO and lz-EGFR in HEK293 cells led to an increased autophosphorylation of lz-EGFR (Figure 31).

These data provide strong evidence for the hypothesis that cytohesins facilitate the activation of already dimerized EGFR.

IV.1.3.3 ARNO facilitates a conformational rearrangement of the intracellular domains in EGFR dimers

Cytohesins enhance the activation of EGFR dimers without altering EGFR receptor endocytosis, clustering or dimerization. These findings suggests the assumption that cytohesins act by facilitating conformational rearrangements in the intracellular domain of EGFRs.

I used steady-state fluorescence anisotropy measurements to visualize conformational changes of the EGFR cytoplasmic domains in living cells.

IV.1.3.3.1 Principles of steady-state fluorescence anisotropy

Anisotropy measurements are based on the principle of photoselective excitation of fluorophores by polarized light and provide information of the size and the shape (=conformation) of the protein to which the fluorophore is coupled.

Fluorophores preferentially absorb photons whose electric vectors are aligned parallel to the transition moment of the fluorophore. Thus, upon excitation with polarized light, one selectively excites those fluorophore molecules whose absorption transition dipole is parallel to the electric vector of the excitation (photoselective excitation). Emission also occurs with the light polarized along a fixed axis in the fluorophore, leading to an anisotropic, directional

emission. The term anisotropy (r) defines the extent of polarization of the emitted light. Anisotropy can be determined by measuring the intensity of emitted light oriented parallel $(I \parallel)$ and perpendicular $(I \perp)$ to the direction of the polarized excitation with the help of an emission polarizer. These intensity values are used to calculate the anisotropy [108]:

$$r = \frac{I \parallel - I \perp}{I \parallel + 2\, I \perp}$$

Several phenomena can affect the anisotropy of a fluorophore. First, rotational diffusion of fluorophores cause a decrease in anisotropy. The extent to which a fluorophore rotates during the excited-state lifetime determines its anisotropy and is described by the Perrin equation (see fluorescence anisotropy measurements):

$$\frac{r0}{r} = 1 + \frac{\tau}{\Theta}$$

where r is the measured anisotropy, r0 is the intrinsic anisotropy of the totally immobile fluorophore, τ is the fluorescence lifetime and θ is the rotational correlation time. That implies, the faster a fluorophore rotates the smaller the anisotropy will be. Second, changes in the fluorescence lifetime of the fluorophore affect anisotropy; the longer the lifetime gets the smaller the anisotropy will be. Third, resonance energy transfer (FRET) between two fluorophores also leads to a decrease in anisotropy due to a "distribution" of the excitation to adjacent fluorophore molecules with differently oriented transition moment (Figure 32).

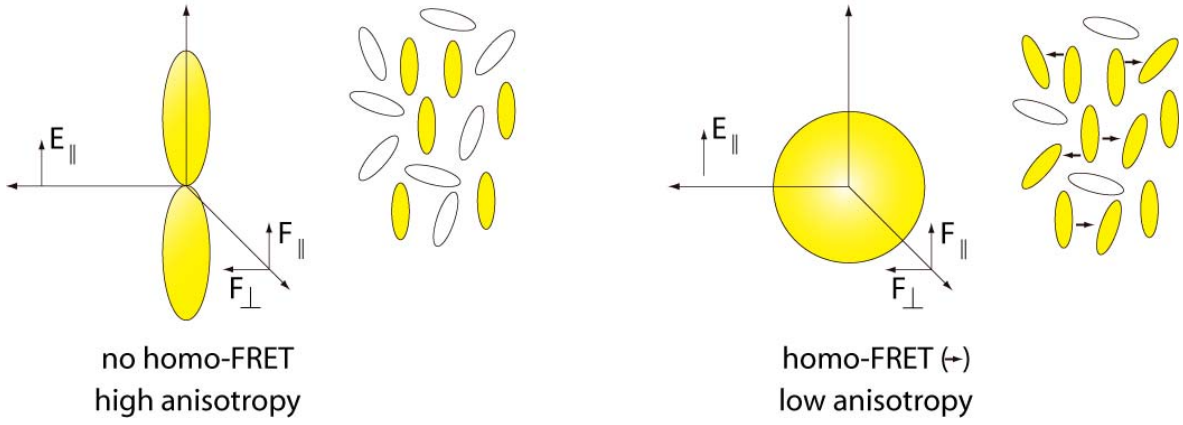

Figure 32 Principle of fluorescence anisotropy measurements

Upon excitation with polarized light $(E \parallel)$, only those fluorophores are excited whose transition moments are aligned parallel to the electric vector of the photons (yellow molecules, left picture). Therefore, emission (fluorescence) occurs only along this axis of the fluorophores $(F \parallel)$, leading to an anisotropic, directional emission (high anisotropy). However, homo-FRET between homologous fluorophores leads to the excitation of adjacent fluorophores and thereby to the "spreading" of the excitation, which results in an undirected, scattered emission (low anisotropy, right picture). Thus, changes in the relative orientation between two fluorophores (results in changes in homo-FRET) can be detected by measurement of anisotropy.

Since resonance energy transfer critically depends on both the distance and the orientation of the fluorophores, anisotropy measurements can be used to visualize conformational changes in the excited proteins [109-112].

I made use of steady-state fluorescence anisotropy measurements to visualize conformational changes in the intracellular domain of EGFR in living cells. For this purpose we constructed a mCitrine-tagged form of the constitutively dimerized lz-EGFR by fusing the fluorescent protein mCitrine to the C-terminus of each lz-EGFR (lz-EGFR-mCitrine, Figure 33, cloning done by Anton Schmitz).
Although fluorescence resonance energy transfer is commonly measured between two different molecules, it can also occur between chemically identical molecules. Such transfer, which is termed homotransfer or homo-FRET, typically occurs for fluorophores which display small Stokes shifts, like citrine (516/529nm, Stoke shift = 13nm).

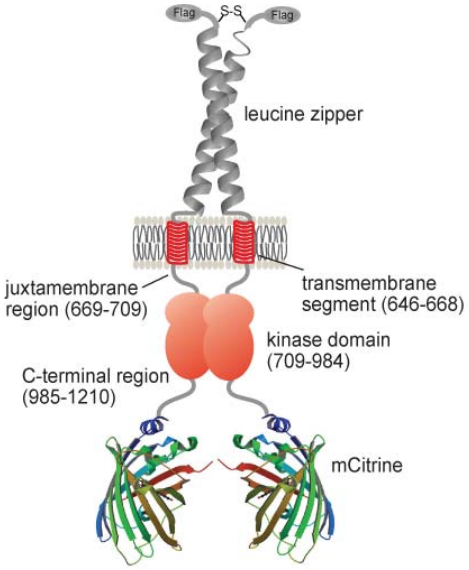

Figure 33 Schematic of the constitutively dimerized lz-EGFR fused to mCitrine (lz-EGFR-mCitrine)
Each molecule in the dimeric lz-EGFR was tagged with the fluorescent protein mCtrine at its C terminus (lz-EGFR-mCitrine).

Changes in the position of the two mCitrine moieties relative to each other result in changes in the fluorescence resonance energy transfer between these proteins (homo-FRET, Figure 32). The efficiency of homo-FRET can be determined by measuring the steady-state fluorescence anisotropy of the transfected cells (the higher the efficiency of homo-FRET the lower the anisotropy will be). This technique has recently been used to monitor conformational changes in the neurotrophin receptor [112].

IV.1.3.3.2 Evaluation of the system

I used Cos-7 cells for all steady-state fluorescence anisotropy measurements because of their flat morphology which simplifies microscopy. First, I transfected Cos-7 cells with lz-EGFR-mCitrine or empty vector, under the same conditions as later used for the steady-state fluorescence anisotropy measurements, to check the integrity of lz-EGFR-mCitrine as described for the lz-EGFR. Like the untagged lz-EGFR, the fusion protein was constitutively dimerized and autophosphorylated (Figure 34). In contrast to HEK293 a strong signal for the endogenous EGFR was detected. Since trans-membrane receptors fused to a fluorescence protein often show defects in subcellular localization, we further confirmed the integrity of lz-EGFR-mCitrine by investigating its expected cellular localization in the plasma membrane. Lz-EGFR-mCitrine reached the membrane, as visualized by fluorescence microscopy on plasma membrane sheets (data not shown), demonstrating that the mCitrine did not perturb receptor localization.

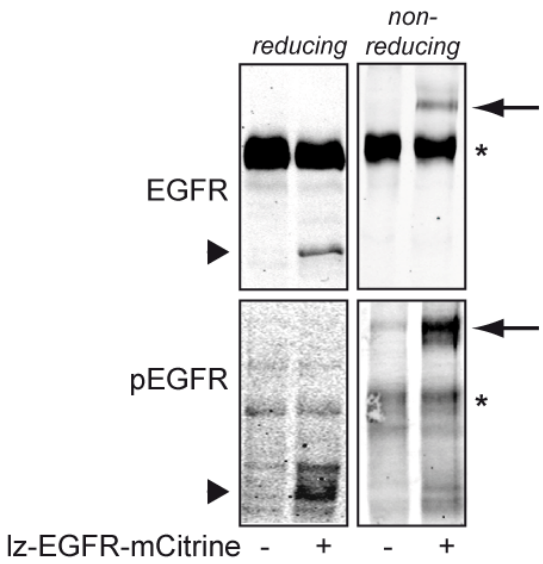

Figure 34 Lz-EGFR-mCitrine is constitutively dimerized and phosphorylated

COS-7 cells were transfected with lz-EGFR-mCitrine or empty vector under the same conditions as used for anisotropy measurements. Proteins were separated by reducing or non-reducing SDS-PAGE. Lz-EGFR-mCitrine was detected by anti-EGFR antibody and by a phosphospecific antibody (pEGFR_Y1086). The arrows indicate receptor dimers, the arrowheads monomers. The asterisk indicated endogenous EGFR.

To test whether this construct is also suited to detect conformational changes in the EGFR cytoplasmic domains, I transfected Cos7-cells with either lz-EGFR-mCitrine alone, together with MIG6 or together with the control protein Rheb (ras homolog enriched in brain, G-protein) and measured steady-state fluorescence anisotropy as described [110]. Shortly, Cos-7 cells were seeded on glass bottom dishes, adhered for at least 6h and transfected with low amounts of the indicated plasmids using FuGene (Roche) for ~ 12-18h. Before microscopy I changed the medium to DMEM without phenol red. Microscopy was done using an inverted

microscope. A linear dichroic polarizer was placed in the illumination path of the microscope, and two identical polarizers were placed at orientations parallel and perpendicular to the polarization of the excitation light. I performed the experiments at the MPI in Dortmund under the supervision of Peter Verveer.

Whereas MIG6 is expected to change the steady-state fluorescence anisotropy of lz-EGFR-mCitrine, Rheb, which is not involved in EGFR signaling, should have no effect. Figure 35 shows representative micrographs of cells transfected with lz-EGFR-mCitrine alone (left) or together with MIG6 (middle) or Rheb (right). The pictures were artificially colorized to visualize the measured values for steady-state fluorescence anisotropy. The diagram shows the statistical evaluation of all experiments.

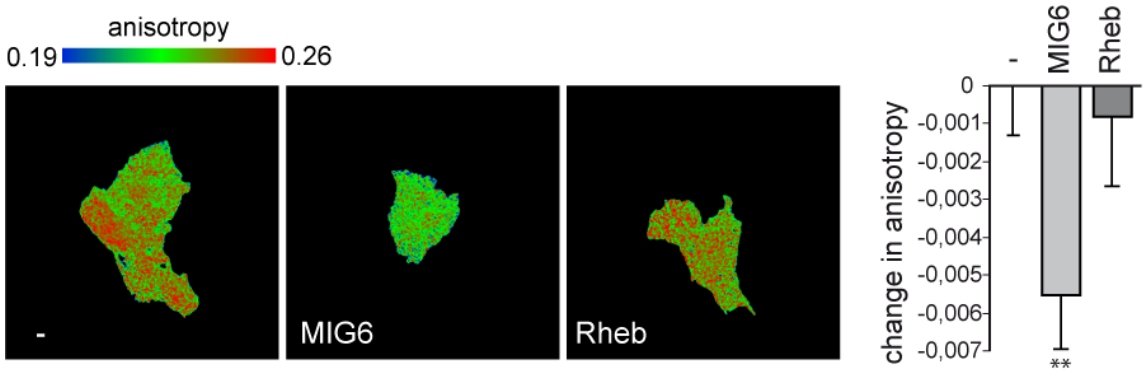

Figure 35 Steady-state fluorescence anisotropy of lz-EGFR-mCitrine

Representative micrographs of Cos-7 cells transfected with lz-EGFR-mCitrine alone (-) or together with either MIG6-EBR (MIG6) or Rheb. Whereas MIG6-EBR is known to prevent the formation of the asymmetric EGFR dimer Rheb is not involved in EGFR signaling. The diagram shows the statistical evaluation of 5 experiments (n=25 fields of view with 1-4 cells each). Data are represented as mean ±SEM. **: $p<0.01$.

As expected, co-expression of MIG6-EBR led to a change in the steady-state fluorescence anisotropy of lz-EGFR-mCitrine whereas co-expression of Rheb did not. Thus, anisotropy measurements are suited to detect differences in lz-EGFR-mCitrine conformation.

IV.1.3.3.3 ARNO induces a change in steady-state fluorescence anisotropy of lz-EGFR-mCitrine

To detect ARNO-dependent conformational changes in the cytoplasmic domains of EGFR dimers, I transfected Cos-7 cells with lz-EGFR-mCitrine either alone or in combination with a low (+) or high (++) amount of ARNO and measured steady-state fluorescence anisotropy as described.

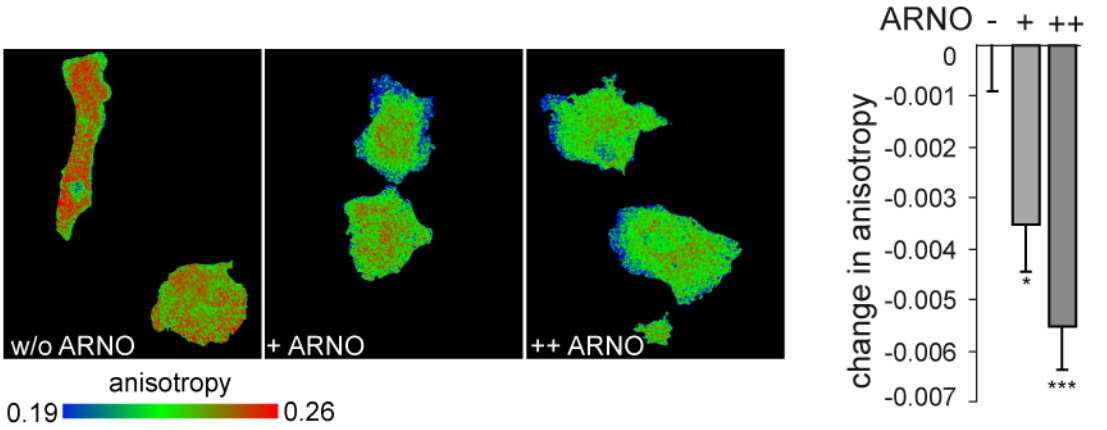

Figure 36 ARNO facilitates a conformational rearrangement of the intracellular domains of constitutively dimerized EGFR

Representative micrographs of Cos-7 cells transfected with lz-EGFR-mCitrine alone or together with increasing amounts of ARNO. Steady-state fluorescence anisotropy was measured as described. The diagram shows the statistical evaluation of 5 experiments (n=25 fields of view with 1-4 cells each). Data are represented as mean ±SEM. *: $p<0.05$ ***: $p<0.001$.

The co-expression of ARNO led to a decrease in anisotropy as compared to lz-EGFR-mCitrine alone indicating that ARNO co-expression resulted in an altered conformation of the cytoplasmic domains of the EGFR dimer (Figure 36).

Although the final geometries of the EGFR dimers in the EGFR-ARNO and EGFR-MIG6 complexes are expected to be different, a decrease in fluorescence anisotropy was detected in both cases. At first view, these results seem mutually contradictory as it might intuitively be anticipated that changes in anisotropy produced by an inhibitor would oppose those of an activator. However, it should be noted that it is not possible to deduce from similar anisotropy values of two situations that the underlying geometries are similar. Fluorescence anisotropy depends on both, the distance and the relative orientation of the fluorophores. Thus, even if the anisotropy is equal in two situations the underlying geometry can be quite different. For instance, in one case the distance between the fluorophores may be larger but the relative orientation may be more favorable for FRET and in the other case the distance may be smaller but the orientation unfavorable. Therefore, although a specific conformation cannot be deduced from a certain value or prefix of changes in anisotropy, they are a reliable indicator for changes in geometry.

The results show that both proteins, ARNO and MIG6, change the geometry of the EGFR dimers. However, it is not possible to deduce the resulting conformation from the change in anisotropy.

Together with the analysis of receptor crosslinking and phosphorylation, these results support the hypothesis that cytohesins enhance ErbB receptor activation by facilitating a conformational rearrangement in the cytoplasmic domains of the dimerized EGFR.

IV.1.3.3.4 Control measurements

Fluorescence anisotropy can also be affected by changes in the fluorescence lifetime. To address this point I repeated fluorescence anisotropy measurements with lz-EFGR-mCitrine and performed fluorescence lifetime measurements at the same time (experiments were done together with Franziska Thorwirth at the MPI in Dortmund). Although ARNO induced a strong decrease in fluorescence anisotropy of lz-EGFR-mCitrine there was no change in the average fluorescence lifetime (τ_{AV}=3.086 ns for lz-EGFR-mCitrine alone and τ_{AV}=3.058 ns for coexpression of lz-EGFR-mCitrine and ARNO). This result strongly argues against the possibility that ARNO decreases fluorescence anisotropy by changing fluorescence lifetime of lz-EGFR-mCitrine.

Another explanation for the obtained decrease in fluorescence anisotropy caused by ARNO coexpression would be that ARNO directly interacts with the citrine moiety of the lz-EGFR-mCitrine. To rule out this possibility of direct interaction between ARNO and mCitrine I used a leucine zipper mCitrine construct (lz-mCitrine, cloning done by Anton Schmitz), in which the mCitrine moiety was directly fused to the transmembrane segment of lz-EGFR, i.e. this construct lacks the intracellular domain of EGFR. In contrast to lz-EGFR-mCitrine, the fluorescence anisotropy of lz-mCitrine was not affected by co-transfection of ARNO (data not shown).

Having shown that ARNO does neither affect lz-mCitrine anisotropy nor the fluorescence lifetime of lz-EGFR-mCitrine the observed decrease in lz-EGFR-mCitrine anisotropy due to co-expression of ARNO is likely explained by a change in homo-FRET, indicating a conformational change in the intracellular domain of the EGFR.

IV.1.4 Cytohesins interact with the EGFR

IV.1.4.1 ARNO forms a complex with EGFR in cells

ARNO´s function as a conformational activator of the EGFR implies ARNO and the EGFR to physically interact. Immunofluorescence microscopy of plasma membrane sheets showed that ARNO and the EGFR colocalize in H460 cells (experiments were performed by David Walrafen, AG Lang, University of Bonn, data not shown [104]). To substantiate this observation I performed coimmunoprecipitation of ARNO and EGFR. I imunoprecipitated EGFR from H460 cell lysates using an EGFR specific antibody coupled to agarose beads. Agarose-coupled normal mouse IgG was used as a control matrix. After washing I eluted the receptor and the elution was analyzed by SDS-PAGE and immunoblotting using an EGFR- or ARNO-specific antibody.

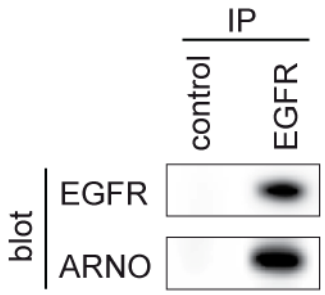

Figure 37 Coimmunopreciptation of ARNO with EGFR

EGFR was coimmunoprecipitated from H460 cells with agarose-coupled anti-EGFR antibody. Coprecipitated ARNO was detected by an ARNO-specific antibody. Agarose-coupled normal mouse IgG was used as control matrix.

Figure 37 indicates complex formation between EGFR and ARNO, whereas no ARNO could be detected in the elution of the control matrix.

In conclusion, these results suggest an interaction between EGFR and ARNO, but, however, do not proof the direct interaction between these two proteins.

IV.1.4.2 Cytohesins directly bind to the intracellular domain of the EGFR

To gain further evidence for direct interaction of ARNO and the cytoplasmic domain of EGFR, I used a cell free reconstitution system. The complete cytoplasmic domain of the EGFR (EGFR-ICD), EGFR-ICD lacking the C-terminal 188 amino acid (EGFR-ICD-1022), segment 1 of MIG6-EBR (MIG6-S1), full length ARNO (ARNO-FL), wild-type and GEF-inactive Sec7 domain of ARNO (ARNO-Sec7wt, ARNO-Sec7-E156K) were heterologously expressed and purified (done by Anton Schmitz and Volkmar Fieberg). Figure 38 shows coomassie stains of the purified proteins and lysozyme. All proteins, except for the EGFR, where labelled with the fluorescent dye fluorescein using Fluorescein isothiocyanate (FITC). Labelling efficiency was between 0.4 and 1 molecules fluorescein per protein molecule, as determined by spectroscopy.

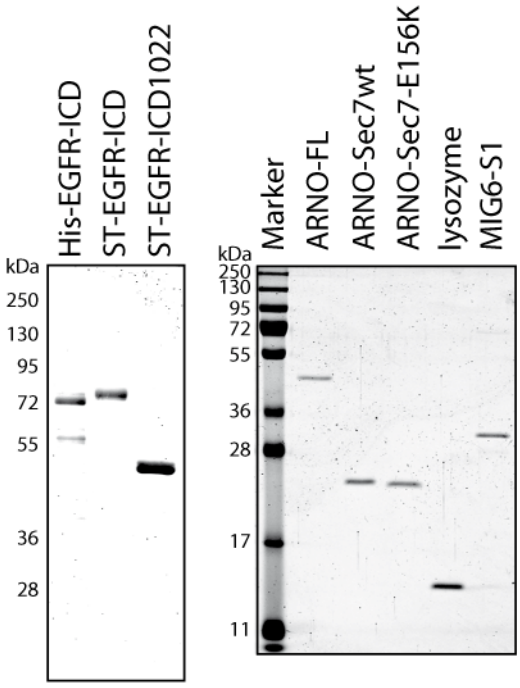

Figure 38 Coomassie stains of proteins used in cell-free binding and autophosphorylation experiments
Proteins were separated by SDS-PAGE and stained with Coomassie. Destained gels were scanned and analyzed.

Interactions between the proteins were analyzed by fluorescence anisotropy measurements. Fluorescence anisotropy can be used to determine the dissociation constant for the interaction between a fluorescently labeled and an unlabeled protein.

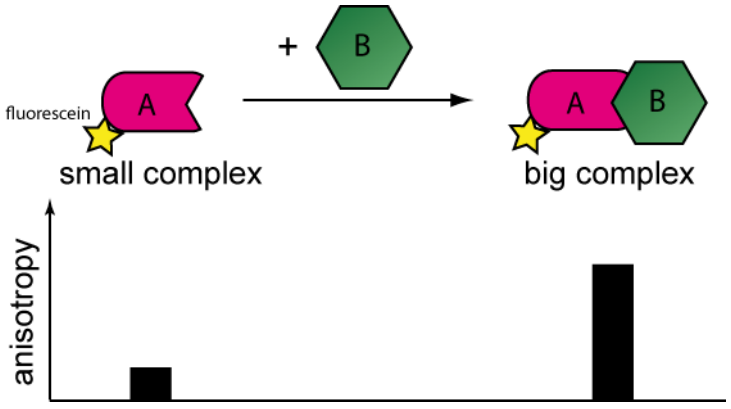

Figure 39 Principle of anisotropy measurements used to detect protein-protein interactions
Fluorescein-labeled protein A interacts with protein B leading to an increase in fluorescence anisotropy. Small fluorescence complexes (protein A) can rotate freely in the solution, thereby emitting fluorescence at a different direction as the exciting light (low anisotropy). Upon interaction with another protein (protein B) the size of the complex is increased, which leads to a deceleration of rotation and a less "scattering" and thus to an increase in anisotropy.

As mentioned above, fluorescence anisotropy depends on the rotation of the fluorophore. If a fluorescence molecule is moving, it will tend to "scatter" the polarization of the light by radiating/emitting at a different direction from the incident/exciting light. According to the Perrin equation, the "scattering" effect is greatest with small fluorescently labeled molecules

freely rotating in solution (low anisotropy) and decreases with reduced rotating rates (high anisotropy). Upon binding of an unlabeled protein to a fluorescein-labeled protein the size of the rotating complex increases, which leads to a deceleration of rotation and thus to an increase in anisotropy (Figure 39).

To exclude the possibility that EGFR-ICD aggregated during binding experiments which could confound the measurements, I first analyzed solubility of EGFR-ICD, under the same conditions as in the binding experiment. I centrifuged the reaction for 5min at 20000x g in order to separate protein aggregates. Figure 40 depicts a western blot of the reaction before (total) and after centrifugation (soluble = supernatant, pellet = aggregated protein). EGFR-ICD was found exclusively in the soluble fraction.

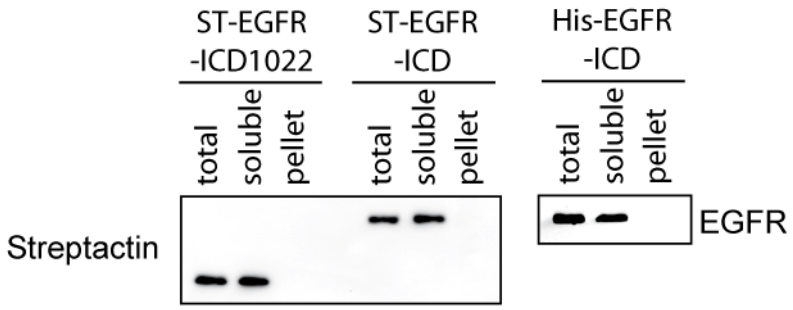

Figure 40 EGFR-ICD is soluble under the conditions used for cell-free binding and autophosphorylation experiments

EGFR-ICD solubility was analyzed by centrifugation under the conditions for a typical binding experiment. Fractions were analyzed by western blot using streptactin or anti-EGFR antibody for detection. Total: before centrifugation, soluble: soluble fraction, pellet: precipitate.

For determination of the dissociation constant, EGFR-ICD was titrated in increasing concentration to the indicated FITC-labeled proteins (constant concentration of 1μM) and fluorescence anisotropy was measured (Figure 41). Blotting the concentration of EGFR-ICD against the measured anisotropy revealed a single-binding site kinetic and the obtained binding curves were fitted using non-linear regression and a one site binding model (GraphPadPrism) to calculate the apparent dissociation constant (K_D).

Full-length ARNO, the isolated Sec7 domain and the GEF-inactive Sec7-E156K domain bound to the EGFR-ICD with apparent dissociation constants around 1μM. Segment 1 of MIG6-EBR (MIG6-S1), a known binding partner of the EGFR-ICD bound with a dissociation constant around 2μM. No binding was observed between lysozyme and EGFR-ICD, nor did ARNO full-length or ARNO-Sec7 show binding to MIG6-S1, indicating that

the observed binding is specific. These data indicate the direct interaction between EGFR and ARNO´s Sec7 domain.

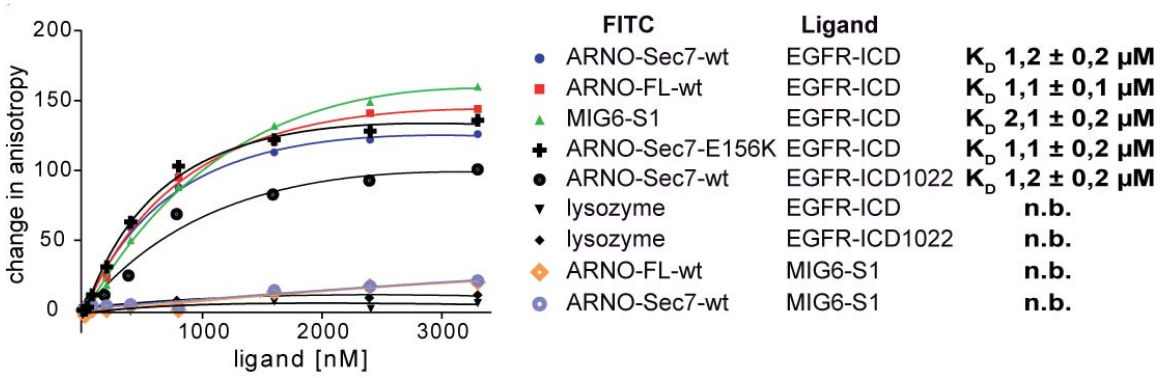

Figure 41 ARNO interacts with the intracellular domain of EGFR in vitro

The indicated proteins were labeled with FITC and the unlabeled ligand was added at increasing concentrations. Binding was measured by fluorescence anisotropy. K_D values were calculated assuming a 1:1 stoichiometry and are given as mean ±SEM, n=4.

In order to restrict the binding site of ARNO in the intracellular domain of EGFR, I titrated EGFR-ICD lacking the C-terminal 188 amino acids (EGFR-ICD-1022) to FITC-labeled ARNO-Sec7-wt (Figure 41). EGFR-ICD-1022 bound to ARNO-Sec7-wt with the same affinity as the complete EGFR-ICD confining ARNO´s binding site to the kinase or juxtamembrane, but not the C-terminal domain of the EGFR.

Recently it was shown, that Dok-7 regulates the activity of the RTK MuSK by binding to the partially phosphorylated receptor [113-114]. To test whether the binding of ARNO-Sec7 to the EGFR-ICD also required phosphorylation of the receptor, I titrated ARNO to EGFR-ICD, preincubated with ATP, which resulted in strong autophosphorylation of EGFR-ICD.

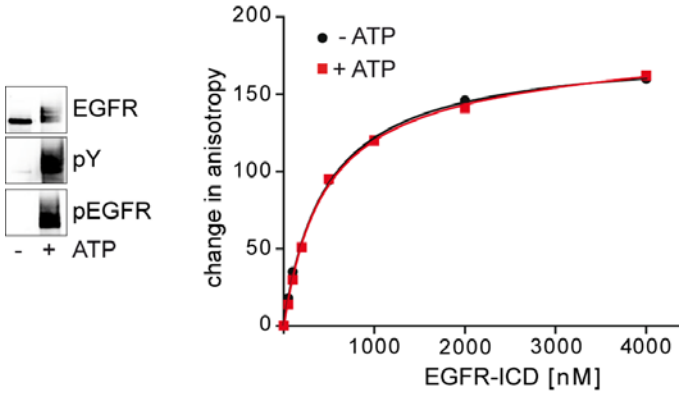

Figure 42 ARNO binds to EGFR independent of the phosphorylation status

Interaction of ARNO-Sec7 and EGFR-ICD was measured by fluorescence anisotropy in the presence or absence of ATP (diagram). Addition of ATP results in autophosphorylation of EGFR-ICD as detected by immunoblotting (left).

As Figure 42 shows, the binding of ARNO-Sec7-wt to the EGFR-ICD did not require phosphorylation of the EGFR-ICD, as binding of ARNO-Sec7 and EGFR-ICD was independent of the phosphorylation status of EGFR-ICD. This result is in agreement with ARNO functioning upstream of EGFR autophosphorylation.

IV.1.5 ARNO stimulates autophosphorylation of EGFR by direct interaction

Having shown that ARNO directly interacts with EGFR-ICD, I analyzed the autophosphorylation of EGFR-ICD in the presence of ARNO in a cell free system. Due to the presence of the juxtamembrane segment, EGFR-ICD forms a dimer resembling the intracellular domains of the ligand-bound EGFR and thus can be used to investigate the autophosphorylation of the EGFR in a cell-free system. Addition of ATP in the presence of DTT and $MgCl_2$, is known to induce autophosphorylation of the receptor. To test whether the conformational requirements for the activation of the authentic EGFR are still preserved in EGFR-ICD, I also included MIG6-S1, which is known to inhibit the formation of the asymmetric dimer of the EGFR, and GST, which was used as a negative control, in the experiment. I preincubated EGFR-ICD either with MIG6-S1, GST or ARNO full-length (ARNO-FL) and initiated the reaction by addition of ATP. At the indicated time points before (0min) and after addition of ATP (1min and 3min) samples were taken and the reaction was stopped by addition of loading buffer and boiling. All samples were analyzed by SDS-PAGE and western blotting, followed by immunodetecting using anti-phosphotyrosine- and His-antibodies.

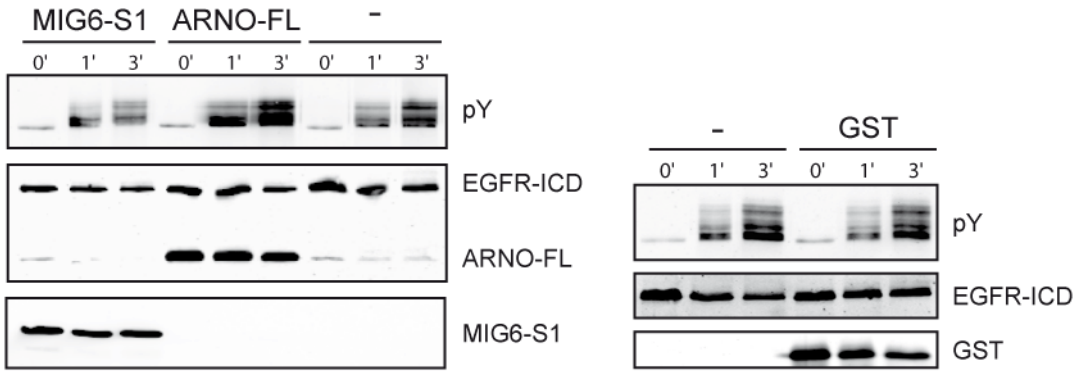

Figure 43 ARNO enhances autophosphorylation of EGFR-ICD

Representative western blots of autophosphorylation experiments of EGFR-ICD in the presence of full-length ARNO (ARNO-FL), segment 1 of MIG6-EBR (MIG6-S1) or GST before (0') or 1min/3min after addition of ATP (1', 3') . Proteins were separated by SDS-PAGE and were analyzed by immunoblotting. EGFR-ICD and ARNO were detected by anti-His antibody, phosphorylated EGFR-ICD by anti-pY antibody, MIG6 and GST by anti-GST antibody.

As expected, addition of ATP led to a time dependent phosphorylation of EGFR-ICD (Figure 43, upper panel). Whereas preincubation with GST had no effect, preincubation with MIG6-S1 reduced EGFR-ICD autophosphorylation, validating that the activation of the EGFR-ICD kinase still depends on the formation of the asymmetric dimer. When ARNO-FL was added to the reaction an increased autophosphorylation or EGFR-ICD was found. Total protein loading was controlled by detection of His or GST, respectively (middle and lower panels).
A similar level of stimulation of EGFR-ICD autophosphorylation was seen when the isolated Sec7 domain or Sec7-E156K of ARNO was added to an autophosphorylation reaction of EGFR-ICD.

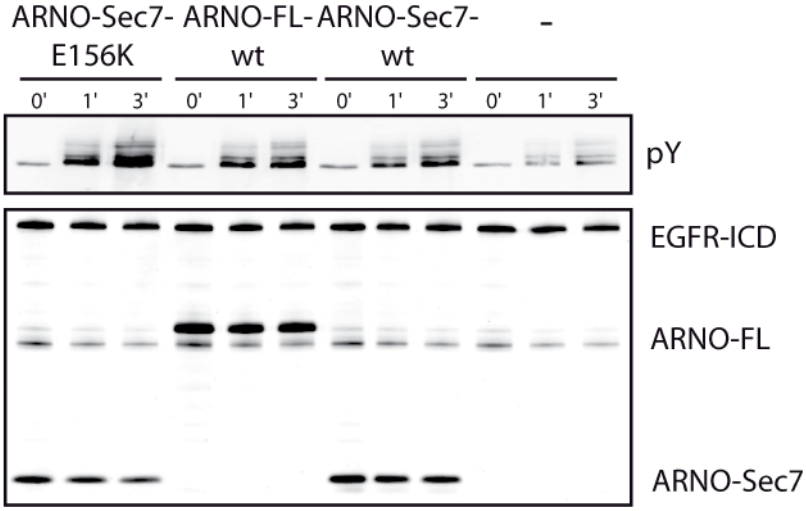

Figure 44 ARNO-Sec7 and GEF-inactive ARNO enhance autophosphorylation of EGFR-ICD
Representative western blots of autophosphorylation experiments of EGFR-ICD in the presence of full-length ARNO (ARNO-FL), ARNO-Sec7 or the GEF-inactive Sec7 mutant ARNO-Sec7-E156K. Proteins were separated by SDS-PAGE and were analyzed by immunoblotting. EGFR-ICD and ARNO were detected by anti-His antibody, phosphorylated EGFR-ICD by anti-pY antibody.

Taken together these results strongly argue for cytohesins acting directly on the intracellular domains of dimerized EGFR as conformational activators.

IV.1.6 Chemical inhibition of cytohesins diminishes proliferation of human lung cancer cell lines in vitro and in vivo

Lung cancer is a multifaceted disease and can broadly be divided into small-cell lung cancer (SCLC, comprising 20% of lung cancers), and non-small-cell lung cancer (NSCLC, comprising 80% of lung cancers). Whereas SCLC is a tumor of neural crest origin, NSCLC is thought to originate in lung epithelial cells, and comprises diverse histological subtypes including adenocarcinoma, bronchioloalveolar, squamous, anaplastic and large-cell carcinomas [48].
Advanced non-small-cell lung cancer (NSCLC) is the leading cause of cancer related deaths in the world and can be divided in different groups based on the status of EGFR: EGFR or its

ligands are overexpressed in 50% of NSCLCs. Furthermore, EGFR mutations are present in ~10% of cases in North America and Western Europe, but ~30–50% of cases in individuals of East Asian descent. Molecular analysis of EGFR in NSCLCs revealed a group of specific mutations in the gene that encodes EGFR. Exon 19 mutations characterized by in-frame deletions of amino-acids 747–750 account for 45% of mutations, exon 21 mutations resulting in L858R substitutions account for 40–45% of mutations, and the remaining 10% of mutations involve exon 18 and 20. Additionally, a second site mutation in Exon 18, T790M, which leads to resistance to Iressa (Gefitinib) is found in ~50% of NSCLCs with mutated EGFR. In addition, about 15–30% of NSCLCs harbor activating mutations in codons 12 and 13 of the KRAS gene. Interestingly, KRAS and EGFR mutations seem to be mutually exclusive in NSCLC [46, 48, 115].

IV.1.6.1 SecinH3 decreases proliferation of human lung cancer cell lines expressing wild-type EGFR

IV.1.6.1.1 SecinH3 inhibits proliferation of H460 and A549 cells

H460 and A549 cells are known to harbor an activating mutation of KRAS and therefore to express normal levels of wild-type EGFR [103]. Although these cells are described as resistant to Iressa they still depend on the signaling of EGFR, since knockdown of EGFR with siRNA resulted in reduced cell proliferation and induction of apoptosis [116-117].

Having shown that ARNO enhances EGFR activation in H460 cells I wondered whether cytohesins may also promote the proliferation of the tumor cells. To test this possibility I determined the proliferation rate of H460 cells in the presence or absence of SecinH3.

I seeded the cells in 96well plates and after adherence cells were treated with different concentrations of SecinH3 or Secin16, the control compound XH1009, the known EGFR kinase domain inhibitor Iressa (Gefitinib) or solvent alone (DMSO, 0.4% final concentration, RPMI, 1%FCS). After 72h the numbers of cells were quantified by using a commercially available 3-(4,5-dimethylthiazol-2-yl)-2,5-diphenyltetrazolium bromide (MTT) assay (CellTiter96 Non-Radioactive Cell Proliferation Assay, Promega). The assay is based on the cellular conversion of a soluble tetrazolium salt into an insoluble formazan product which can be detected colometrically, after lysis of the cells and resolubilisation of the reduced formazan. Figure 45 shows the relative cell number after 72h of proliferation. The cell number in the solvent-treated samples was set to 1.

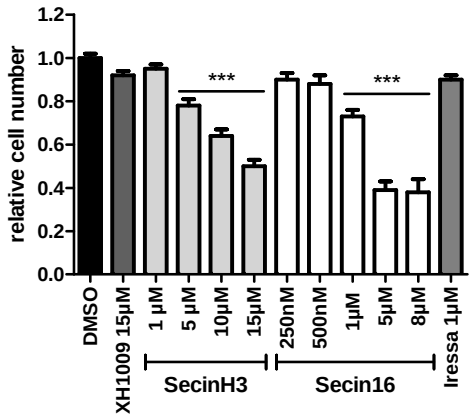

Figure 45 Secins inhibit the proliferation of H460 cells

The diagram represents the relative cell number (MTT assay) after 72h treatment with the indicated compounds and concentrations. The cell number in solvent-treated samples was set to 1. Data are represented as mean ±SEM, ***: $p<0.001$, n=12.

SecinH3 significantly ($p<0.001$, n=12) inhibits cell proliferation in a concentration dependent manner (IC50: SecinH3 14.6µM), whereas the control compound XH1009 showed no effect. Iressa showed only moderate cell proliferation inhibition, confirming the reported resistance of H460 cells to this drug.

The recently identified cytohesin inhibitor Secin16, which showed a significantly better IC50 in vitro as compared to SecinH3, was also tested for inhibition of cell proliferation. Secin16 inhibited proliferation of H460 cells in a concentration dependent manner with an IC50 of 1.4µM ($p<0.001$, n=12).

I also analyzed the effect of SecinH3 and Secin16 on the proliferation of A549 cells, which resemble H460 cells as they express wild-type EGFR and contain an activating mutation in KRAS. The obtained IC50 values (SecinH3: 15µM, Secin16 2.5µM) for the inhibition of proliferation in A549 cells were in a similar range as for H460 cells.

Interestingly, the maximal observed reduction in cell number after treatment with SecinH3 and Secin16 was around 60% in either cell line as compared to the untreated cells. This observation might indicate a cytostatic rather than a cytotoxic effect of the compounds.

Taken together, these results show that inhibition of cytohesins leads to a diminished proliferation of H460 and A549 cells.

IV.1.6.1.2 SecinH3 reduces growth of H460 cell tumor xenografts in nude mice

To test whether SecinH3 was also capable of reducing tumor growth in vivo, tumor xenografts were generated by subcutaneous injection of H460 cells into nude mice (all mice experiments were done by Lukas Heukamp and Katharina König, Pathology, University of

Bonn, with my assistance). After tumor establishment, mice were randomized in two groups and treated with SecinH3 (2.5mM in 50% isotonic glucose/DMSO solution) or carrier alone (50% isotonic glucose/DMSO solution) by daily intraperitoneal injection (100µl). Tumor volume was measured daily and calculated by using the formula $\pi/6 \times$ larger diameter $\times$ (smaller diameter)^2.

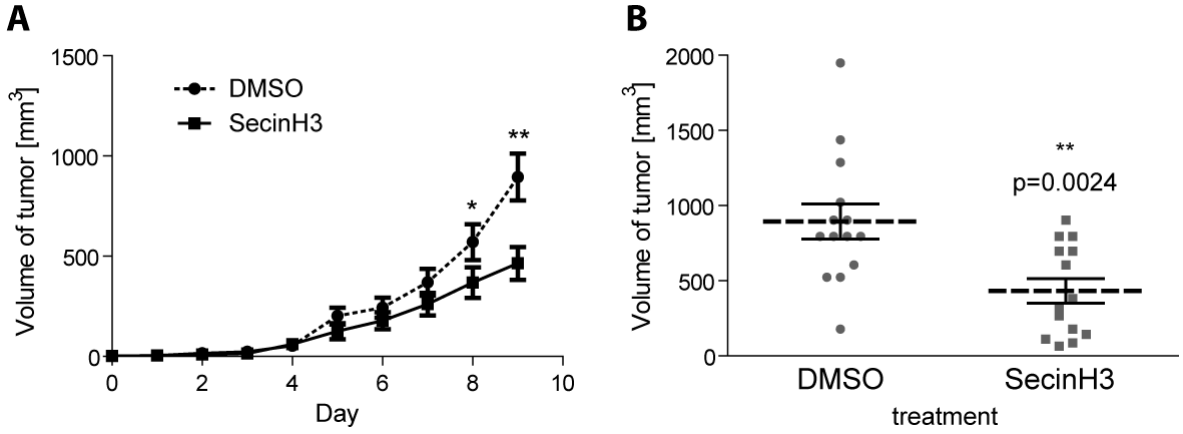

Figure 46 SecinH3 decreases proliferation of H460 xenografts in nude mice

Mice bearing H460 tumor xenografts were treated daily with SecinH3 or solvent by intraperitoneal injection. Tumor volume was measured daily.

A: The diagram summarizes the mean tumor volume measured on the indicated day after begin of treatment (day 8 p=0.035*, day 9 p=0.0024**, n=14 for each group). Data are represented as mean ±SEM.

B: Scatter blot of measured tumor volumes on day 9. Shown are the measured tumor volumes on day 9 and the mean ±SEM (p=0.0024**, n=14 for each group).

As Figure 46 depicts, treatment with SecinH3 resulted in significantly reduced tumor growth. Mice were sacrificed on day 9 after tumor establishment due to a tumor volume of >1000mm^3 in accordance with the German Laws for Animal Protection and with the guidelines of the local animal protection committee.

Furthermore, immunohistochemical staining for apoptosis by terminal deoxynucleotidyl transferase dUTP nick end labelling (TUNEL) revealed an elevated rate of apoptosis in tumor xenografts treated with SecinH3 (Figure 47).

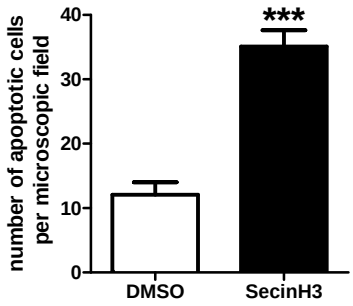

Figure 47 SecinH3 induced apoptosis in H460 xenografts

TUNEL assay of H460 xenografts in nude mice after treatment with SecinH3 or solvent (DMSO) for 9days. Data are represented as mean ±SEM (n=14, ***: p<0.001).

Taken together, these data demonstrate that the chemical inhibition of cytohesins reduces the proliferation of H460 in vitro and in vivo.

IV.1.6.2 SecinH3 also reduces growth of lung cancer cell lines with EGFR mutations

In frame deletion of amino-acids 747–750 of EGFR is the most abundant mutation found in NSCLCs. To test whether cells harboring this mutation still depend on cytohesins, I analyzed the proliferation of PC9 cells, that express the del(747-750) variant of EGFR, in the presence of SecinH3 and Secin16 as previously described.

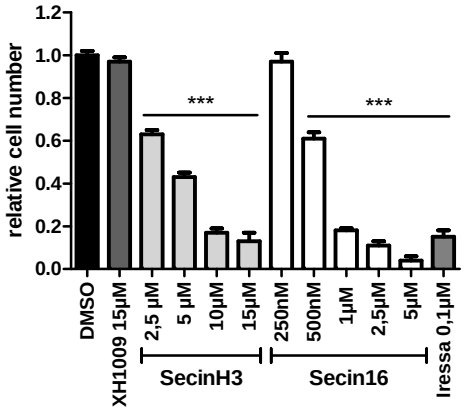

Figure 48 Secins inhibit the proliferation of PC9 cells

The diagram represents the relative cell number (MTT assay) after 72h treatment with the indicated compounds and concentrations. The cell number in solvent-treated samples was set to 1. Data are represented as mean ±SEM, ***: $p<0.001$, n=9.

As Figure 48 demonstrates PC9 are highly sensitive to chemical inhibition of cytohesins. Both SecinH3 and Secin16 showed a concentration dependent inhibition of cell proliferation with an IC50 of 3.3µM and 0.6µM, respectively, whereas XH1009 had no effect. As expected even low concentrations of Iressa (0.1µM) nearly completely blocked cell proliferation.

In summary, proliferation of PC9 cells, which contain the del(747-750) variant of EGFR, still depends on cytohesins.

IV.1.6.3 SecinH3 induces cell-cycle arrest in PC9 cells

As inhibition of EGFR signaling in EGFR-dependent cells results in cell-cycle arrest and induction of apoptosis, I first examined SecinH3-treated PC9 cells for changes in cell-cycle.

The eukaryotic cell cycle is comprised of four phases: G1, S, G2 and M phase. Chromosome duplication occurs during S phase (S for synthesis), which requires 10-12 hours and occupies about half of the cell-cycle time in a rapidly dividing mammalian cell. After S phase, chromosome segregation and cell division occurs in M phase (M for mitosis), which requires

less than an hour. These main phases of cell cycle are separated by two gap phases (G1 and G2 phase), which allow the cell to control and eventually delay the next phase. The G1 phase between M phase and S phase enables the cell to check for external conditions and extracellular signals. In the absence of external proliferation stimuli, cells can delay progress in the cell cycle through G1 and can even enter a permanent resting state called G0. Once extracellular signals are favorable for cell growth, the cells pass a restriction point near the end of G1 and proceed to DNA replication, even if the extracellular signals are removed. After DNA synthesis the cell enters the second gap phase, G2, with the G2/M checkpoint, in which the cells prepare for mitosis. G2 and S phase are often referred to as interphase [118].

One technique to assess the stage that a cell has reached in the cell cycle is by measuring its DNA content. I used flow cytometry in order to analyze the cell-cycle of PC9 cells. Therefore, I preincubated the cells for 12h with SecinH3 or solvent (DMSO 0.4%) in basal medium containing 1% FCS and harvested the cells by trypsinization. Subsequently cells were fixed in methanol and stained with the fluorescent DNA-binding dye TOPRO-3 iodide (Invitrogen). After washing, I analyzed the DNA content of the cells by flow cytometry [118-119].

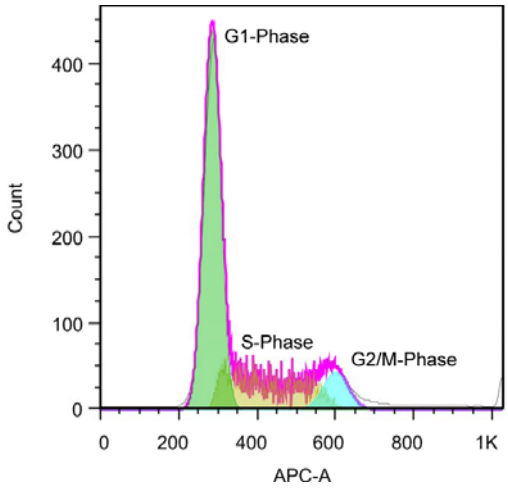

Figure 49 Cell cycle analysis of PC9 cells

Typical histogram obtained for DNA-staining of PC9 cells. The signal distribution was fitted by the Watson model showing G1 (green), S (yellow) and G2/M (blue) phases of cell cycle. PC9 cells were fixed with methanol and stained with TOPRO-3 iodide (DNA dye). DNA content was analyzed by flow cytometry. Count: number of cells, APC-A: DNA content (TOPRO signal).

Figure 49 shows a typical result obtained for proliferating PC9 cells. Since TOPRO-3 iodide becomes fluorescent when it binds to DNA, the amount of detected fluorescence per cell is directly proportional to the amount of DNA in the cell. Two different "peaks" connected by an intermediate signal are visible which correspond to the cells in G1, S or G2/M phase: Cells that have an unreplicated complement of DNA are in G1 (first, green peak, ~50% of all cells), those that have a fully replicated complement of DNA with twice the DNA content compared to G1 are in G2 or in the beginning of M phase (~20% of all cells, last peak, blue), and those

that have an intermediate amount of DNA are in S phase (~30% of all cells, yellow). The histograms were quantitatively analyzed by FlowJo-software to obtain the percentage of cells in the different phases of cell-cycle (Watson model).

Figure 50 illustrates typical histograms of SecinH3-treated and untreated cells. SecinH3 increased the percentage of cells in the G1 phase of the cell-cycle (~68%) and accordingly decreased the cells in S (~23%) and G2/M phases (~10%), indicating an arrest in G1 of the cell cycle. The diagram summarizes the percentage of cells in the indicated cell-cycle phases. All changes were significant (***, $p<0.0001$, $n=6$).

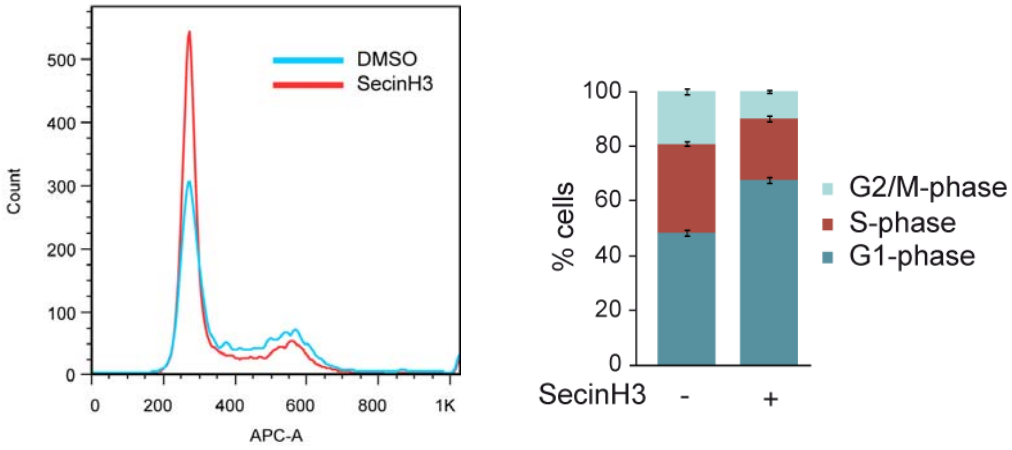

Figure 50 SecinH3 induces G1 arrest in PC9 cells

PC9 cells were treated with SecinH3 (15µM) or DMSO for 24h, fixed and stained with TOPRO-3 iodide. DNA-content was analyzed by flow cytometry. The histogram shows the DNA-content of SecinH3 or DMSO treated cells. The diagram summarizes the percentage of cells in the indicated cell-cycle phases. Data are represented as mean ±SEM. All changes were significant (***, $p<0.0001$, $n=6$). Count: number of cells, APC-A: DNA content (TOPRO signal).

These results indicate that chemical inhibition of cytohesins induces growth arrest in PC9 cells probably as a reaction of diminished EGFR signaling.

IV.1.6.4 SecinH3 induces apoptosis in PC9 cells

Cells arrested in G1 might either enter a resting state (G0) or might initiate apoptosis due to the lack of pro-proliferating or anti-apoptotic signals.

To investigate the fate of G1 arrested PC9 cells I performed an Annexin V apoptosis assay by flow cytometry. This assay is based on characteristic changes in the plasma membrane of apoptotic cells. The negatively charged phospholipid phosphatidylserine is normally exclusively located in the inner leaflet of the lipid bilayer of the plasma membrane, but flips to the outer leaflet in apoptotic cells, where it can serve as a marker. The phosphatidylserine on the surface of apoptotic cells can be visualized with a labelled form of the protein Annexin V, which specifically binds to this phospholipid [120].

I preincubated PC9 cells for 48h with 15µM SecinH3, 1µM Secin16 or solvent (0.4%DMSO) in basal medium containing 1% FBS, harvested by trypsinization and stained the cells with a FITC-labelled form of Annexin V and with TOPRO 3 iodide. Since the cells were not fixed, the membrane impermeable dye TOPRO 3 iodide could only stain cells which already acquired damage in their plasma membrane due to the process of cell death. I analyzed the cells by flow cytometry and blotted the measured signals for Annexin V and TOPRO in a dot blot.

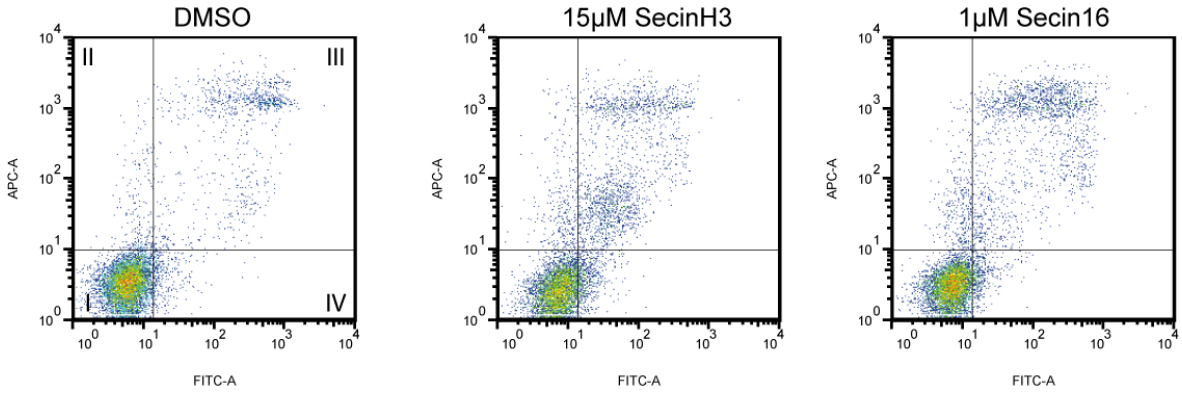

Figure 51 Secins increase the number of apoptotic PC9 cells

Dot blot of TOPRO-3 and FITC-Annexin V stained PC9 cells after 48h treatment with solvent (0.4% DMSO), 15µM SecinH3 or 1µM Secin16. FITC-A: Annexin V, APC-A: TOPRO. Quadrant I: unstained or healthy cells, quadrant II: early apoptotic cell, quadrant III: intermediate apoptotic cells, quadrant IV: late apoptotic cells.

The cells fall into four categories represented by the four quadrants of the dot blot: Unstained or solvent-treated cells show little TOPRO staining of DNA (quadrants 1+2), due to an intact plasma membrane and show only weak staining for phosphatidylserine (quadrants 1+4) and are therefore mainly found in quadrant 1 (FITC -, TOPRO -). Treatment with SecinH3 or Secin16 led to a strong increase in FITC positive/TOPRO negative (quadrant 2, early apoptotic), double positive (quadrant 3, intermediate apoptotic) and TOPRO positive/FITC negativ (quadrant 4, late apoptotic) cells and to a concomitant decrease of double negative cells (quadrant 1, healthy cells). Figure 52 summarizes the percentage of apoptotic cells (quadrants 2-4) in solvent- and SecinH3/Secin16 treated cells (***, $p<0.001$).

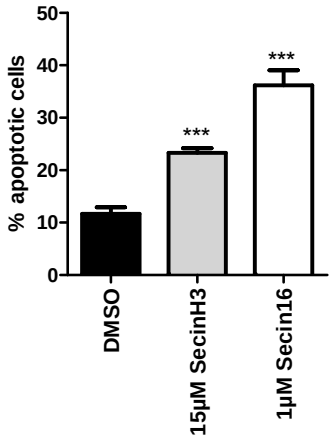

Figure 52 SecinH3 and Secin16 induce apoptosis in PC9 cells

Quantitative analysis of apoptotic PC9 cells (quadrants 2-4) after 48h treatment with solvent (0.4% DMSO), 15µM SecinH3 or 1µM Secin16. (***, $p<0.001$, n=3).

Taken together, these data demonstrate that chemical inhibition of cytohesins in EGFR-dependent PC9 cells inhibits proliferation by inducing a growth arrest in the G1 phase of cell-cycle, which leads to apoptotic cell death.

IV.1.6.5 SecinH3 reduces growth of PC9 tumor xenografts in nude mice

Having shown that SecinH3 decreases the proliferation of PC9 cells by inducing a G1 arrest followed by apoptosis, I was interested whether SecinH3 treatment reduces tumor growth in vivo. Therefore tumor xenografts were generated by subcutaneous injection of PC9 cells into nude mice (experiments were done by Roman Thomas, Roland Ullrich and Sampurna Chatterjee, MPI Köln). After tumor establishment mice were randomized in two groups and treated with SecinH3 (2.5mM in 75% isotonic glucose/25% DMSO solution) or carrier alone (75% isotonic glucose/25% DMSO solution) by daily intraperitoneal injection (100µl). Cell proliferation in the tumor was followed by [^{18}F]fluoro-L-thymidine uptake positron emission tomography ([18F]FLT PET). Therefore [^{18}F]FLT was administered i.v. (tail vein) on day 7 into experimental animals. PET images were performed 60 min after injection. Data evaluation was based on a region of interest (ROI) analysis of PET images to determine maximal radioactivity concentration within the tumors. To determine the uptake ratio a reference ROI was placed in the mediastinum.

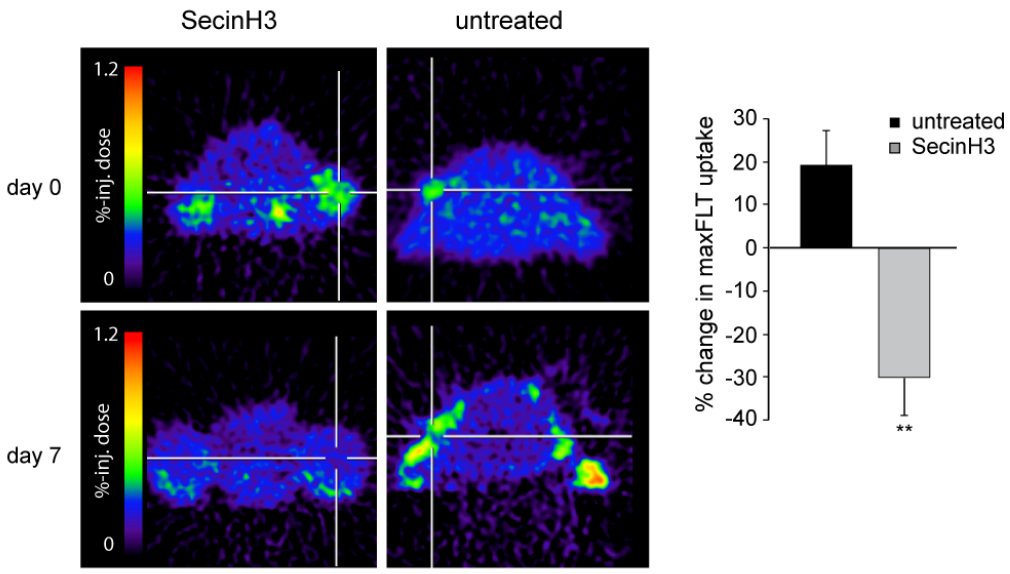

Figure 53 SecinH3 reduces [^{18}F]FLT uptake of PC9 xenografts in nude mice

Representative [^{18}F]fluoro-L-thymidine uptake positron emission tomography ([^{18}F]FLT PET) images of mice bearing PC9 xenografts before and 7 days after treatment with SecinH3 or DMSO. The diagram summarizes the change in maximal FLT uptake. **, $p<0.01$, n=7)

As Figure 53 depicts, tumors in the SecinH3 treated mice showed significantly less uptake of [^{18}F]FLT after 7 days of treatment in comparison to tumors in the solvent treated mice, indicating reduced tumor growth. The diagram represents the mean percentage of injected dose per gram (%ID/g) measured in the tumor of 7 animals (**, $p<0.01$).

Furthermore, immunohistochemical staining of the cell proliferation marker Ki-67 [121-122], which is expressed in all active phases of cell-cycle (G1, S, G2 and M phase) but not in resting cells (G0), in resected tumors confirmed reduced cell proliferation (Figure 54A).

TUNEL staining showed an increase in apoptotic cells in the tumors of SecinH3-treated animals (Figure 54B, experiments done by Lukas Heukamp).

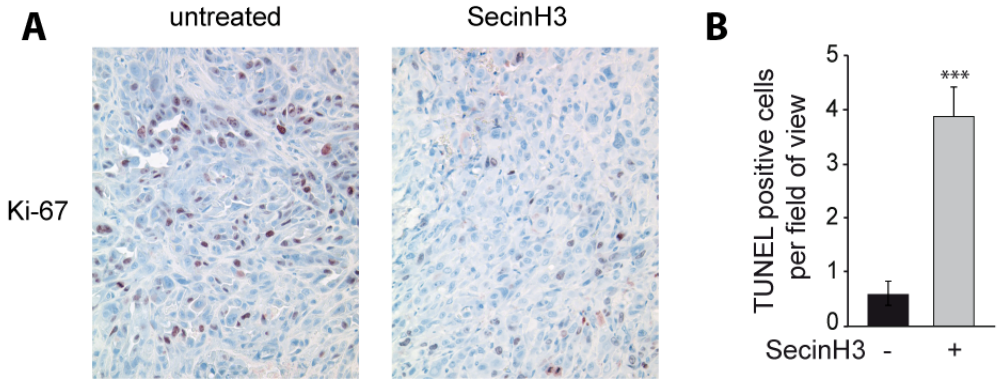

Figure 54 SecinH3 decreases proliferation of PC9 xenografts and induces apoptosis

A: Ki-67 staining of PC9 xenografts in nude mice after treatment with DMSO or SecinH3 for 7 days.
B: TUNEL assay of PC9 xenografts in nude mice after treatment with DMSO or SecinH3 for 7 days. The diagram shows the number of TUNEL-positive cells per high power microscopic field. Per treatment group 10 representative fields were counted, ***$p<0.001$). Data are represented as mean ±SEM.

Taken together, these data demonstrate that chemical inhibition of cytohesins reduces the proliferation of EGFR-dependent tumor cells in vitro and in vivo.

IV.1.6.6 Chemical inhibition of cytohesins decreases proliferation in various EGFR-dependent cell lines independent of the EGFR mutation status

To further substantiate the finding that chemical inhibition of cytohesins reduces proliferation of EGFR-dependent lung cancer cells, I performed cell proliferation assays in a set of different EGFR dependent lung adenocarcinoma derived cell lines, harboring the most common mutations in EGFR. Table 1 summarized the obtained IC50 values for SecinH3 and Secin16, and the known IC50 values for Iressa. XH1009 showed no effect (data not shown).

Cell line	EGFR	KRAS	further anomaly	IC50 SecinH3	IC50 Secin16	IC50 Iressa	
H460	wt	mut, G61H		15µM	1.5µM	>5µM	[103]
A549	wt	mut, G12S		15µM	2.5µM	>5µM	[123]
H3255	L858R	wt		13µM	1.0µM	89nM	[124]
H1975	L858R, T790M	wt		n.d.	5.0µM	>5µM	[124]
PC9	del(E747_A750)	wt		3.3µM	0.6µM	31nM	[124]
H1781	HER2 G776insV_G/C	wt		15µM	0.5µM	>5µM	[125]
H1838	wt, amplf.	wt	MET amplf.	n.d.	n.d.	2µM	[123]

Table 1 Characteristics of the used human lung cancer cell lines

Used human lung cancer cell lines. EGFR status, KRAS status, anomalies and IC50 values for Iressa are given as reported in the literature. IC50 values for SecinH3 and Secin16 were determined by MTT proliferation assays. n.d.: not detectable

Chemical inhibition of cytohesins significantly decreases cell proliferation in all tested EGFR-dependent cell lines except of the cell line H1838, which is described as partially or weakly EGFR-dependent due to strong expression of the receptor tyrosine kinase MET, suggesting an EGFR specific inhibition of proliferation. SecinH3 and Secin16 were even capable of inhibiting proliferation of the HER2 dependent cell line H1781. Since Secin16 showed only a weak inhibitory effect on the cell line H1975 (in comparison to H3255 cells), carrying the gate keeper mutation T790M which renders the receptor resistant to Iressa treatment, I further investigated whether this mutation also mediate resistance to chemical inhibition of cytohesins.

Therefore I made use of the murine bone marrow–derived cell line Ba/F3. Ba/F3 cells depend on the growth factor interleukin-3 (IL-3). Expression of oncogenes, including EGFR, renders the cells IL-3 independent and critically addicts the cells to the oncogene. Therefore,

Ba/F3 cells transfected with EGFR provide valuable system to investigate the selectivity of EGFR targeting compounds.

I treated Ba/F3 cells expressing different variants of EGFR, with SecinH3, Secin16 or Iressa in the absence of IL-3 for 72h and measured cell proliferation by MTT as described.

Iressa efficiently blocked the proliferation of EGFR L858R and EGFR del(E747_A750) dependent Ba/F3 cells, whereas there was no effect on the proliferation of wild-type cells or Ba/F3 cells carrying the gate keeper mutation T790M, validating the EGFR signaling dependency of the cells and the functionality of the EGFR mutations.

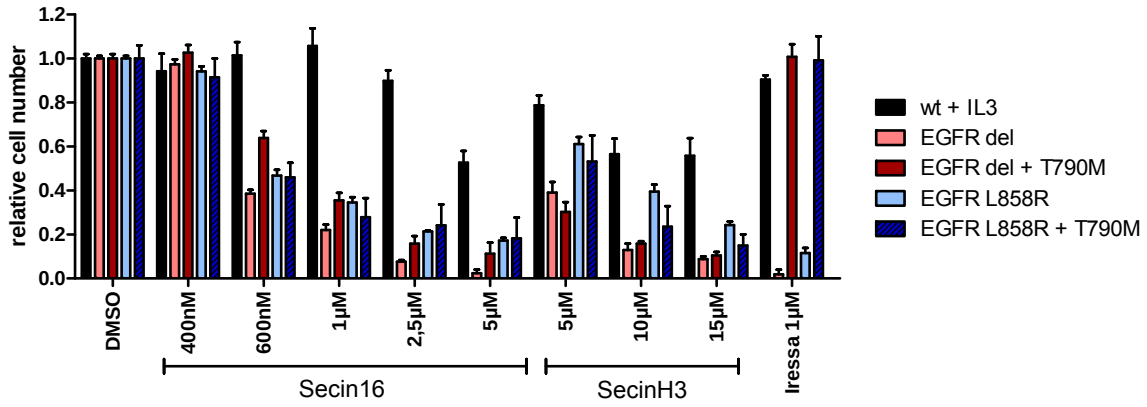

Figure 55 Secins inhibit proliferation of EGFR dependent BA/F3 cells

The diagram shows the relative cell number (MTT assay) after 72h treatment with the indicated compounds and concentrations. Wild-type BA/F3 cells (wt) were grown in the presence of IL-3, whereas BA/F3 cells stably transfected with EGFR del (E747_A750), EGFR L858R alone or in combination with T790M were grown the in the presence of G418. Data are represented as mean ±SEM. ***, $p<0.001$ for all tested concentrations and in comparison to wt BA/F3, n=8.

Ba/F3	SecinH3 IC50	Secin16 IC50
wt, IL-3 dependent	n.d.	n.d.
EGFR L858R	10µM	520nM
EGFR L858R + T790M	10µM	580nM
EGFR E747_A750	4.5µM	560nM
EGFR E747_A750 + T790M	3.5µM	500nM

Table 2 IC50 values of SecinH3 and Secin16 for inhibition of cell proliferation in Ba/F3 cells

IC50 values for SecinH3 and Secin16 were determined in MTT proliferation assays. n.d.: not detectable.

Whereas SecinH3 and Secin16 had only a very weak effect of on the proliferation of untransfected, wild-type and IL-3 dependent Ba/F3 cells, SecinH3 and Secin16 showed a significantly pronounced effect on the proliferation of EGFR-dependent Ba/F3 cells (***, $p<0.001$ for all tested concentrations, n=8). Cells expressing the del(E747_A750) form of EGFR of EGFR showed a higher sensitivity to inhibition of cytohesins by SecinH3 and Secin16 as compared to cells expressing EGFR L858R. There was no significant difference

between cells carrying a second site mutation in EGFR (T790M) in comparison to cells harboring only one mutation in EGFR.

Table 2 summarizes the obtained IC50 values.

In conclusion these data indicate that chemical inhibition of cytohesins diminishes proliferation of EGFR-dependent lung cancer cell lines, independent of their EGFR status.

IV.1.7 Overexpression of cytohesins in human lung adenocarcinoma correlates with enhanced EGFR signaling

IV.1.7.1 Cytohesins are overexpressed in human lung adenocarcinoma

Enhanced EGFR signaling is known to be a hallmark in many cancers. Having shown that ARNO enhances EGFR activation and that proliferation of EGFR-dependent human lung adenocarcinoma derived cell lines is strongly reduced by chemical inhibition of cytohesins; I wondered whether ARNO or other cytohesins are overexpressed in lung cancer.

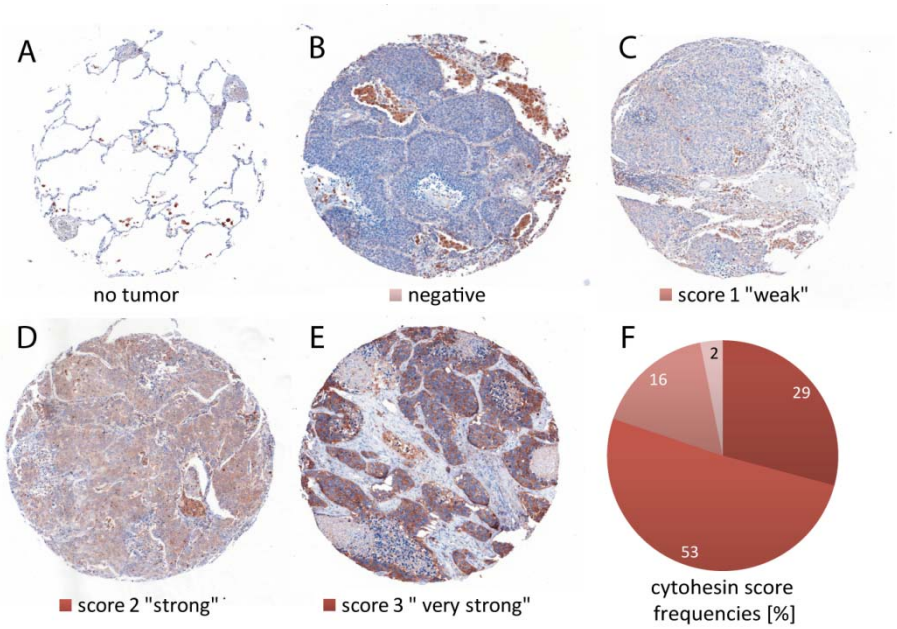

Figure 56 ARNO is overexpressed in human lung adenocarcinoma

Sections of resected human lung adenocarcinomas were stained for ARNO/cytohesin-1 and DAPI. ARNO/cytohesin-1 expression level was analyzed using a four-tier scoring system. Shown are representative images of (A) lung tissue without tumor, (B) tumor with background/negative, (C) weak, (D) strong, (E) very strong ARNO/cytohesin-1 expression. The diagram (F) summarizes the frequencies of tumors with the respective ARNO staining.

To address this question, a collection of primary human lung adenocarcinomas were immunostained with an antibody detecting ARNO and cytohesin-1 (there was no ARNO specific antibody available). Staining intensities were individually evaluated by three independent observers, applying a four-tier scoring system: no or background staining (0),

weak (1), strong intensity (2), very strong (3) (experiments were done by Lukas Heukamp, Sebastian Zimmer and Lisa Meffert, Pathology, University of Bonn).

Whereas normal lung tissue showed only background or weak staining, 82% of the carcinomas showed moderate to strong ARNO/cytohesin-1 staining, demonstrating cytohesin upregulation in a large fraction of lung adenocarcinomas (Figure 56).

IV.1.7.2 Cytohesin overexpression correlates with enhanced EGFR signaling in human lung adenocarcinomas

According to the data obtained in cell culture, increased cytohesin expression should result in enhanced EGFR autophosphorylation in these tumors. To investigate this hypothesis, the same set of adenocarcinomas was stained for phosphorylated EGFR, total EGFR, phosphorylated Akt and phosphorylated p42/p44 and scored as described (Figure 57, experiments were done by Lukas Heukamp, Sebastian Zimmer and Lisa Meffert, Pathology, University of Bonn). To test for a correlation between the expression level of ARNO/cytohesin-1 and the level of phosphorylated EGFR or downstream proteins, I performed a Spearman correlation analysis assuming Gaussian distribution (GraphPadPrism software). Indeed, I found a highly significant correlation between the expression level of ARNO/cytohesin-1 and the levels of EGFR autophosphorylation ($p=0.002$). Increased EGFR phosphorylation was not due to overexpression of the receptor because total EGFR expression was independent of ARNO/cytohesin-1 expression ($p=0.581$). The phosphorylation of Akt and p42/44 (Erk1/2) was also significantly correlated with higher ARNO/cytohesin-1 expression ($p=0.002$ and $p=0.025$, respectively), suggesting that the enhanced activation is not restricted to the EGFR itself but continues along these two major branches of the EGFR signaling pathway.

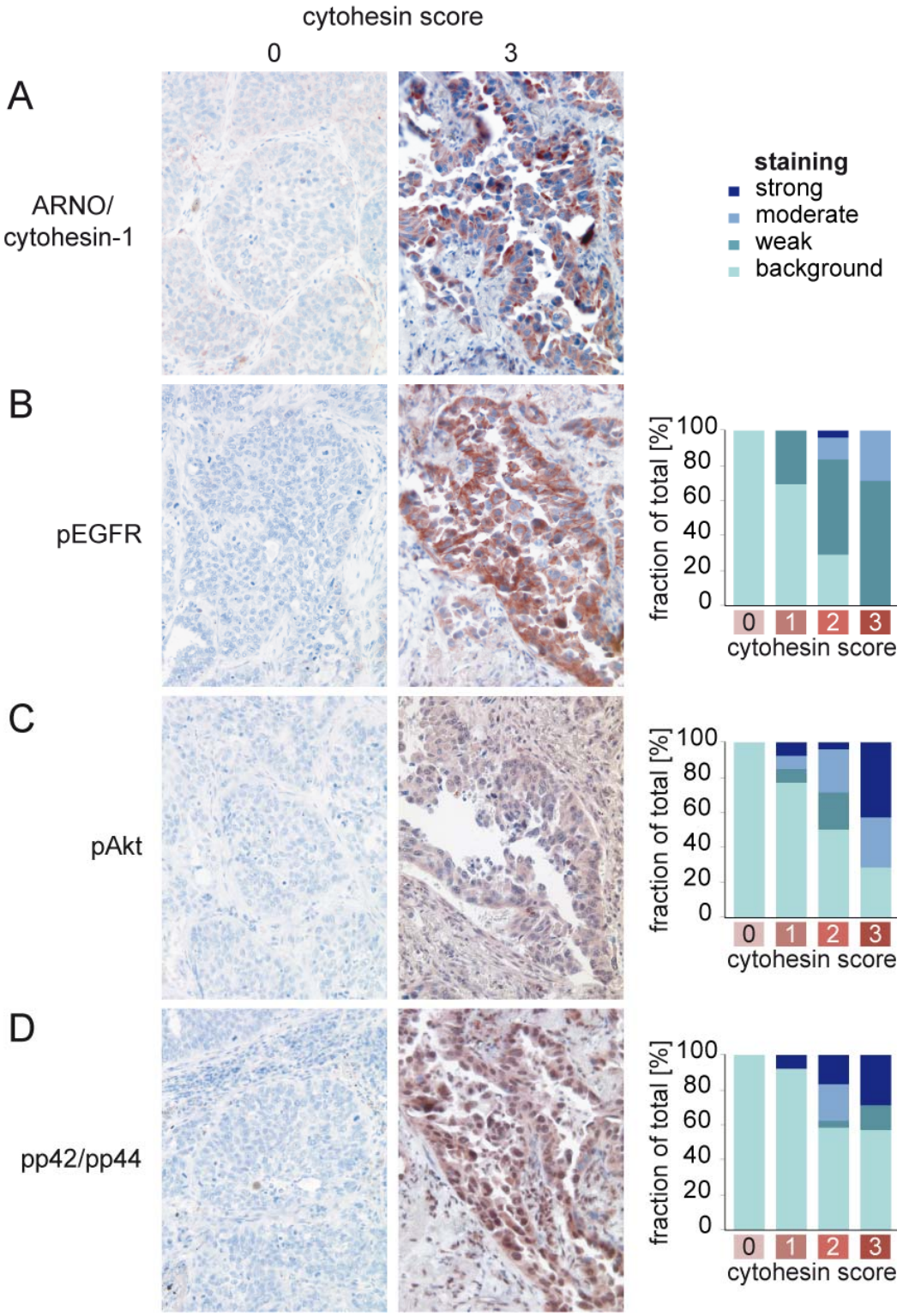

Figure 57 High expression levels of ARNO/cytohesin-1 correlate with increased EGFR signaling in human lung adenocarcinomas

Consecutive sections of human lung adenocarcinoma were stained for ARNO/cytohesin-1 (A), pEGFR_Y1086 (B), pAkt_T308 (C) or pp44/42_T202/Y204 (D). Shown are representative images of tumors with background (left) or high (middle) expression of ARNO/cytohesin-1. The diagrams depict the phosphorylation levels of the respective protein in correlation to the cytohesin score (p=0.002 for pEGFR, p=0.002 for pAkt, p=0.025 for pp44/42, n=45).

IV.2 Identification of improved cytohesin antagonists in vitro

IV.2.1 Virtual screening

High-throughput screening (HTS) currently plays a major role as a source of novel active molecules that serve as leads for drug development and as tools for biomedical research. As an alternative, virtual screening of chemical libraries formatted in silico can be applied to identify new active chemotypes. Virtual screening is based on structural information about the target and/or known ligand. That is why most ligand based methods require as many active and inactive reference compounds as possible, since the probability of success substantially increases with the amount of available compound and structure-activity-relationship (SAR) data. However, in the case of cytohesins, only one inhibitory chemotype, the pan-active cytohesin inhibitor SecinH3 is known. Structure-activity-relationship studies revealed a limited number of SecinH3 related compounds, without significant improvements in the inhibitory potency. Based on these limited information a virtual screening approach combining fingerprint similarity searching and support vector machine was tailored to identify new small molecule chemotypes for the study of cytohesins. In this way, a library containing 145 structures was established (calculations were done by Dagmar Stumpfe and Jürgen Bajorath, University of Bonn) and subsequently named as second generation SecinH3 chemotypes [126].

IV.2.2 Establishment of a GDP/GTP-exchange assay for ARF1

In order to test the predicted structures for an inhibitory effect on cytohesins, I set out to establish a simple and robust assay for monitoring the exchange activity of cytohesins, based on the protocol for an already published exchange assay on ADP ribosylation factor 1 (ARF1) [127].

Guanine nucleotide exchange factors (GEFs) catalyze the dissociation of the nucleotide from the G protein by modifying the nucleotide-binding site in such a way, that the nucleotide affinity is decreased, which results in the release of the nucleotide [77]. Since G proteins show a nanomolar to picomolar affinity for GDP and GTP, the GEF is subsequently replaced by a new nucleotide. Cytohesins bind to the binary complex of ARF and GDP, in which the GDP is sandwiched between two loops called switch 1 and switch 2 (residues 38–52 and 69–84 in Arf1), which are connected by an interswitch region comprising two ß-strands [76, 78, 128-129]. Switch regions 1 and 2 interact with the phosphates of GDP and a coordinating

magnesium ion, thereby stabilizing the GDP bound conformation of ARF. In the cytosolic full-length form of ARF-GDP the myristoylated amphipathic amino-terminal helix locks the interswitch in a retracted conformation that blocks nucleotide exchange. Its reversible binding to membrane releases the hasp and opens up the locked conformation of the interswitch to enable nucleotide exchange [74].

Binding of cytohesin displaces switch 1 to open up the nucleotide binding site and GDP is kicked out of the transiently formed ternary complex between cytohesin, ARF and GDP. A glutamate acid finger of the cytohesin Sec7 domain approaches the negatively charged phosphate of GDP and displaces the coordinated magnesium ion thereby perturbing the interaction surface in the phosphate-binding region, which leads to nucleotide release [129]. In the course of the exchange reaction a new nucleotide displaces the GEF, since the nucleotide weakens the affinity of the G protein for the GEF.

Conformational changes accompanying ARF activation can be monitored by measuring the intrinsic fluorescence of ARF. In proteins, the three aromatic amino acids phenylalanine, tyrosine and tryptophan are fluorescent [108]. A valuable feature of intrinsic protein fluorescence is the high sensitivity to its local environment. Changes in the emission spectra of tryptophan often occur in response to conformational transition. In the case of ARF1, an increase in intrinsic tryptophan fluorescence can be used to monitor GDP to GTP exchange [127].

To enable measurements of nucleotide exchange on ARF1 in the absence of membranes I made use of NΔ17ARF1, a truncated form of ARF1, lacking the first 17 amino acids, holding the protein in an exchange-active state [74-75].

First, I preloaded purified NΔ17ARF1 (1μM) with GDP (80μM) in the presence of EDTA (2mM) by chelating the magnesium ion responsible for nucleotide binding and stabilized the resulting NΔ17ARF1-GDP complexes by addition of $MgCl_2$. Second, 250nM of GDP preloaded NΔ17ARF1 was mixed with 15nM of purified ARNO-Sec7 in the absence or presence of inhibitor. I started the reaction by injection of GTP (50μM) and measured the tryptophan fluorescence at 280nm (excitation) and 340nm (emission). All measurements were performed in PBS, pH 7.4, 3mM $MgCl_2$ at 37°C in 96well plates.

Figure 58 displays the results of a typical exchange reaction. After injection of GTP a linear, ARNO-Sec7 dependent increase in tryptophan fluorescence can be detected, which is inhibited in the presence of SecinH3. For analysis of the exchange rate, I calculated the initial slope of fluorescence increase by linear regression (GraphPadPrism software), as shown in Figure 58. It is important to note, that only initial, linear regions of fluorescence increase were used to calculate the exchange rate of ARNO-Sec7.

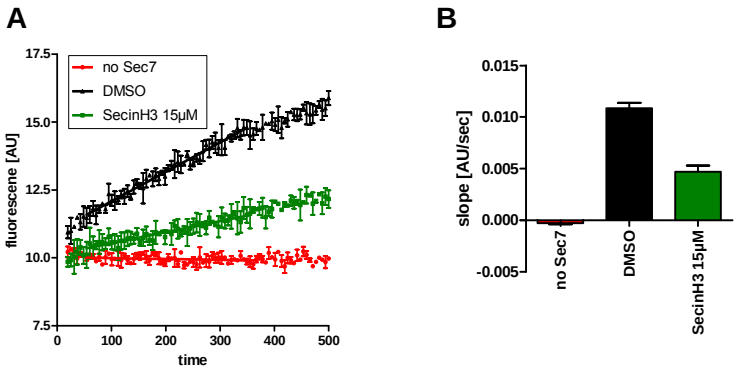

Figure 58 ARNO-Sec7 catalyzed GDP/GTP exchange on NΔ17ARF1

GDP preloaded NΔ17ARF1 was incubated with or without the Sec7 domain of ARNO in the presence of 15µM SecinH3 or DMSO (0.4%DMSO). The exchange reaction was started by addition of GTP. Conformational changes caused by GDP/GTP exchange on NΔ17ARF1 were detected by tryptophan fluorescence (ex280/em340nm).
A: Measured tryptophan fluorescence. The slope of the reaction was calculated by fitting the linear phase in tryptophan fluorescence by linear regression (fit shown as a line).
B: Calculated slope of the reactions
Data are represented as mean ±SEM, n=2.

To "measure" the suitability of the described GDP/GTP exchange assay on ARF1 for use as a screening assay, I calculated the Z'-factor. This coefficient reflects both the dynamic range of the signals (or the signal-to-noise-ratio) and the variation of the obtained signals. The Z'-factor is a useful tool to describe the quality of an assay system and is often utilized for assay validation [130]. It is calculated as:

$$Z' = 1 - \frac{3xSD_{pc} + 3xSD_{nc}}{|\mu_{pc} - \mu_{nc}|}$$

where SD is the standard deviation and µ the mean of the positive control (pc) or negative control (nc) values.

For the described GDP/GTP exchange assay on ARF1 I calculated a Z'-factor of 0.59 out of fourteen independent measurements with the reaction in the presence or absence of ARNO-Sec7 used as a positive or negative control, respectively, rating it as an suitable assay for screening.

IV.2.3 Screening of second generation SecinH3 chemotypes

In order to test the 145 second generation SecinH3 chemotypes predicted by virtual screening, I performed the GDP/GTP exchange assays on NΔ17ARF1 as described in the presence of 5µM compound (0.4% DMSO). All compounds were tested in independent duplicates and the relative exchange rate was calculated with the reaction in the presence of 5µM SecinH3 set to 1.

Figure 59 summarizes the relative exchange rates for all tested compounds which showed at least 10% stronger inhibition than SecinH3. Of these 15 compounds, 3 compounds (Secin69, Secin16, Secin87) showed a relative exchange rate of at most 70% (meaning at least 30% stronger inhibition than SecinH3) and were defined as hits (Figure 60). Retesting of Secin16 and Secin69 validated dose-dependency and yielded IC50 values of 3.7±0.4µM and 2.1±0.3µM, respectively, compared to 11.4±0.7µM for SecinH3. In addition, both compounds were applied in cellular assays. As Secin69 showed severe solubility problems, Secin16 was defined as a new lead compound.

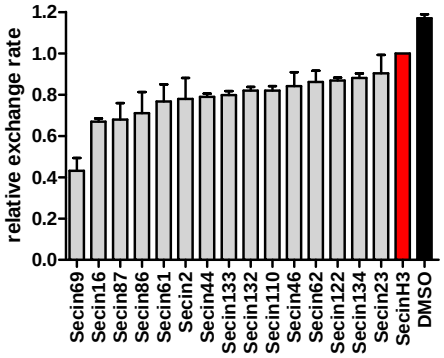

Figure 59 Ranking of second generation SecinH3 chemotypes

Relative exchange rate for second generation SecinH3 chemotypes (5µM) with SecinH3 (5µM) set to 1, shown as mean ±SEM, n=2.

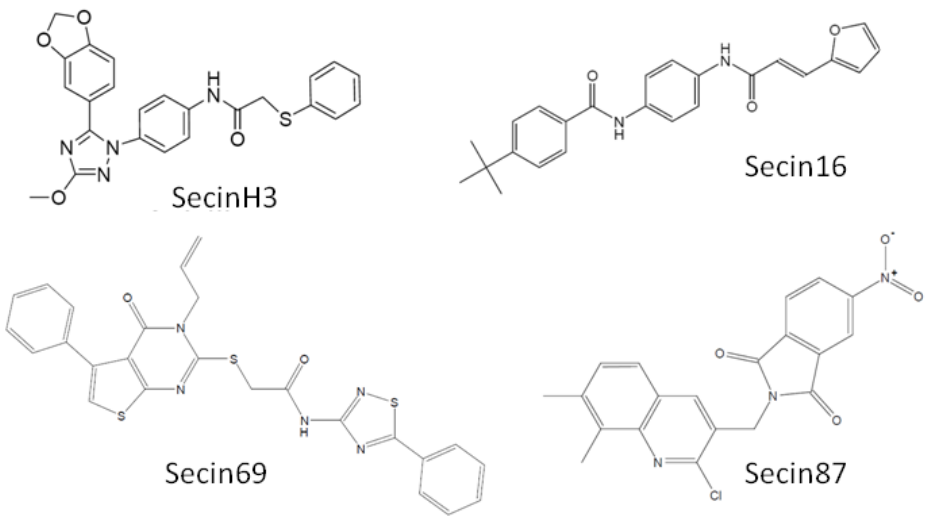

Figure 60 Structures of selected second generation SecinH3 chemotypes and SecinH3

IV.2.4 Structure-activity-relationship studies for Secin16

Although Secin16 displayed a roughly three fold higher potency than SecinH3 in the inhibition of GDP/GTP exchange on NΔ17ARF1, it showed reduced solubility in aqueous solutions (~7µM Secin16, ~15 µM SecinH3), making it difficult to determine further biochemical characteristics. Therefore, I performed a structure-activity-relationship study for a small set of

Secin16 analogs (synthesized by Jeffrey Hannam), to further improve the solubility and inhibitory potency of Secin16.

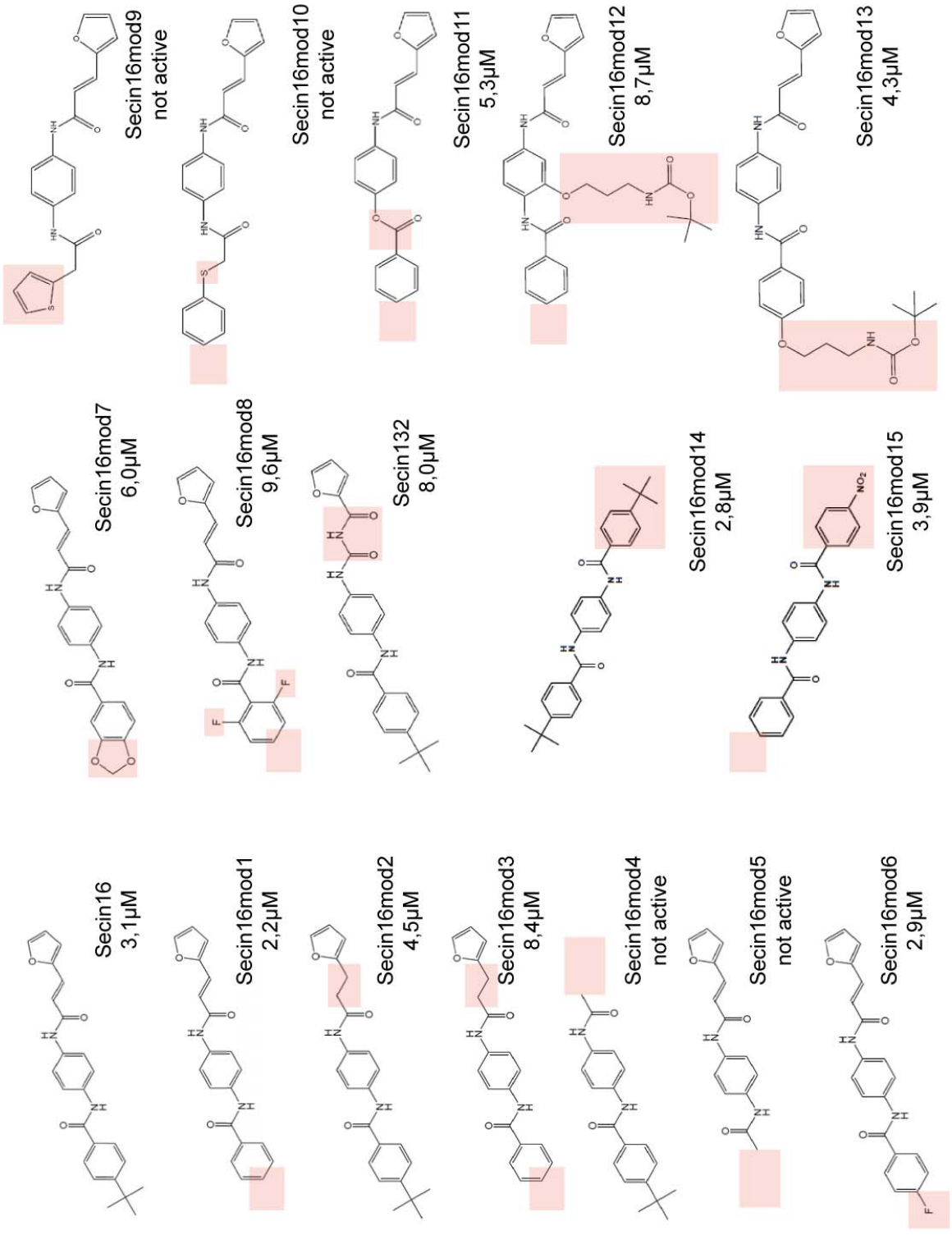

Figure 61 Secin16 modifications

Shown are the structures and the IC50 (GDP/GTP exchange on ARF1) of all tested Secin16 modifications.

Figure 61 gives an overview of the molecules tested, with the nuance indicating the modification. 16 Secin16 analogs were tested in GDP/GTP exchange on NΔ17ARF1 and IC50 values were calculated as described. Table 3 displays the obtained IC50 values.

The solubility of a compound is determined by many factors. The logP (logarithm of the partition coefficient) describes the ratio of concentrations of a compound in the two phases of a mixture of a hydrophobic and hydrophilic solution at equilibrium. Hence it is often used to predict the solubility of the compound, as lipophilic compounds have a high logP value (pure solubility in water) and hydrophilic compounds a low logP value (good solubility in water) [131]. I calculated the predicted clogP value for each molecule (ChemDraw software, using a fragment based prediction, "c" stands for calculated/simulated).

Compound	IC50 [µM]	clogP
Secin16	3.1±0.5	4.31
SecinH3	11.4±0.7	4.35
Secin16mod1	2.2±0.4	2.60
Secin16mod2	4.5±0.6	4.19
Secin16mod3	8.4±1.0	2.48
Secin16mod4	not active	3.45
Secin16mod5	not active	0.70
Secin16mod6	2.9±0.6	2.76
Secin16mod7	6.0±0.9	2.38

Compound	IC50 [µM]	clogP
Secin16mod8	9.6±2.0	2.92
Secin16mod9	not active	2.53
Secin16mod10	not active	2.75
Secin16mod11	5.3±0.5	3.28
Secin16mod12	8.7±0.4	3.08
Secin16mod13	4.3±0.4	3.08
Secin16mod14	2.8±0.3	7.05
Secin16mod15	3.9±0.5	3.24
Secin132	8.0±0.8	3.59

Table 3 Secin16 modifications

Shown are the IC50 and the predicted clogP value (ChemDraw). IC50 values are given as mean ±SEM of at least 4 independent experiments.

Only two Secin16 analogs, Secin16mod1 and Secin16mod6, missing the tertiary-butyl-moiety or 4'-fluoride substituted at the benzoate, respectively, showed an improved IC50 value combined with a predicted >10fold increase in solubility, compare to Secin16. Both compounds were further evaluated in cell proliferation assays, where they did not proof their superior to Secin16 (data not shown). Further substitutions at the benzoate (Secin16mod7, Secin16mod8) did not improve inhibitory potency. Instead substitution of the tertiary butyl benzoate (Secin16mod5) or furoyl-acrylic moiety for acetyl (Secin16mod4) rendered the molecule inactive. Introduction of an acetylthiophene (Secin16mod9) or phenylthioacetyl (Secin16mod10) moiety had the same inactivating effect. Interestingly, substitution of the furoyl-acrylic moiety with a second tertiary-butyl-benzoate slightly improved the IC50 value,

but dramatically worsened the clogP value (Secin16mod14). In respect of subsequent binding studies with immobilized Secin16, two positions for a propylamino-linker were tested (Secin16mod12+13), favoring the terminal position.

IV.2.5 Screening of third generation SecinH3 chemotypes

Based on the results obtained from the structure-activity-relationship study for Secin16 a second virtual screening approach was performed as described, yielding 88 new third generation SecinH3 chemotypes. Again, I tested all 88 compounds for their potential to inhibit the GDP/GTP exchange on ARF1 at a concentration of 2.5µM. I normalized the calculated exchange rates in relation to the exchange rate obtained in the presence of DMSO only.

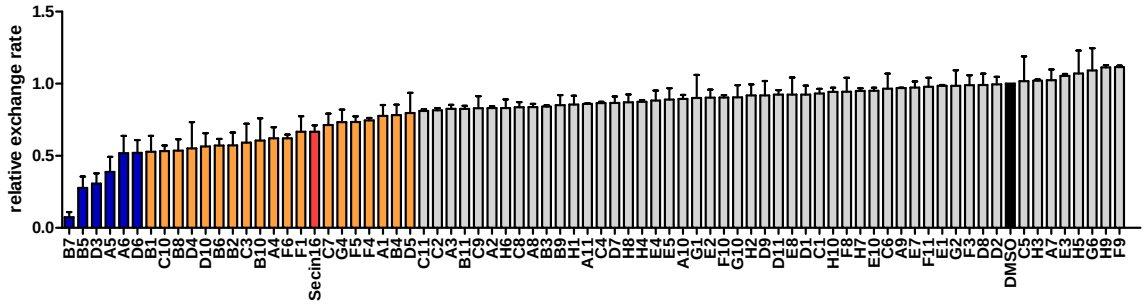

Figure 62 Screening of third generation SecinH3 chemotypes

Relative exchange rates for third generation SecinH3 chemotypes (2.5µM) with the reaction in the presence of DMSO set to 1, shown as mean ±SEM, n=2. Blue bars: 20% stronger activity, orange bars: similar activity as Secin16, grey bars: not active.

In my primary screen 6 compounds which showed at least 20% stronger inhibition compared to Secin16 (Figure 62, blue bars, Secin16 red bar) at a concentration of 2.5µM were classified as a hit (B7, B5, D3, A5, A6, D6, for structure see Figure 63). 19 compounds showed similar activity as Secin16 (+/- 20%, orange bars) and 52 compounds were classified as non active (light grey bars). 11 compounds showed strong autofluorescence and could hence not be evaluated. All 6 hits were re-screened at different concentrations to verify dose-dependency. Table 4 combines the IC50 values for all 6 hits in comparison with Secin16.

Compound	B7	B5	D3	A5	A6	D6	Secin16
IC50 [µM]	0.44 ± 0.06	1.19 ± 0.15	1.34 ±- 0.16	1.18 ± 0.17	0.79 ± 0.15	1.86 ± 0.30	3.74 ± 0.37

Table 4 IC50 values of third generation SecinH3 chemotypes

Numbers represent IC50 values ±SEM for all 6 hits in the GDP/GTP-exchange assay on ARF1. Each individual experiment was performed at least 8 times.

Taken together these data introduce a new class of potent inhibitors for cytohesin-catalyzed GDP/GTP exchange on ARF1.

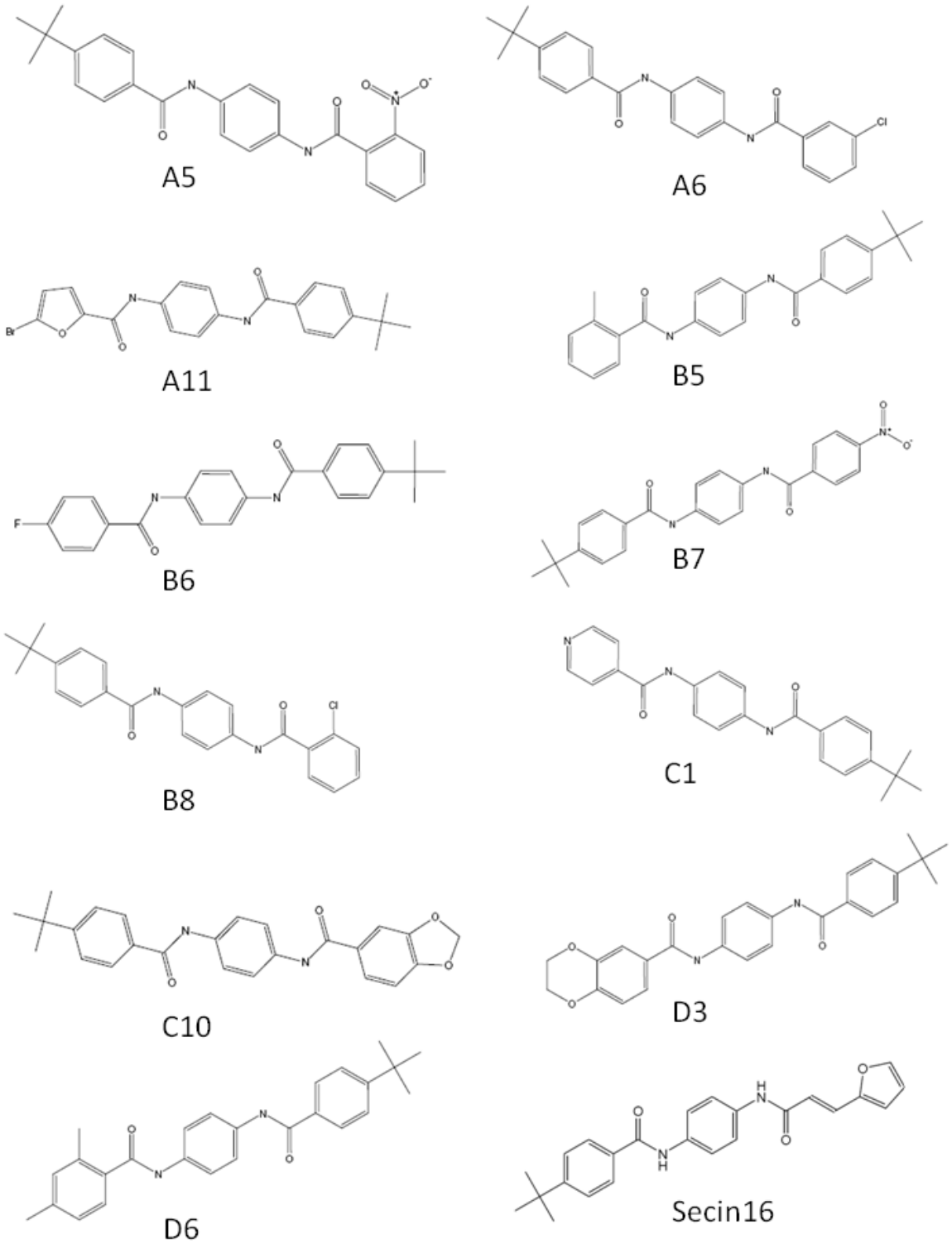

Figure 63 Structure of selected 3rd generation SeicnH3 chemotypes and Secin16

IV.3 Evaluations of 3rd generation SecinH3 chemotypes in human glioblastoma cell lines

IV.3.1 Third generation Secins are potent inhibitors of glioblastoma cell proliferation

Gliomas are the most common subtype of primary brain tumors and are responsible for about 2% of all deaths from cancer. The epidermal growth factor receptor (EGFR) is a primary contributor to glioblastoma initiation and progression. EGFR amplification and overexpression is the most common genetic alteration in primary glioblastoma with a frequency of 40-70%, commonly accompanied with additional mutations in EGFR. The most abundant mutation, which is found in approximately 50-60% of glioblastoma that overexpress the EGFR, is the EGFR variant III (EGFRvIII). This mutant lacks domains I and II of the extracellular part of the EGFR. Although EGFRvIII is incapable of ligand binding it is constitutively tyrosine phosphorylated and therefore constitutively activates EGFR downstream signaling [66, 132].

When grown in vitro, glioblastoma cells lose their native EGFRvIII expression over time, making it necessary to replace this oncogene for further studies. I used two pairs of established glioblastoma cell lines: Gli36 wild-type and U87 wild-type cells and their respective isogenic line, which differs only in the expression of the stably transfected EGFRvIII. By comparing the effect of the compounds on the parental and the EGFRvIII expressing cell line I was able to screen for compounds which selectively inhibit the EGFRvIII dependent cell proliferation.

To identify new inhibitors of glioblastoma cell proliferation I validated all 88 third generation SecinH3 chemotypes for their effect on cell proliferation. Cells were treated with 250nM of the compounds. At this concentration Secin16 shows only weakly affects cell proliferation. After 72h the relative number of cells was quantified by a MTT assay as described before.

The primary screen identified 11 compounds that inhibited the proliferation of both parental cell lines by more than 30% as compared to the solvent only (DMSO) control (Figure 64). These primary hits were classified into two groups: group one, consisting of compounds A4, B5, B7, B8, B10 (Figure 1B, dark blue bars, red box in), showed an inhibitory effect of more than 50% as compared to the solvent only control in both cell lines, whereas group two (compounds A1, A5, A6, B6, D4, D5, B, orange bars or green box in) decreased cell proliferation in both cell lines between 30% and 50%. Comparison of the two parental cell lines U87 and Gli36 revealed a significant correlation ($p<0.0001$, $r=0.9$, Pearson-model,

GraphPadPrism software) between the inhibitory effects of all 88 compounds on the proliferation of both cell lines (Figure 65).

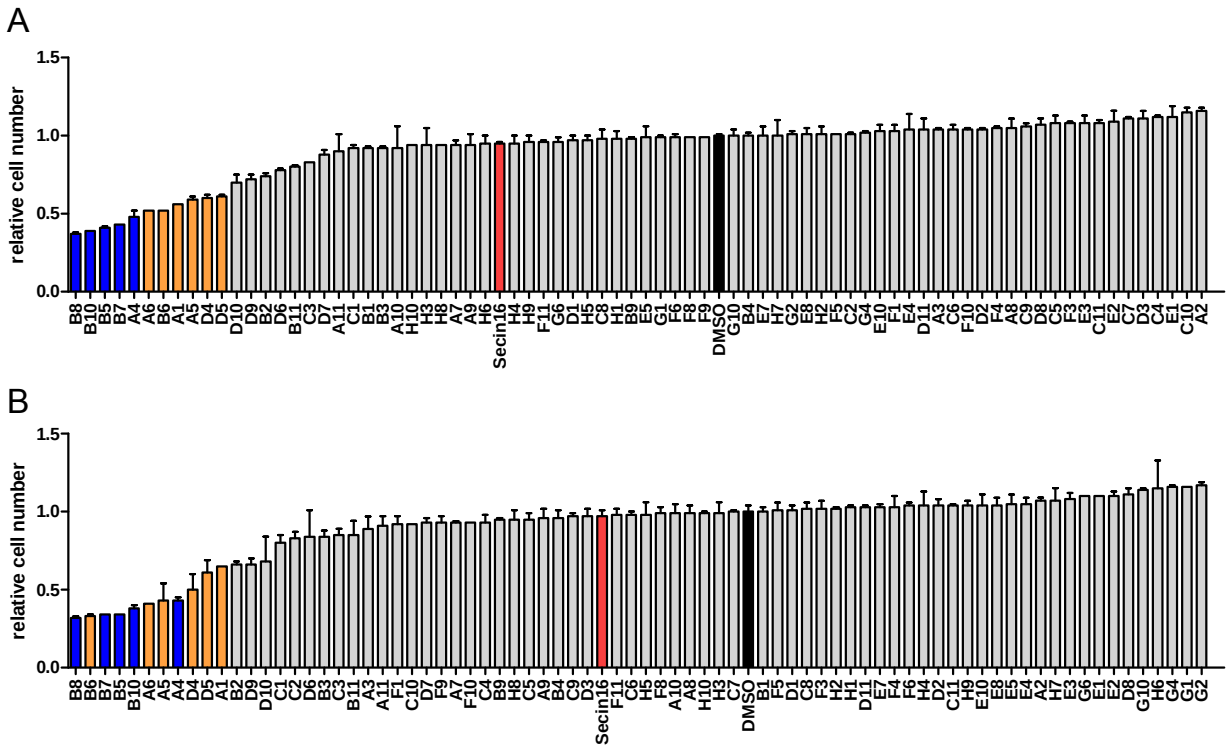

Figure 64 Effect of 3rd generation SecinH3 chemotypes on glioblastoma cell proliferation

Results of the primary screen on glioblastoma cell proliferation. Cells were incubated with the respective compound (250nM) and the relative cell number was determined after 72h using a MTT-assay. Data are normalized with the absorbance in the solvent (DMSO) only control set as 1 and represent the mean values of duplicates ±SEM, error bars correspond to SEM. Blue bars correspond to the most active compounds, which decreased proliferation in both parental cell lines more than 50%, orange bars to compounds with 30-50% inhibition and grey bars to compounds with little effect on cell proliferation.
A: U87 wild-type cells, B: Gli36 wild-type cells

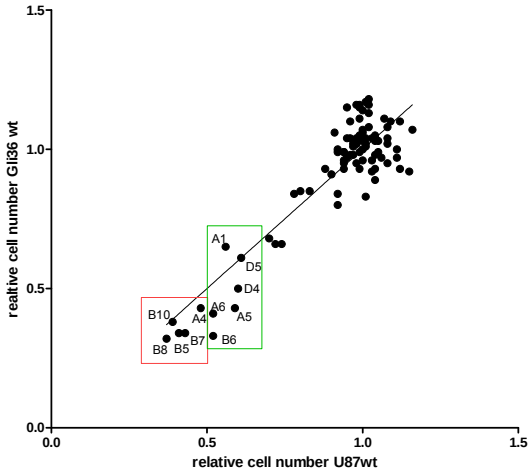

Figure 65 Comparison of the inhibitory effects on proliferation of U87 and Gli36 wild-type cells

Scatter blot showing the relative cell numbers after 72h incubation with the compounds (250nM) with the DMSO treated sample set to 1. Boxes: compounds which inhibit cell proliferation more than 50% (red box) or more than 30% (green box) in both cell lines. Data points represent the mean value of duplicates.

To identify compounds that selectively inhibit proliferation of the EGFRvIII-containing cell lines, the inhibitory effects of all 88 compounds on the proliferation of the parental cell line and on the respective EGFRvIII-expressing cell line was correlated. Whereas there was only little difference in the Gli36 cells, three compounds (A11, C1, C10) preferentially diminished the proliferation of the U87-EGFRvIII cell line (Figure 66).

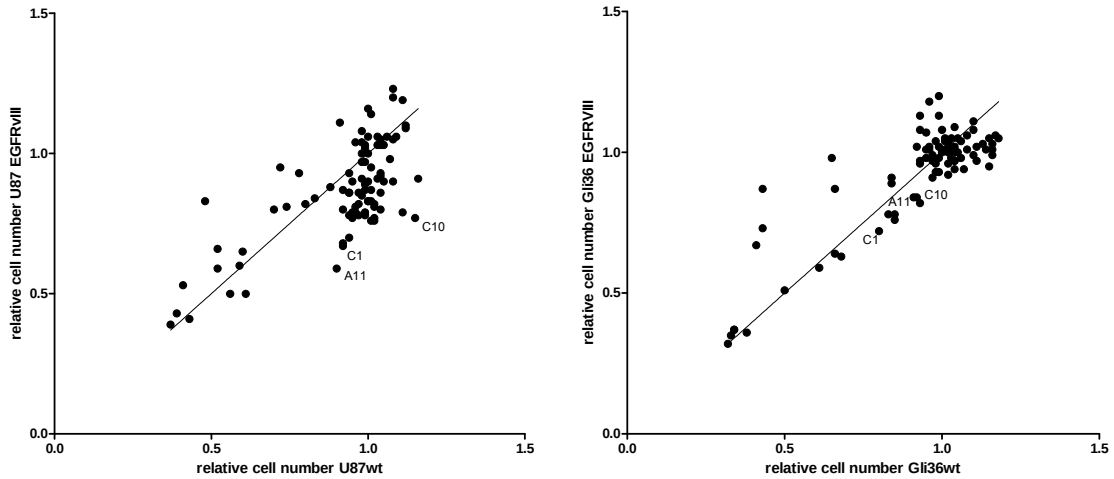

Figure 66 Correlation between relative cell numbers of parental wild-type and EGFRvIII expressing cell lines after treatment with 3rd generation Secin chemotypes

Scatter blot showing the relative cell numbers (left: U87, right: Gli36) after 72h incubation with the compounds (250nM). The DMSO treated sample set to 1. Most selective compounds are labeled. Data points represent the mean value of duplicates ($p<0.0001$, U87 $r=0.71$, Gli36 $r=0.76$).

A secondary screen of 14 compounds (11 pan- and 3 selective inhibitors) confirmed the results of the primary screen and showed dose-dependent effects for all test compounds.

After this second screen five compounds were selected for further testing: compounds B7 and B8 as the most potent pan-inhibitors and compounds A11, C1, C10 as EGFRvIII-selective inhibitors. These compounds were again re-screened at concentrations ranging from 2.5nM to 2µM to determine IC50 values and to test whether there was significant difference in IC50 values between the parental and EGFRvIII-containing cell line (Figure 67). Whereas B7 and B8 showed a very potent inhibition of cell proliferation in all four cell lines, C1 selectively inhibited the proliferation of the EGFRvIII-containing cells. This effect was most prominent in the U87 cell lines. C1 diminished the proliferation of U87 EGFRvIII-cells more than 10-fold better compared to the parental cell line. IC50 values for all 5 compounds in comparison to Secin16 are shown in Table 5.

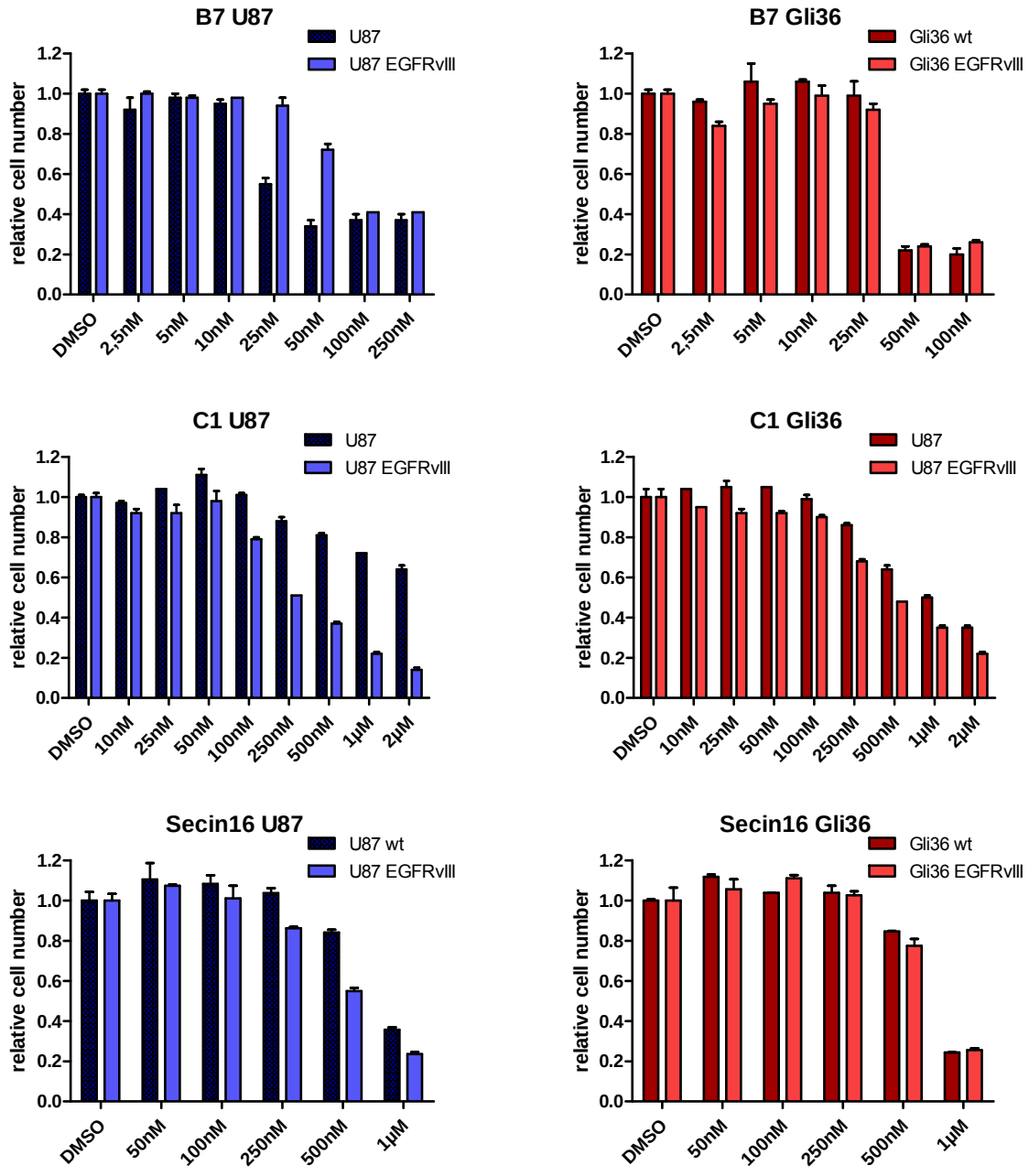

Figure 67 Inhibition of glioma cell proliferation by third generation Secins

Cells were treated 72h with the respective compound or solvent only (DMSO). Relative cell numbers (solvent only control set as 1) are shown. ± SEM, n=3, for each cell line.

IC50/Compound	B7	B8	A11	C1	C10	Secin16
U87 wt	28nM ± 1.3	106nM ± 1.2	1366nM ± 1.4	2086nM ±1.2	922nM ± 1.5	958nM ± 1.4
U87 EGFRvIII	83nM ± 1.2	126nM ± 1.2	198nM ± 1.3	186nM ± 1.2	224nM ± 1.3	453nM ± 1.3
Gli36	40nM ± 1.6	102nM ± 1.2	589nM ± 1.3	732nM ± 1.2	609nM ± 1.3	750nM ± 1.5
Gli36 EGFRvIII	35nM ± 1.5	92nM ± 1.3	360nM ± 1.3	314nM ± 1.1	279nM ± 1.5	724nM ± 1.8

Table 5 IC50 values for inhibition of glioblastoma cell proliferation

Numbers represent IC50 values ±SEM (error of the fit!) for the two most potent (B7 and B8) and three selective (A11, C1, C10) compounds in the glioblastoma cell proliferation assay. Secin16 is shown for comparison. Each individual experiment was performed at least three times.

Furthermore I also analyzed compounds A5, A6, B5 and B6, which showed an inhibition of <30% in the primary screen, and compounds D3 and D6, which were among the 6 most potent inhibitors for GDP/GTP exchange on ARF1, for their potential to inhibit proliferation of U87 wild-type and U87 EGFRvIII cells. Table 6 gives an overview of the obtained IC50 values.

IC50/Compound	A5	A6	B5	B6	D3	D6
U87 wt	168nM ± 1.8	243nM ± 1.3	118nM ± 1.7	89nM ±1.9	297nM ± 1.6	367nM ± 1.9
U87 EGFRvIII	46nM ± 1.2	67nM ± 1.2	148nM ± 1.3	372nM ± 1.2	105nM ± 1.3	84nM ± 1.3

Table 6 IC50 values of 3rd generation Secin chemotypes for the inhibition of glioblastoma cell proliferation

Numbers represent IC50 ±SEM values (error of the fit!) for the indicated compounds in the glioblastoma cell proliferation assay. Each individual experiment was performed at least three times.

In conclusion these results define a new class of potent inhibitors for glioblastoma cell proliferation including potential EGFRvIII selective inhibitors.

IV.3.2 GDP/GTP- exchange assay versus glioma cell proliferation

The Sec7 domain of cytohesins was found to mediate activation of ErbB receptors in lung human adenocarcinoma derived cell lines, while not requiring the GEF function of this domain.

To investigate whether inhibition of glioblastoma cell proliferation by 3rd generation Secin chemotypes is caused by an interference of the compounds with the GEF-independent function of cytohesins or is a mere consequence of decreased GEF-activity, I correlated the relative inhibitory activity of the compounds in the exchange assay with their relative effect on proliferation of the parental cell lines. The scatter blots revealed a significant positive correlation between the inhibitory effect of the compounds (2.5µM) on the exchange activity of the cytohesins (Figure 68) and the inhibition of cell proliferation (250nM) in both parental cell lines ($p<0.0001$, $r=0.6$ U87, $r=0.67$ Gli36, data normalized, Secin16 set to 1).

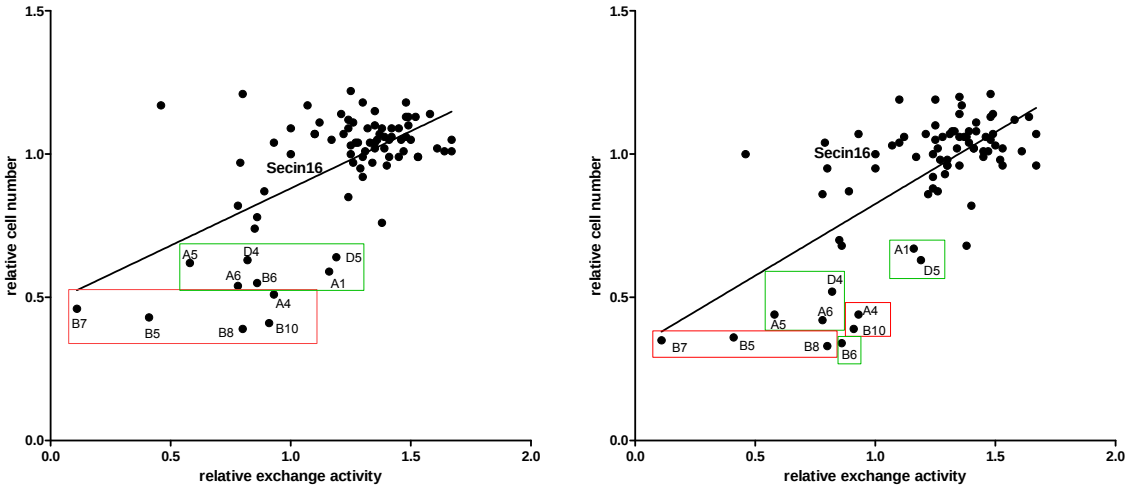

Figure 68 Correlation between the inhibitory effect of 3rd generation Secin chemotypes on GDP/GTP-exchange and cell proliferation

Scatter blots (left: U87, right: Gli36 cells) showing the relative exchange activity in presence of the respective compound (2,5µM) and the relative cell numbers after 72h incubation with the compounds (250nM).The Secin16 treated sample set to 1. Boxes: compounds which inhibited cell proliferation more than 50% (red box) or more than 30% (green box) in both cell lines. Data points represent the mean value of duplicates ($p<0.0001$, $r=0.6$ U87, $r=0.67$ Gli36). Correlation was analyzed using the Pearson model.

Furthermore I compared the obtained IC50 values for inhibition of the GDP/GTP exchange on ARF1 with the IC50 values for inhibition of cell proliferation in U87 and U87 EGFRvIII cells (Figure 69). Statistical analysis revealed a highly significant correlation (***, $p<0.0001$, $r=0.94$) between the IC50 values obtained in both assays. Beyond, a significant correlation between the IC50 value obtained in the exchange assay and for the inhibition of U87 EGFRvIII proliferation was found when the selective compounds A11, C1 and C10 were omitted (*, $p=0.01$, $r=0.76$).

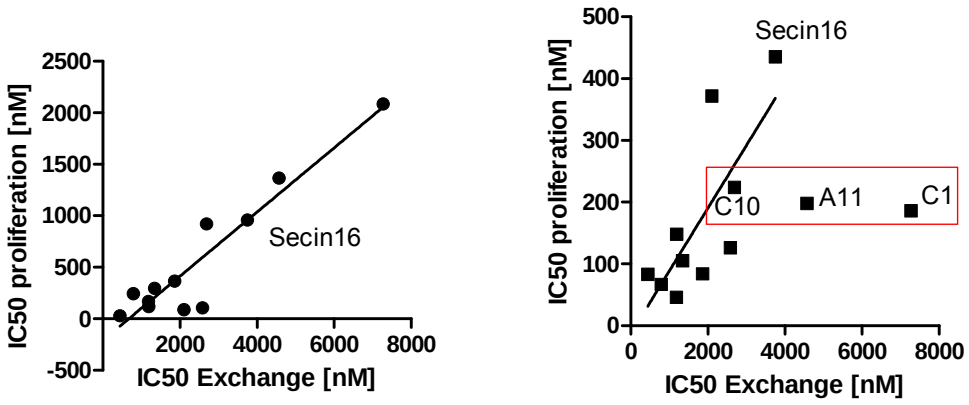

Figure 69 Correlation between the IC50 values in cell proliferation and GDP/GTP exchange

Scatter blots showing the obtained IC50 values for inhibition of cell proliferation and cytohesin catalyzed GDP/GTP-exchange on ARF1. Correlation was analyzed using the Pearson model.
Left: U87 wild-type cells, ***, $p<0.0001$, $r=0.94$
Right: U87 EGFRvIII cells, *, $p=0.01$, $r=0.76$. The red box indicates selective compounds.

In summary these data implicate a correlation between the inhibitory activity on the GDP/GTP-exchange on ARF1 and the potential to inhibit proliferation of glioblastoma cell lines.

IV.3.3 Third generation SecinH3 chemotypes induce distinct phenotypes in glioblastoma cells

To further elucidate the effect of third generation SecinH3 chemotypes on the proliferation of glioblastoma cells, I examined the phenotypes of U87, U87 EGFRvIII, Gli36 and Gli36 EGFRvIII after 18h/36h treatment with 2µM of B7, A11, C1, 5µM Secin16, 15µM SecinH3 or solvent (0.4% DMSO) alone. Figure 70 displays representative micro photographs of treated cells after 18h and 36h incubation with the indicated compounds.

Only B7 affected the growth of the typically outstretched, foci forming U87 wild-type cells, detected as a decrease in total cell number. Whereas C10 and A11 had only little effect on the proliferation of the parental U87 cell line, both compounds clearly reduced the number of vital cells in the EGFRvIII expressing U87 cell line, underlining the observed selectivity for EGFRvIII expressing cells. Similar to its effect on the parental cell line, B7 simply diminished the total number of U87 EGFRvIII cells without affecting the appearance of the cells. On the other hand, C10 and A11 dramatically altered the phenotypes of the cells. U87 EGFRvIII cells normally appear as fusiforme cells. Treatment of these cells with C10 or A11resulted in more rounded phenotype and an increase in detached, floating cells. Again SecinH3 and Secin16 showed no effect.

The same result was obtained for Gli36 wild-type and Gli36 EGFRvIII expressing cells. Again B7 reduced the cell number of both cell lines, without altering the phenotype of the cells. In contrast, C10 and A11, only slightly influenced proliferation of the wild-type Gli36 cells but clearly reduced the number of attached, vital Gli36 EGFRvIII cells. Whereas Secin16 inhibited the proliferation of EGFRvIII expressing Gli36 cells, SecinH3 had no effect on either cell line.

Taken together, these data confirm the high potency of B7 to inhibit glioblastoma cell proliferation and indicate a distinct effect of C10 and A11 on EGFRvIII expressing glioblastoma cells.

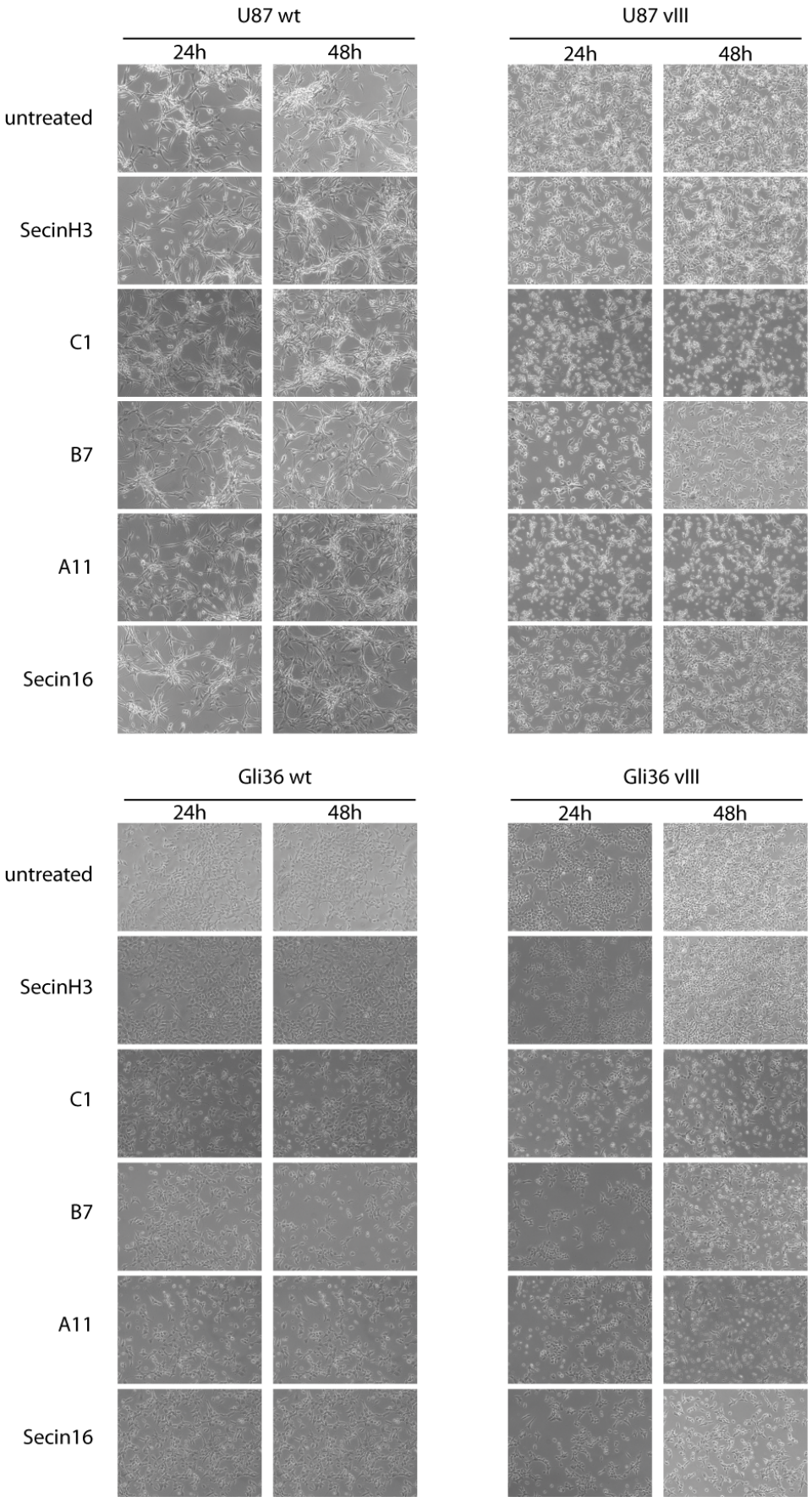

Figure 70 Phenotypes of glioblastoma cells after treatment with third generation Secins

Representative microphotographs of glioblastoma cells after treatment with the indicated compounds (15μM SecinH3, 2μM C1, B7, A11, 5μM Secin16) or DMSO (0.4%, untreated).

IV.3.4 Compounds A11, C1 and C10 induce apoptosis selectively in EGFRvIII expressing glioblastoma cells

The obtained reduction in cell number after treatment of glioblastoma cells with the compounds Secin16, B7, A11 or C10 might be due to the induction of a resting state or an increase in apoptosis due to the lack of pro-proliferation signals. Therefore, the distinct phenotypes observed after treatment with the compounds suggest different fates of the cells.
To test this possibility I performed an Annexin V apoptosis assay by flow cytometry as described above. I preincubated U87/Gli36 wt or EGFRvIII expressing cells for 48h with 5µM Secin16, 2µM B7, A11, C1 or C10 or solvent (0.4%DMSO) in basal medium containing 1% FBS, harvested by trypsinization and stained the cells with a FITC-labelled form of Annexin V and with TOPRO 3 iodide. I analyzed the cells by flow cytometry as previously described.

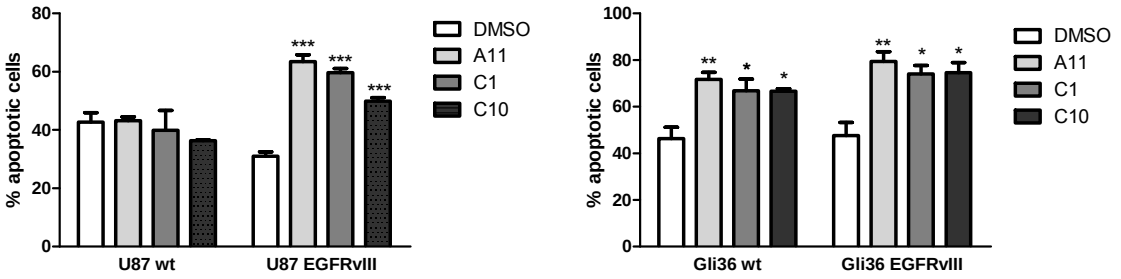

Figure 71 Selective third generation Secins induce apoptosis in EGFRvIII expressing glioblastoma cell lines

Quantitative analysis of apoptotic glioblastoma cells (quadrants 2-4) after 48h treatment with solvent (0.4% DMSO) or 2µM A11, C1, C10 (*** $p<0.001$, ** $p<0.01$, ** $p<0.05$, n=3).

Whereas Secin16 and B7 had no effect in any cell line (data not shown), treatment with compounds A11, C1 and C10 led to a significant increase in apoptotic cells (defines as quadrants 2-4) most pronounced in EGFRvIII expressing cells as compared to the wild-type cells (Figure 71). Again, the selective effect was more distinct in the U87 cell line. These data support the selectivity of compounds A11, C1 and C10 for EGFRvIII expressing glioblastoma cell lines and are in line with the observed distinct phenotype of rounded, detached cells induced by treatment with A11 or C10, which is likely explained by apoptosis. B7 and Secin16 do neither induce apoptosis nor change the phenotype of the cells, but inhibit glioblastoma cell proliferation. This finding might indicate a different mode of cell proliferation inhibition, like the induction of a resting state.

IV.3.5 Effect of compounds A11, C1 and C10 on EGFR phosphorylation

Having shown that chemical inhibition of cytohesins leads to a decreased EGFR activation in human lung and breast adenocarcinoma derived cell lines, I investigated whether the selective effect of A11, C1 and C10 on the proliferation of EGFRvIII expressing U87 glioblastoma cells can be explained by reduced EGFR signaling.

Therefore, I treated the cells overnight with 5μM A11, C1, C10 or 2μM B7 (highest possible concentration due to the weak solubility) in basal media containing 1% FBS (0.4% DMSO end concentration). Wildtype U87 cells were stimulated with 50ng/ml EGF for 5min at 37°C before harvesting. EGFRvIII expressing U87 were harvested without stimulation, since addition of EGF showed no increase in EGFR phosphorylation. Phosphorylation levels of EGFR were detected as described using immunoblotting and an antibody against pY1068 of EGFR.

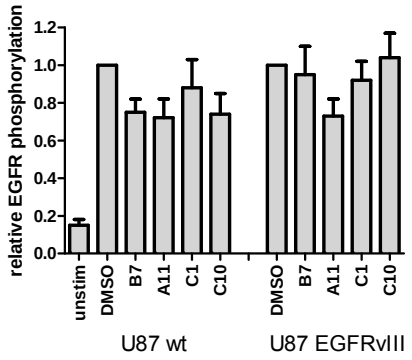

Figure 72 Third generation Secins do not inhibit EGFR phosphorylation in U87 cells

Quantitative analysis of EGFR phosphorylation (EGFR_Y1086) after overnight treatment of U87 wild-type and U87 EGFRvIII cells with the indicated compounds (2μM B7, 5μM A11, C1, C10). Data are represented as mean ±SEM, n≥2.

Treatment of wild-type U87 cells with B7, A11 and C10 resulted in a weak inhibition of EGFR phosphorylation (Figure 72). Although the cells showed severe changes in the phenotype (rounding, detaching, and beginning fragmentation) no clear effect on the phosphorylation level of EGFR could be observed in the EGFRvIII expressing U87 cells, indicating that the induction of apoptosis is not a results of EGFR inhibition.

IV.3.6 Compounds A11, C1 and C10 influence repair of DNA double strand breaks in glioblastoma cells

Apoptosis can be induced by several intracellular and extracellular stimuli.One of the most potent inducer of apoptosis is DNA damage [133]. Every cell is under constant attack not

only from exogenous also from endogenous mutagenic influences (chemicals, radiation, free radicals) causing DNA damage. The accumulation of DNA damage can lead to oncogenesis, cell death, and severe dysfunction of cells. Therefore, the DNA repair system is crucially important for survival of cells. In most cells an elevated level of DNA damage causes delay in the cell cycle via checkpoint mechanisms, which ensure that DNA damage is repaired before a cell divides. Accumulation of DNA damage, however, leads to apoptotic cell death.

DNA damage targeting the bases or nucleotides itself typically involves only one strand (single-strand break), preserving the information of the other strand. An accidental lesion on one strand can therefore be cut out and resynthesized by referring to the information in the undamaged strand (base and nucleotide excision repair). Repair of double-strand brakes in the DNA helix, however, often leads to rearrangements in the DNA sequence. The repair of double-strand breaks in somatic cells is mediated through non-homologous or homologous recombinatorial repair. In non-homologous repair (non-homologous end-joining, NHEJ) the broken ends of both strands are simply brought together and rejoined by DNA ligation, leading to the loss of one or more nucleotides at the site of joining. On the other hand, homologous recombination results in the transfer of genetic information between two DNA duplex segments of similar nucleotide sequence and is essential for both, the error-free repair of chromosome damage in all cells and for crossing-over of chromosomes that occur during meiosis. The recombination event is guided by a specialized set of proteins, involving the mammalian homolog of RecA, called RAD51. Binding of RAD51 to double-strand breaks in the DNA helix is initiated by the phosphorylation of a member of the histone family H2A, which is one of the five types of histones that package and organize eukaryotic DNA into chromatin. In response to double-strand breaks, the conserved C-terminal tail of H2AX becomes rapidly phosphorylated at serine-139 by PI3-K like kinases, including ATM, ATR and DNA-PKcs (DNA-dependent protein kinase catalytic subunits). The phosphorylated H2AX, named γH2AX, is one of the first proteins involved in DNA damage response pathways and is required for DNA damage signal amplification and subsequent accumulation of numerous repair proteins (like RAD51) at double-strand breaks sites [134-136].

To test whether the induction of apoptosis in EGFRvIII expressing glioblastoma cells induced by treatment with the selective compounds A11, C1 and C10 is caused by an accumulation of double-strand breaks, I incubated wild-type or EGFRvIII expressing Gli36 cells for 24h with 2μM of A11, B7, C1, C10 or Secin16. Cell lysates were subjected to SDS-PAGE followed by immunoblotting. Levels of RAD51 or γH2AX were detected by using specific antibodies.

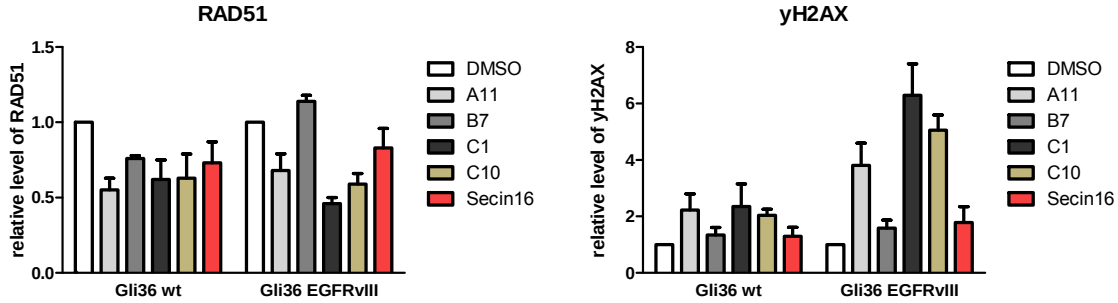

Figure 73 Third generation Secins lead to an increase in DNA double-strand breaks in glioblastoma
Quantitative western blot analysis of RAD51 and γH2AX levels in Gli36 glioblastoma cells after 24h treatment with 2μM of the indicated compounds (Secin16 5μM). Data are represented as the mean ±SEM of relative expression levels, with the solvent (DMSO) treated sample set to 1, n=2-3.

Whereas treatment of wild-type Gli36 cells with the selective compounds A11, C1 and C10 only weakly induces phosphorylation of H2AX, it resulted in a strong increase in γH2AX in EGFRvIII expressing Gli36 cells, indicating an accumulation of double-strand breaks in these cells (Figure 73, right panel). B7 and Secin16 had no effect on the level of γH2AX in either cell line, demonstrating once more the differential mode of inhibition. An increase in phosphorylation of H2AX and thereby an increase in double-strand breaks can be either caused by facilitating double-strand breaks or by inhibition of double-strand break repair and the subsequent accumulation of double-strand breaks. To distinguish between these possibilities I detected the protein level of RAD51. The increase in γH2AX was accompanied by a reduction in RAD51 protein level, rather than an increase in RAD51 expression due to enhanced double-strand repair activity, indicating an effect of the compounds on double-strand repair (Figure 73, left panel). Again, the effect on RAD51 expression level was more pronounced in EGFRvIII expressing Gli36 cells as compared to the wild-type cell line. B7 and Secin16 showed no effect on RAD51 protein level in EGFRvIII Gli36 cells.

To gain further insight into the underlying mechanism of the EGFRvIII selective proliferation inhibition and the subsequent induction of apoptotic cell death in Gli36 cells, I performed a kinetic for the appearance of double-strand breaks after treatment with C1. Therefore, I incubated the cells 4h, 8h or 24h with 2μM C1 as described above. To exclude any effects due to different proliferation times all cells were harvested at the same time, after transfer in basal media containing 1% FBS and addition of C1 at the indicated time points. In addition, untreated cells were analyzed for every time point.

Figure 74 depicts a representative blot for detection of RAD51 and γH2AX. In correlation with the previous experiments, γH2AX level was elevated in cells treated with C1 after 24h, accompanied by a decrease in RAD51 protein level. Shorter incubation times had no effect.

Again, the effect in EGFRvIII expressing Gli36 cells was more pronounced compared to the wild-type cell line.

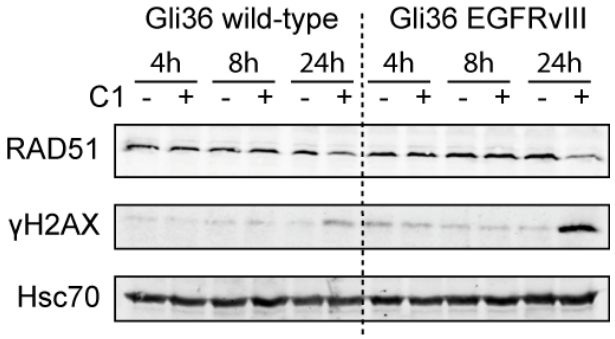

Figure 74 Kinetic for C1 induced accumulation of DNA double-strand breaks
Gli36 wild-type or EGFRvIII expressing cells were treated for the indicated time periods with 2μM C1. RAD51 and γH2AX levels were detected by western blotting using specific antibodies. Hsc70 served as loading control.

Taken together, these data suggest an accumulation of double-strand breaks due to reduced RAD51 levels in cells treated with compounds A11, C1 and C10, which subsequently leads to increased apoptotic cell death. Hence, the selective effect of the compounds might be explained by the slightly higher proliferation rate of EGFRvIII expressing cells. A higher replication rate could facilitate replication prone double-strand breaks. Reduced RAD51 expression levels, would lead to a faster accumulation of double-strand breaks and to induction of apoptosis in EGFRvIII expressing cells.
Unfortunately, no signals for RAD51 or γH2AX could be obtained in U87 cells.

IV.3.7 EGFRvIII expressing glioblastoma cell lines show an increase in ARF6 expression

Recently it has been shown, that ARF6 is required for EGF dependent proliferation of glioblastoma cells [137]. However, the precise mechanism is still unknown. Since the third generation SecinH3 chemotypes bore a high inhibitory effect on the cytohesin catalyzed GDP/GTP-exchange on ARF1 in vitro and also decreased ARF6 activation in cells (data not shown), the selectivity for EGFRvIII expressing cells might be explained by a higher dependency on ARF6 activity. To investigate this hypothesis, I analyzed the expression level of ARF1 and ARF6 in wild-type and EGFRvIII expressing U87 and Gli36 glioblastoma cells by quantitative real-time PCR.
Figure 75 depicts the relative expression of ARF1 and ARF6 in EGFRvIII expressing cells normalized to the respective expression in wild-type cells. ARF6 showed a ~6fold higher expression in EGFRvIII expressing U87 cells as compared to the wild-type cell line.

Expression of ARF1 was almost doubled. In EGFRvIII expressing Gli36 cells, both ARF1 and ARF6 expression level were elevated ~2fold as compared to the wild-type cell line.

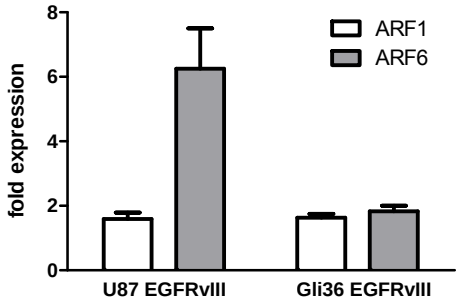

Figure 75 ARF expression is increased in EGFRvIII expressing glioblastoma cell lines

Quantitative PCR analysis of ARF1 and ARF6 expression levels in EGFRvIII expressing glioblastoma cells in comparison to wild-type glioblastoma cells. Bars represent the relative increase in ARF expression (mean ±SEM, n=3) as compared to the respective wild-type cell line.

These results might indicate an increased dependency of EGFRvIII expressing glioblastoma cells on ARF proteins and might provide an explanation for the observed high sensitivity of EGFRvIII expressing cells for the tested cytohesin inhibitors.

IV.4 A new real-time FRET-based assay to monitor GDP/GTP exchange on NΔ17ARF1

IV.4.1 Recent approaches

Multiple techniques are available to study the activation of small GTPases by their GEFs [138]. Based on the step of the activation reaction used for analysis they can be divided in different classes: The first group directly monitors the activation of the GTPase by utilizing conformational changes induced upon binding of the GEF and the subsequent exchange of the nucleotide. As an alternative, one can directly measure binding of GTP to the GTPase which is relative to the exchange rate of the protein. The third group of assays is based on the selective interaction of the activated GTP-bound GTPase with its effector protein. Whereas the first two methods are based on fluorescence spectroscopy which allows for real-time monitoring, analysis of protein interactions are commonly end point measurements lacking kinetic information.

ARF1 lacking the first 17 amino acids (NΔ17ARF1) is the most often used ARF protein to measure GDP/GTP exchange in vitro. The lack of the N-terminal part of the proteins renders its activation independent from the presence of liposomes. Various assays to monitor GDP/GTP exchange on NΔ17ARF1, referring to all three classes described, can be found in literature. The most abundant assay is based on the change in the tryptophan fluorescence of NΔ17ARF1 upon activation by its GEF, which can be monitored in real-time by measuring tryptophan excitation and emission at 280/340nm, respectively [127]. However, some small molecules show a strong absorption of light, especially of shorter wavelength and may interfere with the intrinsic fluorescence assay. An alternative approach to measure the GEF-catalyzed activation of NΔ17ARF1 is to use GDP or GTP analogs labeled with an environment sensitive fluorescent group, like N-methylanthranyloyl (or mant) group [139-140]. The fluorescence of the mant GDP/GTP analogs is sensitive to the environment of the fluorophore, exhibiting both an increased fluorescence quantum yield upon protein binding and a blue-shift of 10–20 nm in fluorescence emission maximum. Mant guanine nucleotides can be excited at a wavelength of ~360nm and show protein-binding dependent emission at 440nm, remote from the wavelength region where proteins or small molecules absorb. By using mant-nucleotides, activation of NΔ17ARF1 can be followed kinetically in two ways: First one can simply monitor binding of mant-GTP to NΔ17ARF1, by measuring the fluorescence of mant-GTP at ex360/em440nm. As a variant, the displacement of mant-GDP by GTP on mant-GDP preloaded NΔ17ARF1 can also be measured. Furthermore, it is possible to use fluorescence resonance energy transfer (FRET) between tryptophan and mant

nucleotide to follow the exchange reaction (ex280nm/em440nm). Here the tryptophan residue is excited and acts as a donor to induce the fluorescence of the acceptor mant group. Although the mant fluorescent group is small and in general does not disturb the binding of small molecules, this point has to be considered when using mant-labeled nucleotides.

A different, fluorescence independent approach to measure GDP/GTP exchange on NΔ17ARF1 makes use of radioactive labeled nucleotides [127]. For this purpose, the exchange reaction is conducted in the presence of radioactive labeled GTP. GTP loading on NΔ17ARF1 is detected after washing and separation of NΔ17ARF1 by quantification of the bound radioactivity. To prevent hydrolysis of the bound GTP, an uncleavable form of GTP, in which the γ-phosphate group is substituted by sulfur (GTPγS), is commonly used in these kinds of experiments. However, because of limited sample number, determination of kinetic parameters is difficult.

The last group of assays is based on the specific interactions of ARF1-GTP with its effector proteins, which mediate ARF1 function [141]. ARF1-GTP is an important regulator of membrane traffic and binds to coat proteins such as coatomers, clathrin adaptor protein (AP) complexes 1 and 3, and γ-adaptin homology-Golgi associated ARF-binding (GGA) proteins [142-143]. By binding to ARF-GTP these proteins are recruited to the cell membrane where they initiate the formation of transport vesicles. Whereas coatomers and AP proteins exist as multimeric protein complexes, the GGA proteins are monomeric polypeptides, which are comprised of four domains: VHS (binds to DXXLL sorting motifs), GAT (binds ARF-GTP), hinge (binds clathrin), and GAE (binds various proteins involved in vesicle formation). The GAT domain of GGAs 1-3, which can be expressed separately in bacteria, specifically interact with the switch regions 1 and 2 of ARF1-GTP and can be used as a tool to quantify the amount of ARF1-GTP in vitro and in vivo. For this purpose, a GTS tagged GGA-GAT domain can be added to an exchange reaction or cell lysate and after precipitation of GGA-GAT the amount of bound NΔ17ARF1-GTP can be detected by SDS-PAGE and western blotting [138]. Although this technique provides important information about the ability of NΔ17ARF1 to interact with its endogenous effector protein in the presence of a small molecule, it is very elaborate and therefore incompatible with high throughput screening approaches.

In order to combine the advantages of the rapid and high-sensitive real-time fluorescence measurements with the possibility to identify small molecule inhibitors of the interaction between NΔ17ARF1-GTP and GGA3, I developed a new FRET-based assay for the cytohesin catalyzed GDP/GTP exchange on NΔ17ARF1.

IV.4.2 A new FRET-based assay for the cytohesin catalyzed GDP/GTP exchange on NΔ17ARF1

Figure 76 displays the principles of the assay. NΔ17ARF1, C-terminally tagged with the fluorescent protein CyPET, is preloaded with GDP in the presence of EDTA and subsequently incubated with the Sec7 domain of ARNO. To monitor binding of NΔ17ARF1-CyPET-GTP to its effector protein GGA3, GGA3-GAT domain with its N-terminus fused to the fluorescent protein YPET is added. After starting the exchange reaction by addition of GTP, one can follow NΔ17ARF1-CyPet activation by detection of tryptophan fluorescence at ex280/em340 nm. Furthermore, binding of NΔ17ARF1-CyPET-GTP to YPET-GGA3 can be analyzed in real-time by FRET between the CyPET moiety of NΔ17ARF-CyPET and the YPET moiety of YPET-GGA3 at ex436/em535 nm at the same time.

CyPET is excited at 436nm and acts as a donor to induce fluorescence of YPET. CyPET and YPET are FRET-optimized variants of the fluorescence proteins CFP and YFP, respectively, and have been recently used to monitor ARF6 activation in living cells [144]. Since fluorescence energy transfer critically depends on the proximity of the two fluorophores involved, binding of GTP-loaded NΔ17ARF-CyPET to YPET-GGA3 leads to an increase in FRET between CyPET and YPET, and therefore to enhanced emission of YPET at 535nm.

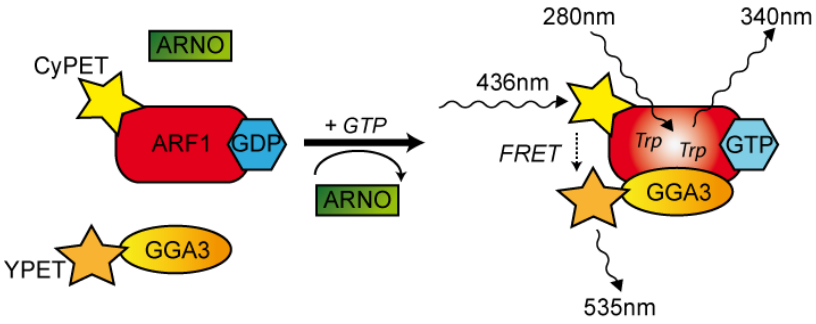

Figure 76 A FRET-based assay for the cytohesin catalyzed GDP/GTP exchange on NΔ17ARF1

GDP preloaded NΔ17ARF1-CyPET is incubated with the Sec7 of ARNO and YPET-GGA3. The exchange reaction is started upon addition of GTP. Conformational changes caused by GDP/GTP exchange on NΔ17ARF1-CyPET are detected by tryptophan fluorescence (ex280/em340nm). Simultaneously, the amount of GTP loaded NΔ17ARF1-CyPET in the reaction can be monitored by FRET (ex436/em535), resulting from the interaction between NΔ17ARF1-CyPET-GTP with YPET-GGA3.

IV.4.2.1 Proof of principle I: The FRET signal depends on the concentration of YPET-GGA3

To test whether GDP/GTP exchange on NΔ17ARF-CyPET can still be induced by ARNO-Sec7 in the presence of YPET-GGA3, I measured the exchange on NΔ17ARF-CyPET (0.7μM) in the presence and absence of ARNO-Sec7 (15nM) and added increasing amounts of

YPET-GGA3 (0.2-1µM) to the reaction. All measurements were performed in PBS, pH 7.4, 3mM $MgCl_2$ at 37°C in black 96well plates, in a total volume of 200µl.

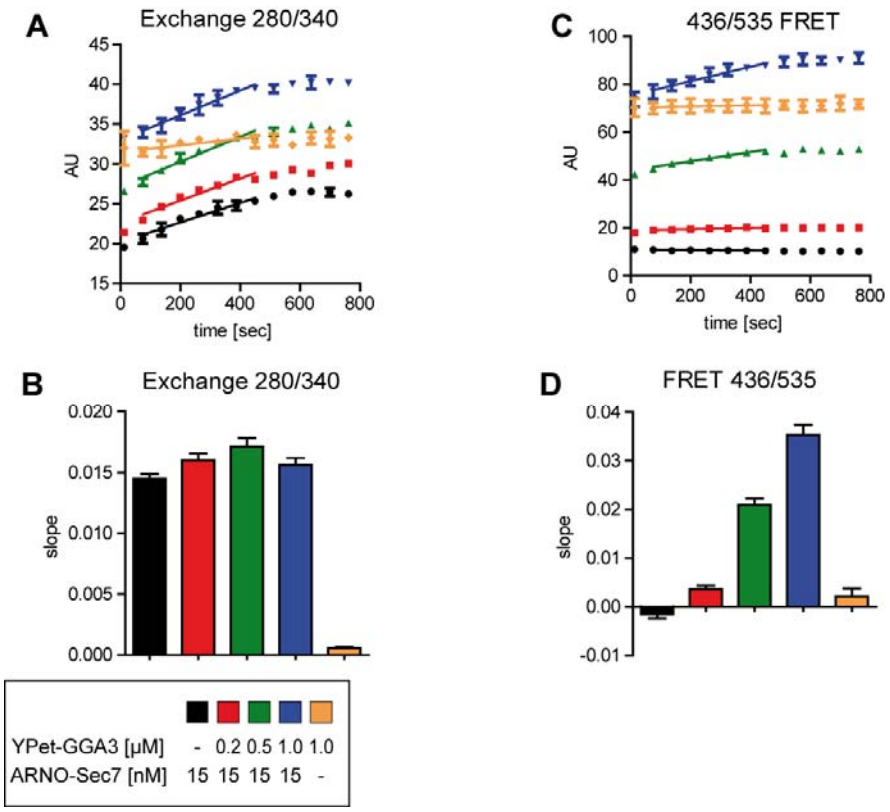

Figure 77 The FRET signal depends on the concentration of YPET-GGA3

A/C: Detected tryptophan fluorescence (A) or FRET (C) of NΔ17ARF1-CyPET in the presence (black, red, green, blue) or absence (orange) of ARNO-Sec7 or different concentrations of YPET-GGA3 (red, green, blue). The slope of the reaction was calculated by fitting the linear increase in tryptophan fluorescence or FRET by linear regression (shown as a line).

B/D: Calculated slope for the initial increase in tryptophan fluorescence (B) or FRET signal (D).The color scheme is the same as in A/C.

All measurements were performed in PBS, pH 7.4, 3mM $MgCl_2$ at 37°C in black 96well plates, in a total volume of 200µl and 0.7µM NΔ17ARF1-CyPET. Fluorescence was measured every ~20sec. Data represent the means of duplicates of one representative measurement (out of three independent measurements).

Figure 77 depicts the obtained signals at 280/340nm (exchange = tryptophan fluorescence, A) and 436/535nm (FRET = interaction between NΔ17ARF-CyPET-GTP and YPET-GGA3, C) and the calculated slope for the initial, linear phase of the reaction (B, D). GDP/GTP exchange on NΔ17ARF-CyPET critically depends on the presence of ARNO-Sec7 (Figure 76, black and orange bars). Although increasing amounts of YPET-GGA3 raised the fluorescence signal at the starting point due to higher absolute protein concentrations they did not influence the slope of the reaction (red, green, blue). Thus, YPET-GGA3 does not interfere with the Sec7-catalyzed exchange reaction. No FRET signal could be detected in the absence of YPET-GGA3 (black, Figure 77C/D). As expected, increasing amount of YPET-GGA3 enhanced the FRET signal (red, green, blue), which was detected simultaneously to the tryptophan fluorescence, due to increased complex formation between Δ17ARF-CyPET-GTP

and YPET-GGA3. In agreement to tryptophan fluorescence, only a weak FRET signal was detected in the absence of ARNO-Sec7 with the highest concentration of YPET-GGA3 (orange). Based on these results a concentration of 0.5µM of YPET-GGA3 was selected for further experiments.

Taken together, these data show that fusion of Δ17ARF with CyPET does not interfere with its exchange activity and that the FRET-signal obtained for the interaction of Δ17ARF-CyPET-GTP and YPET-GGA3 critically depends on the presence of Δ17ARF-CyPET-GTP and the concentration of YPET-GGA3.

IV.4.2.2 Proof of principle II: The FRET signal depends on the amount of Δ17ARF-CyPET-GTP

To demonstrate, that different amounts of Δ17ARF-CyPET-GTP can be detected with this FRET assay, I conducted an exchange assay in the presence of increasing concentrations of ARNO-Sec7 (3.5-30nM) or Δ17ARF-CyPET (0.1-1.3µM).

As expected, the measured slopes for tryptophan fluorescence were directly dependent on the concentration of ARNO-Sec7 and Δ17ARF-CyPET, reflecting increasing concentrations of Δ17ARF-CyPET-GTP (Figure 78). The slopes of the signals obtained for FRET between Δ17ARF-CyPET-GTP and YPET-GGA3 directly mirrored the slopes of the tryptophan fluorescence, demonstrating the suitability of this assay to quantitatively monitor the GDP/GTP exchange on Δ17ARF1.

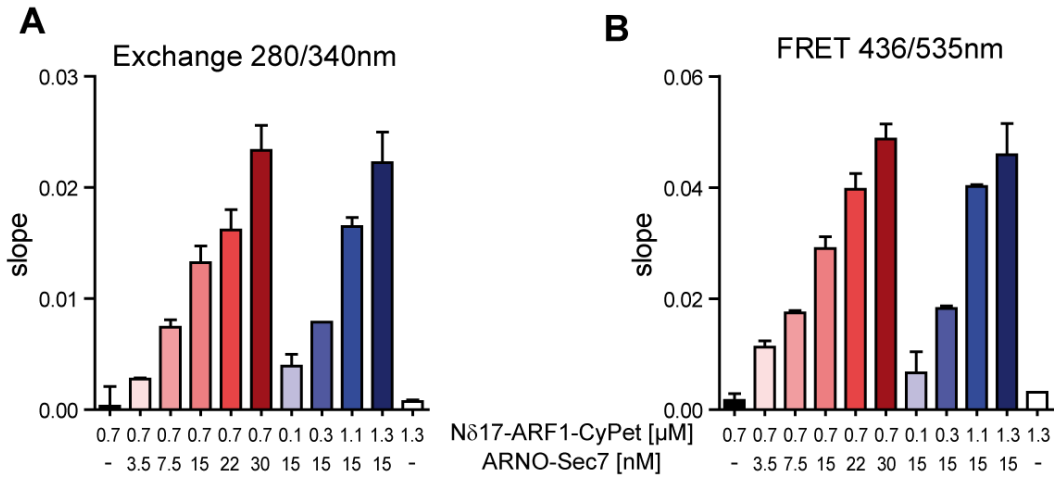

Figure 78 The FRET signal depends on the amount of NΔ17ARF1-CyPET-GTP

Calculated slope for the initial increase in tryptophan fluorescence (A) or FRET signal (B). Increasing concentrations of ARNO-Sec7 (0-30nM) were titrated to 0.7µM NΔ17ARF1-CyPET (red bars) or the concentration of NΔ17ARF1-CyPET was varied in the presence of 15nM ARNO-Sec7 (blue bars).
All measurements were preformed in the presence of 0.5µM YPET-GGA3.

IV.4.2.3 Proof of principle III: The FRET-based assay is suitable for screening

Next I examined whether the FRET based exchange assay is suited to detect chemical inhibition of cytohesins by SecinH3 and Secin16. For this purpose I performed an exchange assay on Δ17ARF1-CyPET in the presence of SecinH3 (15µM), Secin16 (2.5µM) or solvent (1%DMSO). As Figure 79 shows, inhibition of ARNO-Sec7 with SecinH3 or Secin16 is detected by a reduced slope in both, the tryptophan fluorescence (Figure 79A) and the FRET signal (Figure 79B). Again, both detection methods revealed consistent results.

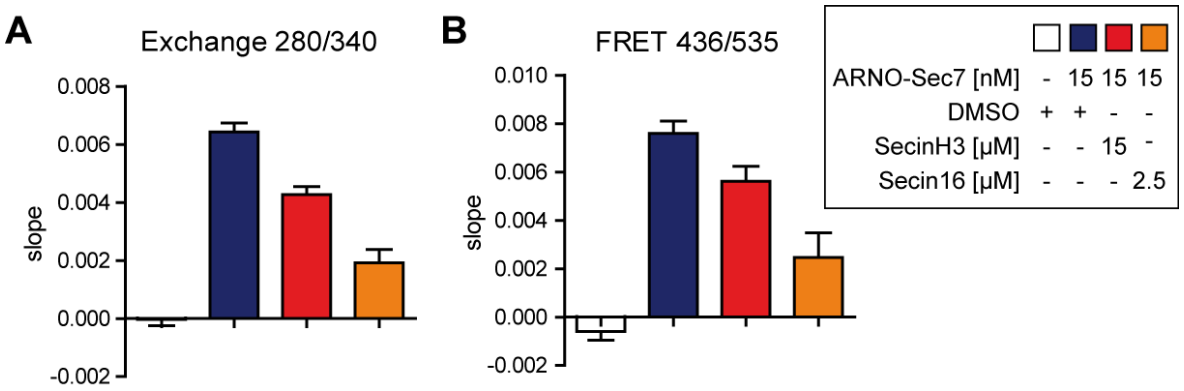

Figure 79 Inhibition of cytohesin with SecinH3 or Secin16 decreases the FRET signal for GDP/GTP exchange on Δ17ARF-CyPET

Calculated slopes for the initial increase in tryptophan fluorescence (A) or FRET signal (B) of NΔ17ARF1-CyPET (0.7µM) in the presence of 15µM SecinH3 (red), 2.5µM Secin16 (orange) or solvent (0.4% DMSO, blue). All measurements were preformed in the presence of 0.5µM YPET-GGA3. Data represent the mean of 3 independent measurements.

To test the suitability of the FRET based GDP/GTP exchange assay on Δ17ARF1-CyPET for use as a screening assay, I determined the Z'-factor [130]. This factor reflects both the dynamic range of the signals (or the signal-to-noise-ratio) and the variation of the obtained signals and is therefore a useful tool to describe the quality of an assay system. For the tryptophan fluorescence as well as for FRET based detection of GDP/GTP exchange on Δ17ARF1-CyPET a Z'-factor of 0.6 was calculated out of six independent measurements with the reaction in the presence or absence of ARNO-Sec7 used as a positive or negative control, respectively. This Z´-value rates the assay as being suitable for screening.

V Discussion

V.1 Cytohesins are cytoplasmic ErbB receptor activators

The known function of cytohesins is to act as a GEF on ARF proteins. In the last years, several publications furthermore implemented cytohesins in the regulation of cell signaling. Kliche et al. have shown that cytohesin-1 binds to and enhances the transforming potential of transmembrane protein kaposin A in tumor cells by selective activation of the mitogen-associated protein (MAPK)-signaling pathway [88]. Recently, Hafner et al. reported the involvement of cytohesins in insulin-signaling. Inhibition of cytohesins with SecinH3 blocks the transcription of insulin-dependent genes in human HepG2 cells and in murine liver cells in vivo: SecinH3 most likely inhibits the binding of adapter molecules like IRS-1 (insulin receptor substrate 1) to the activated insulin receptor. In parallel, Fuss et al. described a Drosophila mutant in which expression of the only cytohesin homolog Steppke is strongly reduced [102]. These flies show the typical phenotype caused by diminished insulin signaling. These findings where substantiated by an additional study of Lim et al. showing that cytohesins interact with the Connector Enhancer of KSR1 (CNK1), thereby promoting insulin receptor signaling [96].

The results described in this work are the first evidence that cytohesins act as cytoplasmic ErbB receptor activators.

V.1.1 Inhibition of cytohesins reduces ErbB receptor signaling

Treatment of H460 cells with the cytohesins antagonist SecinH3 reduces EGFR phosphorylation and signaling in H460 cells (Figure 13). This effect can be directly ascribed to cytohesin inhibition for the following reasons: First, transfection of the cytohesin specific aptamer M69 [95] mirrored the effect of SecinH3 (data not shown, experiments were done by Jin-Na Song [104]). Second, treatment with the control compound XH1009 [145] that is structurally related to SecinH3 but does neither bind nor inhibit cytohesins had no effect on EGFR phosphorylation (Figure 14). Third, knockdown of cytohesins with specific siRNAs also decreased EGFR phosphorylation (data not shown, experiments were done by Jin-Na Song). In addition, the re-expression of ARNO in siRNA-treated cells rescued the effect of ARNO knockdown in EGFR autophosphorylation (Figure 20), showing a direct connection between cytohesins protein level and EGFR phosphorylation.

Cytohesins are not only involved in EGFR signaling but in the signaling of the whole ErbB receptor subfamily of receptor tyrosine kinases (RTKs). In agreement, treatment of HER2/HER3 expressing SkBr3 cells with SecinH3 decreases HER3 phosphorylation and signaling (Figure 15). Again, the involvement of cytohesins in the activation of HER3 was confirmed by the aptamer M69, the control compound XH1009 and cytohesin specific siRNAs.

Interestingly, M. Theis observed an inhibition of serum mediated MAPK activation upon treatment of HeLa cells with the cytohesin specific aptamers M69 and K61 [89], which might now be explained by ErbB receptor signaling inhibition.

V.1.2 Cytohesins enhance ErbB receptor activation independently of their GEF activity

Overexpression of cytohesin-2 (ARNO) enhances ligand-induced EGFR phosphorylation (H460 cells, Figure 16) and HER3 phosphorylation (SkBr3 cells, Figure 17). In this thesis, ARNO was selected for all overexpression studies, since it shows higher expression than cytohesin-1 and -3 in both cell lines.

The Sec7 domain of ARNO is sufficient to enhance ligand-induced EGFR phosphorylation (Figure 18). However, overexpression studies with the GEF-inactive ARNO mutant ARNO-E156K [79] showed that the GEF activity of the Sec7 domain is not required for the ARNO-mediated activation of ErbB receptors (Figure 19). The ability of ARNO-E156K to enhance ErbB receptor activation is not due to its overexpression. This is because ARNO-E156K expressed as endogenous ARNO protein level is able to rescue the inhibition of EGFR phosphorylation induced by ARNO knockdown (Figure 20).

Besides, knockdown of neither ARF1 nor ARF6 by RNA interference had an influence on the activation of the EGFR (data not shown, experiments were done by Jin-Na Song [104]), substantiating the finding that the cytohesin-mediated activation of ErbB receptors is independent of GEF activity.

Summing up, cytohesins facilitate the activation of ErbB receptors in a GEF-activity independent mechanism.

These results establish a new function of cytohesins, since the so far described functions of cytohesins in cell signaling all depend on the GEF activity of those proteins. Only two reports of GEF-independent activity of cytohesins can be found in the literature. Firstly, Theis et al. developed an aptamer that specifically binds to cytohesin-2 without disturbing the GEF activity toward ARF1. Transfected into HeLa cells this aptamer abrogated MAP-signaling and

reporter gene transcription directed by serum response elements [89]. Based on the function of cytohesins as ErbB receptor activators described in this work, the inhibition of MAPK signaling might be explained by reduced ErbB signaling due to cytohesin inhibition. Secondly, Kolanus et al. identified cytohesin-1 as a regulator of integrin β binding to ICAM-1 in immune cells [83]. The GEF-inactive cytohesin E157K enhanced integrin β binding to ICAM-1 as efficiently as the wild-type protein [87]. Interestingly, the Sec7 domain of cytohesin-1 was found to be sufficient for interaction with integrin β. However, the presence of the PH domain is crucial for cytohesin-mediated integrin activation [80, 83].

The finding that the Sec7 domain of cytohesins is sufficient to mediate activation of ErbB receptors while not requiring the GEF function of this domain, thus implicate a hitherto unknown GEF-independent function of cytohesins.

SecinH3 targets the Sec7 domain of cytohesins and inhibits its GEF function [90, 145]. The finding that cytohesin-mediated activation of ErbB receptors is independent of GEF activity raises the question, why SecinH3 inhibits cytohesin-mediated ErbB receptor activation.

To address this point it is important to consider that SecinH3 was identified as a cytohesin Sec7-domain inhibitor completely independently of whether or not the binding had an effect on the GEF activity of the Sec7 domain [90]. Thus, SecinH3 (which stands for Sec7-domain inhibitor) should be seen as a Sec7 inhibitor rather than (exclusively) as a GEF inhibitor. Apparently, binding of SecinH3 to the Sec7 domain inhibits both, the GEF-dependent and the GEF-independent functions of this domain. To understand the molecular basis of this dual function of the Sec7 domain as well as the inhibitory function of SecinH3 on GEF activity and ErbB receptor activation, the EGFR should be co-crystallized with the Sec7 domain in both the presence and absence of SecinH3. Such an analysis will give more insights into the mechanism of cytohesin-mediated ErbB receptor activation that can be useful to explain the inhibitory function of SecinH3.

V.1.3 Cytohesins facilitate a conformational rearrangement in the intracellular domains of EGFR dimers

Activation of ErbB receptors was originally considered to result solely from the ligand induced dimerization of the intracellular domains which leads to subsequent kinase activation [22]. From crystallographic, biochemical and biophysical data it is becoming increasingly evident that EGFR dimerization and activation of the kinase domains are distinctly regulated and thoroughly balanced processes. The mechanisms by which this balance is achieved are still largely elusive.

In 2002, two papers were published back to back shedding new light on the ligand induced dimerization of EGFR. The studies of Garret et al. and Ogiso et al. [15-16] redeem the prior model, in which the bivalent ligand, by binding to both receptor monomers, functions as a clamp driving receptor dimerization [13], as it can often be found in receptor tyrosine kinases. Opposed of this, EGFR dimerization is solely mediated by receptor-receptor contacts facilitated by rearrangements of the extracellular domains due to ligand binding (see introduction). Although these data enormously advanced the understanding of EGFR activation, there are still some open questions that cannot be explained by this model. Since the early studies of EGFR, it has been known that there are two affinity classes for EGF binding to its cell surface receptor [146]. Several studies try to correlate the two affinity states of EGFR with the current models, but come to conflicting results [17, 147-148]. Another issue is the existence of preformed EGFR dimers on the cell surface, showing that the mere dimerization of the EGFR is not sufficient for activation [149-151]. Recent crystallographic studies extend the model of dimerization-driven EGFR activation by the finding, that only a subset of the dimers are catalytically active. These are those that adopt a distinct conformation called the asymmetric dimers, where one kinase acts as an allosteric activator for the other [23, 25-26] (see introduction, II.1.4.2). Activity studies with the purified kinase domains indicate the existence of an autoinhibited state of the kinase domains and further substantiate an allosteric model of EGFR activation, in which the activation of EGFR results from the intrinsic ability of the receptor kinase domains to form active (asymmetric) dimers as soon as they are released from their default autoinhibited state [23, 152-155]. The only activator required in this model is the ligand itself, which binds to the ectodomain of the receptor and induces or stabilizes the structural rearrangements that release the kinase domains from their autoinhibited state [17, 47]. The finding that EGFR activation is enhanced by cytohesins indicates that EGFR activation is likely not to be comprehensively explained by ligand-induced release from autoinhibition and the subsequent spontaneous formation of the asymmetric dimer. The question arises, how the cytohesins can be implemented into this system.

ErbB receptor clustering on the cell membrane has been intensively discussed in the literature as an additional effect that may affect ErbB receptor activation. However, several studies have reported contradictory findings about the connection between ErbB activation and receptor clustering [156-158]. These contradictions may be due to the application of different imaging methods with different resolution scales or to varying expression levels of the studied receptors. In our system, using superresolution light microscopy (STED microscopy = stimulated emission depletion microscopy) on H460 plasma membrane sheets, EGF

stimulation induces a slight increase in the measured EGFR cluster size, which was not affected by SecinH3 (data not shown, experiments were done by David Walrafen and Arne Schreiber), indicating that the reduction of EGFR signaling observed after cytohesin inhibition is not a result of alterations in cluster size at the observed ~100nm scale.

Cytohesins are known as GEFs for ARF proteins and are thus involved in endocytosis [82]. Although this function involves the GEF activity of cytohesins, which is not important for their activity on ErbB receptors, cytohesins may affect EGFR activation indirectly by modulation of endocytosis or degradation of the ErbB receptors. However, SecinH3 does not reduce EGF-triggered receptor internalization (Figure 21), arguing against such an indirect effect. Furthermore, this result also suggests that cytohesins do not affect dimerization of the EGFR, since dimerization rather than phosphorylation of the EGFR was reported as the inducer for EGFR endocytosis [106]. Indeed, cytohesins do not alter ErbB receptor dimerization in HER2/HER3 coimmunoprecipitations (Figure 26) and ErbB receptor crosslinking studies (Figure 22, Figure 23, Figure 24, Figure 25), indicating that cytohesins act independently of the dimerization of ErbB receptors and facilitate the activation of already dimerized receptors.

This hypothesis is further supported by the result that cytohesins enhance the activation of constitutively dimerized EGFR (lz-EGFR experiments, Figure 30, Figure 31). Having shown that cytohesins do neither affect receptor clustering, nor trafficking, nor dimerization, but instead act on the already dimerized EGFR receptor, suggests the assumption that cytohesins enhance EGFR activation by facilitating conformational changes in the intracellular part of the receptor. Steady state fluorescence anisotropy measurements of cells transfected with the mCitrine labeled constitutively dimerized EGFR are in full agreement with this assumption (Figure 36).

To further understand the mechanism by which cytohesins facilitate the activation of ErbB receptors, it is necessary to distinguish between a direct and an indirect effect of cytohesins on the conformation of the intracellular part of the receptor. This is the question whether cytohesins directly interact with and activate the receptor or an additional factor is needed. To gain evidence for a direct interaction of cytohesins and the cytoplasmic domain of EGFR, I used a cell-free reconstitution system. Purified full-length ARNO or the Sec7 domain of ARNO directly interacts with purified cytoplasmic domain of EGFR with an apparent dissociation constant around 1μM (Figure 41). In addition, ARNO directly stimulates autophosphorylation of EGFR in the cell-free reconstitution system (Figure 43, Figure 44). Together with the data obtained in the cellular assays, these results strongly argue for

cytohesins acting on the intracellular domains of dimerized EGFR as conformational activators.

In a cellular context, the transition from the inactive symmetric to the active asymmetric dimer represents a stage where additional layers of modulation of receptor activation, inhibitory as well as stimulatory, might come into play. This additional layer of regulation would allow the cell to modulate or fine tune, for a given amount of ligand-bound receptor, the number of activated receptors according to cellular needs. Recently, MIG6 was identified as an inhibitor of EGFR signaling [32-33, 35, 159] that acts by blocking the formation of the asymmetric dimer [34], indicating that a layer of negative regulation appears actually implemented. Except for Dok-7, cytoplasmic activators have not been described for any receptor tyrosine kinase. Dok-7, a SH2-domain-containing adaptor protein for the MuSK receptor tyrosine kinase, enhances the activity of the muscle-specific receptor kinase MuSK by dimerizing partially autophosphorylated and thus partially activated receptor monomers [113-114, 160]. In contrast, cytohesins do neither influence receptor dimerization nor require receptor autophosphorylation (Figure 42) for binding but function as conformational activators of receptor dimer. Thus, these results establish cytohesins as the first cytoplasmic conformational activators of ErbB receptors. It is important to point out that the existence of cytoplasmic EGFR activators like cytohesins does not abolish ligand dependency of receptor activation, since the autoinhibition imposed on the kinase domain by the extracellular domains still has to be released by ligand binding [155]. Furthermore, it does not preclude receptor activation to occur in the absence of activators as can be seen for the intracellular domain of EGFR in the cell free autophosphorylation experiments (Figure 43). It remains to explain, how cytohesins activate the EGFR.

A first insight into the mechanism of cytohesin-mediated EGFR activation can be obtained by summarizing the obtained results (Figure 80). ARNO (i) binds to intracellular region of the EGFR (Figure 41), (ii) does not require EGFR autophosphorylation for binding (Figure 42), (iii) enhances EGFR autophosphorylation by direct interaction (Figure 43), (iv) does not modify receptor dimerization but acts on EGFR dimers (Figure 23, Figure 31), (v) modulates the conformation of the EGFR dimers (Figure 36).

Further experiments showed that the Sec7 domain of cytohesins most likely interacts with either the kinase domain or the juxtamembrane domain of the EGFR, since it also bound to an EGFR construct lacking the C-terminal 188 amino acids (EGFR-ICD1022, Figure 41). The C-terminal part of the EGFR has been demonstrated to exhibit regulatory activity on the EGFR kinase [161-162]. However, the “more N-terminal” located binding site of ARNO on

the EGFR might argue against a direct involvement of the C-terminus in the cytohesin-mediated activation of ErbB receptors.

Furthermore, ARNO does not interact with MIG6 (Figure 41), excluding a direct influence of ARNO on the MIG6 function.

Even if the exact conformational rearrangement has not been established, these results show that ARNO functions as a conformational activator of EGFR dimers and, thus, acts by an unprecedented mechanism. Structural analyses of the complex between cytohesins and ErbB receptors are necessary to further understand the detailed mechanism of cytohesin-mediated ErbB receptor activation.

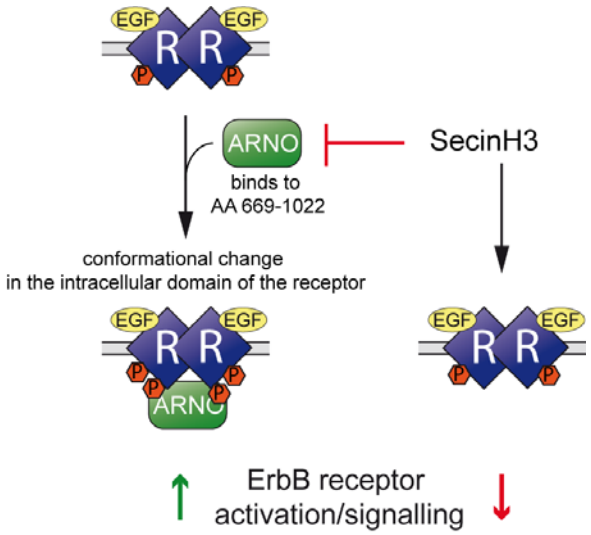

Figure 80 Model of cytohesin mediated ErbB activation

ARNO binds to the intracellular domain of EGFR dimers and induces a conformational change that facilitates EGFR activation. The cytohesin antagonist SecinH3 inhibits ARNO and reduces EGFR activation and signaling.

Although the precise mechanism of cytohesin-mediated EGFR activation is not known, the cytohesin mediated activation of EGFR signaling show many features that are distinct to the function of cytohesins on the insulin receptor [90, 96]. In both pathways cytohesins facilitate the downstream signaling of the receptors. Yet, cytohesins do not increase the phosphorylation of insulin receptor, but instead facilitate the formation of the complex between the insulin receptor and the insulin receptor substrate 1 (IRS-1). This effect has been shown to be ARF dependent and to require the coiled-coil domain of cytohesins, which stands in clear contrast to the GEF activity independent function of the cytohesin Sec7 domain on ErbB receptors. How can these differences in the mechanism of RTK signaling activation by cytohesins be explained?

For one thing, both receptors are activated in a dimeric state, but the insulin receptor exists as a constitutive dimer on the cell membrane, whereas the ErbB receptors exist as a dynamic assembly of monomers, dimers and oligomers. The associated difference in the mechanism of receptor activation may account for different regulation mechanisms. Whereas in insulin signaling the phosphorylation of adaptor proteins seems to be the important step, ErbB receptor activation is regulated already at the level of receptor autophosphorylation. For another thing, the mechanism of kinase activation is quite distinct and might therefore demand a different mode of action for cytoplasmic activators. The insulin receptor kinase requires the trans-phosphorylation of specific tyrosine residues in the so called activation loop of the kinase to render the kinase fully active [163]. On the contrary, EGFR kinase activation does not depend on phosphorylation in the activation loop of the kinase but instead requires the formation of an asymmetric kinase dimer [23]. However, the detailed mechanisms underlying the activation of different RTKs by cytohesins can just be speculated about. Structural analysis and crystallographic data of the complexes between cytohesins and RTK are needed to fully understand the mechanism of cytohesin-mediated modulation of RTK signaling.

V.2 Pathophysiological relevance of cytohesins in lung cancer

V.2.1 Cytohesins are overexpressed in human lung adenocarcinomas

Enhanced EGFR signaling is known to be a hallmark in many human cancers including non-small cell lung cancer (NSCLC) [48]. Having shown that cytohesins enhance EGFR activation in H460 cells, a human NSCLC cell line, one may assume that deregulation of cytoplasmic EGFR activators like cytohesins might play a role in tumorgenesis.

Immunostaining of primary human lung adenocarcinomas with an antibody detecting ARNO and cytohesin-1 revealed that these two cytohesins are strongly expressed in >80% of the carcinomas (Figure 56), demonstrating cytohesin upregulation in a large fraction of human lung adenocarcinomas. In agreement with the cellular data, high expression levels of ARNO/cytohesin-1 also correlate with increased EGFR phosphorylation and signaling (MAPK- and Akt-pathway) in human lung adenocarcinoma (Figure 57).

Cancer cell commonly critically depend on a specific signaling molecular for growth and survival (oncogene addiction [164]). Lung cancer cells are often addicted to EGFR. The

majority of these tumors has either upregulated or mutant EGFR and initially responds well to EGFR tyrosine kinase inhibitors [48-49]. Hence, the response rate to EGFR tyrosine kinase inhibitor therapy can be used as a measure for EGFR addiction. Nevertheless, a significant fraction of lung cancers with apparently normal EGFR status also responds to EGFR inhibitors, reflecting their EGFR addiction [48]. How these tumor cells maintain a sufficient level of EGFR signaling to satisfy their EGFR addiction in the absence of activating EGFR mutations or increased expression levels of EGFR, is currently unclear. The observation that ARNO/cytohesin-1 overexpression is associated with an activated EGFR signaling pathway in human lung adenocarcinoma provides a possible explanation for the EGFR addiction of these cancer cells.

V.2.2 Chemical inhibition of cytohesins diminishes proliferation of EGFR dependent lung cancer cell lines

The observation that ARNO/cytohesin-1 expression correlates with increased EGFR signaling in human lung adenocarcinomas raises the questions whether cytohesins also promote the proliferation of the tumor cells. In this case attenuation of ErbB activity by antagonizing cytohesins with Secins (SecinH3 or Secin16) should lead to a decrease in cell proliferation. Indeed, treatment of a set of EGFR-dependent human lung adenocarcinomas with the cytohesin antagonists SecinH3 or Secin16 significantly diminishes cell proliferation (Figure 48, Table 1). Interestingly, the "gate keeper mutation" (T790M) which renders the cells resistant to Iressa treatment, does not affect the sensitivity of proliferating cells for cytohesin inhibition. In agreement with an EGFR-dependent inhibition of proliferation, the partially or weakly EGFR-dependent cell line H1838 [123, 165-166] is not affected by cytohesin inhibition. This EGFR-specific effect of cytohesin inhibition on the proliferation of EGFR-addicted tumor cells is further supported by the results obtained by using the BA/F3 cell system. BA/F3 cells do not express ErbB receptors and critically depend on IL-3 in their proliferation. By transfection of oncogenes it is possible to addict the cells to the function of these genes rendering them independent of IL-3. Chemical inhibition of cytohesins does not affect the IL-3 dependent proliferation of the parental wild-type BA/F3 cell line, but does significantly reduce proliferation in EGFR-addicted BA/F3 cells (Table 2, Figure 55), underlining the EGFR-specific inhibitory effect of Secins on the proliferation of EGFR-dependent cancer cell lines. Again, the T790M mutation did not affect the sensitivity of the cells for cytohesin inhibition.

One of the major effects of receptor tyrosine kinase inhibition in sensitive EGFR-dependent cells lines is the induction of apoptosis [167-168]. In accordance, chemical inhibition of cytohesins in EGFR-dependent PC9 cells induces a G1 arrest in cell cycle which results in the induction of apoptosis (Figure 49, Figure 50). The inhibitory effect of SecinH3 on the proliferation of PC9 can also be observed in nude mice bearing PC9 xenografts. Treatment of these mice with SecinH3 results in decreased tumor cell proliferation measured as the uptake of radiolabeled thymidine in the tumor and visualized with positron emission tomography (Figure 53). Histological investigations of the SecinH3 treated xenografts substantiated the observed decrease in proliferation (Ki-67 staining was strongly reduced) and revealed a strong increase in TUNEL positive cells as compared to untreated xenografts, indicating apoptosis (Figure 54).

Taken together, all these results argue for an EGFR-specific effect of cytohesin inhibition on the proliferation of EGFR-dependent cell lines.

However, treatment of the two cell lines H460 and A549 with SecinH3 or Secin16 also results in a distinct inhibition of proliferation (Figure 45, Table 1). Both cell lines harbor an activating mutation in KRAS and do neither have amplified nor mutated EGFR. Based on their weak sensitivity to EGFR tyrosine kinase inhibitors (TKI), they are classified as TKI-resistant and EGFR-independent [103, 123]. At first sight, these results seem mutually contradictory as it might be expected that (i) these cells are addicted to KRAS and that (ii) inhibition of EGFR activation by Secins, similar to TKI treatment, should not affect proliferation of these cells. However, several studies show that these cells still depend on EGFR [116-117, 169], as knockdown of EGFR results in decreased proliferation of both cell lines. Nevertheless, the lack of sensitivity to TKI still remains unclear and might support the hypothesis that the mode of action for EGFR TKIs is more complex than simply blocking EGFR-kinase activity and might involve the inhibition of further RTKs [169-171].

Again, the impact of cytohesin inhibition on cell proliferation was also found in mice bearing H460 xenografts. In agreement with the results obtained for the PC9 cells, treatment of these tumors with SecinH3 led to a reduction in cell proliferation and tumor size as well as to the induction of apoptosis (Figure 46, Figure 47).

In summary, these results implement cytohesins as cytoplasmic conformational activators of ErbB receptors that are of pathophysiological relevance for the proliferation of EGFR-dependent lung cancer cell lines.

V.3 Identification of improved cytohesin antagonists in vitro

The pathophysiological significance of cytohesins in human cancer is underlined by the finding that the proliferation of EGFR-dependent tumor cells is drastically reduced by inhibition of cytohesins, making them an interesting target for cancer therapy.

Yet, GEFs are not classically considered as druggable targets. Protein-protein interactions commonly show a high affinity and involve large contact surfaces with little cavities or possible binding sites for small molecules [93]. The discovery of more and more small molecules that target protein-protein interaction in the last years, however, sheds new light on the drug-ability of these targets [172]. The small molecule SecinH3, discovered by Hafner et al. [90], is another important example that highlights the potential of cytohesins as new targets for small molecule inhibitors.

Small molecules that specifically target GEFs would also represent valuable tools to indirectly target another class of undruggable proteins: small GTPases of the Ras superfamily.

Upregulated activity of small GTPases is involved in various human diseases. Unlike in the case of the three Ras proteins (HRas, KRas and NRas), the upregulated activity of the other small GTPases is commonly not caused by direct mutations but instead involves the altered expression or activity of their regulating proteins, like GEFs [93]. Also ARFs, regulated by GEFs of the cytohesin family, play an important role in the regulation of the proliferation and invasive capacity of cancer cells, making them attractive targets for cancer therapy [93, 137, 173-174]. Unfortunately, no specific, direct ARF inhibitor has been described. However, indirect inhibition of ARFs by targeting their specific GEFs has been proven very useful to elucidate the cellular functions of ARFs. The fungal metabolite brefeldin A (BFA) binds to the complex of GDP-bound, inactive ARF1 and the Sec7 domain of large GEFs, thereby inhibiting GDP/GTP exchange catalyzed by this subgroup of GEFs [175]. By a similar mechanism, the small molecule LM11 targets the complexes of ARF1-GDP with both the large GEF BIG1 and BFA-insensitive ARNO. Both molecules have been shown to inhibit ARF-regulated traffic at the Golgi apparatus in cells [92].

The usefulness of the cytohesin-specific inhibitor SecinH3 as an indirect inhibitor of ARF1 and ARF6 has been proven in various studies [90, 96-101, 126]. However, the biochemical properties of SecinH3 make it difficult to further continue along the long way towards its development as a clinically applicable drug. The limited solubility of approximately 15µM in aqueous solution containing 0.5% DMSO and a dissociation constant in about the same concentration range, makes it hard to perform any biochemical characterization of the

compound. Although in the experiments carried out during this thesis impressive activity data of SecinH3 in mice was obtained, post mortal autopsies showed precipitates of the compound in the abdomen of the mice. Improvements in the solubility of SecinH3 may therefore lead to great advances in the in vivo performance of the compound.

In order to further elucidate the potential of cytohesin inhibitors in anti-cancer therapy improved small molecule inhibitors are needed.

As a first step towards this goal, I established a simple and robust assay suitable for high throughput screening that monitors the exchange activity of cytohesins on ARF1. It should be noted that this assay allows the screening of compounds that inhibit the GEF activity of cytohesins, but gives no information about the inhibition of GEF-independent function of cytohesins. However, the inhibition of GEF activity can be used as an indicator for the binding of the compound to the Sec7 of cytohesins. The interference of the identified molecules with the GEF independent function of cytohesin can then be tested in separate assays.

V.3.1 2nd generation Secin chemotypes

In order to identify more potent cytohesin inhibitors, 145 compounds (referred to as second-generation Secin chemotypes) were tested for their potential to inhibit cytohesin catalyzed GDP/GTP exchange on ARF1. These 2nd generation Secin chemotypes were predicted by virtual screening based on structure activity relationship data for SecinH3 previously obtained in the lab. The two most potent compounds showed a 3- respectively 6-fold better inhibition of GDP/GTP exchange on ARF1 as compared to SecinH3 and were subjected to further analysis in cell culture. Because of severe solubility problems, the testing of the most potent compound Secin69 had to be discontinued, leaving Secin16 as the new lead compound.

In addition to the characterization in the GDP/GTP exchange assay, all compounds were tested in two further assays in order to monitor their interference with cytohesin-mediated insulin signaling (dFOXO assay, group of Prof. Hoch, University of Bonn) [102] or cytohesin dependent adhesion of human leukocytes (cell adhesion assay, group of Prof. Kolanus, University of Bonn) [83, 126].

Only two compounds (Secin16 and Secin132, which share a similar structure) were identified as hits in all three assays [126]. Secin16 was the most active compound in inhibiting the insulin signaling which led to the transcription of the dFOXO target gene 4EB-P and clearly decreased human leukocyte adhesion. Secin132 also showed inhibitory activity in all three assays, but was less potent than Secin16 (IC50 exchange assay; Secin16: 3.7μM, Secin132:

8µM). Secin69 exhibited a cytotoxic effect in the cell adhesion assay, probably due to its limited solubility, but was also active in the dFOXO-assay.

Compound	Hit
Secin16	Consensus
Secin132	Consensus
Secin67	Cell adhesion
Secin92	Cell adhesion
Secin105	Cell adhesion
Secin107	Cell adhesion
Secin114	Cell adhesion
Secin144	Cell adhesion
Secin111	Cell adhesion
Secin110	Cell adhesion, exchange
Secin134	Cell adhesion, exchange
Secin2	Exchange
Secin23	Exchange
Secin44	Exchange
Secin46	Exchange
Secin61	Exchange
Secin62	Exchange
Secin86	Exchange
Secin87	Exchange
Secin122	Exchange
Secin133	Exchange
Secin69	FoxO, exchange
Secin3	FoxO
Secin7	FoxO
Secin13	FoxO
Secin15	FoxO

Table 7 Activity of selected 2nd generation Secin chemotypes in different cytohesin-dependent assays
Exchange: ARNO-Sec7 catalyzed GDP/GTP exchange on Δ17-ARF1, cell adhesion: assay to measure the adhesion of human leukocytes, FOXO: insulin signaling dependent transcription of FOXO target genes in Schneider 2 insect cells, Consensus: compounds were active in all three assays.

All other compounds were either not active in all assays, active in only one assay or showed activity in only two assays (Table 7). Interestingly, there was no compound that showed activity in the cell adhesion- and dFOXO-assay without being active in the exchange assay, which might indicate the dependence on GEF activity inhibition. Although the facilitation of ß integrin binding to ICAM-1 is demonstrated to be GEF-activity independent [83], the LFA-1 induced cell adhesion and cell spreading involve the GEF activity of cytohesins [80, 87]. Seven compounds were found to be active only in the cell adhesion assay and 4 compounds in the dFOXO-assay (Table 7). Whether these compounds target GEF-activity independent functions of cytohesins can only be speculated on, until it is demonstrated that they indeed target cytohesins. In a similar way, it has to be shown that the 10 compounds identified as hits only in the exchange assay actually target cytohesins (instead of ARF1). The lack of activity in cell-based assays might also be caused by solubility problems, since the concentrations used in these assays are much higher than in the exchange assay.

V.3.2 Secin16

As the new lead compound, Secin16 not only exhibits an improved IC50 value for the inhibition of ARNO-Sec7 catalyzed GDP/GTP exchange on Δ17-ARF1 (IC50 3.7µM), but also shows higher potency in reducing proliferation of EGFR-dependent lung cancer cell lines (Table 1, Figure 45, Figure 48). However, Secin16 showed a decreased solubility in aqueous solution as compared to SecinH3 (8µM versus 15µM, data not shown). The approximately 3 fold improvement in potency is partially abolished by the two-fold decrease in solubility. In

order to optimize the relationship between potency and solubility a set of Secin16 based structures was tested that display a lower clogP value as compared to Secin16 (Table 3, Figure 61). Two Secin16 analogs showed a slightly improved IC50 value combined with a predicted >10-fold increase in solubility, as compared to Secin16, but did not prove their superiority to Secin16 in cell based assays (data not shown). The latter is being probably caused by aggravated membrane permeability.

In conclusion the structure activity relationship studies for Secin16 were not efficient to further improve the biochemical or biological properties of the lead compound Secin16.

V.3.3 3rd generation Secin chemotypes

As the modifications on Secin16 with the goal of improving its solubility and optimizing the ratio between potency and solubility were unsuccessful, a second virtual screening based on the information obtained from the 2nd generation Secin chemotypes was performed. This screening resulted in 88 3rd generation Secin chemotypes which were subsequently tested in the exchange assay. Six compounds were classified as hits (Figure 62). Although these hits showed IC50 values between 0.4 and 1.9μM for the inhibition of ARNO-Sec7 catalyzed GDP/GTP exchange on Δ17-ARF1 (Table 4), they showed severe solubility problems (data not shown) probably due to the shared backbone structure of three amido linked benzoic rings and the associated phenomena of aromatic ring stacking that is known to reduce solubility. However, all of these hits demonstrated dose-dependency in the exchange assay as well as in cell culture experiments. Furthermore, despite the highly similar backbone structure that is shared by all 3rd generation Secin chemotypes and the expected low solubility associated with it, only the mentioned six compounds exhibited potency in the tested assays. Hence it is unlikely that his effect is solely based on unspecific interference caused by compound aggregation. These contradictory results raise the question of how to deal with insoluble but apparently active compounds.

Solubility is defined as the amount of a substance that dissolves in a given solvent under given conditions. Solubility is an important issue in drug development since it directly affects the ADMET parameters of the potential drug [131]. Likewise, low solubility of compounds in screening assays can cause false-positive hits [176] or as stated by Di and Kerns "low solubility affects bioassays by causing […] discrepancies between enzyme and cell assays" and it is important to ensure that "low-solubility compounds are fully solubilized in bioassays"[177]. In order to answer this claim it is necessary to determine the solubility of a given compound. Various methods are available to measure the solubility of small molecules.

The most common methods involve the addition of different serial dilutions of the compound in DMSO to the buffer used in the screening assay. Compound solubility is either measured directly by UV-absorption after separation of aggregated compound by centrifugation or filtration, or indirectly by light scattering of the aggregates [131, 178]. However, all these assays only predict the solubility in the given test system which may vary from the conditions used for cell-based assays. Furthermore, the set up of the solubility measurement itself may influence the solubility of the compounds. Therefore, the measured solubility should be understood as an important benchmark and can serve as an early warning of possible difficulties [179]. In such a case special attention should be given to the compounds behavior in vitro or in cell based assays to avoid false-positive results. It is important to point out that such an interpretation of the solubility problem may cause work and costs for no purpose and that there is no guarantee of success. However, the interpretation of the specific activity pattern of a given compound in different assays may be more meaningful as its (bio)chemical *in-vitro* characterization.

V.3.4 Further directions

In silico prediction of potential small molecule chemotypes for the inhibition of cytohesins has proven to be useful. However, in order to combine the improvement in solubility and potency at the same time, it is inevitable to include the solubility as an additional parameter in the algorithm. This combined approach may yield more valuable inhibitors of cytohesins for *in vivo* applications. In addition, the value of a compound should not only be scored by its potency or IC50 value but should also include biochemical properties like solubility.

Virtual screening uses structure-activity data of already known inhibitors and is, therefore, intrinsically biased. As an alternative approach for an unbiased screen, I developed a new FRET-based assay to monitor GDP/GTP exchange on ARF1 (Figure 76) that combines the advantages of rapid and high-sensitive real-time fluorescence measurements with the possibility of identifying small molecule inhibitors of the interaction between NΔ17ARF1-GTP and GGA3. In addition to the commonly used tryptophan fluorescence to monitor the GDP/GTP-exchange on ARF1, this assays utilizes a second longer wavelength for the detection of activated ARF1, reducing the probability of detecting false-positive hits due to interference of the compounds with the intrinsic fluorescence. The interaction between NΔ17ARF1-GTP and its effector protein GGA3 has already been widely used to monitor the level of activated ARF in the sample. For this purpose, a GTS tagged GGA-GAT domain can

be added to an exchange reaction or cell lysate, and after precipitation of GGA-GAT the amount of bound NΔ17ARF1-GTP can be detected by SDS-PAGE and western blotting [138]. However, these analyses of protein interactions are commonly end-point measurements lacking kinetic information. Although this technique provides important information about the ability of NΔ17ARF1 to interact with its endogenous effector protein in the presence of a small molecule, it is very elaborate and therefore incompatible with high throughput screening approaches. The new established assay represents the first system to directly measure the interaction between NΔ17ARF1-GTP and its effector protein GGA3 in real-time and in a homogenous format using FRET. It allows the simultaneous identification and distinction of small molecule inhibitors that interfere with the cytohesin-catalyzed NΔ17ARF1-activation and/or with the interaction between NΔ17ARF1-GTP and its effector protein GGA3. By applying this assay it is possible to identify new inhibitors for the cytohesin-catalyzed GDP/GTP exchange on NΔ17ARF1 and to screen for inhibitors of the interaction between NΔ17ARF1-GTP and GGA3. Those inhibitors could make major contributions to the development of new drugs for anti cancer therapy.

V.4 Third generation Secins are potent inhibitors of glioblastoma cell proliferation

V.4.1 Inhibition of glioblastoma cell proliferation

Third generation Secin chmotypes have been proven to be very effective inhibitors of cytohesin catalyzed GDP/GTP-exchange in ARF1. It is therefore likely that they bind either to the Sec7 domain of ARNO, to ARF1 or to the complex between the two proteins. However, this observation gives no hints about their potential to inhibit GEF-activity independent cytohesin functions and raises the question whether 3rd generation Secins are also capable to interfere with cytohesin mediated GEF-activity independent functions.

In order to answer this question and to concurrently explore a new potential application field for cytohesin inhibitors, I decided to move to a new test system: the proliferation of glioblastoma cells. Gliomas are the most common subtype of primary brain tumors. EGFR is a primary contributor to glioblastoma initiation and progression. The most abundant mutation found in glioblastomas is the EGFR variant III (EGFRvIII), which lacks domains I and II of the extracellular part of the EGFR and is demonstrated to constitutively activate EGFR downstream signaling [66, 132]. Since these cells are clearly addicted to EGFR signaling, glioblastomas are a useful and promising system to test the potency of cytohesin inhibitors.

The third generation Secin chemotypes appeared to be extremely effective in reducing the proliferation of the two human glioblastoma cell lines U87 and Gli36 (Figure 64). Comparison of the impact of every single compound in each cell line revealed a clear correlation, indicating that the active compounds are effective in inhibiting both independent cell lines (Figure 65). In order to gain more evidence for an EGFR-dependent mechanism of inhibition, I tested the compounds for their effect on the proliferation of two further cell lines (directly arising from the two cell lines U87 and Gli36, tested previously) which stably overexpress EGFRvIII. The comparison yielded a significant correlation between the effects on proliferation in the parental and EGFRvIII expressing cell lines (Figure 66). Most of the compounds showed a slightly better inhibition in the EGFRvIII expressing cell lines, supporting an EGFR dependent effect. Three compounds (A11, C1 and C10) selectively reduced the proliferation of EGFRvIII expressing cell lines and were subsequently classified as EGFRvIII selective compounds. This effect was more pronounced in the U87 cell line system.

V.4.2 Inhibition of proliferation versus inhibition of GDP/GTP-exchange

Interestingly, compounds which were found to be most active in inhibiting the proliferation of glioblastomas were also most potent in inhibiting GDP/GTP-exchange on ARF1 (Figure 68, Figure 69). Table 8 summarizes the features of the most active compounds in both assays. Compounds which are extremely active in diminishing GDP/GTP-exchange on ARF1 are shown in orange (dark: IC50<1μM, light: IC50>1μM) and compounds inhibiting glioblastoma cell proliferation are shown in green (dark: IC50<200nM, light: IC50<400nM). EGFRvIII selective compounds are marked in violet.

These findings raise the question how the clear correlation between inhibition of GEF-activity and inhibition of proliferation can be explained. The clear correlation between the inhibition of exchange and proliferation suggests that the inhibition of proliferation is GEF-activity- or even ARF-dependent rather than EGFR-dependent. There are some results, however, which argue against this assumption.

	exchange	proliferation			
		U87wt	U87vIII	Gli36wt	Gli36vIII
A5	1,18µM	168nM	46nM		
A6	0,79µM	243nM	67nM		
A11	4,57µM	1366nM	198nM	589nM	360nM
B5	1,19µM	118nM	148nM		
B6	2,1µM	89nM	372nM		
B7	0,44µM	28nM	83nM	40nM	35nM
B8	2,58µM	106nM	126nM	102nM	92nM
C1	7,27µM	2086nM	186nM	732nM	314nM
C10	2,69µM	922nM	224nM	609nM	279nM
D3	1,34µM	297nM	105nM		
D6	1,86µM	367nM	84nM		
Secin16	3,71µM	958nM	435nM	750nM	724nM
SecinH3	11,4µM	-	-	-	-

Table 8 Characteristics of most active 3rd generation Secin chemotypes

Shown are the IC50 values for the indicated compounds in the GDP/GTP-exchange assay on ARF1 (exchange) and in glioblastoma proliferation assays (proliferation, cell line indicated). Colors highlight most active compounds. Exchange: dark orange: IC50<1µM, light orange: IC50>1µM. Proliferation: dark green: IC50<200nM, light green: IC50<400nM, violet: EGFRvIII selective compounds.

Firstly, most of the compounds show a slightly better inhibition in the EGFRvIII expressing cell lines supporting EGFR-dependency. Secondly, the compounds that were found to be active in reducing glioblastoma proliferation were also active in reducing the proliferation of EGFR-dependent lung cancer cell lines, but were not active in EGFR-independent H1838 cells. For a discussion of the EGFRvIII-selective compounds see below (V.4.3). Thirdly, concentrations needed to inhibit the GDP/GTP-exchange on ARF1 are approximately 10fold higher than the concentration needed to inhibit glioblastoma cell proliferation. Although a direct and quantitative comparison between these two assays is difficult it might indicate an inefficient inhibition of the cellular GEF activity of cytohesins at the used concentrations.

On the other hand, in support of a GEF activity dependent inhibition of glioblastoma cell proliferation, Li et al. demonstrated that the EGF-dependent proliferation of U87 cells depends on ARF6 [137]. EGF stimulation of U87 wild-type cells led to ARF6 expression and an increase in proliferation. Knockdown of ARF6 with siRNA reduced U87 cell proliferation. In agreement with these results, I found an increased expression level of ARF1 and ARF6 in EGFRvIII expressing glioblastoma cells in comparison to the parental cell lines (Figure 75). The increased expression of ARFs might provide an alternative explanation for the slightly higher sensitivity of EGFRvIII expressing glioblastoma cells towards 3rd generation Secin chemotypes. Furthermore, B7, the most active compounds in both assays, showed no effect on the phosphorylation of EGFRvIII or on the downstream signaling (Figure 72) in U87 cells, making it unlikely that this compound directly interferes with EGFR signaling.

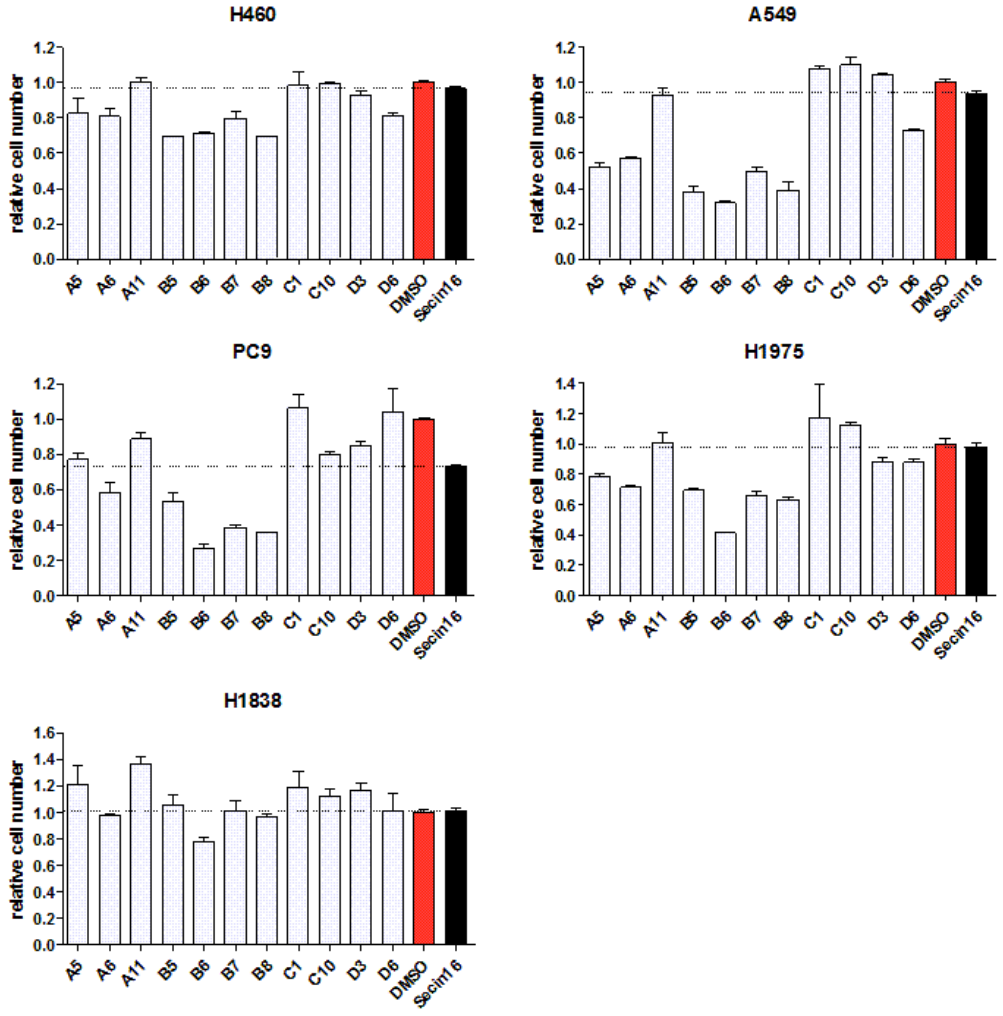

Figure 81 Effect of 3rd generation Secin chemotypes on the proliferation of EGFR dependent lung cancer cell lines

The diagram represents the relative cell number (MTT assay) after 72h treatment with the indicated compounds (250nM). The cell number in solvent-treated samples was set to 1. Data are represented as mean ±SEM, n=2.

In summary, the current results suggest, that 3rd generation Secin chemotypes reduce glioblastoma cell proliferation in an indirectly EGFR-dependent mechanism, i.e. they do not directly interfere with EGFR signaling but do clearly show a preference for EGFR dependent cell lines. If this activity directly depends on the inhibition of the GEF-activity of cytohesins has to be further elucidated, since the high potency in the exchange assay may simply represents the high affinity of these compounds for cytohesins and might therefore explain the good correlation between the inhibitory activities in both assays.

V.4.3 EGFRvIII selective compounds

The existence of EGFRvIII selective compounds adds new information to the mechanism of glioblastoma cell proliferation inhibition by 3rd generation Secins. These compounds do not

exhibit a significantly improved activity in the exchange assay, instead C1 shows an nearly two fold less inhibitory potential as compared to Secin16 (Table 8). In accordance to the observed correlation between inhibition of exchange and proliferation, these compounds only weakly inhibit proliferation of the wild-type glioblastoma cell lines. However, they efficiently inhibit the proliferation of EGFRvIII expressing glioblastoma cell lines (Table 8, Figure 66, Figure 69).

So how is this selective effect of compounds A11, C1 and C10 characterized? Firstly, it has to be pointed out, that these compounds show an EGFRvIII-dependent rather than a commonly EGFR-dependent activity, since they do not inhibit the proliferation of EGFR-dependent lung cancer cell lines (Figure 81). This finding differs from the results obtained for the "unselective" 3rd generation Secin chemotypes. Secondly, a closer look on the phenotypes of glioblastoma cells after treatment with 3rd generation Secin chemotypes reveals an additional difference between the two classes of compounds: Whereas the "unselective" compounds B7 and Secin16 seem "simply" to reduce the cell number without altering the appearance of the cells, the selective compounds A11 and C10 induce drastic changes in the phenotype of the EGFRvIII expressing cells (Figure 70). Apoptosis assays further support this difference, as in contrast to A11, C1 and C10, the compounds Secin16 or B7 did not induce apoptosis in glioblastoma cells (Figure 71). In agreement with the selective quality, the proapoptotic effect of compounds A11, C1 and C10 was more pronounced in EGFRvIII expressing glioblastoma cells. In conclusion, compounds A11, C1 and C10 clearly show selectivity for EGFRvIII expressing cells and induce a distinct, apoptotic phenotype in glioblastoma cells. These characteristics obviously separates compounds A11, C1 and C10 as an own class of 3rd generation Secin chemotypes (Table 9, Table 10).

	exchange	proliferation		phenotype		apoptosis	
		wt	vIII	wt	vIII	wt	vIII
B7	0,44µM	28nM	83nM	⇩	⇩	-	-
A11	4,57µM	1366nM	198nM	-	✞	-	+++
C1	7,27µM	2086nM	186nM			-	+++
C10	2,69µM	922nM	224nM	-	✞	-	+++
Secin16	3,71µM	958nM	435nM	-	-	-	-
SecinH3	11,4µM	-	-	-	-		

Table 9 Characteristics of selected 3rd generation Secin chemotypes in U87 glioblastoma cells

Summary of characteristics for selected 3rd generation Secin chemotypes in comparison to Secin16 and SecinH3. Orange: most active compound in the exchange assay, violet: EGFRvIII selective compounds, red: Secin16, blue: SecinH3. ⇩: reduction in cell number, ✞: cell death, -: no effect, blank: not tested, + to +++: positive effect.

	exchange	proliferation		phenotype		apoptosis		RAD51		yH2AX	
		wt	vIII	wt	vIII	wt	vIII	wt	vIII	wt	vIII
B7	0,44µM	40nM	35nM	⇩	⇩	-	-	+	-	-	-
A11	4,57µM	589nM	360nM	-	✞	++	+++	+	+	+	+++
C1	7,27µM	732nM	314nM			++	+++	+	+++	+	+++
C10	2,69µM	609nM	279nM	-	✞	++	+++	+	++	+	+++
Secin16	3,71µM	750nM	724nM	-	⇩	-	-	+	-	-	+
SecinH3	11,4µM	-	-	-	-						

Table 10 Characteristics of selected 3rd generation Secin chemotypes in Gli36 glioblastoma cells

Summary of characteristics for selected 3rd generation Secin chemotypes in comparison to Secin16 and SecinH3. Orange: most active compound in the exchange assay, violet: EGFRvIII selective compounds, red: Secin16, blue: SecinH3. ⇩: reduction in cell number, ✞: cell death, -: no effect, blank: not tested, + to +++: positive effect.

So how can the EGFRvIII selectivity of compounds A11, C1 and C10 be explained? The simplest explanation of an EGFRvIII selective effect would be a direct impact on EGFRvIII. However, the compounds showed no clear effect on the phosphorylation of wild-type EGFR or EGFRvIII (Figure 72), making this scenario rather unlikely. To gain further insight into the molecular mechanisms induced by the EGFRvIII selective compounds I focused on a potential connection between inhibition of EGFRvIII signaling and induction of apoptosis in glioblastoma cells. Inhibition of EGFRvIII signaling in glioblastoma cell lines is known to induce apoptosis in a yet not totally identified mechanism involving the appearance of DNA double-strand breaks. As nicely reviewed by Norbury and Zhivotovsky [133] DNA damage is a potent inducer of apoptosis. Glioblastomas are reported to critically depend on DNA repair mechanisms, accounting for their resistance to radiotherapy or treatment with cis-platin. This dependency on the DNA repair machinery seems to be controlled by EGFRvIII, as EGFRvIII inhibition results in an increased sensitivity for radiotherapy and the appearance of DNA double strand breaks [72, 136, 180-182]. And indeed, in agreement with this mechanism, treatment of Gli36 glioblastoma with compounds A11, C1 and C10 led to an increased occurrence of DNA double-strand breaks, as detected by an increase in the phosphorylation of the histone H2AX. The increase in DNA double-strand breaks was accompanied by reduced protein levels of RAD51, an important mediator of double strand repair (Figure 73, Figure 74) [134-135]. These effects were again more pronounced in the EGFRvIII expressing Gli36 cell line. Unfortunately, no signals for yH2AX could be obtained in U87 cells. In summary these results are consistent with an effect of the compounds on the EGFRvIII controlled regulation of DNA damage, probably by affecting the expression level of RAD51. The precise role of cytohesins in this mechanism, however, has still to be investigated.

Interestingly, recently another small molecule has been published that selectively inhibits the proliferation of EGFRvIII expression glioblastoma cells [73]. NSC-154829 selectively induces apoptosis in EGFRvIII expression glioblastoma cells without affecting matched wild-type cell lines. Although this compound comprises a typically purine-like structural component, it does not seem to interfere directly with EGFR signaling. Rather it has been shown that is moderately affects the expression levels of p21, without affecting p53 levels or Akt phosphorylation [73]. p21, a cyclin dependent kinase inhibitor, has itself been shown to be interrelated with RAD51 expression. Further it had been demonstrated that downregulation of p21 inhibits RAD51 foci formation [183]. These reports might indicate an important and general connection between the selectivity of some compounds for EGFRvIII expressing glioblastoma cells and interference with DNA double-strand break repair.

Although the precise molecular inhibitory mechanism of the compounds cannot yet be explained, they demonstrate the high potential of cytohesins as a new target in glioblastoma therapy.

V.5 Cytohesins as new targets in cancer therapy

Cytohesins are the first class of cytoplasmic ErbB receptor activators, comprising a new, promising target for the therapy of ErbB receptor-dependent cancers. Human lung adenocarcinomas highly express cytohesins and the expression can directly be correlated to the activation level of EGFR signaling, clearly demonstrating the pathophysiological relevance of cytohesins in lung cancer. Inhibition of ErbB receptor activation with the cytohesin inhibitors SecinH3 or Secin16 results in a pronounced reduction in cell proliferation not only in wild-type EGFR-dependent but also in EGFR mutation harboring human lung cancer cell lines. The same holds true for HER2/HER3-dependent breast cancer cell lines (previously shown in my diploma thesis and supported by unpublished results). Although the precise mechanism is not yet fully understood, cytohesins have also been shown to be involved in the proliferation of human glioblastoma cell lines. Thus, cytohesins provide a new layer of regulation in tumorgenesis and open up new avenues for fighting ErbB receptor-dependent cancers (Figure 82).

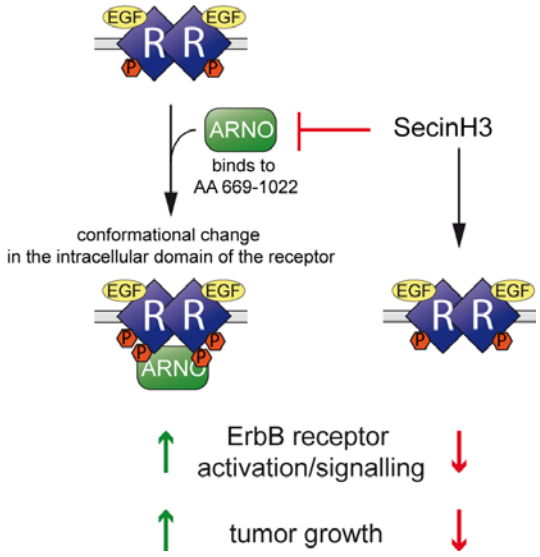

Figure 82 Cytohesin facilitate ErbB receptor activation and signaling
Cytohesins are cytoplasmic conformational ErbB receptor activators that are of pathophysiological relevance.

What is the advantage to target cytohesins instead of the respective ErbB receptor? The great difference in both approaches lies in the nature of the target. Whereas tyrosine kinase inhibitors (TKI) or humanized antibodies directly affect one particular ErbB receptor, inhibition of cytohesins does not target the receptor itself but instead the cofactor of ErbB receptors. This indirect impact on receptor inhibition is of paramount importance. The problem of acquired resistance, due to the induced activation of other receptor tyrosine kinases [184-186] or the occurrence of single amino acid mutations in the receptor [46, 187], accounts for the only temporarily successful effect of receptor-targeting therapy in most ErbB dependent cancers and often renders the therapy totally inactive. Targeting cytohesins as a general ErbB receptor- or even RTK-activating cofactor would hamper the occurrence of acquired resistance due to the compensating activation of other ErbB receptor members or RTKs. In addition, commonly found single point mutations of EGFR that mediate resistance to TKIs, for example the T790M mutation which renders the EGFR resistant to Iressa (Gefitinib) [188], are shown to not interfere with the cytohesin-mediated inhibition of human lung cancer cell lines. In fact, it has been demonstrated that inhibition of cytohesins can synergistically improve the impact of TKIs on the proliferation of a TKI-resistant human lung cancer cell line (previously shown in my diploma thesis). Furthermore, the remarkable effect of cytohesin inhibitors on the proliferation of EGFR-dependent human lung cancer xenografts in nude mice might partially be explained by the concurrent inhibition of additional cytohesin-dependent processes, like ARF dependent proliferating properties of the cells [93].

In summary, the obtained results establish cytohesins as promising targets in cancer therapy and open up new avenues for fighting ErbB receptor-dependent cancers by targeting not the receptors themselves but their activators.

VI Methods

VI.1 Cell culture

VI.1.1 Cell lines

Cells were grown at 37°C and 5% CO_2 in the indicated media (Table 11) until they reached a maximal confluency of ~80% and were subsequently splitted every 2-3 days. Suspension cells were maintained at a cell density of 0,05-1,0*10^6 cells per milliliter.

VI.1.2 Plasmids

For expression of ARNO in mammalian cells the complete coding sequence of human ARNO (GenBank NM_017457) or sequences covering the indicated domains (amino acids 52 – 400 for ARNO-ΔCC, 1 – 246 for ARNO-ΔPH, 52 – 246 for ARNO-Sec7) were cloned into pCMV-Tag2 (Stratagene) introducing a FLAG tag at the N-terminus of the protein.
For expression of MIG6-EBR in mammalian cells the EGFR binding region of MIG6 including surrounding stabilizing sequences (NM_018948; amino acids 282 – 396) was inserted into pCMV3Tag2 (Stratagene).
For the construction of lz-EGFR the region coding for the extracellular domain of L-gp130 was amplified by PCR out of pMOWS-L-gp130 [189] and ligated in-frame with the sequence coding for the transmembrane and intracellular domains of the EGFR (NM_005228). This construct was cloned into pRLuc-N3 (PerkinElmer) such that it replaced the luciferase gene in the vector. The resulting fusion protein contains the signal peptide of gp130, a FLAG tag, a linker with a single cysteine residue which forms a disulfide bridge upon dimerization of the protein, the leucine zipper of c-jun, the membrane-proximal 15 amino acids of the extracellular region of gp-130, and the transmembrane and intracellular regions of the EGFR.
The coding sequences of all constructs were verified by sequencing (GATC Biotech).

Cell line	culture	media	species	source/type
CAL 120	adherent	RPMI+10%FBS	human	breast cancer (AC)
HCC1143	adherent	DMEM+10%FBS	human	breast cancer (AC)
MDA-MB-231	adherent	RPMI+10%FBS	human	breast cancer (AC)
HCC1395	adherent	RPMI+10%FBS	human	breast cancer (AC)
HCC1599	suspension	RPMI+10%FBS	human	breast cancer (AC)
BT20	adherent	RPMI+10%FBS	human	breast cancer (ID)
T74D	adherent	RPMI+10%FBS	human	breast cancer (ID)
MCF7	adherent	DMEM+10%FBS	human	breast cancer (ID)
SkBr3	adherent	RPMI+10%FBS	human	breast cancer (ID)
PC9	adherent	RPMI+10%FBS	human	NSCLC (AC)
H1975	adherent	RPMI+10%FBS	human	NSCLC (AC)
H3255	adherent	RPMI+10%FBS	human	NSCLC (AC)
HCC827R	adherent	RPMI+10%FBS	human	NSCLC (AC)
H1838	adherent	RPMI+10%FBS	human	NSCLC (AC)
A549	adherent	RPMI+10%FBS	human	NSCLC (AC)
H460	adherent	RPMI+10%FBS	human	NSCLC (AC)
H1993	adherent	RPMI+10%FBS	human	NSCLC (AC)
H1781	adherent	RPMI+10%FBS	human	NSCLC (AC)
BA/F3	suspension	RPMI+10%FBS+10ng/ml IL-3	mouse	pro B cell
BA/F3 L858R	suspension	RPMI+10%FBS	mouse	pro B cell
BA/F3 L858R T790M	suspension	RPMI+10%FBS	mouse	pro B cell
BA/F3 del1	suspension	RPMI+10%FBS	mouse	pro B cell
BA/F3 del1 T790M	suspension	RPMI+10%FBS	mouse	pro B cell
U87	adherent	DMEM+10%FBS+sodium pyruvate	human	glioblastoma
U87dEGFR	adherent	DMEM+10%FBS+sodium pyruvate+1µg/ml puromycin	human	glioblastoma
U87dEGFR-LITG	adherent	DMEM+10%FBS+sodium pyruvate+1µg/ml puromycin+500µg/ml G418	human	glioblastoma
Gli36	adherent	DMEM+10%FBS+sodium pyruvate	human	glioblastoma
Gli36dEGFR	adherent	DMEM+10%FBS+sodium pyruvate+500µg/ml G418	human	glioblastoma
Gli36dEGFR-LITG	adherent	DMEM+10%FBS+sodium pyruvate+1µg/ml puromycin+500µg/ml G418	human	glioblastoma
HeLa	adherent	DMEM+10%FBS	human	cervix carcinoma (AC)
Hek	adherent	DMEM+10%FBS	human	embryonal kidney cells (transformed with Ad5)
COS-7	adherent	DMEM+10%FBS	african green monkey	kidney cells (transformed with SV40)

Table 11 Used cell lines

List of all used cell lines, culture type, media and origin. AC: adenocarcinoma, ID: invasive ductal, NSCLC: non-small cell lung cancer

VI.1.3 Transfection

$1.3x10^6$ SkBr3 or H460 cells were seeded in a 6cm plate, cultured for at leat 12 h and transfected with a total amount of 1.2 µg DNA using 4 µl Lipofectamine LTX and 1 µl Plus-Reagent (Invitrogen). For siRNA-transfections $2,4x10^6$ SkBr3 or H460 cells were seeded in 6well plates, cultured for 24 h and transfected with 10-15 nM siRNA (Ambion) using 4 µl Lipofectamine RNAimax (Invitrogen). Aptamer transfection was carried out using 1-20 nM M69 aptamer or pool RNA and 4 µl Metafectene (Biontex) per 6well.

For cotransfection of siRNA and plasmid, $2x10^6$ H460 cells were seeded on a 6cm plate, incubated for at least 2h and subsequently transfected with 20nM siRNA and 1,2µg total DNA using 7,2µl MetafectenePro.

$3.6x10^6$ HEK-293T cells per 6well plate were reverse transfected with a total amount of 1.6 µg DNA per well (0.8 µg lz-EGFR, 0.8 µg ARNO or empty vector) using 4.8 µl Metafectene. Transfected cells were analyzed 36-48 h after transfection, with the exception of aptamer-transfected cells, which were analyzed 5 h after transfection.

$1x\ 10^5$ COS-7 cells were seeded in a 3.5 cm glass bottom dishes (Matek), cultured for 6h and transfected with 1.2 µg DNA (0.6 µg lz-EGFR-mCitrine and 0.6 µg ARNO, MIG6, Rheb or empty vector, respectively) using 3.6 µl FuGene6 (Roche). Anisotropy was measured 12h after transfection.

Lipofectamin reagents or Metafectene were premixed with serum free media, incubated for 5min and the diluted DNA was subsequently added. FuGene6 and MetafectenePro were directly added to the diluted DNA/RNA.

Transfection was performed after an additional 20min incubation by adding the transfection mixture to 2ml (6well plate well) or 4ml (6cm plate) of complete growth media.

VI.2 Cellular assays

VI.2.1 Protein biochemistry

VI.2.1.1 Preperation of cell lysates

Cells were serum-starved overnight in the presence of the indicated concentrations of SecinH3 or DMSO (final DMSO concentration 0.4%). The medium and inhibitors were refreshed 1 h prior to stimulation. H460/U87/Gli36 and SkBr3 cells were stimulated for 5 min with 50 ng/ml EGF (Peprotech) or 25 ng/ml Heregulin-β1 (Peprotech), respectively, and the stimulation media was discarded (Table 12).

Cell line	starvation media	stimulation
H460	RPMI	50ng/ml EGF
SkBr3	RPMI	25ng/ml HRG
HEK 293	DMEM, 0,1% FBS	
COS-7	DMEM	
U87/Gli36 wt	DMEM, 1% FBS	50ng/ml EGF

Table 12 Conditions used for stimulation

Cells were harvested in cold 1xPBS, 5mM EDTA on ice using a cell scraper and were subsequently centrifugated (500rpm, 5min, 4°C). Pellets were resuspended and lysed in (~30µl/6cm dish) lysis buffer supplemented with the protease-inhibitor-mix HP (Serva) for 15min on ice. After seperation of cell debris (12000rpm, 15min, 4°C) lysates were subjected to protein determination by a bradford-assay. For SDS-PAGE samples were boiled in 1x SDS sample buffer (lämmli buffer).

1x Lysis buffer
20 mM Tris-Cl, pH7.5
150 mM NaCl
1 mM EDTA
1 mM EGTA
2.5 mM sodium pyrophosphate
1 mM β-glycerophosphate
1 mM sodium vanadate
1% (v/v) Triton X-100

1x SDS sample buffer
8,25mM Tris-HCl pH6,8
100mM DTT
2,5 % (w/v) SDS
5 % (v/v) Glycerin
bromphenolblue

VI.2.1.2 Immunoprecipitation

Cell lysates were diluted with 1x lysis buffer to a total protein concentration of 4mg/ml. Normalized amounts of cells lysates (~8mg) were immunoprecipitated using 25µg agarose-conjugated EGFR-antibody (sc-120, SantaCruz Biotechnology) or 40µg agarose-conjugated HER3-antibody (sc-285) over night at 4°C. Beads were seperated by centrifguation (300rpm, 3min, 4°C) and subsequently washed three times with 200µl 1x lysis buffer. Precipitated proteins were eluted in 55µl sample buffer for 10 min at 55°C.

VI.2.1.3 SDS-PAGE

Protein lysates (~40-60µg/lane) or precipitates were separated by discontinuous SDS-PAGE (sodium dodecyl sulfate polyacrylamid gel electrophoreses). Polyacrylamide gels are formed from the polymerization of two compounds, acrylamide and N,N-methylene-bis-acrylamide.

The polymerization is initiated by the addition of ammonium persulfate (APS) along with N,N,N,N,- tetramethylethylenediamine (TEMED).

The separation of molecules within a gel is determined by the relative size of the pores formed within the gel and the charge of the protein. For SDS-PAGE samples were boiled in 1x SDS sample buffer (lämmli buffer). SDS binds to polypeptides in a constant weight ratio of 1.4 g/g of polypeptide. In this process, the intrinsic charge of proteins becomes negligible when compared to the negative charges contributed by SDS, providing the same net negative charge per peptide.

In discontinuous SDS-PAGE two different gels are put on top of each other. First, the proteins pass through the large pore stacking gel. This gel is prepared with buffer about 2 pH units lower than that of the running buffer or the separating gel, providing the conditions for a yet not fully understood process based on molar conductivity that leads to the concentration of the protein in a thin starting zone. This gel is cast on top of the separating gel in which the proteins are separated based on their size [190]

The indicated reactions were mixed and gels were cast between two thin glass slides (Table 13). Protein samples were loaded (~40-60µg) and separated for ~1h at 200V. Page Ruler Prestained Protein Marker (Fermentas) served as a size standard.

Separating gel buffer (4x)
1,5M Tris-HCl pH 8,8
0,4 % (w/v) SDS

Running buffer (5x)
125mM Tris-HCl pH8,2
960mM Glycin
0,5 % (w/v) SDS

Stacking gel buffer (4x)
500mM Tris-HCl pH6,8
0,4 % (w/v) SDS

	Separating gel			stacking gel
	6%	7,50%	10%	4%
(Bis)-acrylamide	1000 µl	1250 µl	1667 µl	213 µl
water	2712 µl	2462 µl	2045 µl	975 µl
separating gel buffer (4x)	1250 µl	1250 µl	1250 µl	-
stacking gel buffer (4x)	-	-	-	400 µl
TEMED	8 µl			2 µl
APS	30 µl			10,4 µl

Table 13 Pipet scheme for the preparation of SDS-PAG

VI.2.1.4 Blotting

After separation by SDS-PAGE proteins were transferred on nitrocellulose membranes using the technique of discontinuous blotting describes by Kyhse-Andersen [191]. For this purpose the gel was piled between different layers of filter papers, equilibrated in the indicated buffer (semi-dry transfer system, Table 14). Proteins were transferred on a nitrocellulose membrane by applying a constant power of 2mA/cm^2 gel for 45min.

Cathode
2 filter papers in Cathode buffer
Gel in Cathode buffer
nitrocellulose membrane in Anode II buffer
1 filter paper in Anode II buffer
1 filter paper in Anode I buffer
Anode

Table 14 Stacking in the semi dry transfer system

Cathode buffer
25mM Tris-HCl, pH 9,4
40mM Glycin

Anode I buffer
300mM Tris-HCl pH 10,4

Anode II buffer
25m Tris-HCl pH 10,4

For transfer of high size proteins (for example crosslinked ErbB receptors) a tank (or wet) transfer systems was used (Criterion Blotter, BioRad). In this system the gel and membrane sandwich is held within a gel holder cassette and submerged entirely in transfer buffer. Transfer was performed at 4°C for 60-90min at 100V.

Transfer buffer:
25mM Tris
192mM glycine

VI.2.1.5 Immunodetection

After transfer of proteins on a nitrocellulose membrane, membranes were rinsed with 1xTBS-T and blocked by incubation in 5% (w/v) milk powder or 5% (w/v) BSA in 1xTBS-T for at least 45min at RT. Subsequently, the membranes were rinsed once in 1xTBS-T and incubated with the primary antibody diluted 1:500-1:1000 in 5% (w/v) BSA, 1xTBS-T, 0,02% (v/v) thimerosal (Table 15).

	antigen	epitope	species		company	number	clone
	ARF-1	N-terminus	goat	polyclonal	SantaCruz	sc-7622	
	ARF-6	aa 1-174	mouse	monoclonal	SantaCruz	sc-7971	3A-1
	ARNO	full length	mouse	monoclonal	SantaCruz	sc-59451	CYT2-21
	cytohesin-1	full length	mouse	monoclonal	Sigma	Cyt1-82	C8979
	cytohesin-2	aa 314-399	mouse	monoclonal	Abnova	H00009266	6H5
	cytohesin-3	full length	rat		Hafner et al.		
	EGFR	cytopl. domain aa1140-1160	mouse	monoclonal	nanoTools	0168-100	10F4
	EGFR	c-terminus	mouse	monoclonal	SantaCruz	sc-120	528
	EGFR	cocktail R19/48	mouse	monoclonal	Thermo Scientific	Ab-12	MS-400-P
agarose-coupled	EGFR	extracell. domain	mouse	monoclonal	SantaCruz	sc-120 AC	528
	FLAG-M2		mouse	monoclonal	Sigma	F1804	M2
	GST		mouse	monoclonal	SantaCruz	sc-138	B-14
	HER2	c-terminus	rabbit	polyclonal	SantaCruz	sc-284	
	HER3	c-terminus	rabbit	polyclonal	SantaCruz	sc-285	
agarose-coupled	HER3	c-terminus	goat	polyclonal	SantaCruz	sc-285 AC	
	His		mouse	monoclonal	SantaCruz	sc-8036	B-14
	Hsc70		mouse	monoclonal	Stressgen	SPA-820	N27F3-4
	normal goat IgG				SantaCruz	sc-2346	
	normal mouse IgG				SantaCruz	sc-2343	
	pAkt	pT308	mouse	monoclonal	Cell Signaling	4056	244F9
	pEGFR	pY1173	rabbit	monoclonal	Cell Signaling	4407	53A5
	pEGFR	pY1068	mouse	monoclonal	Cell Signaling	2236	1H12
	pEGFR	pY1068	rabbit	monoclonal	Epitomics	1138-1	Y38
	pEGFR	pY1086	rabbit	monoclonal	Epitomics	1139-1	Y39
	pHER2	pY1221/1222	rabbit	monoclonal	Cell Signaling	2243	6B12
	pHER3	pY1289	rabbit	monoclonal	Cell Signaling	4791	21D3
	pIRS-1	pY612	rabbit	polyclonal	Biosource	44-816	
	pp44/42	pT202/pY204	rabbit	monoclonal	Cell Signaling	4377	197G2
	pShc	pY239/240	rabbit	polyclonal	Cell Signaling	2434	
	pY	pY	mouse	monoclonal	SantaCruz	sc-7020	pY-99
	RAD51		rabbit	polyclonal	SantaCruz	sc-8349	
	Survivin	AS 1-142	mouse	monoclonal	SantaCruz	sc-17779	D-8
	yH2AX	S139	rabbit	monoclonal	Cell Signaling	9718	20E3
HRP-coupled	goat-IgG		rabbit		SantaCruz	sc-2768	
NIRD(680)-coupled	goat-IgG		donkey		Licor	926-32224	
HRP-coupled	mouse-IgG		goat		SantaCruz	sc-2005	
NIRD(800)-coupled	mouse-IgG		goat		Thermo Scientific	35521	
HRP-coupled	rabbit-IgG		goat		SantaCruz	sc-2004	
NIRD(800)-coupled	rabbit-IgG		goat		Thermo Scientific	35571	

Table 15 Antibodies used for immunoprecipitation and immunodetection

Membranes were washes three times in 1xTBS-T to discard unbound primary antibody and incubated in HRP- (horseradish peroxidase) or NIR dye-coupled secondary antibody (diluted 1:10000-1:20000 in 5% (w/v) BSA, 1xTBS-T) for 1h at RT (in the dark). Visualization was done by enhanced chemiluminescence (Millipore) and a VersaDoc 5000 CCD camera (BioRad) or by near infrared (NIR) immunofluorescence and an Odyssey scanner (Licor), respectively. Bands were quantified with the QuantityOne software (BioRad).

TBS-T buffer
20 mM Tris-HCl pH 7,4
136 mM NaCl
0,1 % (v/v) Tween-20

VI.2.1.6 Crosslinking

H460 or SkBr3 cells ($1.5x10^6$ per 6 cm plate) were cultured for 24h and starved overnight in the presence of SecinH3 (15 μM) or DMSO (final DMSO concentration 0.4%). For crosslinking cells were washed twice in prewarmed (37°C) 1xPBS and stimulated as previously described in 2ml 1xPBS. After stimulation, freshly prepared BS3 (Pierce, solubilized in DMSO) was added to a final concentration of 2 mM and cells were incubated on a rocker for 5 min at 37 °C. The reaction was quenched with 100 mM Tris-Cl, pH7.5 for 5 min at 37 °C. Cells were harvested as previously described and lysed in RIPA buffer (1x lysis buffer supplemented with 1 % (v/v) NP40 / 0.1 % (w/v) SDS / 0.5 % (w/v) NaDoc). Normalized amounts of proteins were separated by SDS-PAGE using precast 3 % - 8 % gradient Tris-acetate gels (Invitrogen). Western transfer was done with the Criterion Blotter system (BioRad). Hi Mark Protein Standard (Invitrogen) was used as a size standard.

VI.2.2 Analysis of expression levels

VI.2.2.1 RNA purification

Cells were lysed in 175µl RNA lysis buffer (Promega) per 24well and RNA lysates were stored at -80°C. RNA was purified using the SV total RNA Isolation Kit (Promega) according to the manufacturer`s instructions and eluted in 100µl RNAse-free water.

VI.2.2.2 Reverse Transcription (RT)

After purification the RNA was reverse transcribed using the High Capacity cDNA Archive Kit (AppliedBiosystems) according to the manufacturer`s instructions. 35,5µl RNA (without further concentration determinations) were used in every reaction.

reagent	amount	stock	endconcentration
RT buffer	5 µl	10x	1x
dNTPs	2 µl	25x	1x
Primer	5 µl	10x	1x
RT (Multiscripe)	2,5 µl		
RNA	35,5 µl		

Table 16 RT reaction (50µl)

RT program
10min at 25°C
120min at 37°C

VI.2.2.3 Quantitative real time PCR

cDNA was analyzed by quantitative real time PCR using gene-specific TaqMan-probes (Applied Biosystems, Table 19). 2,5µl of cDNA (diluted 1:3 in water) was used in every reaction (total volume 10µl, 2xPlatinum-qPCR-Supermix, Invitrogen). The amplification reaction (40cycles) was performed according to the manufacturer`s instructions using a pPCR-thermocycler (BioRad) and fluorescence was measured after every cycle. The obtained threshold cycle (C_T) for every probe was normalized to the C_T-value of ß2-microglobulin ($\Delta C_T = C_T gene - C_T B2M$). Relative expression levels were calculated using the formula: relative expression level $= 2^{-\Delta CTgene1} / 2^{-\Delta CTgene2}$.

reagent	amount	stock	endconcentration
Platinum-qPCR-Mix	5 µl	2x	1x
probe	0,5 µl	20x	1x
cDNA (1:3 diluted)	2,5 µl		
water	2 µl		

Table 17 qPCR reaction

step	temperature	duration
1. initiale denaturing	95°C	2min
2. denaturing	95°C	15sec
3. extension	60°C	60sec

Table 18 qPCR cycling
Steps 2 and 3 were repeated 40times.

target mRNA	species	number
PSCD1	human	Hs00245092_m1
PSCD2	human	Hs00244669_m1
PSCD3	human	Hs00188456_m1
PSCD4	human	Hs00203581_m1
ARF1	human	Hs00734523_m1
ARF4	human	Hs00743745_s1
ARF6	human	Hs01922781_g1
B2M	human	Hs99999907_m1

Table 19 TaqMan Gene Expression probes

Hs: homo sapiens, _m1: probe spans an exon junction, _s1: primer and probe in same exon, _g1: position of probe not known (www.appliedbiosystems.com)

VI.2.3 Microscopy

VI.2.3.1 Immunofluorescence

H460 cells were plated onto Ø 25 mm poly-L-lysine– coated coverslips as previously described [192], starved over night, treated with compounds and stimulated as described. The following antibodies were used for immunostaining: ARNO/cytohesin 1 (Santa Cruz, sc-9729), EGFR (Santa Cruz, sc-03). As secondary antibodies, donkey-anti-goat coupled to Alexa488 (Invitrogen, A11055), donkey anti-rabbit coupled to Alexa594 (Invitrogen, A21207) were used. Before application, all antibodies were diluted (primary and Atto coupled secondary antibodies 1:100, all other secondary antibodies 1:200) into PBS containing 1% (w/v) BSA.

Membrane sheets were generated and immunostained using standard protocols as previously described [193] and imaged in PBS containing 10 % of a TMA-DPH–saturated PBS solution. Membrane sheets were imaged using a Zeiss Axio Observer D1 fluorescence microscope with a 100x 1.4 NA plan apochromate objective. For image acquisition, we used a cooled digital 12bit CCD camera (Sensicam QE, 6.45 x 6.45µm pixel size, PCO AG). The following filter sets were used (all filter sets were purchased from AHF Analysentechnik AG, Tübingen, Germany): Alexa488 fluorescence was detected using filter set F36-525 EGFP (BrightLine HC 472/30, BS 495 and BrightLine HC 520/35), Alexa594 fluorescence was detected using filter set F36-503 TRITC (BrightLine HC 543/22, BS 562 and Bright Line HC 593/40) and TMA-DPH fluorescence was detected using filter set F11000 (excitation filter D 350/50, 400 DCLP and emission filter E 420 LP). Comparative quantitation of immunostaining intensities was performed as previously described [194] using ImageJ 1.38x Software. Experiments were performed by the laboratory of Thorsten Lang, University of Bonn.

VI.2.3.2 STED

For STED experiments membrane sheets were prepared as describe and stained for EGFR and goat anti-rabbit coupled to Atto 647N (Atto-Tec, Siegen, Germany). After immunostaining membrane sheets were mounted on glass slides in Mowiol. Images were acquired by Stimulated Emission Depletion (STED) Microscopy using a Leica TCS STED microscope (Leica Microsystems GmbH, Mannheim, Germany) with a resolution in the range of 100 nm applying a 1.4 numerical aperture HCX PL APO CS 100x oil objective and a standard STED filter set. For excitation a 635 nm pulsed diode laser (PicoQuant GmbH, Berlin, Germany) and for depletion a MaiTai tunable Ti:sapphire femtosecond laser at 750 nm (Spectra-Physics Lasers, Mountain View, USA) were applied. An Avalanche Photodiode (APD) was used for signal detection. At a pixel size of 20.22 nm and a 10 Hz scan frequency a 2-line average was performed. At least 10-12 sheets for each condition and experiment were imaged, and 3 independent experiments were performed. Cluster size analysis was performed semi automized by using a self-written routine in Matlab (The MathWorks, Natick, USA). A 3-pixel broad and 30-pixel long line scan was laid through the centres of single clusters within a randomly chosen 150x150 pixel region of interest (ROI) in an analyzed membrane sheet (original images were 512x512 pixels). Linescan traces for every measured spot were fitted with a Gaussian function using Origin and the size corresponding to the full width at half maximum (FWHM) was determined in pixel units. FWHM values were multiplied with the size of a single pixel (20.22 nm) and averaged. Experiments were performed by the laboratory of Thorsten Lang, University of Bonn.

VI.2.3.3 Anisotropy Microscopy

Anisotropy microscopy was done as described [110] in COS-7 cells. 1x 10^5 COS-7 cells were seeded in a 3.5 cm glass bottom dishes (Matek), cultured for 6h (until cells were attached and streched) and transfected with 1.2 µg DNA (0.6 µg lz-EGFR-mCitrine and 0.6 µg ARNO, MIG6, Rheb or empty vector, respectively) using 3.6 µl FuGene6 (Roche). Media was changed to phenol red-free media one hour before measurement.

Images were acquired 15–24 h posttransfection, using a Olympus IX81 inverted microscope equipped with a MT20 illumination system. A linear dichroic polarizer (Meadowlark Optics) was placed in the illumination path of the microscope, and two identical polarizers were placed in an external filter wheel at orientations parallel and perpendicular to the polarization of the excitation light. The fluorescence was collected via a 20× 0.7 NA air objective, and parallel and polarized emission images were acquired sequentially on an Orca CCD camera

(Hamamatsu Photonics). Data acquisition was controlled by the CellR software (Olympus). In each experiment at least 25 fields of view, with 1-4 cells each, were analyzed per condition.

VI.2.3.4 FLIM measurements

For fluorescence lifetime imaging microscopy (FLIM), cells were seeded and transfected as transcribed for anisotropy microscopy. FLIM measurements of mCitrine were performed in the presence and absence of ARNO overexpression. FLIM images were obtained using a Fluoview 1000 microscope (Olympus, Hamburg, Germany), equipped with a Picoharp 300 photon counting setup (Picoquant, Berlin, Germany). Images of 512 x 512 pixels were acquired until approximately 30.000 photons were collected per image. Images of mCitrine fluorescence were processed using the SymPhoTime software package (v4.2, Picoquant). The images were analyzed on a pixel-by-pixel basis using a mono-exponential fitting model including background.

VI.2.4 Proliferation assays

$3x10^3$ cells per 96well were seeded into a clear, flat bottom 96well plate (TPP). After 24hours the media was discarded by inversion of the plate and cells were treated with the respective concentration of SecinH3 or solvent (final DMSO concentration 0.4%) in fresh media containing 1% FCS. Media was changed daily for additional 3 days and cell proliferation was analyzed after 72h treatment using a 3-(4,5-dimethylthiazol-2-yl)-2,5-diphenyltetrazolium bromide (MTT) assay as described in the manufacturer's protocol. The assay is based on the cellular conversion of a tetrazolium salt into a formazan product that can be detected colometrically. Briefly, 15µl of Dye solution media was added directly into the media of the cells (100µl). After 4h incubation at 37°C, 5% CO_2, 100µl solubilization solution was added to solubilize the formazan product and the absorbance at 570nm was measured in a Varioscan microplate reader (Thermo Scientific).

12000 Ba/F3 cells (50µl, FBS free media) per well were seeded into a clear, flat bottom 96well plate (TPP) and the same volume of media (2% FBS) containing the 2-fold concentration of compound and solvent was added. Proliferation was analyzed 72h after addition of the compounds.

All assays were performed at least in triplicates. For calculation of the relative proliferation rate/cell number the mean absorbance in the solvent (DMSO) only treated cells were set as 1.

Commercially available solutions were later on substituted by self-made solutions.

MTT staining solution
5mg/ml MTT in PBS

MTT lysis buffer
250ml DMF
250ml water
100g SDS
10ml acetic acid
pH~4,7

VI.2.5 Apoptosis assays

1,3x10^6 cells were seeded on 10 cm dishes in full growth media containing 10% FBS. After 24 h incubation media was changed to growth media containing 1%FBS and cells were treated with compound or solvent (final DMSO concentration 0.4) for 24h-48h. Cells (<70% confluence!) were harvested by trypsinization (keep media!) and were collected in the kept media to include already detached cells. Subsequently cells were centrifuged at 300rpm for 3min, washed twice in PBS and counted. 1x10^6 cells per sample were resuspended in 1x Annexin V binding buffer and stained with 5µl Annexin-V-FITC (Annexin-V-FITC Apoptosis Detection Kit I, BD Biosciences) and 5µl TOPRO-3-iodide (10µM in DMSO, Invitrogen) as described in the manufacturer´s instructions for 15min at room temperature. Samples were diluted with 400 µl 1x Annexin V binding buffer directly before measurement. FACS analysis was performed on a FACS Canto II Flow Cytometer (BD Biosciences) in the FITC and 7-AAD setups, analyzing 10.000 cells. Unstained and untreated cells were used for live gate settings and TOPRO only stained cells were used to set the gates for FITC and TOPRO (TOPRO showed an intensive background staining of live cells, therefore FITC only stained cells could not be used to set TOPRO gates). Results were calculated using FlowJo Software (Treestar). Apoptotic cells were defined as being TOPRO+/FITC- (late apoptotic), TOPRO-/FITC+ (early apoptotic) or TOPRO+/FITC+ (intermediate apoptotic) and all three quadrants were summarized.

1x Annexin V binding buffer
0,1M Hepes/NaOH pH 7,4
1,4M NaCl
25mM $CaCl_2$

VI.2.6 Cell-cycle analysis

For cell cycle analysis cells were prepared and harvested as described for the apoptosis assay. $1x10^6$ cells were resuspended in 300µl PBS and 700µl ice cold methanol was added drop wise under constant vortexing. Cells were incubated at least 1 h on ice, diluted with 1ml PBS and washed twice in PBS and were finally resuspended in 100µl PBS. DNA was stained with 100 nM TOPRO-3-iodide and treated with RNAse A (50 µg/ml) for 15 min at 37°C. FACS analysis was performed on a FACS Canto II Flow Cytometer (BD Biosciences) in the 7-AAD setup, analyzing 10.000 cells. Untreated, unstained cells were used to set up the live gate and the laser power/7-AAD gate. Histograms were analyzed using FlowJo Software (Treestar) and the percentage of cells in the indicated phases of cell-cycle was calculated based on the Watson-model.

VI.3 Mouse experiments

VI.3.1 Xenograft models

VI.3.1.1 H460 cells

All animal procedures were in accordance with the German Laws for Animal Protection and were approved by the local animal protection committee and the local authorities (Bezirksregierung Bonn). Tumors were generated by s. c. injections of $5x10^6$ H460 cells into nu/nu athymic male mice. After tumor establishment mice were randomized into two groups, control (vehicle) and SecinH3-treated mice. Mice were treated by daily i. p. injections (Volume 100µl, dosage 2.5 mM SecinH3 in 50% DMSO/50% isotonic Glucose solution). Tumor volume was measured daily and calculated by using the formula $\pi/6 \times$ larger diameter $\times$ (smaller diameter)^2.

The TUNEL assay was performed according to the manufacturer´s manual (ApopTag Plus Peroxidase In Situ Apoptosis Kit, Millipore).

H460 xenograft studies were performed in cooperation with L.C. Heukamp, University of Bonn.

VI.3.1.2 PC9 cells

All animal procedures were in accordance with the German Laws for Animal Protection and were approved by the local animal protection committee and the local authorities (Bezirksregierung Köln). Tumors were generated by s. c. injections of $5x10^6$ PC9 cells into nu/nu athymic male mice as described previously [195]. After tumor establishment mice were

randomized into two groups, control (vehicle) and SecinH3-treated mice. Mice were treated by daily i. p. injections (Volume 100µl, dosage 2.5 mM SecinH3 in 25% DMSO/75% isotonic Glucose solution). Ki-67 staining was done as described [196-197] and the TUNEL assay was performed according to the manufacturer´s manual (ApopTag Plus Peroxidase In Situ Apoptosis Kit, Millipore). PC9 xenograft studies were performed by the laboratory of R.T.Ullrich, MPI Köln.

VI.3.2 [^{18}F]FLT PET imaging

Tumor bearing mice were investigated using a FOCUS microPET scanner (Siemens Microsystems, Inc., Knoxville, TN). [^{18}F]FLT synthesis was performed as described previously [198]. No-carrier-added [^{18}F]FLT (3'-deoxy-3'-[^{18}F]fluorothymidine) was administered i.v. (tail vein) into experimental animals with a dose of 200 µCi/mouse. PET images were performed 60 min after injection. Data evaluation was based on a region of interest (ROI) analysis of PET images to determine maximal radioactivity concentration within the tumors. To determine the uptake ratio a reference ROI was placed in the mediastinum. Data were decay corrected and divided by the total injected dose to represent percentage injected dose per gram (%ID/g). PET imaging was performed by the laboratory of R.T.Ullrich, MPI Köln.

VI.4 Analysis of human tumor samples

All primary tumor samples stem from the CIO Biobank at the Institute of Pathology, University of Bonn, Germany. All tumors were clinically and pathologically identified as being the primary and only neoplastic lesion and classified in accordance with WHO guidelines [44]. 3 µm formalin fixed paraffin embedded sections were stained for pEGFR, pAkt, pStat3, pp44/42 and evaluated as previously described [196-197]. The ARNO / cytohesin-1 specific antibody (sc-9729, SantaCruz) was used according to the manufacturer´s instructions. Staining intensities were individually evaluated as described before [196] by three independent observers and the average score was used for statistical analysis. When the individual scores differed by more than 1 the results were re-evaluated by the panel of the three pathologists. A four-tier scoring system was employed to quantify the respective staining: no or background staining (0), weak (1), distinct and of moderate intensity (2), strong (3). Immunofluorescence double-staining of cytohesin, pEGFR, pp44, pAkt was performed as described [199].

VI.5 Cell-free assays

VI.5.1 Proteins

For expression of ARNO and ARNO-Sec7 in E. coli the complete coding sequence of human ARNO (GenBank NM_017457) or amino acids 52 – 246 for ARNO-Sec7 were inserted into pET-15 vector introducing a N-terminal 6xHis tag. For bacterial expression of MIG6-EBR amino acids 325 – 375 were fused to the C-terminus of GST (pGEX-2T, TEV cleavage site). For the construction of EGFR-ICD and EGFR-ICD1022 the complete intracellular domain of the EGFR (amino acids 669 – 1210) or the intracellular domain truncated after amino acid 1022 were cloned into pIEx/Bac-1 (Novagen) such that they contained a 6xHis tag (His-EGFR-ICD) or a StrepTag (ST-EGFR-ICD and ST-EGFR-ICD1022) at the N-terminus. Recombinant baculovirus was produced using the BacMagic DNA Kit (Novagen). The coding sequences of all constructs were verified by sequencing (GATC Biotech). EGFR-ICD was expressed in baculovirus-infected SF9 cells. Purification of His-EGFR-ICD by anion exchange and nickel affinity chromatography was performed as described [23]. ST-EGFR-ICD and ST-EGFR-ICD1022 were purified by StrepTactin affinity chromatography. ARNO and its domains and MIG6-EBR were expressed in E. coli and purified by standard nickel or glutathion affinity chromatography, respectively.

NΔ17ARF1-CyPET, YPET-GGA3 and ARNO-Sec7 were subcloned into pET15 vectors (Novagen) as described previously. N-terminal truncated [Δ17]ARF1 (amino acids 18-181), lacking the first 17 amino acids and ARNO-Sec7 (amino acids 50-255 of ARNO) were expressed in E. coli and purified by Ni-NTA chromatography (Ni-NTA agarose, Quiagen).

Cloning, expression and purification were performed by Anton Schmitz and Volkmar Fieberg (AK Famulok).

VI.5.2 Fluorescence anisotropy

VI.5.2.1 Labeling of proteins

Proteins were slowly thawed on ice and centrifuged for 15min at 20000rpm to separate protein aggregates. The supernatant was subjected to buffer exchange (1x protein buffer) using NAP-5 columns (GE Healthcare Lifescience). Protein concentration of the eluted proteins was determined by Bradford or absorption at 280nm. Proteins were labelled with fluoresceine isothiocyanate (FITC, dissolved in DMSO, Sigma) using 10-20fold molecular excess for 1h at 4°C in the dark. The reaction was stopped by the addition of 75mM Tris-HCl, pH 6.8. Free dye was separated by buffer exchange using NAP-5 columns. Concentration and

labelling efficiency of the labelled proteins were calculated using the following formulas and the absorption at the indicated wavelengths:

$$\text{Protein concentration (M)} = \frac{A_{280} - (A_{max} \times CF)}{\varepsilon} \times \text{dilution factor}$$

$$\text{Moles dye per mole protein} = \frac{A_{max} \text{ of the labeled protein}}{\varepsilon' \times \text{protein concentration (M)}} \times \text{dilution factor}$$

Table 20 Formulas for concentration determination of labeled proteins
A: absorption, A_{max}: absorption 495nm, CF: correction factor 0.35, ε': extinction factor protein

Protein buffer
25mM HEPES-NaOH pH 7,8
300mM NaCl
3mM MgCl2
10% Glycerin

VI.5.2.2 Anisotropy measurements

Fluorescein-labelled ARNO, ARNO-Sec7-wt/E156K, MIG6-EBR or lysozyme (Sigma) at a final concentration of 1μM was mixed with unlabelled His-EGFR-ICD, ST-EGFR-ICD, ST-EGFR-ICD1022 or MIG6-EBR (20 nM-3.5 μM) in 1x binding buffer containing 0,05% Triton X-100 at room temperature in a 384well Proxiplate (PerkinElmer). Where indicated the reactions contained 1 mM ATP. Fluorescence anisotropy was measured after 45min incubation in a microplate reader (TecanUltra, Tecan). For comparison, the anisotropy value of the labelled protein without ligand was set as 0.

1x binding buffer
20 mM HEPES-KOH, pH 7.4
50 mM NaCl
5 mM $MgCl_2$
0.2 mM DTT

VI.5.2.3 Aggregation of EGFR-ICD

To analyze the aggregation of EGFR-ICD an aliquot of the binding reactions was separated by centrifugation (20000 rpm, 5 min) into pellet and supernatant. Both fractions were boiled in sample buffer and analyzed by SDS-PAGE and immunoblotting.

VI.5.3 EGFR-ICD autophosphorylation assays

For the autophosphorylation assays, His- or ST-EGFR-ICD (100nM) was incubated in 1x binding buffer with the indicated protein (200nM) at room temperature for 5min (reaction size: 90µl). The reaction was started by addition of 1 mM ATP (10µl). After the indicated time aliquots (40µl) were removed, boiled in SDS sample buffer, separated by SDS-PAGE (10µl) and analyzed by immunoblotting.

VI.5.4 GDP/GTP-exchange assays

VI.5.4.1 Tryptophan fluorescence

GDP/GTP exchange was measured on NΔ17ARF1 by tryptophan fluorescence. All measurements were performed in PBS pH 7.4, 3 mM MgCl2 at 37°C.

NΔ17ARF1 (2.8 µM) was preincubated with GDP (80 µM) in the presence of EDTA (2 mM) for 15 min in PBS pH 7.4 (without $MgCl_2$) at 37°C. The bound GDP was stabilized by addition of $MgCl_2$ (final concentration 3 mM) and incubation for further 5 min at 37°C. If not otherwise indicated, for each exchange reaction 700 nM of GDP loaded NΔ17ARF1 was mixed with 15 nM ARNO-Sec7 in the absence or presence of inhibitor or solvent (0,5% DMSO) in PBS pH 7.4, 3 mM MgCl2 (total volume 180 µl). The reaction was started by injection of 20µl GTP (50 µM). Fluorescence was detected approximately every 5secs, depending on sample number for a total of 600sec. The tryptophan fluorescence was measured at excitation and emission wavelength of 280 nm and 340 nm, respectively. All fluorescent measurements were performed with a Varioskan microplate reader (Thermo Scientific), in black 96-well plates. For data analysis the linear increase in fluorescence signal (200sec-600sec) was fitted by linear regression using GraphPadPrism software.

VI.5.4.2 FRET

GDP/GTP exchange was measured on NΔ17ARF1-CyPET by FRET. All measurements were performed in PBS pH 7.4, 3 mM MgCl2 at 37°C.

NΔ17ARF1-CyPET (2.8 µM) was preincubated with GDP (80 µM) in the presence of EDTA (2 mM) for 15 min in PBS pH 7.4 (without $MgCl_2$) at 37°C. The bound GDP was stabilized by addition of $MgCl_2$ (final concentration 3 mM) and incubation for further 5 min at 37°C. If not otherwise indicated, for each exchange reaction 700 nM of GDP loaded NΔ17ARF1-CyPET was mixed with 15 nM ARNO-Sec7 in the absence or presence of inhibitor or solvent (1% DMSO) in PBS pH 7.4, 3 mM MgCl2 and after 5min incubation at room temperature 500nM YPET-GGA3 was added (total volume 180 µl). The reaction was started by injection of 20µl

GTP (50 μM). Fluorescence was detected approximately every 10secs, depending on sample number for a total of 600sec. The tryptophan fluorescence was measured at excitation and emission wavelength of 280 nm and 340 nm, respectively, whereas FRET was measured at 436nm and 535nm, respectively. To detect possible quenching effects of the compounds CyPET and YPET was detected at ex436/em465 nm and ex500/em535, respectively, at the beginning of each measurement. All fluorescent measurements were performed with a Varioskan microplate reader (Thermo Scientific), in black 96-well plates. For data analysis the linear increase in fluorescence signal (200sec-600sec) was fitted by linear regression using GraphPadPrism software.

GTP Mix

	for 250Rxn		Stock	End
PBS + 3mM MgCl2	4975	µl		
GTP	25	µl	100mM	200µM
Gesamt	5000	µl		

Prime tubes with GTP-Mix!!!

ARF Mix

	for 30Rxn		Stock	End
PBS	1353	µl	1x	1x
Δ17ARF1	16,5	µl	235µM*	2.59µM (final 0.65µM)
EDTA pH 8,0	6	µl	500mM	2mM
GDP	120	µl	1000µM	80µM
Gesamt	1495.5	µl		
incubate @37°C, shaking (10% speed) for 15min			* nach Gel, OD: 650µM	
add				
MgCl2	4.5	µl	1000mM	3mM
and incubate for 3-5min @37°C				

hCyt2-Sec7 Mix

dilute hCyt2-Sec7 (80µM) 1:8 in PBS/MgCl2 to get 10µM				
PBS + 3mM MgCl2	992.5	µl	1x	1x
hCyt2-Sec7	7.5	µl	10µM	75nM (final 15nM)
Gesamt	1000	µl		

1. Prepare Mixes
2. add to plate 89µl plate buffer PBS + 3mM MgCl2
   1µl Compound/DMSO (200x)
   40µl Cyt-Mix (just before addition of ARF)
   and mix thoroughly
3. add to plate 50µl ARF-Mix
4. start measurement by injecting 20µl GTP-Mix

Table 21 Exemplary pipet scheme for a GDP/GTP-exchange reaction on NΔ17ARF1

VI.6 Statistics

Results are given as the mean +/- SEM (standard error of the mean). Statistical analyses were performed with Prism (GraphPad Software) applying the two-tailed t-test or one-way-ANOVA, as appropriate. All data sets passed the Kolmogorov and Smirnov test for Gaussian distribution. For the analysis of the tumor samples the Spearman nonparametric correlation test was used. Differences of means were considered significant at a significance level of 0.05 (Table 22).

p-value	meaning	symbol
>0.05	non significant	
0.01 to 0.05	significant	*
0.001 to 0.01	highly significant	**
<0.001	extremely significant	***

Table 22 Meaning of the p-value

VI.7 Materials

VI.7.1 Instruments

instrument, type	manufacturer
blotting chamber; semi-dry-blotter PEGASUS	Phase
CCD-Camera; VersaDoc 5000	Bio-Rad
centrifuge; 5417C	Eppendorf
centrifuge; 5810R	Eppendorf
electronic micro pipette; multidispenser	Eppendorf
fluorescence plate-reader	Thermo
hemocytometer; T728.1	Roth
incubator, Hera Cell	Heraeus
magnetic stirrer; Combimag	IKA
micoscope; Axiovert25	Zeiss
micro pipette; research	Eppendorf
Odyssey	LICOR
PAGE-chamber; Mini-Protean 3 Cell	Bio-Rad
PCR-cycler; T3 thermocycler	Biometra
pH-Meter MP220	Mettler Toledo
pipette controller; Accu-Jet	Brand
power supply: Power Consort E865	Consort
real-time PCR Cycler; iCycler iQ5	Bio-Rad
scale; BL 1500S	Sartorius
scale; JL-200	Chyo Balance

sterile hood; HeraSafe	Heraeus
thermoblock; Block Heater	Stuart-Scientific
thermomixer; KTM 100RP	HLC
UV-transilluminator; MiniBis	Bio-Imaging-Systems
water purifications system; HP6 UV/UF	TKA-Lab

VI.7.2 Materials

article	**manufacturer**
cell scraper	TPP
cryo tubes	Roth
culture dishes	TPP
culture flasks	TPP
culture plates	TPP
filter paper GB005	Whatman
nitrocellulose membrane; Protran 0,45µM	Schleicher&Schuell
PCR-plate sealer	Bio-Rad
PCR-plates, 96well	Bio-Rad
pipette tipps for micro pipettes	Peske, Biozym
pipette tipps for micro pipettes, multidispenser	Eppendorf
reaction tube (1,5ml und 2ml)	Eppendorf or Sarstedt
reaction tube (PCR 0,2ml und 0,5ml)	Eppendorf or Sarstedt
serological pipettes 2, 5, 10, 25, 50ml	TPP
tubes 15ml, 50ml	Falcon

VI.7.3 Cell culture reagents

article	**manufacturer**
cell culture media	PAA
EGF; AF-100-15	Peprotech
Fetal Bovine Serum (FBS), DE14-870F	Lonza
FuGene	Roche
G-418 sulphate solution (50mg/ml)	PAA
HRG-ß-1; AF-100-03	Peprotech
Lipofectamin	Invitrogen
Lipofectamin LTX + Plus reagent	Invitrogen
Lipofectamin RNAiMax	Invitrogen
Metafecten	Biontex
Metafecten Pro	Biontex
PBS Dulbecco's (1x), pH 7,4	PAA
Penicillin/Streptomycin (100x)	PAA
Trypsin/EDTA (10x)	PAA

VI.7.4 Standards for DNA- and protein-gels

DNA-ladder	manufacturer
peqGOLD 100bp 0,5mg DNA/ml	peqLab

protein-ladder	manufacturer
SeeBluePlus2	Invitrogen
Page Ruler Prestained Protein Ladder	Fermentas
HiMark Prestained HMW Protein Standard	Invitrogen

VI.7.5 Kits

article	manufacturer
CellTiter96 Non Radioactiv Cell Proliferation Assay (MTT-Assay)	Promega
High Capacity cDNA-Kit	AppliedBiosystems
Platinum Quantitative PCR Supermix	Invitrogen
SV Total RNA Isolation Kit	Promega

VII Literature

1. Blume-Jensen, P. and T. Hunter, *Oncogenic kinase signalling.* Nature, 2001. **411**(6835): p. 355-65.
2. Schlessinger, J., *Cell signaling by receptor tyrosine kinases.* Cell, 2000. **103**(2): p. 211-25.
3. Downward, J., et al., *Close similarity of epidermal growth factor receptor and v-erb-B oncogene protein sequences.* Nature, 1984. **307**(5951): p. 521-7.
4. Bublil, E.M. and Y. Yarden, *The EGF receptor family: spearheading a merger of signaling and therapeutics.* Curr Opin Cell Biol, 2007. **19**(2): p. 124-34.
5. Olayioye, M.A., et al., *The ErbB signaling network: receptor heterodimerization in development and cancer.* Embo J, 2000. **19**(13): p. 3159-67.
6. Zhang, H., et al., *ErbB receptors: from oncogenes to targeted cancer therapies.* J Clin Invest, 2007. **117**(8): p. 2051-8.
7. Hynes, N.E. and H.A. Lane, *ERBB receptors and cancer: the complexity of targeted inhibitors.* Nat Rev Cancer, 2005. **5**(5): p. 341-54.
8. Yarden, Y. and M.X. Sliwkowski, *Untangling the ErbB signalling network.* Nat Rev Mol Cell Biol, 2001. **2**(2): p. 127-37.
9. Graus-Porta, D., et al., *ErbB-2, the preferred heterodimerization partner of all ErbB receptors, is a mediator of lateral signaling.* Embo J, 1997. **16**(7): p. 1647-55.
10. Guy, P.M., et al., *Insect cell-expressed p180erbB3 possesses an impaired tyrosine kinase activity.* Proc Natl Acad Sci U S A, 1994. **91**(17): p. 8132-6.
11. Shi, F., et al., *ErbB3/HER3 intracellular domain is competent to bind ATP and catalyze autophosphorylation.* Proc Natl Acad Sci U S A, 2010. **107**(17): p. 7692-7.
12. Tzahar, E., et al., *A hierarchical network of interreceptor interactions determines signal transduction by Neu differentiation factor/neuregulin and epidermal growth factor.* Mol Cell Biol, 1996. **16**(10): p. 5276-87.
13. Gullick, W.J., *A new model for the interaction of EGF-like ligands with their receptors: the new one-two.* Eur J Cancer, 1994. **30A**(14): p. 2186.
14. Lemmon, M.A., et al., *Two EGF molecules contribute additively to stabilization of the EGFR dimer.* Embo J, 1997. **16**(2): p. 281-94.
15. Garrett, T.P., et al., *Crystal structure of a truncated epidermal growth factor receptor extracellular domain bound to transforming growth factor alpha.* Cell, 2002. **110**(6): p. 763-73.
16. Ogiso, H., et al., *Crystal structure of the complex of human epidermal growth factor and receptor extracellular domains.* Cell, 2002. **110**(6): p. 775-87.
17. Ferguson, K.M., *Structure-based view of epidermal growth factor receptor regulation.* Annu Rev Biophys, 2008. **37**: p. 353-73.
18. Ferguson, K.M., et al., *EGF activates its receptor by removing interactions that autoinhibit ectodomain dimerization.* Mol Cell, 2003. **11**(2): p. 507-17.
19. Burgess, A.W., et al., *An open-and-shut case? Recent insights into the activation of EGF/ErbB receptors.* Mol Cell, 2003. **12**(3): p. 541-52.
20. Moasser, M.M., *The oncogene HER2: its signaling and transforming functions and its role in human cancer pathogenesis.* Oncogene, 2007.
21. Schlessinger, J., *Ligand-induced, receptor-mediated dimerization and activation of EGF receptor.* Cell, 2002. **110**(6): p. 669-72.
22. Yarden, Y. and J. Schlessinger, *Epidermal growth factor induces rapid, reversible aggregation of the purified epidermal growth factor receptor.* Biochemistry, 1987. **26**(5): p. 1443-51.
23. Zhang, X., et al., *An allosteric mechanism for activation of the kinase domain of epidermal growth factor receptor.* Cell, 2006. **125**(6): p. 1137-49.
24. Jeffrey, P.D., et al., *Mechanism of CDK activation revealed by the structure of a cyclinA-CDK2 complex.* Nature, 1995. **376**(6538): p. 313-20.

25. Jura, N., et al., *Mechanism for activation of the EGF receptor catalytic domain by the juxtamembrane segment.* Cell, 2009. **137**(7): p. 1293-307.
26. Red Brewer, M., et al., *The juxtamembrane region of the EGF receptor functions as an activation domain.* Mol Cell, 2009. **34**(6): p. 641-51.
27. Jura, N., et al., *Structural analysis of the catalytically inactive kinase domain of the human EGF receptor 3.* Proc Natl Acad Sci U S A, 2009. **106**(51): p. 21608-13.
28. Hackel, P.O., M. Gishizky, and A. Ullrich, *Mig-6 is a negative regulator of the epidermal growth factor receptor signal.* Biol Chem, 2001. **382**(12): p. 1649-62.
29. Fiorentino, L., et al., *Inhibition of ErbB-2 mitogenic and transforming activity by RALT, a mitogen-induced signal transducer which binds to the ErbB-2 kinase domain.* Mol Cell Biol, 2000. **20**(20): p. 7735-50.
30. Zhang, Y.W., et al., *Evidence that MIG-6 is a tumor-suppressor gene.* Oncogene, 2007. **26**(2): p. 269-76.
31. Anastasi, S., et al., *Loss of RALT/MIG-6 expression in ERBB2-amplified breast carcinomas enhances ErbB-2 oncogenic potency and favors resistance to Herceptin.* Oncogene, 2005. **24**(28): p. 4540-8.
32. Ferby, I., et al., *Mig6 is a negative regulator of EGF receptor-mediated skin morphogenesis and tumor formation.* Nat Med, 2006. **12**(5): p. 568-73.
33. Anastasi, S., et al., *The evolutionarily conserved EBR module of RALT/MIG6 mediates suppression of the EGFR catalytic activity.* Oncogene, 2007. **26**(57): p. 7833-46.
34. Zhang, X., et al., *Inhibition of the EGF receptor by binding of MIG6 to an activating kinase domain interface.* Nature, 2007. **450**(7170): p. 741-4.
35. Anastasi, S., et al., *Feedback inhibition by RALT controls signal output by the ErbB network.* Oncogene, 2003. **22**(27): p. 4221-34.
36. Turjanski, A.G., J.P. Vaque, and J.S. Gutkind, *MAP kinases and the control of nuclear events.* Oncogene, 2007. **26**(22): p. 3240-53.
37. Cantley, L.C., *The phosphoinositide 3-kinase pathway.* Science, 2002. **296**(5573): p. 1655-7.
38. Quesnelle, K.M., A.L. Boehm, and J.R. Grandis, *STAT-mediated EGFR signaling in cancer.* J Cell Biochem, 2007. **102**(2): p. 311-9.
39. Kim, H., et al., *The c-Src tyrosine kinase associates with the catalytic domain of ErbB-2: implications for ErbB-2 mediated signaling and transformation.* Oncogene, 2005. **24**(51): p. 7599-607.
40. Foster, K.G. and D.C. Fingar, *Mammalian target of rapamycin (mTOR): conducting the cellular signaling symphony.* J Biol Chem, 2010. **285**(19): p. 14071-7.
41. Hanahan, D. and R.A. Weinberg, *The hallmarks of cancer.* Cell, 2000. **100**(1): p. 57-70.
42. Hunter, T. and B.M. Sefton, *Transforming gene product of Rous sarcoma virus phosphorylates tyrosine.* Proc Natl Acad Sci U S A, 1980. **77**(3): p. 1311-5.
43. Di Fiore, P.P., et al., *Overexpression of the human EGF receptor confers an EGF-dependent transformed phenotype to NIH 3T3 cells.* Cell, 1987. **51**(6): p. 1063-70.
44. Brambilla, E., et al., *The new World Health Organization classification of lung tumours.* Eur Respir J, 2001. **18**(6): p. 1059-68.
45. Veale, D., et al., *Epidermal growth factor receptors in non-small cell lung cancer.* Br J Cancer, 1987. **55**(5): p. 513-6.
46. Sharma, S.V., et al., *Epidermal growth factor receptor mutations in lung cancer.* Nat Rev Cancer, 2007. **7**(3): p. 169-81.
47. Bose, R. and X. Zhang, *The ErbB kinase domain: structural perspectives into kinase activation and inhibition.* Exp Cell Res, 2009. **315**(4): p. 649-58.
48. Sharma, S.V. and J. Settleman, *ErbBs in lung cancer.* Exp Cell Res, 2009. **315**(4): p. 557-71.
49. Pao, W. and J. Chmielecki, *Rational, biologically based treatment of EGFR-mutant non-small-cell lung cancer.* Nat Rev Cancer, 2010. **10**(11): p. 760-74.

50. Wheatley-Price, P. and F.A. Shepherd, *Epidermal growth factor receptor inhibitors in the treatment of lung cancer: reality and hopes.* Curr Opin Oncol, 2008. **20**(2): p. 162-75.
51. Rowinsky, E.K., *The erbB family: targets for therapeutic development against cancer and therapeutic strategies using monoclonal antibodies and tyrosine kinase inhibitors.* Annu Rev Med, 2004. **55**: p. 433-57.
52. Matsubara, D., et al., *Co-Activation of Epidermal Growth Factor Receptor and c-MET Defines a Distinct Subset of Lung Adenocarcinomas.* Am J Pathol, 2010.
53. *http://www.breastcancer.org/*.
54. Slamon, D.J., et al., *Human breast cancer: correlation of relapse and survival with amplification of the HER-2/neu oncogene.* Science, 1987. **235**(4785): p. 177-82.
55. Slamon, D.J., et al., *Studies of the HER-2/neu proto-oncogene in human breast and ovarian cancer.* Science, 1989. **244**(4905): p. 707-12.
56. Sliwkowski, M.X., et al., *Nonclinical studies addressing the mechanism of action of trastuzumab (Herceptin).* Semin Oncol, 1999. **26**(4 Suppl 12): p. 60-70.
57. Nahta, R., et al., *Mechanisms of disease: understanding resistance to HER2-targeted therapy in human breast cancer.* Nat Clin Pract Oncol, 2006. **3**(5): p. 269-80.
58. Giampaglia, M., et al., *Lapatinib in breast cancer: clinical experiences and future perspectives.* Cancer Treat Rev, 2010. **36 Suppl 3**: p. S72-9.
59. Xia, W., et al., *Anti-tumor activity of GW572016: a dual tyrosine kinase inhibitor blocks EGF activation of EGFR/erbB2 and downstream Erk1/2 and AKT pathways.* Oncogene, 2002. **21**(41): p. 6255-63.
60. Badache, A. and N.E. Hynes, *A new therapeutic antibody masks ErbB2 to its partners.* Cancer Cell, 2004. **5**(4): p. 299-301.
61. *http://www.gene.com/gene/news/press-releases/display.do?method=detail&id=8431*.
62. Gutierrez, C. and R. Schiff, *HER2: biology, detection, and clinical implications.* Arch Pathol Lab Med, 2011. **135**(1): p. 55-62.
63. Mukai, H., *Targeted therapy in breast cancer: current status and future directions.* Jpn J Clin Oncol, 2010. **40**(8): p. 711-6.
64. Maher, E.A., et al., *Malignant glioma: genetics and biology of a grave matter.* Genes Dev, 2001. **15**(11): p. 1311-33.
65. Huang, P.H., A.M. Xu, and F.M. White, *Oncogenic EGFR signaling networks in glioma.* Sci Signal, 2009. **2**(87): p. re6.
66. Gan, H.K., A.H. Kaye, and R.B. Luwor, *The EGFRvIII variant in glioblastoma multiforme.* J Clin Neurosci, 2009. **16**(6): p. 748-54.
67. Huang, H.S., et al., *The enhanced tumorigenic activity of a mutant epidermal growth factor receptor common in human cancers is mediated by threshold levels of constitutive tyrosine phosphorylation and unattenuated signaling.* J Biol Chem, 1997. **272**(5): p. 2927-35.
68. Grandal, M.V., et al., *EGFRvIII escapes down-regulation due to impaired internalization and sorting to lysosomes.* Carcinogenesis, 2007. **28**(7): p. 1408-17.
69. Ding, H., et al., *Oligodendrogliomas result from the expression of an activated mutant epidermal growth factor receptor in a RAS transgenic mouse astrocytoma model.* Cancer Res, 2003. **63**(5): p. 1106-13.
70. Sampson, J.H., et al., *Unarmed, tumor-specific monoclonal antibody effectively treats brain tumors.* Proc Natl Acad Sci U S A, 2000. **97**(13): p. 7503-8.
71. Perera, R.M., et al., *Treatment of human tumor xenografts with monoclonal antibody 806 in combination with a prototypical epidermal growth factor receptor-specific antibody generates enhanced antitumor activity.* Clin Cancer Res, 2005. **11**(17): p. 6390-9.
72. Nagane, M., et al., *Human glioblastoma xenografts overexpressing a tumor-specific mutant epidermal growth factor receptor sensitized to cisplatin by the AG1478 tyrosine kinase inhibitor.* J Neurosurg, 2001. **95**(3): p. 472-9.
73. Trembath, D.G., et al., *A novel small molecule that selectively inhibits glioblastoma cells expressing EGFRvIII.* Mol Cancer, 2007. **6**: p. 30.

74. Kahn, R.A., et al., *The amino terminus of ADP-ribosylation factor (ARF) is a critical determinant of ARF activities and is a potent and specific inhibitor of protein transport.* J Biol Chem, 1992. **267**(18): p. 13039-46.
75. Franco, M., et al., *Myristoylation of ADP-ribosylation factor 1 facilitates nucleotide exchange at physiological Mg2+ levels.* J Biol Chem, 1995. **270**(3): p. 1337-41.
76. Goldberg, J., *Structural basis for activation of ARF GTPase: mechanisms of guanine nucleotide exchange and GTP-myristoyl switching.* Cell, 1998. **95**(2): p. 237-48.
77. Bos, J.L., H. Rehmann, and A. Wittinghofer, *GEFs and GAPs: critical elements in the control of small G proteins.* Cell, 2007. **129**(5): p. 865-77.
78. Mossessova, E., J.M. Gulbis, and J. Goldberg, *Structure of the guanine nucleotide exchange factor Sec7 domain of human arno and analysis of the interaction with ARF GTPase.* Cell, 1998. **92**(3): p. 415-23.
79. Beraud-Dufour, S., et al., *A glutamic finger in the guanine nucleotide exchange factor ARNO displaces Mg2+ and the beta-phosphate to destabilize GDP on ARF1.* Embo J, 1998. **17**(13): p. 3651-9.
80. Kolanus, W., *Guanine nucleotide exchange factors of the cytohesin family and their roles in signal transduction.* Immunol Rev, 2007. **218**: p. 102-13.
81. Moss, J. and M. Vaughan, *Molecules in the ARF orbit.* J Biol Chem, 1998. **273**(34): p. 21431-4.
82. D'Souza-Schorey, C. and P. Chavrier, *ARF proteins: roles in membrane traffic and beyond.* Nat Rev Mol Cell Biol, 2006. **7**(5): p. 347-58.
83. Kolanus, W., et al., *Alpha L beta 2 integrin/LFA-1 binding to ICAM-1 induced by cytohesin-1, a cytoplasmic regulatory molecule.* Cell, 1996. **86**(2): p. 233-42.
84. Chardin, P., et al., *A human exchange factor for ARF contains Sec7- and pleckstrin-homology domains.* Nature, 1996. **384**(6608): p. 481-4.
85. Klarlund, J.K., et al., *Signaling by phosphoinositide-3,4,5-trisphosphate through proteins containing pleckstrin and Sec7 homology domains.* Science, 1997. **275**(5308): p. 1927-30.
86. Ogasawara, M., et al., *Similarities in function and gene structure of cytohesin-4 and cytohesin-1, guanine nucleotide-exchange proteins for ADP-ribosylation factors.* J Biol Chem, 2000. **275**(5): p. 3221-30.
87. Geiger, C., et al., *Cytohesin-1 regulates beta-2 integrin-mediated adhesion through both ARF-GEF function and interaction with LFA-1.* Embo J, 2000. **19**(11): p. 2525-36.
88. Kliche, S., et al., *Signaling by human herpesvirus 8 kaposin A through direct membrane recruitment of cytohesin-1.* Mol Cell, 2001. **7**(4): p. 833-43.
89. Theis, M.G., et al., *Discriminatory aptamer reveals serum response element transcription regulated by cytohesin-2.* Proc Natl Acad Sci U S A, 2004. **101**(31): p. 11221-6.
90. Hafner, M., et al., *Inhibition of cytohesins by SecinH3 leads to hepatic insulin resistance.* Nature, 2006. **444**(7121): p. 941-4.
91. Cherfils, J. and P. Melancon, *On the action of Brefeldin A on Sec7-stimulated membrane-recruitment and GDP/GTP exchange of Arf proteins.* Biochem Soc Trans, 2005. **33**(Pt 4): p. 635-8.
92. Viaud, J., et al., *Structure-based discovery of an inhibitor of Arf activation by Sec7 domains through targeting of protein-protein complexes.* Proc Natl Acad Sci U S A, 2007. **104**(25): p. 10370-5.
93. Vigil, D., et al., *Ras superfamily GEFs and GAPs: validated and tractable targets for cancer therapy?* Nat Rev Cancer, 2010. **10**(12): p. 842-57.
94. Hafner, M., et al., *Displacement of protein-bound aptamers with small molecules screened by fluorescence polarization.* Nat Protoc, 2008. **3**(4): p. 579-87.
95. Mayer, G., et al., *Controlling small guanine-nucleotide-exchange factor function through cytoplasmic RNA intramers.* Proc Natl Acad Sci U S A, 2001. **98**(9): p. 4961-5.
96. Lim, J., et al., *The CNK1 scaffold binds cytohesins and promotes insulin pathway signaling.* Genes Dev, 2010. **24**(14): p. 1496-506.

97. Jones, C.A., et al., *Slit2-Robo4 signalling promotes vascular stability by blocking Arf6 activity.* Nat Cell Biol, 2009. **11**(11): p. 1325-31.
98. Ikenouchi, J. and M. Umeda, *FRMD4A regulates epithelial polarity by connecting Arf6 activation with the PAR complex.* Proc Natl Acad Sci U S A, 2010. **107**(2): p. 748-53.
99. Oh, S.J. and L.C. Santy, *Differential effects of cytohesins 2 and 3 on beta1 integrin recycling.* J Biol Chem, 2010. **285**(19): p. 14610-6.
100. Torii, T., et al., *Cytohesin-2/ARNO, through its interaction with focal adhesion adaptor protein paxillin, regulates preadipocyte migration via the downstream activation of Arf6.* J Biol Chem, 2010. **285**(31): p. 24270-81.
101. El Azreq, M.A., et al., *Cytohesin-1 regulates the Arf6-phospholipase D signaling axis in human neutrophils: impact on superoxide anion production and secretion.* J Immunol, 2010. **184**(2): p. 637-49.
102. Fuss, B., et al., *The cytohesin Steppke is essential for insulin signalling in Drosophila.* Nature, 2006. **444**(7121): p. 945-8.
103. Janmaat, M.L., et al., *Enhanced cytotoxicity induced by gefitinib and specific inhibitors of the Ras or phosphatidyl inositol-3 kinase pathways in non-small cell lung cancer cells.* Int J Cancer, 2006. **118**(1): p. 209-14.
104. Bill, A., et al., *Cytohesins Are Cytoplasmic ErbB Receptor Activators.* Cell, 2010. **143**(2): p. 201-11.
105. Kao, J., et al., *Molecular profiling of breast cancer cell lines defines relevant tumor models and provides a resource for cancer gene discovery.* PLoS One, 2009. **4**(7): p. e6146.
106. Wang, Q., G. Villeneuve, and Z. Wang, *Control of epidermal growth factor receptor endocytosis by receptor dimerization, rather than receptor kinase activation.* EMBO Rep, 2005. **6**(10): p. 942-8.
107. Mattson, G., et al., *A practical approach to crosslinking.* Mol Biol Rep, 1993. **17**(3): p. 167-83.
108. Lacowicz, J.R., *Principles of fluorescence spectroscopy.* Springer Verlag, 2006. **3rd edition**.
109. Lidke, D.S., et al., *Imaging molecular interactions in cells by dynamic and static fluorescence anisotropy (rFLIM and emFRET).* Biochem Soc Trans, 2003. **31**(Pt 5): p. 1020-7.
110. Squire, A., et al., *Red-edge anisotropy microscopy enables dynamic imaging of homo-FRET between green fluorescent proteins in cells.* J Struct Biol, 2004. **147**(1): p. 62-9.
111. Tramier, M. and M. Coppey-Moisan, *Fluorescence anisotropy imaging microscopy for homo-FRET in living cells.* Methods Cell Biol, 2008. **85**: p. 395-414.
112. Vilar, M., et al., *Activation of the p75 neurotrophin receptor through conformational rearrangement of disulphide-linked receptor dimers.* Neuron, 2009. **62**(1): p. 72-83.
113. Bergamin, E., et al., *The cytoplasmic adaptor protein Dok7 activates the receptor tyrosine kinase MuSK via dimerization.* Mol Cell, 2010. **39**(1): p. 100-9.
114. Inoue, A., et al., *Dok-7 activates the muscle receptor kinase MuSK and shapes synapse formation.* Sci Signal, 2009. **2**(59): p. ra7.
115. Charpidou, A., et al., *Review. EGFR mutations in non-small cell lung cancer--clinical implications.* In Vivo, 2008. **22**(4): p. 529-36.
116. Li, S.D., et al., *Tumor-targeted delivery of siRNA by self-assembled nanoparticles.* Mol Ther, 2008. **16**(1): p. 163-9.
117. Zhang, M., et al., *Inhibition of epidermal growth factor receptor expression by RNA interference in A549 cells.* Acta Pharmacol Sin, 2004. **25**(1): p. 61-7.
118. Harper, J.V. and G. Brooks, *The mammalian cell cycle: an overview.* Methods Mol Biol, 2005. **296**: p. 113-53.
119. Tavecchio, M., et al., *Multi-parametric flow cytometric cell cycle analysis using TO-PRO-3 iodide (TP3): detailed protocols.* Acta Histochem, 2008. **110**(3): p. 232-44.
120. van Engeland, M., et al., *Annexin V-affinity assay: a review on an apoptosis detection system based on phosphatidylserine exposure.* Cytometry, 1998. **31**(1): p. 1-9.

121. Gerdes, J., et al., *Production of a mouse monoclonal antibody reactive with a human nuclear antigen associated with cell proliferation.* Int J Cancer, 1983. **31**(1): p. 13-20.
122. Scholzen, T. and J. Gerdes, *The Ki-67 protein: from the known and the unknown.* J Cell Physiol, 2000. **182**(3): p. 311-22.
123. Yauch, R.L., et al., *Epithelial versus mesenchymal phenotype determines in vitro sensitivity and predicts clinical activity of erlotinib in lung cancer patients.* Clin Cancer Res, 2005. **11**(24 Pt 1): p. 8686-98.
124. Kubo, T., et al., *MET gene amplification or EGFR mutation activate MET in lung cancers untreated with EGFR tyrosine kinase inhibitors.* Int J Cancer, 2009. **124**(8): p. 1778-84.
125. Shigematsu, H., et al., *Somatic mutations of the HER2 kinase domain in lung adenocarcinomas.* Cancer Res, 2005. **65**(5): p. 1642-6.
126. Stumpfe, D., et al., *Targeting multifunctional proteins by virtual screening: structurally diverse cytohesin inhibitors with differentiated biological functions.* ACS Chem Biol, 2010. **5**(9): p. 839-49.
127. Kahn, R.A. and A.G. Gilman, *The protein cofactor necessary for ADP-ribosylation of Gs by cholera toxin is itself a GTP binding protein.* J Biol Chem, 1986. **261**(17): p. 7906-11.
128. Casanova, J.E., *Regulation of arf activation: the sec7 family of Guanine nucleotide exchange factors.* Traffic, 2007. **8**(11): p. 1476-85.
129. Cherfils, J., et al., *Structure of the Sec7 domain of the Arf exchange factor ARNO.* Nature, 1998. **392**(6671): p. 101-5.
130. Zhang, J.H., T.D. Chung, and K.R. Oldenburg, *A Simple Statistical Parameter for Use in Evaluation and Validation of High Throughput Screening Assays.* J Biomol Screen, 1999. **4**(2): p. 67-73.
131. Lipinski, C.A., et al., *Experimental and computational approaches to estimate solubility and permeability in drug discovery and development settings.* Adv Drug Deliv Rev, 2001. **46**(1-3): p. 3-26.
132. Zawrocki, A. and W. Biernat, *Epidermal growth factor receptor in glioblastoma.* Folia Neuropathol, 2005. **43**(3): p. 123-32.
133. Norbury, C.J. and B. Zhivotovsky, *DNA damage-induced apoptosis.* Oncogene, 2004. **23**(16): p. 2797-808.
134. Yuan, J., R. Adamski, and J. Chen, *Focus on histone variant H2AX: to be or not to be.* FEBS Lett, 2010. **584**(17): p. 3717-24.
135. Tarsounas, M., A.A. Davies, and S.C. West, *RAD51 localization and activation following DNA damage.* Philos Trans R Soc Lond B Biol Sci, 2004. **359**(1441): p. 87-93.
136. Golding, S.E., et al., *Double strand break repair by homologous recombination is regulated by cell cycle-independent signaling via ATM in human glioma cells.* J Biol Chem, 2004. **279**(15): p. 15402-10.
137. Li, M., et al., *Adenosine diphosphate-ribosylation factor 6 is required for epidermal growth factor-induced glioblastoma cell proliferation.* Cancer, 2009. **115**(21): p. 4959-72.
138. Zeeh, J.C., et al., *In vitro assays to characterize inhibitors of the activation of small G proteins by their guanine nucleotide exchange factors.* Methods Enzymol, 2008. **438**: p. 41-56.
139. John, J., et al., *Kinetics of interaction of nucleotides with nucleotide-free H-ras p21.* Biochemistry, 1990. **29**(25): p. 6058-65.
140. Lenzen, C., R.H. Cool, and A. Wittinghofer, *Analysis of intrinsic and CDC25-stimulated guanine nucleotide exchange of p21ras-nucleotide complexes by fluorescence measurements.* Methods Enzymol, 1995. **255**: p. 95-109.
141. Nie, Z., D.S. Hirsch, and P.A. Randazzo, *Arf and its many interactors.* Curr Opin Cell Biol, 2003. **15**(4): p. 396-404.
142. Bonifacino, J.S., *The GGA proteins: adaptors on the move.* Nat Rev Mol Cell Biol, 2004. **5**(1): p. 23-32.
143. Takatsu, H., et al., *GGA proteins associate with Golgi membranes through interaction between their GGAH domains and ADP-ribosylation factors.* Biochem J, 2002. **365**(Pt 2): p. 369-78.

144. Hall, B., et al., *A fluorescence resonance energy transfer activation sensor for Arf6.* Anal Biochem, 2008. **374**(2): p. 243-9.
145. Bi, X., et al., *Affinity-based labeling of cytohesins with a bifunctional SecinH3 photoaffinity probe.* Angew Chem Int Ed Engl, 2008. **47**(49): p. 9565-8.
146. Gullick, W.J., et al., *A radioimmunoassay for human epidermal growth factor receptor.* Anal Biochem, 1984. **141**(1): p. 253-61.
147. Klein, P., et al., *A structure-based model for ligand binding and dimerization of EGF receptors.* Proc Natl Acad Sci U S A, 2004. **101**(4): p. 929-34.
148. Walker, F., et al., *CR1/CR2 interactions modulate the functions of the cell surface epidermal growth factor receptor.* J Biol Chem, 2004. **279**(21): p. 22387-98.
149. Gadella, T.W., Jr. and T.M. Jovin, *Oligomerization of epidermal growth factor receptors on A431 cells studied by time-resolved fluorescence imaging microscopy. A stereochemical model for tyrosine kinase receptor activation.* J Cell Biol, 1995. **129**(6): p. 1543-58.
150. Moriki, T., H. Maruyama, and I.N. Maruyama, *Activation of preformed EGF receptor dimers by ligand-induced rotation of the transmembrane domain.* J Mol Biol, 2001. **311**(5): p. 1011-26.
151. Chung, I., et al., *Spatial control of EGF receptor activation by reversible dimerization on living cells.* Nature, 2010.
152. Landau, M. and N. Ben-Tal, *Dynamic equilibrium between multiple active and inactive conformations explains regulation and oncogenic mutations in ErbB receptors.* Biochim Biophys Acta, 2008. **1785**(1): p. 12-31.
153. Mohammadi, M., et al., *Aggregation-induced activation of the epidermal growth factor receptor protein tyrosine kinase.* Biochemistry, 1993. **32**(34): p. 8742-8.
154. Wedegaertner, P.B. and G.N. Gill, *Activation of the purified protein tyrosine kinase domain of the epidermal growth factor receptor.* J Biol Chem, 1989. **264**(19): p. 11346-53.
155. Zhu, H.J., et al., *Epidermal growth factor receptor: association of extracellular domain negatively regulates intracellular kinase activation in the absence of ligand.* Growth Factors, 2003. **21**(1): p. 15-30.
156. Nagy, P., et al., *Distribution of resting and ligand-bound ErbB1 and ErbB2 receptor tyrosine kinases in living cells using number and brightness analysis.* Proc Natl Acad Sci U S A, 2010. **107**(38): p. 16524-16529.
157. Nagy, P., et al., *Activation-dependent clustering of the erbB2 receptor tyrosine kinase detected by scanning near-field optical microscopy.* J Cell Sci, 1999. **112 (Pt 11)**: p. 1733-41.
158. Abulrob, A., et al., *Nanoscale imaging of epidermal growth factor receptor clustering: effects of inhibitors.* J Biol Chem, 2010. **285**(5): p. 3145-56.
159. Reschke, M., et al., *Mitogen-inducible gene-6 is a negative regulator of epidermal growth factor receptor signaling in hepatocytes and human hepatocellular carcinoma.* Hepatology, 2010. **51**(4): p. 1383-90.
160. Maselli, R.A., et al., *Mutations in MUSK causing congenital myasthenic syndrome impair MuSK-Dok-7 interaction.* Hum Mol Genet, 2010. **19**(12): p. 2370-9.
161. Cadena, D.L., C.L. Chan, and G.N. Gill, *The intracellular tyrosine kinase domain of the epidermal growth factor receptor undergoes a conformational change upon autophosphorylation.* J Biol Chem, 1994. **269**(1): p. 260-5.
162. Landau, M., S.J. Fleishman, and N. Ben-Tal, *A putative mechanism for downregulation of the catalytic activity of the EGF receptor via direct contact between its kinase and C-terminal domains.* Structure, 2004. **12**(12): p. 2265-75.
163. Huse, M. and J. Kuriyan, *The conformational plasticity of protein kinases.* Cell, 2002. **109**(3): p. 275-82.
164. Weinstein, I.B., *Cancer. Addiction to oncogenes--the Achilles heal of cancer.* Science, 2002. **297**(5578): p. 63-4.
165. Wang, X., et al., *Does hepatocyte growth factor/c-Met signal play synergetic role in lung cancer?* J Cell Mol Med, 2010. **14**(4): p. 833-9.

166. Yoshida, T., et al., *Effects of Src inhibitors on cell growth and epidermal growth factor receptor and MET signaling in gefitinib-resistant non-small cell lung cancer cells with acquired MET amplification.* Cancer Sci, 2010. **101**(1): p. 167-72.
167. Sharma, S.V., et al., *A common signaling cascade may underlie "addiction" to the Src, BCR-ABL, and EGF receptor oncogenes.* Cancer Cell, 2006. **10**(5): p. 425-35.
168. Sordella, R., et al., *Gefitinib-sensitizing EGFR mutations in lung cancer activate anti-apoptotic pathways.* Science, 2004. **305**(5687): p. 1163-7.
169. Chang, G.C., et al., *Molecular mechanisms of ZD1839-induced G1-cell cycle arrest and apoptosis in human lung adenocarcinoma A549 cells.* Biochem Pharmacol, 2004. **68**(7): p. 1453-64.
170. Normanno, N., M.R. Maiello, and A. De Luca, *Epidermal growth factor receptor tyrosine kinase inhibitors (EGFR-TKIs): simple drugs with a complex mechanism of action?* J Cell Physiol, 2003. **194**(1): p. 13-9.
171. Culy, C.R. and D. Faulds, *Gefitinib.* Drugs, 2002. **62**(15): p. 2237-48; discussion 2249-50.
172. Wells, J.A. and C.L. McClendon, *Reaching for high-hanging fruit in drug discovery at protein-protein interfaces.* Nature, 2007. **450**(7172): p. 1001-9.
173. Muralidharan-Chari, V., et al., *ADP-ribosylation factor 6 regulates tumorigenic and invasive properties in vivo.* Cancer Res, 2009. **69**(6): p. 2201-9.
174. Boulay, P.L., et al., *ADP-ribosylation factor 1 controls the activation of the phosphatidylinositol 3-kinase pathway to regulate epidermal growth factor-dependent growth and migration of breast cancer cells.* J Biol Chem, 2008. **283**(52): p. 36425-34.
175. Mossessova, E., R.A. Corpina, and J. Goldberg, *Crystal structure of ARF1*Sec7 complexed with Brefeldin A and its implications for the guanine nucleotide exchange mechanism.* Mol Cell, 2003. **12**(6): p. 1403-11.
176. Feng, B.Y., et al., *A high-throughput screen for aggregation-based inhibition in a large compound library.* J Med Chem, 2007. **50**(10): p. 2385-90.
177. Di, L. and E.H. Kerns, *Biological assay challenges from compound solubility: strategies for bioassay optimization.* Drug Discov Today, 2006. **11**(9-10): p. 446-51.
178. Alsenz, J. and M. Kansy, *High throughput solubility measurement in drug discovery and development.* Adv Drug Deliv Rev, 2007. **59**(7): p. 546-67.
179. Kerns, E.H., *High throughput physicochemical profiling for drug discovery.* J Pharm Sci, 2001. **90**(11): p. 1838-58.
180. Fischer, U. and E. Meese, *Glioblastoma multiforme: the role of DSB repair between genotype and phenotype.* Oncogene, 2007. **26**(56): p. 7809-15.
181. Golding, S.E., et al., *Pro-survival AKT and ERK signaling from EGFR and mutant EGFRvIII enhances DNA double-strand break repair in human glioma cells.* Cancer Biol Ther, 2009. **8**(8): p. 730-8.
182. Huse, J.T. and E.C. Holland, *Targeting brain cancer: advances in the molecular pathology of malignant glioma and medulloblastoma.* Nat Rev Cancer, 2010. **10**(5): p. 319-31.
183. Raderschall, E., et al., *Formation of higher-order nuclear Rad51 structures is functionally linked to p21 expression and protection from DNA damage-induced apoptosis.* J Cell Sci, 2002. **115**(Pt 1): p. 153-64.
184. Engelman, J.A., et al., *ErbB-3 mediates phosphoinositide 3-kinase activity in gefitinib-sensitive non-small cell lung cancer cell lines.* Proc Natl Acad Sci U S A, 2005. **102**(10): p. 3788-93.
185. Engelman, J.A., et al., *MET amplification leads to gefitinib resistance in lung cancer by activating ERBB3 signaling.* Science, 2007. **316**(5827): p. 1039-43.
186. Hutcheson, I.R., et al., *Inductive mechanisms limiting response to anti-epidermal growth factor receptor therapy.* Endocr Relat Cancer, 2006. **13 Suppl 1**: p. S89-97.
187. Ciardiello, F. and G. Tortora, *EGFR antagonists in cancer treatment.* N Engl J Med, 2008. **358**(11): p. 1160-74.

188. Ogino, A., et al., *Emergence of epidermal growth factor receptor T790M mutation during chronic exposure to gefitinib in a non small cell lung cancer cell line.* Cancer Res, 2007. **67**(16): p. 7807-14.
189. Stuhlmann-Laeisz, C., et al., *Forced dimerization of gp130 leads to constitutive STAT3 activation, cytokine-independent growth, and blockade of differentiation of embryonic stem cells.* Mol Biol Cell, 2006. **17**(7): p. 2986-95.
190. Laemmli, U.K., *Cleavage of structural proteins during the assembly of the head of bacteriophage T4.* Nature, 1970. **227**(5259): p. 680-5.
191. Kyhse-Andersen, J., *Electroblotting of multiple gels: a simple apparatus without buffer tank for rapid transfer of proteins from polyacrylamide to nitrocellulose.* J Biochem Biophys Methods, 1984. **10**(3-4): p. 203-9.
192. Avery, J., et al., *A cell-free system for regulated exocytosis in PC12 cells.* J Cell Biol, 2000. **148**(2): p. 317-24.
193. Lang, T., et al., *SNAREs are concentrated in cholesterol-dependent clusters that define docking and fusion sites for exocytosis.* EMBO J, 2001. **20**(9): p. 2202-13.
194. Lang, T., et al., *SNAREs in native plasma membranes are active and readily form core complexes with endogenous and exogenous SNAREs.* J Cell Biol, 2002. **158**(4): p. 751-60.
195. Ullrich, R.T., et al., *Early detection of erlotinib treatment response in NSCLC by 3'-deoxy-3'-[F]-fluoro-L-thymidine ([F]FLT) positron emission tomography (PET).* PLoS One, 2008. **3**(12): p. e3908.
196. Zimmer, S., et al., *Epidermal growth factor receptor mutations in non-small cell lung cancer influence downstream Akt, MAPK and Stat3 signaling.* J Cancer Res Clin Oncol, 2009. **135**(5): p. 723-30.
197. Heukamp, L.C., et al., *Podocalyxin-like protein 1 expression in primary hepatic tumours and tumour-like lesions.* Histopathology, 2006. **49**(3): p. 242-7.
198. Machulla, H.J., et al., *Simplified Labeling Approach for Synthesizing 3'-Deoxy-3'-[18F]fluorothymidine ([18F]FLT).* Journal of Radioanalytical and Nuclear Chemistry, 2000. **243**(3): p. 843-846.
199. Friedrichs, N., et al., *Immunohistochemical expression patterns of AP2alpha and AP2gamma in the developing fetal human breast.* Histopathology, 2007. **51**(6): p. 814-23.